Optical Tweezers: A tool to control, manipulate and quantify immune cell interaction

A thesis presented by

David Gavin Glass BSc Hons

A thesis submitted in the fulfilment of the requirements for the degree of Doctor of Philosophy

2014

Strathclyde Institute of Pharmacy and Biomedical Sciences

&

The Institute of Photonics

University of Strathclyde

This thesis is the result of the author's original research. It has been composed by the author and has not been previously submitted for examination which has led to the award of a degree.

Signed:

Date:

This thesis is dedicated to the memory of my mother,

Angela Glass (1954 – 2014),

For inspiring me to do my best, offering the support and encouragement to make it possible, and being the greatest influence on my life – It is all for you.

ACKNOWLEDGEMENTS

PUBLICATIONS

Glass, D G., Butcher, J., McAlinden, N., Schroeder, J., Plevin, R., Culshaw, S., Wright, A J., Millington, O R., Antigen citrullination enhances T-cell recognition and is associated with increased forces of cell-cell interaction as measured using optical trapping (In preparation).

Morrison, V., James, M J., Grzes, K., Cook, P., Glass, D G., Savinko, T., Lek, S H., Gawden-Bone, C., Watts, C., Millington, O R., Macdonald, A S., Fagerholm, S C. Loss of beta2-integrin-mediated cytoskeletal linkage reprograms dendritic cells to mature migratory phenotype. *Nature Communications*, **5**, 5355-5359 (2014).

McAlinden, N., Glass, D G., Millington, O R., Wright, A J., Accurate position tracking of optically trapped live cells. *Biomedical Optics Express*, **5**, 1026-1037 (2014).

McAlinden, N., Glass, D G., Millington, O R., & Wright, A J., Designing an experiment to measure cellular interaction forces. *Proceesings of SPIE*, **8810**, 88101L (2013).

McAlinden, N., Glass, D G Millington, O R., Wright, A J., Viability studies of optically trapped T-cells. *Proceedings of SPIE*, **8097**, 80970J (2011).

CONFERENCE POSTERS

Glass, D G., McAlinden, N., Millington, O R., Wright, A J., Assessing the viability of T-cells in a single and triple spot optical trap. Microscopy Applied to Bio-photonics, Enrico Fermi School in Varenna (2011).

Glass, D G., McAlinden, N., Kropf, P., Wright, A J., Millington, O R., Optical Tweezers: Manipulating and Quantifying cell interactions to understand the importance of L-arginine on T-cell function. British Society for Immunology Congress, Liverpool, UK (2013).

Chapter 1 - General Introduction.

Chapter 2 – Materials and Methods.

LIST OF FIGURES

CHAPTER 7.

LIST OF TABLES

LIST OF ABBREVIATIONS

ACPAs	Anti-citrullinated peptide antibodies
APC	Antigen presenting cell
BMDC	Bone marrow-derived dendritic cells
BSA	Bovine serum albumin
CCP	Cyclic citrullinated peptides
CD	Cluster of Differentiation
CFA	Complete Freunds' adjuvant
CFSE	5, 6-carboxy-succinimidyl-fluorescein-ester
cRPMI	Complete Roswell Park Memorial Institute Medium
cSMAC	Central supramolecular activation cluster
CTLA	Cytotoxic T-lymphocyte associated antigen
DC	Dendritic cell
DLN	Draining lymph node
DNA	Deoxyribonucleic acid
dSMAC	Distal supramolecular activation cluster
EDTA	Ethylenediaminetetraacetic acid
ELISA	Enzyme-linked immunosorbent assay
ERK	Extracellular signal regulated kinase
FACS	Fluorescence-activated cell sorter
FBS	Foetal bovine serum
FCS	Foetal calf serum
FITC	Fluorescein isothiocyanate
FSC	Forward scatter
GFP	Green fluorescent protein
GM-CSF	Granulocyte-macrophage colony-stimulating factor
HBSS	Hanks' buffered salt solution
HEL	Hen egg lysozyme
ICAM	Intercellular adhesion molecule
IFN	Interferon

IL	Interleukin
iNOS	Inducible nitric oxide synthase
IS	Imunological synapse
ITAM	Immunoreceptor tyrosin-based activation motif
JNK	c-jun N-terminal kinase
LFA	Lymphocyte function-associated antigen
LPS	Lipopolysaccharide
MAb	Monoclonal antibody
MACS	Magnetic assorted cell sorting
MFI	Mean fluorescence intensity
mg	Milligrams
MHC	Major histocompatibility complex
ml	Millilitres
MKP	MAP kinase phosphatase
mm	millimetre
mM	Millimolar
MTOC	Microtubule-organizing centre
N.A	Numerical Aperture
ng	Nanogram
nN	Nanonewton
OVA	Ovalbumin
PAD	Petidylarginine deiminase
PBS	Phosphate buffered saline
PE	Phycoerythrin
PI	Propidium iodide
pMHC	peptide Major histocompatibility complex
PMA	Phorbol 12-myristate 13-acetate
pN	Piconewton
pSMAC	Peripheral supramolecular activation cluster
RSA	Rat serum albumin
RPE	R-Phycoerythrin

SD	Standard deviation
SEM	Standard error mean
SSC	Side scatter
TCR	T-cell receptor
T_H	T helper cell
T_{reg}	Regulatory T-cell
µg	Microgram
%	Percentage
°C	Degree celsius

ABSTRACT

Cellular contacts are crucial in determining function, yet these complex interactions are difficult to delineate due to their dynamic nature. This complexity is evident in the antigen-specific interactions between antigen-presenting cells (APCs, such as dendritic cells, B-cells or macrophages), and $CD4^+$ T-cells. Recognition of cognate antigen by T-cells results in a rapid initiation of an intracellular signalling cascade, leading to translocation of specific transcription factors to the nucleus of the cell: factors that are important in determining the functional outcome of T-cell activation. These early interactions between T-cell and APC can determine the fate of a $CD4^+$ T-cell. Factors such as quality, quantity, duration and strength of interaction between a T-cell and APC, can influence whether an effective immune response is initiated (and which type of response) or if a state of anergy is induced. Therefore understanding more about these factors that control this decision would help in the development of therapeutics that aim to initiate protective immunity or to improve selective suppression in autoimmunity and restore immune anergy.

Within this thesis a novel approach is presented to dissect this interaction using optical tweezers. A novel optical tweezer setup is developed, providing greater control over cells and enhancing cell viability. This system is used to demonstrate quantification of the interactions between individual T cell and APC pairs, whereby the force of interaction increased from 3.3 ($\pm$ 1.4) Piconewton (pN) in steady-state to 8.5 ($\pm$ 5.7) pN upon antigen recognition. Importantly, the applicability of optical tweezers in addressing important biological questions was tested, investigating how T cell/APC interactions were altered during L-arginine deprivation, upon recognition of citrullinated antigen or in cells lacking an important signalling molecule. The approach presented here provides a novel tool for further understanding cell-cell interactions as well as demonstrating the potential for wide-ranging pharmaceutical screening applications.

Chapter 1 - General Introduction

1.1   Introduction.

The aim of this project was to develop and build an optical tweezer system that could directly trap T-cells and manipulate their contact with dendritic cells (DCs) and quantify their subsequent interactions. Therefore, my research crosses two major areas, immunology and optics for which I have implemented and used an optical tweezer system to control and manipulate T-cell and DC interaction and demonstrated for the first time that the strength of interaction can be quantified using the system. In this chapter, I first give a brief introduction to immunology, specifically concentrating on T-cell activation. I next go on and detail the controversy surrounding how T-cell receptor (TCR) triggering is initiated and detail some aspects which can determine this; peptide major histocompatibility complex (pMHC) dose; affinity of interaction; duration of interaction. Following on from this I introduce optical tweezers; the construction of optical tweezers; and highlight some of the biological applications of this tool, especially in Immunology. The final part of the intro provides a background to 3 biological applications of the optical tweezer system – namely L-arginine deficiency, citrullinated antigen and MAP kinase phosphatase II (MKP-II) and support the objectives for subsequent chapters.

1.2   Overview of immune system.

The immune system is a complex, organised and adaptable system which can respond to any insult. Foreign particles, chemicals or invading micro-organisms can be inhaled, swallowed, or invade skin and mucous membranes and cause disease. This is dependent on the pathogenicity of the organism and the integrity of the host defence [1]. The mammalian immune system is divided into two parts termed the innate and adaptive immune response, dependent on speed and specificity. The innate immune response is rapid and non-specific and plays a critical role for the first line of defence. It consists of phagocytes, macrophages, granulocytes and finally natural killer cells. However, the innate immune system is restricted and can only bind to a number of pattern-associated molecular patterns. Recognition of these by pattern recognition receptors (such as toll-like receptors) leads to the initiation of the

innate immune response [2]. The adaptive immune response on the other hand, has evolved to protect a host against a wide range of pathogens through the recognition of self and non-self-antigens presented on the surface of antigen presenting cells (APCs) such as dendritic cells, B-cells and to a lesser extent, macrophages. Whilst the innate immunity can detect the same pathogen on repeated exposure, the adaptive immune response learns and can develop memory to the same antigen, resulting in a quicker and more efficient secondary response. Critically, it is the interactions between cells of the immune system that dictate the magnitude and type of immune response generated and defining how cell-cell contact relates to effector function has become an area of intense research.

1.2.1 Adaptive immunity.

The cells of the adaptive immune response are T-cells and B-cells, collectively known as lymphocytes. There are two types of T-cells; CD4^{+} T-cells which recognise antigens presented on the surface of major histocompatibility complex (MHC) class II complex and CD8^{+} T-cells which are restricted to MHC class I associated antigens [3]. CD4^{+} T-cells play a central role in an immune response, helping to co-stimulate and activate B-cells to make antibody; regulate the function and activation of macrophages; produce cytokines to orchestrate an immune response specific to pathogenic microorganisms; help effective CD8^{+} T-cell activation. As well as having a positive effect on immune response they also play a critical role in controlling autoimmunity, development of immunological memory and supressing immune responses to minimise tissue damage [4]. On the other hand, CD8^{+} T-cells, also called cytotoxic T-cells, can directly clear viruses as well as kill virally infected cells [5].

In order to prime a naïve T-cell, cells that present antigen in the context of MHC are required and these include dendritic cells, B-cells and macrophages, collectively known as antigen presenting cells. Antigen presenting cells present antigen which they have captured during activation of the innate immune response.

Lymphocytes constitute about 20-40% of the white blood cell population and arise from common lymphoid progenitor cells within the bone marrow. B-cells develop in the marrow, whilst T-cells develop and mature in the thymus. During this stage antigen-specific receptors are generated in both cell types through random rearrangements and splicing as well as splicing of multiple deoxyribonucleic acid (DNA) segments [1]. Importantly this generates a population of over 10^8 T-cell receptors and 10^{10} antibody specificities, generating a sufficient number of cells that are adequate to detect a range of pathogens [6]. However, once rearrangements are made antigen is presented to the T-cell in the context of a peptide binding groove of a self MHC molecule. The process of positive selection ensures cells that interact too strongly or too weakly are removed. Following this, negative selection ensures that T-cells are removed that may cause autoimmunity. Thymocytes that bind too strongly with self-MHC peptides will receive an apoptotic signal leading to cell death, whilst remaining cells exit the thymus as mature naïve T-cells. Therefore, as well as generating diversity, the maturation process is also an important component of central tolerance in preventing auto-reactive T-cells that may induce autoimmunity exiting the thymus. Upon maturation, lymphocytes exit the bone-marrow or the thymus and begin to circulate around the body via the vasculature and lymphatic system, migrating through secondary lymphoid organs until they encounter their cognate antigen [3,7–9]. APCs from the innate immune response act as a bridge to the initiation of an adaptive response and take up and process a number of antigens which are then presented to T-cells [10,11]. It is these interactions that provide the antigen-specific immune response and the development of memory to that specific antigen. Following activation the lymphocytes exit the lymph nodes and spleen and migrate to the site of infection to initiate an immune response [7].

1.3 Dendritic cells.

Dendritic cells are an essential component of the immune system and are termed "professional" APCs. They can efficiently recognise and phagocytose pathogens through expressing a variety of toll-like receptors and pattern recognition receptors.

Dependent on the type of pathogens they encounter, DCs will produce a variety of cytokines and chemokines and undergo both phenotype and functional modifications [3,11–17]. For example, mature DCs resist IL-10 suppression and produce a large quantity of IL-12, which stimulates T-cell development. Furthermore, they can up-regulate surface proteins such as lymphocyte function-associated antigen 3 (LFA-3)/CD58, intercellular adhesion molecule 1 (ICAM-1)/CD54, B7-1/2/CD80 & CD86, MHC-class II − all of which promote adhesion, activation and co-stimulation of T-cells [18,19]. See also **Figure 1.1** below.

IL-10

pathogens
cytokines
T cells

IMMATURE DC

High intracellular MHCII (MIICs)
Endocytosis, including FcR
Low CD54, 58, 80, 86
Low CD40, CD25, IL-12
Low CD83, p55
Low granule antigens
Actin cables

MATURE DC

High surface MHCII
Low endocytosis and FcR
High CD54, 58, 80, 86
High CD40, CD25, IL-12
High CD83, p55
High M342, 2A1, MIDC-8 antigens
No actin cables
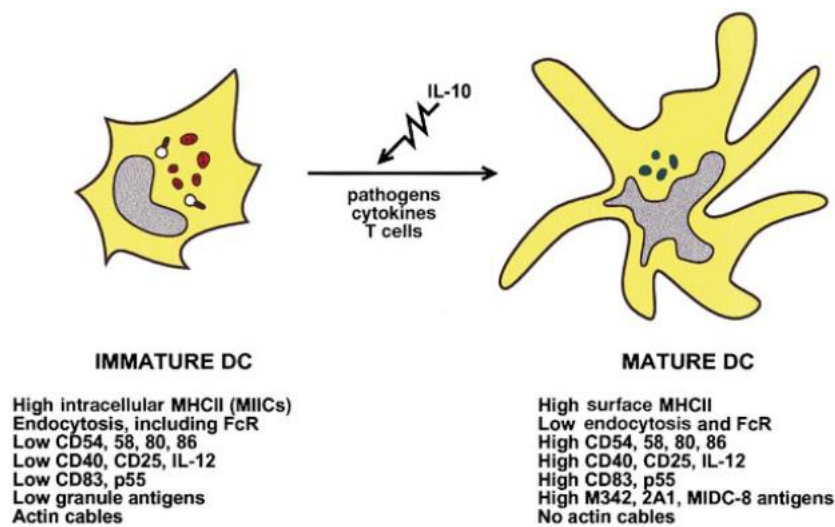
Figure 1.1: <u>**Phenotypic changes between immature and mature DCs.**</u>

Shows phenotypic changes of DCs following stimulation with pathogenic molecules, such as Lipopolysaccharide (LPS), TNF-α or the CD40-binding (from CD40L) on T-cells. IL-10 can inhibit the maturation of DCs, as indicated [11].

After internalising pathogens, DCs process antigens into peptides and load the peptides on MHC class I or class II molecules. Although other phagocytes such as neutrophils and macrophages are capable of this, it is only DCs that can initiate primary immune response and activate naïve T-cells [3,9,11,20]. Therefore, DCs lie at the crossroads between the innate immunity and adaptive immunity where they can

process and take up antigen and then present this to naïve T-cells for the initiation of an antigen-specific immune response [12].

1.4   T-cell activation.

Activation of naïve T-cells requires the interaction between a TCR, co-receptors and accessory molecules present on the T-cell that will bind with the appropriate ligands on the surface of DC. Following the interaction between a TCR and its cognate antigen presented in the peptide-binding groove of an MHC molecule, there is the initiation of TCR signalling and subsequent intracellular signalling. In order for T-cells to activate fully they require specific peptide/MHC class II complexes (signal 1) as well as co-stimulation through the interaction of CD28 on the T-cell with CD80/86 on the APC (signal 2). Upon receiving both signals, a T-cell will proliferate, differentiate and provide effector functions. However, when a T-cell only receives signal 1 without co-stimulation, then the T-cell can become anergic or die by apoptosis [3,8,21–24].

As shown in **Figure 1.2**, following ligation of the TCR with peptide-MHC complex, the Src family of protein tyrosine kinases, lymphocyte-specific tyrosine kinase Lck and Fyn are all activated, which then phosphorylate motifs known as immunoreceptor tyrosine-based activations motifs (ITAMs) present on the CD3 subunits of the TCR complex [25–29]. Subsequently, ZAP-70 is activated and recruited to the ITAMs for phosphorylation by Lck which in turn then activates several target proteins including linker of activated T-cells (LAT) and SH2-domain-containing leukocyte protein of 76 kDa (SLP-76) which allow the aggregation of signalling complexes around these proteins [30–32]. These promote the phosphorylation of phospholipase Cγ1, with the latter contributing to the production of second messengers such as inositol 1,4,5-trisphosphate (IP$_3$) and diacyglycerol (DAG), important factors in the triggering of Ca^{2+} flux, protein kinase C (PKC) and Ras activation [33].

The above are important for the activation of mitogen-activated protein kinases such as p38, extracellular signal regulated kinase (ERK) and c-jun-N-terminal kinase (JNK), which are controlled through dephosphorylation by MKP-II. This is later discussed in **Section 1.18.3**. The use of selective inhibitors on mitogen-activated protein kinases has helped to understand the complex signalling cascade following T-cell activation and activation of transcription factors NF-κB and AP-1 [34,35].

A lot of work has been carried out investigating the signalling cascade during T-cell activation. Differing signalling pathways could be initiated dependent upon the strength and interaction dynamics between T-cells and DCs. For instance, Katzman *et al*. 2010 showed tolerance was characterised by transient T-cell signalling, with parallel live cell imaging showing that interactions between T-cells and APCs were brief, which was in contrast to T-cell activation where long-term interactions with APCs was observed, followed by development of effector cells [36]. The TCR itself can sense external forces and upon the application of sufficient force can initiate signalling, which is further described in **Section 1.7**. Therefore, the implementation of a tool that could control T-cell/DC interaction, whilst quantifying the interaction force between the cells would help decipher if an altered interaction force can influence T-cell signalling.
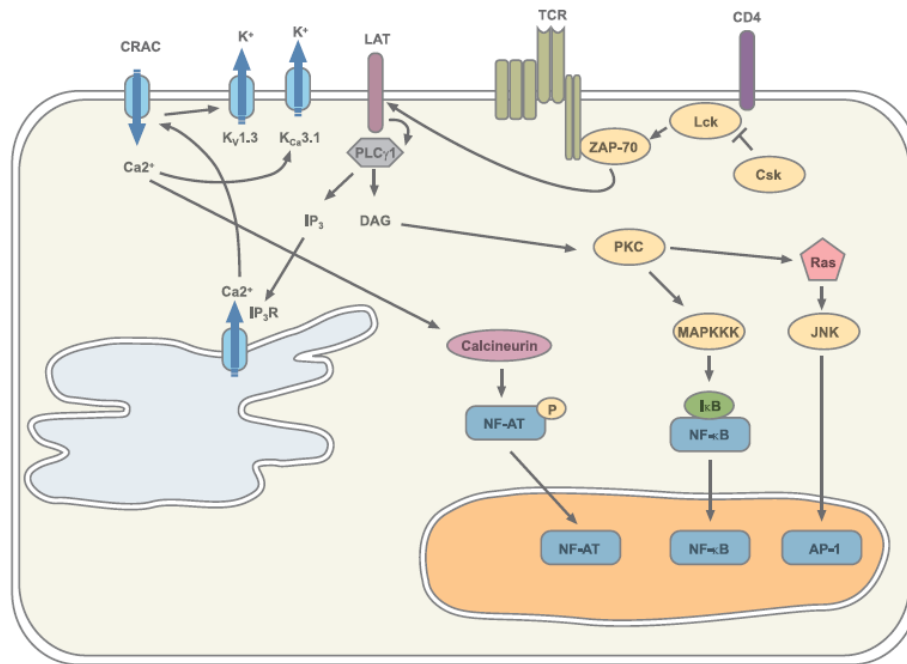
Figure 1.2: <u>**Signalling pathways in T-cell activation.**</u>

Shows the main signalling molecules and pathways in T-cell activation following ligation of TCR with p-MHC receiving signal 1 and signal 2. Taken from [25].

1.4.1 CD4$^+$ T-cell differentiation.

Upon recognition of cognate antigen bound to MHC-class II on the surface of APCs, and in the presence of co-stimulation, a naïve T-cell will activate and proliferate. The cytokine environment can influence the development of either a T_H1 or T_H2 effector response, however as highlighted in **Section 1.5** the effector function of T-cells can also be influenced by pMHC dose, affinity of TCR with pMHC and finally the interaction dynamics between T-cells and DCs.

T_H1 cells produce Interleukin 2 (IL-2), Interferon γ (IFN-γ) and TNF-α. IFN-γ promotes further T_H1 differentiation in a positive feedback loop by up-regulating IL-12 production by DCs and macrophages and by down regulating IL-4 production. T_H1 cells contribute to the cellular T_H1 immune response by enhancing intracellular

killing of phagocytosed bacteria by macrophages via the JAK1/2-STAT1 pathway [37]. T_H2 cells produce cytokines IL-4, IL-5, IL-6, IL-10, IL-13 and express the transcription factor GATA2 [38]. By stimulating B-cells and the secretion of IgG1 antibodies, T_H2 cells influence the adaptive immune response towards a humoral immune response. IL-4 stimulates T_H cells to differentiate into T_H2 cells, whilst IL-10 inhibits the production of IL-2 and IFN-γ, and IL-12 by DCs and macrophages.

T_H17 cells are another lineage of $CD4^+$ T-cells and are characterised by the RORγT expression and production of the cytokine IL-17, IL-17F and IL-6 [39]. To produce this lineage TGF-β is required and the differentiation of this lineage is distinct from T_H1 and T_H2 lineages [40,41].

Subsets of $CD4^+$ T-cells that co-express high levels of CD25 and Foxp3 also exist. Commonly known as regulatory T-cells they play a major role in regulating an immune response through suppressing immune response to self-antigens or foreign antigens [42]. They down-regulate the proliferative capacity of other populations of T-cells, both *in vitro* and *in vivo*. Both naturally occurring T_{regs} (which are generated in the thymus) and adaptive or induced (T_H3 or Tr1 respectively) T_{regs} (generated in the periphery) exist. These T_{regs} have developed from an immune response, upon recognition of low levels of antigen or antigen presented in inappropriate cytokine environment. $CD4^+$ $CD25^-$ T_H cells have been shown to up-regulate the expression of Foxp3 [43].

1.4.2   Immune tolerance.

Immune tolerance describes a state of unresponsiveness to a substance or tissue that could initiate an immune response. Whilst the primary mission of the immune system is to defend against pathogens, discriminating between self and non-self-antigens is a must as well as being able to encounter and respond to new antigens. A decision is made as to whether a productive immune response is induced or antigen-specific tolerance is induced [44,45]. This is a tightly regulated process which ensures foreign pathogens are eliminated whilst tolerance to self-antigens is maintained, preventing autoimmune disease. Tolerance in T-cells is mediated in the thymus

through negative selection where self-reactive T-cells are deleted. However, some self-reactive T-cells can escape and therefore central tolerance is incomplete. Another mechanism known as peripheral tolerance is involved and helps to ensure that tolerance is maintained to self-antigens, development antigen and food and environmental antigens. T-cells may be deleted and/or rendered inactive (anergic) upon exposure to self-antigens, due to increased expression of inhibitory receptors or negative signalling molecules. Furthermore, T_{reg} cells can also suppress the activation of antigen-specific T-cells. A comprehensive review on immune tolerance and the mechanisms involved in maintaining tolerance can be found in [46,47].

1.5   The challenges for TCR triggering.

The mechanism by which TCR-pMHC ligation initiates signalling, a process termed TCR triggering is controversial. There are a number of factors that can determine the plausibility of the type of TCR triggering model and these fall into 4 areas; sensitivity; discrimination; versatility; and structural diversity [48,49].

One of the first challenges is **sensitivity** and being able to detect very low amount of antigenic peptide-MHC on APCs. As only a few antigenic peptides may be present amongst the "noise" of other peptides, the TCR has to be sensitive enough to detect very rare signals. Indeed TCRs can be triggered by only a single antigenic peptide bound on the groove of MHC [50–52] as well as being able to detect as low as 1-10 pMHC among thousands of self-pMHC [50,51,53–55].

Another challenge is **discrimination**, whereby the TCR must be able to discriminate between self-peptide-MHC molecules and antigenic-peptide-MHC molecules. During positive selection in the thymus, only T-cells that bind with self-peptides will survive and therefore all peripheral T-cells have the ability to bind to self-pMHC, albeit with a much lower affinity threshold than foreign peptide. Indeed there is evidence to show that recognition of self-peptides is important for the migration and survival of peripheral T-cells [56–58]. Although negative selection makes sure that T-cells don't bind with high affinity to self-peptides, the affinity threshold for this is

close to the affinity threshold for antigenic-peptide-MHC recognition and therefore poses a problem for TCR triggering, especially in the detection of rare foreign peptides in amongst self-peptides [59].

Another challenge is **versatility** whereby T-cells must be versatile to respond to ligands of varying affinities in order to determine their effector function. This can be during T-cell development in the thymus, where cells must respond to both high and low affinity self-peptides[60]. Furthermore, T-cells must respond to a range of affinities for foreign peptide-MHC which can influence the activation and proliferative capacity of T-cells, as well as produce distinct signals within the T-cell, depending on the strength of interaction [48].

Whilst interactions between T-cells and APCs share common structural features, such as formation of IS and a diagonal orientation, the interface at the atomic level has great **structural diversity**. Here no common contacts or conformational changes have been identified that are related to all TCR-peptide MHC complexes (at atomic level) [48, 61–63]. Therefore, any triggering mechanism has to also take into consideration the differences in the diversity at atomic level.

Several groups have investigated how TCR signalling is triggered and from these studies three mechanisms have been proposed – aggregation of TCRs, conformational change and segregation, as reviewed in [48,64]. Precisely how T-cells can distinguish between agonist and self-ligands is not fully understood, but it is suggested that differences in the force of binding between TCR to pMHC complexes may play a role in determining different signalling patterns within the T-cell, which may influence T-cell effector function [65]. Furthermore, a number of other parameters can also influence and correlate with the robustness of T-cell activation and these are shown in **Figure 1.3** and in various studies [66–75]. These are discussed in more detail in the next few sections.
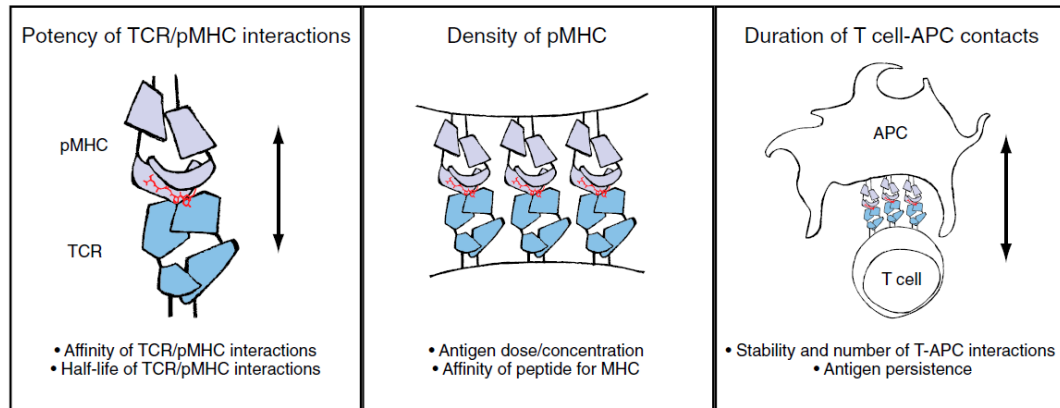
Figure 1.3 <u>**Parameters that can influence TCR stimulation and responses.**</u>

The diagram highlights parameters that can influence the strength of TCR stimulation and functional responses of T-cells. These include such things as affinity and half-life of TCR/pMHC interactions; Antigen dose and affinity of peptide for MHC and finally the duration of T-cell/APC interactions. (discussed in the next few sections). Figure is taken from [75].

1.5.1 pMHC dose and its effect on T-cell function.

pMHC dose can influence the effector function of T-cells as well as alter the interaction dynamics between T-cell/DC interactions. For example, it has been shown that higher doses of peptide are required for effective proliferation and effector function of T-cells and that this can decrease the time it takes for CD8 [+] and CD4 [+] T-cells to form stable interactions as well as the amount of clustering around DCs [76–79]. This evidence shows that when higher doses of antigen is present then there is more chance that a cognate T-cell will recognise its foreign peptide and arrest on a DC. Furthermore, it highlights the requirement for a sufficient antigen dose to be present to induce stable interactions followed by proliferation. A stable interaction is the mean time that a T-cell remains in contact with the same DC, with cell-cell contact times lasting longer than 30 minutes being defined as stable [80]. In fact as little as a 2-fold change in pMHC concentration is required to switch T-cells from resting to dividing cells [77] with a similar response being observed *in vivo* [78].

Therefore from the above literature it is clear that the pMHC dose can have an influence on not only the duration of T-cell/DC interactions but also the robustness of T-cell activation.

Interestingly there are suggestions that T-cells can accumulate "signals" with DCs. This was demonstrated by Henrickson *et al.* who showed that T-cells form stable interactions with DCs quicker when DCs are presenting both low and high doses of peptide [81]. Again this links in well with the proposal that T-cells receive "tonic" signals and perhaps suggests that T-cells accumulate signals to survey the amount of antigen present to determine the level of "threat" and perhaps achieve certain thresholds of stimulation in order for expansion phase [82]. Indeed continued antigen presence is required for continued effector and proliferative function of $CD4^+$ T-cells, whilst $CD8^+$ proliferative function is also affected; its effector function is less impacted by antigen persistence [78,82].

Moreover, antigen dose has been shown to affect the immune response *in vivo*. Studies have highlighted that antigen dose correlates with the cytotoxic function of $CD8^+$ T-cells and that in the presence of more antigen there is a larger development of memory cells, especially IFN-γ producing memory cells [77,83–85]. Interestingly the effect of antigen dose seems to be more affiliated with the earlier expansion phase of T-cells rather than the direction in which effector memory differentiation goes [86]. The differentiation of naïve $CD4^+$ T-cells can also be affected by the antigen dose. In the presence of low doses of pMHC T-cells are more likely to differentiate into IL-4 producing T-cells and it is thought this may be down to ERK activity which inhibits IL-4 production when T-cells are stimulated with higher doses of antigen [87–89].

Interestingly in the absence of inflammation, when low doses of pMHC are present then naive $CD4^+$ T-cells are pushed towards a regulatory T-cell expressing the marker Foxp3$^+$ [90,91]. Interestingly, using *in vitro* assays, Gottschalk *et al.* and Turner *et al.* showed that peptides with varying affinities but a low dose of the peptide induced only weak TCR stimulation resulting in Foxp3 induction [92,93]. This suggests

that there may be an interplay between the amount of antigen dose and the relative affinity between TCR/pMHC. However, this was contradicted *in vivo* where only peptides with high-affinity interactions induced the production of Foxp3^{+} T-cells and in the case of low affinity peptides, increasing the antigen dose had no effect on generation of Foxp3^{+} T-cells [93].

1.5.2 Affinity of TCR-pMHC and its effect on T-cell function.

The affinity of a single TCR for pMHC can be wide ranging, but may be crucial in determining the effector function of T-cells and the robustness of T-cell activation [67,94–97]. This has been investigated experimentally by altering single amino acid residues of pMHC, to generate peptides with less stimulatory effects on the TCR. Altered peptide ligands (APLs) were defined in the 1990s by Evavoid and Allen, 1991; Sloan-Lancaster *et al.,* 1993). These studies demonstrated that altered peptide could become a partial agonist, antagonist or fail to activate that specific T-cell [94,98,99]. Such altered pMHC ligands can bind to a TCR with varying affinities and can be ranked according to their ability to result in CD69 up-regulation (lowest affinity), proliferation (middle affinity) or cytokine production (highest affinity) [100].

The affinity of TCR/pMHC can alter the signalling of T-cells, specifically low affinity APLs have been shown to induce distinct and incomplete patterns of CD3 phosphorylation [99,101–103]. This perhaps may be down to low affinity APLs being insufficient to induce conformational changes in CD3 molecules, linking back to the proposal that the TCR can sense external forces [104,105]. In the context of high affinity APLs the TCR-pMHC will bind with high affinity, which could be sufficient to make conformational changes in CD3 molecules and as a result ITAMs are more accessible for phosphorylation and efficient T-cell activation [106–110]. Interestingly this links with the proposal that T-cells can bind to not only antigenic peptides (high affinity) but also to self-peptides (low affinity) [111]. The low affinity interactions may be essential for maintaining survival and migration of T-cells.

Furthermore, Ca^{2+} responses are also affected with low affinity pMHC ligands inducing a delayed increase in intracellular Ca^{2+} concentration [112,113]. Different patterns of Ca^{2+} flux have also been observed, with a sustained calcium flux present when tumour-reactive T-cells bind to high affinity pMHC whilst recognition of low affinity pMHC induces an oscillating Ca^{2+} response [114]. Interestingly Ca^{2+} has been suggested to play a role in inducing the "stop" signal and influencing the interaction dynamics between T-cells and DCs. This was demonstrated by Skokos *et al.* who investigated the interaction dynamics between T-cells and APLs with varying affinities. They found that higher affinity peptides resulted in a sharp decrease in T-cell velocity and migration, which was associated with a rapid increase in calcium flux [115]. The recruitment of molecules within the immunological synapse (IS) is also affected by varying affinities of TCR-pMHC interaction. CD3ζ recruitment is delayed when pMHC ligands with low affinity are present [116].

Interestingly T-cell signalling intermediates within T-cells activated with pMHC is slower and more sustained compared to T-cells activated with pMHC after stimulation with anti-CD3 [113,117,118]. This data suggests the importance of integrating multiple signals and suggests that T-cells prior survey the amount of antigen present before committing to proliferation and cytokine release [119]. This is further backed up by data showing that phosphorylated c-Jun is delayed when T-cells interact with weaker affinity pMHC [113]. Moreover, *in vivo* data shows that TCR stimulation with weaker affinity ligands will eventually reach maximal proliferative capacity if given enough time to make numerous cumulative interactions [92]. Collectively, the above suggests that accumulative signals and different affinities may function to influence the dynamics of T-cell/DC interaction and certainly may link and explain the 3-phase model of T-cell activation, discussed later in **Section 1.5.3**.

Whilst *in vitro* experiments have highlighted T-cells effector function following interaction with pMHCs with varying affinities [120], a recent study revealed the effector function *in vivo*. There is an expansion and generation of cytotoxic and memory T-cells in response to *Listeria* in the context to low-affinity pMHC ligands, however lower affinity ligands resulted in a quicker generation of antigen-specific T-

cells which exited the lymphoid organs quicker, compared to T-cells interacting with higher affinity pMHC ligands. Similar results were also observed in CD4$^+$ T-cells although the proliferative capacity and cytokine release was somewhat to a lesser extent than high affinity peptides [121,122].

The different responses of T-cells with varying affinities of altered peptide ligands is summarised in **Table 1.1** below.

Table 1.1: <u>**Differences in T-cell signalling dependent on ligand affinity.**</u>

pMHC ligand	Affinity	CD3ζ phosphorylation	IS formation	Ca^{2+} flux	ERK phosphorylation
Agonist	1-10 μM	+++	+++	+++	+++
Partial agonist APL		++	++	++	++
Positively selecting APL		?	+	+	+
Self-pMHC	>500 μM	?	?	-	?

The table above is adapted from [65]. Differences in ligand affinity and the relationship with various activation components of the TCR, including IS formation are shown.

Overall these studies highlight the importance of altered interaction affinities between T-cells and DCs and how these changes can affect T-cell activation. Therefore, this would be an important parameter to measure and the above highlights the importance of providing a tool that could dissect the role of affinity further in altering T-cell activation.

1.5.3 Time/duration of interaction and its effect on T-cell function.

Naïve T-cells spend around 25 hrs in a lymph node but upon being exposed to its cognate antigen this is extended to around 3-4 days [9]. Earlier *in vitro* experiments supported the idea that T-cells arrest and remain in contact with the same DC upon recognition of cognate antigen [123–125]. However, these initial findings were challenged when naïve T-cells and DCs were placed in a collagen matrix and the duration of interaction was very short lived, around 10 minutes [126].

The introduction of two-photon laser scanning microscopy was an ideal way to resolve the controversy and determine whether a long term or short term interaction with a DC was required for efficient T-cell activation. This technique has enabled researchers to image the interactions between T-cells and DCs in secondary lymphoid organs [127,128] to decipher exactly how cell-cell interactions lead to T-cell activation. However, it was soon established that there was an even higher degree of diversity in T-cell and DC interactions and ultimately this led to the exciting idea that the duration of interaction may be a potential mechanism as to how T-cell activation is regulated and tolerance is maintained [9]. The first experiment to use two-photon microscopy to study CD4$^+$ T-cell activation in explanted inguinal lymph nodes was by Cahalan *et al.* [128]. Since then interactions have been studied using intravital imaging of the inguinal and popliteal lymph nodes described in [80,129,130]. It was clear from these experiments that T-cells within lymph nodes were highly motile and interactions were very dynamic with DCs.

Specifically two photon laser scanning microscopy has revealed that T-cells make around 500-5000 interactions with DCs every hr [79,131]. Whilst a high interaction rate may increase the chances of detecting rare antigen, there are suggestions that these interactions are functionally important. For instance, upon interacting with a DC, T-cells decelerate and show some level of calcium response [132,133]. These may functionally be important in order to maintain immune homeostasis and maintain a population of mature CD4$^+$ T-cells. In fact CD4$^+$ T-cells progressively lose their

motility and ability to interact with cognate antigen bearing DCs if MHC class II molecules are deleted highlighting the importance of these interaction – even in the absence of antigen [111].

In the presence of antigen the duration of T-cell/DC interaction is controversial. They may be transient [80,134] or stable [9,133,135]. Stable interactions are important for both IFN-γ and IL-22 production by T-cells [136,137] whilst T-cells interacting transiently up-regulate CD69, accumulate activation signals over several hrs, and these interactions are more associated with tolerance induction, especially in the presence of low potency ligand [80,115,119,130,138–143]. However, during an oral immunization regime it was observed that stable T-cell/DC interaction occurs during both tolerance and priming conditions [144]. Furthermore, a study has observed the interaction dynamics following secondary exposure to antigen and found that in both tolerising and priming regimes CD4$^+$ T-cells display slower migration with multiple short contacts with DCs [145]. This adds to the complexity in understanding T-cell/DC interactions and their role in affecting functional outcome of T-cells.

T-cell/DC interactions can change over time, which may explain the controversy described above. Mempel *et al*. first demonstrated the contact dynamics between T-cells and DC over time which lead to the proposed "3 phase model" where CD8$^+$ T-cells transiently interact with DCs in the first 8 hrs in the lymph node (Phase 1) which then progressed into long stable interactions after this (Phase 2), followed by the return to transient interactions (Phase 3) [80]. This suggests that T-cells may "remember" signals with low peptide pulsed DCs and as a result are more sensitive to subsequent interactions and therefore from stable interactions quicker [77]. The transient phase 1 was also observed in Miller *et al*. and Hugues *et al*. [134,146]. However, this was contradicted by Shakhar *et al*. Wei *et al*; and Celli *et al*. where these reports did not detect an initial phase of transient interactions but instead visualised the formation of long stable interactions even at the very early stage of immunization [133,147,148]. Some of these controversies may lie in the diversity of experimental set-ups, however there is a general agreement that T-cells which receive strong signals immediately arrest on DCs surface, whereas T-cells that

receive weaker signals may go through a transient phase of interaction, followed by a stable phase of interaction. This in turn may be influenced by factors such as the pMHC dose and/or the affinity of T-cell/DC interaction.

Factors that may influence T-cell/DC contact dynamics include maturation of DCs [143,149,150], dose of antigen [79], Ca^{2+} flux [115,135], IS formation [151] and finally the presence of $CD4^+$ $CD25^+$ regulatory T-cells that inhibit the formation of long lived T-cell/DC interactions [152,153]. The "types" of interaction and the parameters that can influence this is summarised below in **Table 1.2**.

Table 1.2: <u>**Parameters that can alter T-cell/DC interaction dynamics.**</u>

	Transient interactions	Stable interactions
Duration	3-11 minutes	Several hours
T-cell behaviour during contact	Crawling	Sessile
Calcium flux	To date not detected	High intense flux, spikes of Ca^{2+}
Influenced by	- High numbers of T-$_{regs}$ - High number of antigen-specific T-cells - No DC maturation stimulus - PKCθ and CTLA-4 expression	- High dose of peptide - High affinity peptide ligands - High DC maturation - ICAM-1 adhesion, chemokine bound to DC and length of time a T-cell spends in lymph node

The table above summarises the duration of T-cell/DC interaction and the parameters that may influence whether interactions are transient or stable [9].

Overall the above highlights the complexity of **peptide dose** and **affinity** in affecting the function of T-cells. Moreover, the controversy surrounding T-cell/DC interaction dynamics and its precise role in altering T-cell function has been discussed. Longer

interactions between a T-cell/DC suggest that those cells are interacting with a greater force than those interacting transiently. However, despite multi-photon microscopy proving invaluable in understanding the dynamics of T-cell and DC interaction, this tool has been limited by the ability to measure parameters such as migration, velocity and level of clustering. Given the clear role of affinity in affecting T-cell function and perhaps longer durations suggesting a greater interaction force, it would therefore be important to dissect T-cell/DC interaction further by being able to develop a tool that could determine how strong the cells are interacting. This would help to understand the role of force and its effect on T-cell function.

1.6   Formation of immunological synapse.

In 1998 Kupfer and colleagues demonstrated a specialised structure formed at the interface between T-cells and APCs. The structure was a doughnut like structure that consisted of a central supramolecular activation cluster containing protein kinase Cθ and Lck and a peripheral supramolecular cluster containing lymphocyte function-associated antigen-1 and talin [154,155]. However, it was later shown that a "multifocal IS" containing multiple clusters of TCRs forms at the interfaces between T-cells and DCs [156]. A number of reviews are available that describe the events and components of the IS [157–161].

The formation of IS micro clusters, which can be motile or stationary, has been observed and can affect the interaction dynamics between a T-cell and APC – especially the motility of a T-cell interacting with a APC [162,163]. Furthermore, as discussed later in **Section 1.5.3**, *in vivo* imaging has suggested that T-cell and DC interactions are very dynamic and therefore the formation of an IS may influence this. Moreover, IS formation may have a role in determining the interaction forces between T-cells and DCs, and as a result measuring how strong T-cells interact with DCs could be linked to those studies that observe different T-cell/DC interaction dynamics (**discussed in Section 1.7**).

A model by Dustin and colleagues (2005) explained how IS can affect T-cell/DC interactions. They proposed the formation of a hemi-synapse *in vivo* and *in vitro* [164]. **Figure 1.4** indicates the difference between a IS and a hemi-synapse (HS).
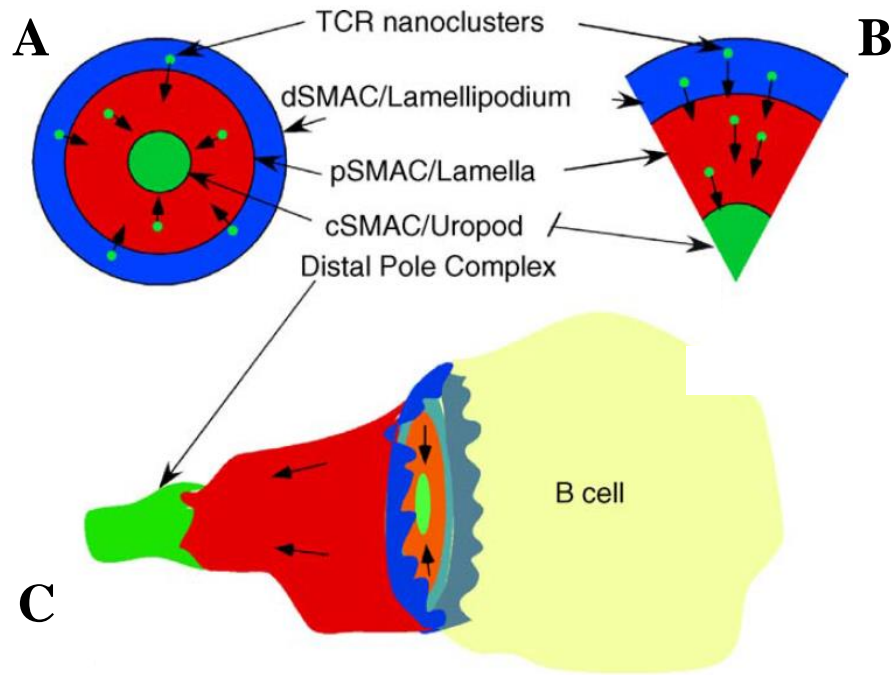
Figure 1.4:   <u>**Model of Immunological synapse and hemi-synapse.**</u>

Figure shows green cSMAC (composed of protein kinase C, CD2, CD4, CD8, CD28, Lck and Fyn), red pSMAC (composed of LFA-1 and talin) and blue dSMAC (enriched with CD43 and CD45), as indicated.   Green TCR nanoclusters are indicated with arrows indicating direction of nanocluster movement. **A:** Shows surface view of IS which mediates sustained contact and signalling as defined by Kupfer [154] [165]. **B:** Shows view of hemi-synapse formed by a migrating T-cell on an antigen presenting APC as proposed by Michael Dustin (2005) [164,166]. In migrating cells the leading edge is the lamellipodium, followed by the lamella and finally the trailing uropod. **C:** Shows a 3D representation of the IS formed when an antigen-specific T-cell is in contact with a B-cell.

This hemi-synapse model proposes that as T-cells crawl over the surface of DCs, the leading edge of the lamellipodia signals, as it is rich in TCR nanoclusters. The main difference between a IS and HS is that when T-cells form an IS they spend longer interacting with a DC, whilst when forming a HS, the T-cell can serially interact with a number of DCs. Importantly, this model suggest a way that solves the controversy in T-cell/DC interaction dynamics and suggests that with stable interactions a IS forms, whilst in transient interactions a HS forms [126]. Interestingly this links in well with the proposal that the TCR can mechanosense as discussed later in **Section 1.7**. That particular section describes a proposed model whereby a TCR can mechanosense. As a T-cell migrates across an APC, a pulling force would exert on the TCR-pMHC complex. If a cognate antigen is present then the pulling force would be sufficient to trigger the TCR and induce a conformational change in the CD3 chain to allow the ITAMs to be phosphorylated. Importantly, if this model is right then it highlights the importance of TCR scanning on APC surface. Whilst *in vitro* T-cells would be unlikely to crawl over the surface of the DC, the above highlights the importance of building a tool whereby T-cells are allowed to freely scan the surface of DCs.

In 2009 a study by Hosseini *et al*. manipulated T-cell/DC interaction and revealed that the formation of the IS correlates with the interaction forces between T-cells and DC, as measured by AFM [167]. However, a limitation in using AFM is that a T-cell is not able to freely scan the surface of an APC. This is due to one cell type being fixed to surface of the slide and the other being fixed to the AFM cantilever. Therefore, this might not be an appropriate tool to manipulate T-cell/DC interaction and quantify subsequent interaction strength.

As the IS may influence how long a T-cell stays in contact with a DC, which in turn can determine the interaction forces between the cells, it would be important to decipher this interaction using an appropriate tool/method. The importance of this could be that differences in the interaction forces may drive T-cells to become tolerant or influence the initiation of an antigen-specific immune response.

1.7 The role of force in initiating TCR stimulation.

Forces are increasingly being recognised to play a vital role in initiating many biological events and have been described in epithelial, endothelial and muscle cells [168]. This also holds true for T-cells as well where the application of external forces is enough to initiate TCR signalling. There are suggestions that the TCR can mechanosense and subsequently sense external forces and upon the application of sufficient force the TCR will initiate signalling [105].

This was shown in a series of papers where application of sufficient mechanical forces could initiate TCR signalling [169–172]. Zhen-Yu *et al*. (2001) suggested that following ligand binding the CD3γ chain may mediate a piston-like movement of the TCR complex within the cell. This movement would be provided by external forces following cell-cell interaction [108]. Furthermore, another model known as the receptor deformation model was suggested by Zhengyu *et al*. (2008); Zhengyu & Finkel (2009); and Kim *et al*. (2009). This model proposed that as T-cells/APC interactions are highly dynamic within the lymphoid organs, then the binding of a TCR with its specific antigen doesn't trigger TCR signalling but instead the triggering stems from a pulling force generated by the migrating T-cell's cytoskeleton. Upon weak interactions when specific antigen is not present or upon the recognition of self-peptides then the pulling force is not sufficient to trigger TCR signalling. However, upon recognition of cognate antigen the higher interaction strength would result in a stronger pulling force, inducing a conformational change to trigger signalling and make ITAMs of CD3 complex more accessible for phosphorylation by Lck kinases [104,105,173].

Furthermore, TCR can mechanosense and this was demonstrated by Chen Li *et al*. who compared the calcium response of T-cells bound to artificial APCs which were designed not to activate T-cells. Under static conditions there was only a background level of calcium flux within T-cells. In contrast they found that upon application of a shear flow and a pulling force on the T-cell/APC complex by a

micropipette there was a strong calcium flux [172]. Further evidence for TCR acting as a mechanosensor was highlighted in Judokusumo *et al.* Using a mixture of anti-CD3 and anti-CD28 to stimulate naïve CD4$^+$ T-cells in polyacramide gels of varying elastic modulus, this study revealed that there was stronger activation as measured through the secretion of IL-2 with increasing polyacramide thickness/density, [170].

It is clear from these studies that the TCR can initiate signalling upon sufficient mechanical forces with both pulling and pushing forces. Hence, to initiate TCR signalling may require an interaction strength between T-cell and APC to be above a specific threshold [174]. Indeed this has been demonstrated experimentally using an electromagnetic tip to pull on magnetic particles that were designed to engage TCR or CD3 receptors. It revealed that T-cell activation (as measured by calcium flux intensity) was achieved with forces ranging from 200 pN to 600 pN and that the calcium flux appeared only upon application of force and not in non-specific binding situations [175]. The evidence above supports the proposed model of TCR signalling where mechanical forces play a role in the deciphering and transduction of the message contained in the TCR/CD3-pMHC interaction [175].

It is clear that mechanical force may play a key role in initiating TCR signalling and forces between T-cell/APC interface may determine the functional outcome of T-cell activation. Therefore it would be important to probe these interactions and quantify their cell-cell interaction strength. Techniques such as single cell force spectroscopy and atomic force microscopy are useful tools as they can measure forces ranging from 5 pN to tens of nN [176]. Indeed single cell force spectroscopy and atomic force microscopy has been used to demonstrate that binding affinities between T-cells and DC increase in the presence of antigenic peptides and that higher binding affinities resulted in a more efficient T-cell activation response, as measured by IL-2 secretion and calcium mobilisation [167,169]. A more recent technique has used what is called a bio membrane force probe which was pioneered by E.Evans in the late 1990s. This technique allows the analysis of single molecular bond strengths at a range of 0.1 pN to 1 nN and again has highlighted the dynamic nature of mechanical forces within T-cells [171,174,177].

Despite these approaches being useful in understanding the molecular interactions involved in synapse formation and the dynamics of calcium flux, it is unclear what affect the mechanical manipulation by the AFM tip or micropipette has on normal cell function. Moreover, as it has been suggested that the initiation of TCR signalling may come from the actin skeleton, as proposed in the receptor deformation model [104,105], it is important to allow a T-cell to freely scan the surface of a DC to maintain dynamic receptor scanning during such studies. In addition, experimentally investigating T-cell/DC interactions at a single cell level perhaps may reveal novel insights that could be missed at a population level. Some of the tools that are available to quantify forces of cell-cell interaction are described below.

There are a number of approaches to control cell interaction whilst quantifying forces. A review of these is available in [178–181] with some of the major ones and the working principles of each technology summarised in **Table 1.3**.

Table 1.3: <u>Comparison of tools that can quantify cell interaction forces.</u>

	Working mechanism	Range of forces that can be measured	Limitations
Atomic force microscopy	Deformation of cantilever tip with attached cell is used to estimate forces	~ 5 – 10,000 pN	Large minimal force measurement and Large stiffness probe
Magnetic tweezers	Magnetized ferromagnetic beads are moved by weaker directional magnetic fields	2 pN – 50 pN	Not able to manipulate
Optical tweezers	Particles with high refractive index are moved by laser beam	0.1 – 100 pN	Sample heating and photo-damage

The above table compares the tools that can be used to manipulate cell-cell interaction and the range of forces that can be measured, including the limitations of each tool. Table adapted and taken from [179] and [181].

Atomic force microscopy involves using a sharp tip which is attached to a flexible cantilever. A cell is attached to the tip and the amount of bend and relative deformation of the cantilever can be used to estimate forces of interaction between two cells, with the other cell being left to adhere to surface of sample slide. Whilst this technique has successfully been used to probe the viscoelastic properties of platelets [182,183] one of the major limitations is that the tip can cause cell damage [179]. Moreover, many different shapes of tips are used and as the shape of each tip determines the overall force deformation curve, having to constantly re-calibrate the AFM would not be ideal if experiments were needed to be replicated or repeated [179]. Moreover, although the amount the cell is stretched or deformed by the tip can be

controlled by gently bringing the tip into contact with a cell, it is often difficult to view the structural deformation of the cell and therefore the user has no way of determining how much the cell is deformed and if any morphological changes associated with necrosis of the cell is visible [179]. Although not mentioned in the table, micropipette aspiration solves the problem of being able to visualise the deformation of the cell membrane as the cell is fixed due to the suction of the micropipette. This technique was used by Husson *et al.* to determine the mechanical interaction between a T-cell and APC [171]. However, one limitation is that the technique can limit the ability of T-cells to freely scan the surface of DCs. As highlighted in **Section 1.7** a TCR may initiate signalling following sufficient binding force as the T-cells migrate across surface of DCs (termed "receptor deformation model"). Therefore, this tool may not be ideal for addressing the main aim of this thesis. Magnetic tweezers rely on using beads that have been exposed to magnetizing coils to induce a magnetic dipole. However, as we wanted as true a representation of cell-cell interaction as possible, it was important to minimise the use of beads and also there would be no idea of what effect the magnetic coils would have on cell viability [179]. Furthermore, the beads have to be re-magnetised after a period of time and as a result experiments lasting more than 1 hr may not be feasible, therefore again this tool may not be ideal. Moreover, the above techniques also use artificial beads and if these are coated with anti-CD3 to activate T-cells, it may not be a true representation of T-cell activation.

1.8 Understanding the role of interaction forces – manipulation?

To further understand how differences in the interactions between T cells and DCs may influence the functional outcome of the immune response, a strategy capable of experimentally manipulating cell contact is necessary. This was elegantly conducted by Celli *et al.* who demonstrated that whilst T-cells formed antigen-specific stable interactions with DCs following immunisation, injecting a monoclonal antibody directed against MHC class II molecules resulted in these stable interactions

dissociating. This meant that by varying the time between peptide injection and anti-MHC class II antibody injection it was possible to control the duration of interaction between T-cells and DC. From this study it was established that a 2 hr interaction with a DC was not sufficient to drive T-cell proliferation and that a minimum duration of 6 hrs was required, with longer durations of 24 hrs showing a more robust clonal expansion. Cytokine production was detected only when stimulation was extended over several days, indicating that both a long term interaction is required for effective T-cell activation and that T-cells are able to receive signals during prolonged interactions with DCs [148].

An alternative approach that has been used to manipulate single cells is optical tweezers. Although the major limitations with this technique are photo-induced damage and the upper limits of the amount of force that can be measured, these can be addressed in part by using an appropriate wavelength of light and higher laser powers [184,185]. Recently optical tweezers have been used to manipulate cells directly and to study the interaction forces between erythrocytes [186] and human osteoblast cells and various implant surfaces [187]. Therefore, optical tweezers may provide the capacity to directly manipulate the contact between T-cells and DCs as well as to quantify the interaction forces between these cells, providing a unique approach to address novel questions about how such interactions are altered by modified peptide antigen, by the local environment or by alterations in the signalling capacity of T cells.

1.9 Aim.

As described above, several studies have shown that T-cell and DC interaction is very dynamic. This has led to the hypothesis that either the duration [9,36,74,76,77,80,126,147–149,188–190] or strength [104,169–172,175,191–194] of contact (or a combination) determines T-cell activation and effector function or whether tolerance is induced. Optical tweezers represent a useful tool that may be able to explore this experimentally. Whilst the tool has previously been used to optically manipulate T-

cells, to date no-one has successfully controlled the interaction between T-cells and DCs, whilst quantifying the interaction force between the cell pair.

Therefore, the main aim of this thesis was to develop and build an optical tweezer system that could directly trap T-cells to manipulate their contact with DCs and quantify their subsequent interactions.

1.10 Optical tweezers.

1.10.1 History of optical tweezers.

The year 2014 marks the 54th anniversary of the laser and one area in which the laser has played a significant role in biology is its use in optical tweezer systems. The basic physics of radiation pressure was first observed by the German astronomer Johannes Kepler in the 17th century who proposed that due to the pressure of light comet tails always pointed away from the sun [195]. In 1873 James Clerk Maxwell, a Scottish theoretical physicist, showed optical forces can be exerted by light. However, due to radiation pressure being very feeble this was not demonstrated experimentally until the advent of lasers in the 1960s, which enabled studies to be conducted on radiation pressure using a high intensity coherent light source [196]. Arthur Ashkin pioneered the field of optical tweezers and published a number of papers with colleagues demonstrating the work up and development of a single-beam optical trap [197–200]. A schematic diagram of the experiment conducted by Ashkin *et al*. in 1986 and the first single-beam optical trap is shown in **Figure 1.5**.
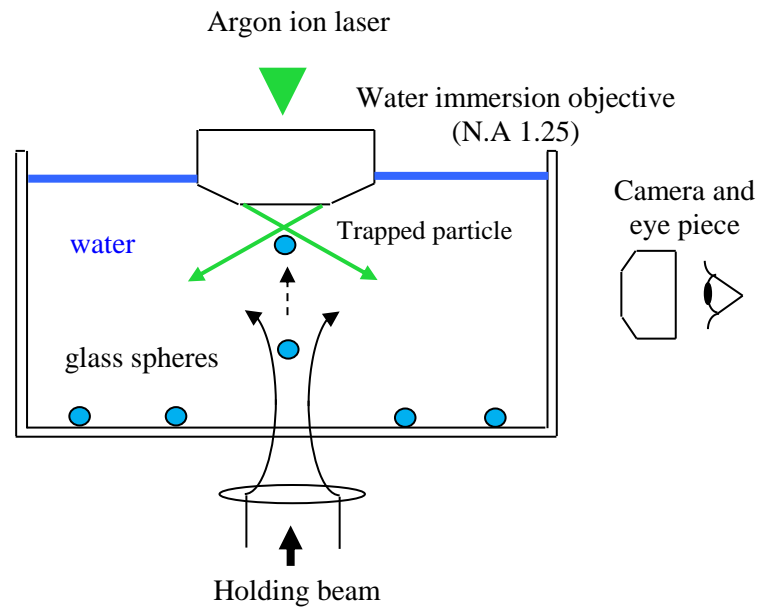
Figure 1.5: <u>**Schematic diagram of first single beam optical trap.**</u>

A diagram of the first three dimensional optical trap built by Arthur Ashkin. A holding beam was used to lift the particles off the bottom of the sample cell using radiation pressure. A highly focused argon laser beam was then used to trap the particles in 3D. Adapted from Ashkin *et al*. (1986) [197]

The single-beam gradient trap is now an established method for the manipulation of micron-sized objects and is having a major impact in many fields of biology. There has been a recent push to use optical tweezers to measure and assess forces in biological systems, for example looking at the weak forces involved in bacterial and cell adhesion [201–203], protein folding [204–210] and the stretching and un-winding of DNA [211,212].

1.11 The key forces in optical tweezers.

The combination of a high numerical aperture (N.A) lens with a laser beam causes a particle to be trapped in three dimensions. A particle within an optical trap experiences three main forces: scattering force, axial force and the transverse force.

A schematic diagram showing the directions of the three forces involved in trapping a particle is shown in **Figure 1.6.**
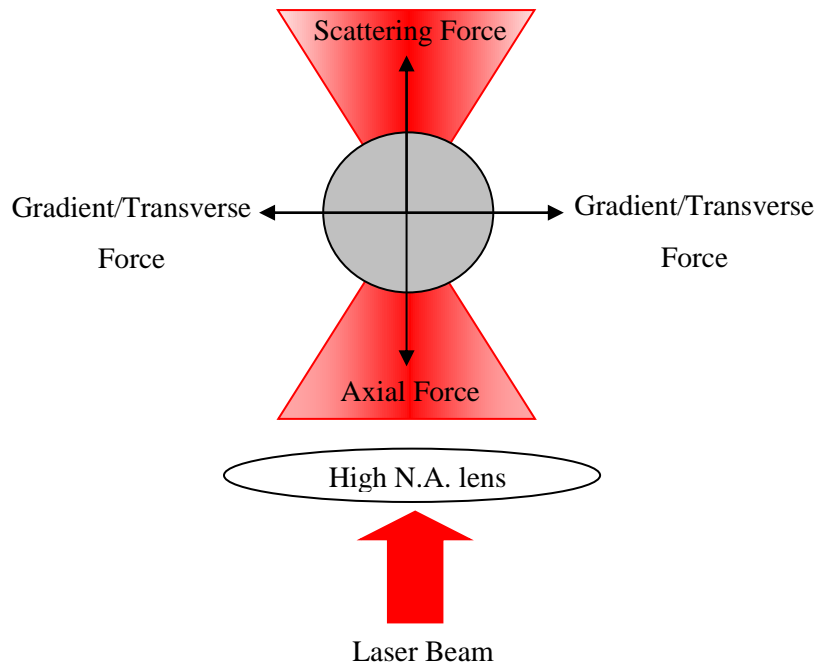
Figure 1.6: <u>Schematic diagram showing the three forces in optical tweezers.</u>

Schematic diagram shows the scattering force, gradient force and the axial force.

The scattering force acts in the direction of beam propagation, is proportional to the intensity, due to radiation pressure and often is thought of as a photon "fire hose". Light coming from one direction and acting on the particle is scattered in a variety of directions while some of the light is absorbed resulting in a net momentum transfer to the particle from the incident light [185,213]. The gradient force, is due to the intensity gradient of the light. When a particle has a higher refractive index than its surrounding medium the particle will be pulled to the higher intensity region of the beam. In order to achieve stable trapping in three dimensions the axial gradient force must equal the scattering force, which is pushing the particle away from the focal

region. The axial gradient force pulls the particle towards the focal region of the beam and to overcome the scattering force a steep gradient is required. A laser beam that is sharply focused using an objective with high N.A achieves this. The axial equilibrium position of a trapped particle is situated slightly beyond the focal point due to the balance between the scattering and gradient forces [213,214].

The light-particle interaction can be determined mathematically. However, the way it is treated depends on the ratio between the trapped particle's radius and the wavelength of the laser [214]. The ray optics regime is valid for particles which are larger than the wavelength of light whilst the Rayleigh regime is valid for particles whose size is smaller than the wavelength of light. Ashkin derived a theory based on the ray optics approximation [215], based around reflection and refraction of light. As T cells fall into the ray optics regime, the next section describes this in more detail, concentrating on the interaction between a dielectric sphere with a refractive index greater than the medium it is suspended in and a Gaussian laser beam.

1.11.1 Gradient/transverse force.

Ray optics is a way to describe the trapping forces for particles in the Mie regime, where particle size is larger than the wavelength of the laser beam [197,216]. This relationship holds true for T-cells trapped and described later in **Chapter 3**.

Shown in **Figure 1.7** it is clear that a particle is attracted to the more intense region of a Gaussian profile laser beam. Consider two rays, ray *a* (more intense) and ray *b* (less intense), that strike the dielectric particle symmetrically. The two rays are refracted due to the particle's higher refractive index relative to the surrounding medium, leading to the forces $\underline{F}_a$ and $\underline{F}_b$ in the opposite direction of the momentum change from ray a and ray b. The bottom of the figure illustrates the change in momentum (ΔT), of rays *a* and *b* due to refraction of light. Both forces contribute to the force in the direction of propagation, however as ray *a* is more intense than ray *b*, $\underline{F}_a$ is greater than that of $\underline{F}_b$ and therefore $\underline{F}_a$ also creates a force that pulls the particle towards the beam axis (the region of higher intensity and in the direction of the higher intensity gradient).

The above concerns a particle of refractive index greater than that of the surrounding medium, however with a particle with a lower refractive index than that of the surrounding medium (for example, an air bubble in water) $\underline{F}_a$ is less than that of $\underline{F}_b$ and as a result the particle is pushed away from the intense regions of the beam [217].

The transverse force or gradient force, as it is sometimes referred to, explains why Ashkin observed particles aligning with the beam axis and propelling forward in the direction of light propagation [200] It is simply a result of the intensity gradient of the laser beam.

A

Momentum Changes

B

^{a}IN

^{a}OUT ΔT^a
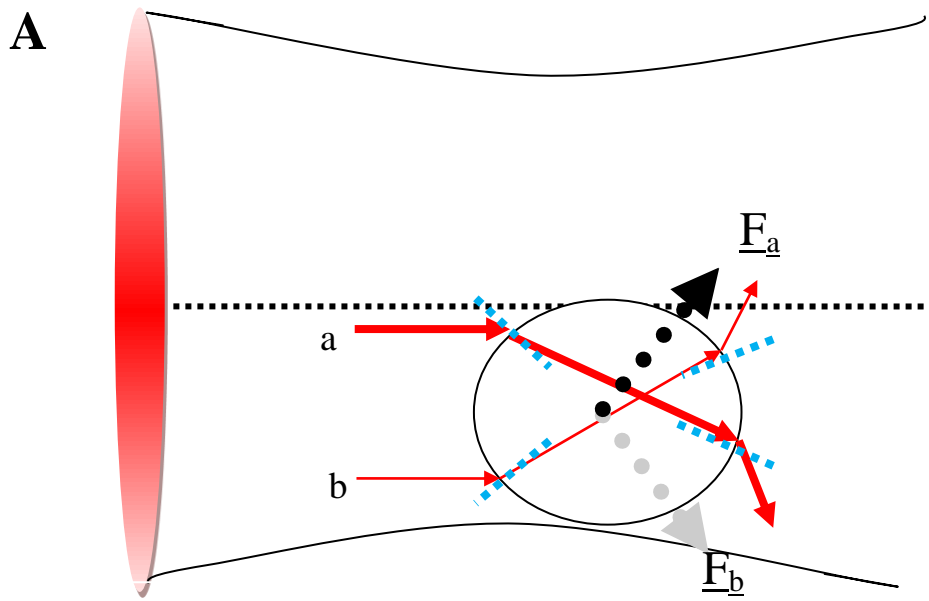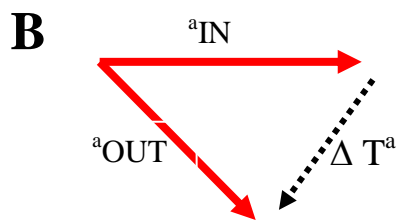
Momentum change for ray a
(more intense)

C

^{b}OUT ΔT^b

^{b}IN
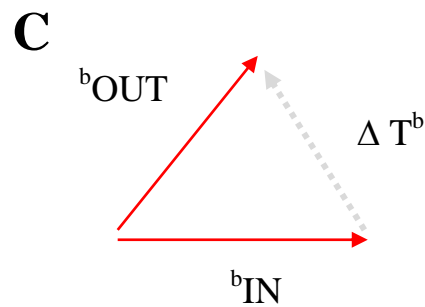
Momentum change for ray b
(less intense)

Figure 1.7:   Gradient force.

A schematic diagram of a trapped particle with a refractive index greater than
the surrounding medium optically trapped with a Gaussian intensity profile. **A:**
Shows the forces attributed to the gradient force as well as the momentum
changes of **B:** higher intensity ray and **C:** lower intensity ray. Adapted from
[218].

1.11.2 Axial force.

The transverse trapping force arises from the intensity profile of a laser beam and draws a particle towards the most intense regions of a beam. However, this force alone will not trap a particle in three dimensions; an additional axial force is required to counter-balance the scattering force and create a stable trap in three dimensions. **Figure 1.8** shows a Gaussian mode laser beam, tightly focussed onto a dielectric sphere using a high N.A lens. Since a light beam carries a linear momentum of h/λ per photon, the refraction of light by transparent objects results in a change in photon momentum and a resulting reaction force that acts on the object (ultimately the change in direction, results in a change in momentum resulting in a force equal to but opposite in direction). Considering two rays, *a* and *b*, the resulting forces can be seen from the diagram as $\underline{F}_a$ and $\underline{F}_b$, and as you can see the forces are opposite in direction to the change in momentum of the light $\underline{\Delta T}_a$ and $\underline{\Delta T}_b$. The resultant force $\underline{F}$ pulls the particle towards the focus of the laser beam.

In order to trap a particle in 3-dimensions, the axial force caused by the convergent rays must balance the strong scattering force of the laser beam. This is achieved using a high N.A objective. The combination of this and the intensity profile of the laser beam will trap a particle in both the transverse and axial directions, holding it in three dimensions. At this point the scattering and axial forces are in equilibrium and, for an inverted microscope, the particle will normally sit just above the focus of the laser beam [218].
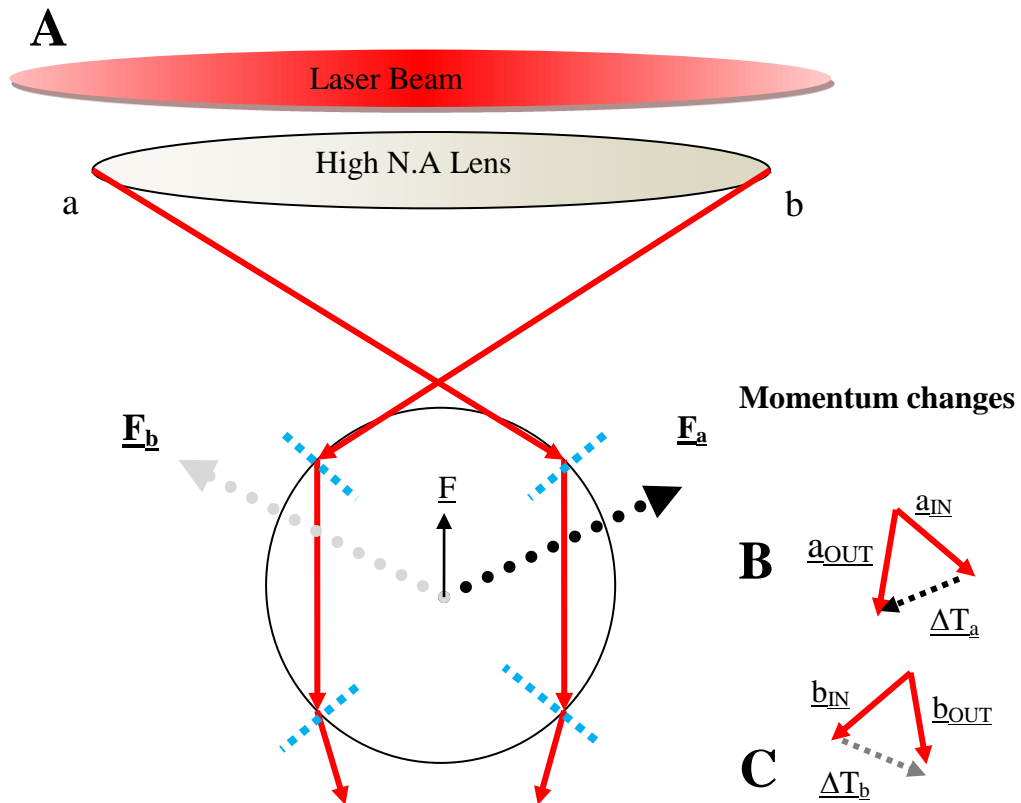
Figure 1.8: <u>**Axial trapping force.**</u>

A schematic diagram illustrating the origin of the axial trapping force, including momentum changes. **A:** Shows the forces attributed to the axial force as well as the momentum changes of **B:** higher intensity ray and **C:** lower intensity ray Adapted from [218].

1.12   Construction of optical tweezer system.

The implementation of an optical tweezer system is relatively straightforward. There are eight main components that are used to construct an optical tweezer system. A laser source; objective lens; sample of interest; illumination source; steering mirrors; dichroic mirror; camera and finally any specialist equipment such as a SLM in between the laser and objective lens that may be required. An optical tweezer system is usually built around a commercial microscope with the laser entering the microscope from below or above depending on if it's an up-right or inverted

microscope. However, for biological applications it is better to build a system around an inverted microscope where biologists can access samples. Extensive reviews are available that outline the components of optical tweezers and why each one is necessary [185,213,218–223]. A detailed description of the components used in my optical tweezer set-up can be seen later in **Chapter 3**

1.13 Measuring forces with optical tweezers.

1.13.1 Position detection.

Sensitive and accurate position measurements of the trapped particle are key to the majority of methods for determining the strength of the trapping force. It is possible to trap irregularly shaped particles, such as cells. However, due to their irregular shape and varying local refractive indices it makes it difficult to accurately track the position of the cell over time [185]. Many studies have relied on attaching beads to act as handles or use beads alone to calibrate an optical tweezer system prior to carrying out force measurements. Displacements of trapped particles are commonly measured using a quadrant photo-diode or fast camera with an accuracy in tens nanometers [185,214,224]. By calibrating the size of a pixel, then digitally processing the signal acquired from the camera and using a centroid fitting algorithm such as the centre of mass tracking, it is possible to determine the position of the centroid of a trapped particle to within 5nm or better [225,226]. There are a number of studies that have used video to track the position of a trapped particle over time; however this method can be limited to acquisition rates of roughly 25-120 Hz [227,228]. To improve the temporal resolution, high speed charge-coupled device (CCD) cameras and complementary metal-oxide semiconductor (CMOS) cameras have been used which improved the frame rate to a few KHz and is only limited by the computers central processing unit (CPU) power and memory [224,229].

1.13.2 Trap stiffness.

For small displacements from equilibrium position, optical tweezers behave like a Hookean spring i.e. the displacements of a trapped particles from the trap centre is

opposed by a restoring force which is proportional to the displacement, $F = -\kappa\Delta x$ Thus, if a known force is applied, and positional variance of a trapped particle $\langle x^2 \rangle$ is known, then the trapping stiffness k can be quantified

One method of determining trap stiffness is the Equipartition theorem where the potential energy stored in an optical trap is equated to the thermal energy of the system. The trap stiffness of an optical trapping system can then be determined using: with stiffness k:

Equation 1.1

$$\frac{1}{2}k_B T = \frac{1}{2}k\langle x^2 \rangle$$

Where k_B is Boltzmann's constant, T is the absolute temperature and x the displacement of the particle from its trapped equilibrium position. Therefore, if one can measure the position of a trapped particle over time and determine the variance of its position then the stiffness of the optical trap can be calculated. An advantage of this method is that it is independent of shape and size of the trapped particle as well as viscosity of the medium surrounding the trapped object [185,213,222,230,231].

The key to this method is accurate and reliable position sensing and particle tracking leading to the determination of the time-dependent variance in the particle position $\langle x^2 \rangle$. Any added noise or drift throughout the measurement could result in a larger variance in x^2 resulting in a decreased estimation of trap stiffness [185]. By lowering the acquisition time this can be improved. Moreover, the centre of mass tracking algorithm used to determine the position over time works best on a dark background, and for this reason before starting the measurement a threshold is applied to enhance the contrast between background and the trapped particle of interest to obtain a suitable image to track. Doing this for a bead is relatively easy but it may prove difficult to threshold properly for a cell due to varying refractive indices associated with intracellular structures such as the nucleus and light-scattering organelles..

Another method for calibrating the stiffness of an optical trap is the viscous drag method [232–235]. This approach subjects a trapped particle to a viscous drag which is proportional to the velocity of the flow and can be achieved by either moving the fluid around the trapped particle or by moving the trapped particle itself. By moving the stage at velocity v, the force is calculated using Stokes Law, assuming a low Reynolds number fluid, $(F) = -6\pi\eta r \boldsymbol{v}$ where η is the viscosity of surrounding medium, $\boldsymbol{v}$ the stage velocity and r the radius of the trapped particle. The velocity of the sample stage is typically increased until the object is released from the trap and at the point of release the trapping force is said to be equal to the viscous drag force. However, factors that can affect this measurement include particle size and viscosity of trapping medium, which might not always be clear [185]. Furthermore, if a particle is trapped close to the proximity of a wall then Faxen's Law needs to be included to account for any wall effects. Although a study by Andersson *et al*. showed that the additional drags by walls can be neglected at distances over 5 μm for a 2.8 μm sized bead, which corresponds to just over 3 times the beads radius [187]. However, caution has to be taken when trapping deeper into a solution as this can lead to spherical aberrations which degrade the quality of optical trap [185]. This has been demonstrated in several papers where the efficiency of trapping is decreased with an increase in trapping depth from the cover slip [236,237].

1.14 Viability in optical tweezers.

Optical tweezers have proved to be vital in the manipulation and control of small biological objects [213]. Despite their effectiveness in bridging the gap between Biology and Physics one drawback is that the high intensity trapping light can cause damage to biological material. The trapping of small objects such as polystyrene beads can be made using a HeNe laser with relatively low power [178]. However, due to the high viscous resistance of the cytoplasm or extracellular matrix of biological materials and in order to measure forces in biological materials a high laser power is needed [178]. High laser powers increase the risk of affecting the object to be studied such as inducing stress response reactions in cells, which is often not visible through

the use of microscopic observation. As recognised by Ashkin., Dziedzic & Yamane in 1987 infrared laser wavelengths are crucial to avoid the death of biological samples [215] The absorption spectrum for water and biological material are at their lowest between 800 -1200 nm, and therefore a wavelength within this "window" would allow the trapping of cells, without compromising viability. As can be seen in **Figure 1.9** the red highlighted area shows the "therapeutic window" where there is a relative window of transparency.
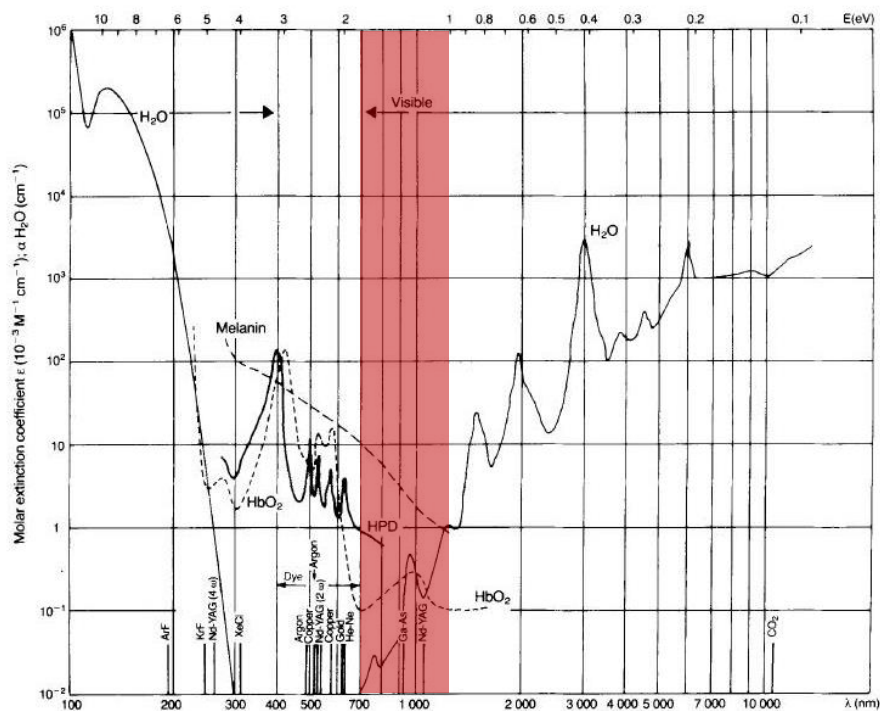
Figure 1.9: <u>**Absorption spectrum of biological materials at different wavelengths.**</u>

The red section represents the "therapeutic window" whereby the absorption of haemoglobin and water is at its lowest, adapted from [238].

The main effect associated with trapping is localised heating, which could potentially induce the stress responses in cells, causing them to become apoptotic or necrotic. Indeed previous work has investigated this and found that the temperature increases

associated with the trapping of human sperm cells, hamster ovary cells and liposomes was in the order of roughly 10°C, 11.5°C and 14.5°C, respectively [184,239,240].

Healthy cells have the ability to keep a constant pH gradient over the cell wall, while cells that are damaged are unable to do this. Therefore, by measuring pH gradient in cells exposed to a high intensity laser beam it is possible to investigate for optical damage. A study conducted in 2008 by Rasmussen *et al*. investigated the effect of laser power on bacterial cells, optically trapped for extended periods of time with a 1064 nm laser. They found that viability decreased through time and higher laser powers resulted in the degradation of cell viability at a quicker rate. Importantly, this study also revealed variance in the viability half-life of different bacterial cells trapped at the same laser power [241].

The precise mechanism of photo-damage is not fully understood, meaning that cell damage caused by a trapping laser could vary dependent on the cell. Indeed from the studies described above this can vary between different cell types. Therefore, it is necessary to conduct photo-damage or photochemical studies on individual experiments to avoid "optication", a term first coined by Ashkin describing the laser-induced death of specimens [184] and any attempts to develop optical tweezers for application to cells must also monitor cell viability using such a system.

1.15 Optical tweezers in biology.

The success of optical tweezers in biological studies is due to the picoNewton forces that they can exert on a trapped object, which is within the magnitude of forces detected in biological samples. For instance, the force require to convert DNA from a double helix to a ladder is around 50 pN and the force required to break protein-protein interactions is around 20 pN [218]. Moreover, the tool provides biologists with a non-invasive technique that can be readily built around a commercially available microscope.

Optical manipulation has made an impact across many fields of science, including chemistry [242,243], biology [203,244–247] as well as combining optical tweezers with microfluidic devices [248–252]. Specifically, within the past two decades optical tweezers have been used for cell sorting and measuring the forces in molecular motors of the cytoskeleton [253,254], protein studies and measuring the transcription and translation of DNA and RNA and their related enzymes [255–257]. It is impossible to review all of the publications that use optical tweezers to make measurements of biological materials due to the vast number of papers. However, review papers with emphasis on biological applications [218,258], photo-physics and photo-chemistry of manipulated particles [259] and optical manipulation using optical tweezers [220] are available.

1.16 Optical tweezers in immunology.

Optical tweezers have found uses in immunology before. For example, in a study by Seeger *et al*. a Natural Killer cell (NK cell) attack on a cancer cell line (Human erythroleukemia cells, K562) was observed from the first few seconds after contact with the help of optical tweezers [260]. Conventional methods rely on mixing the two types of cells together, centrifuging them at low speed and then observing the cellular responses using a fluorescence microscope. This has a limitation as the initial stages of cell activation can be missed due to the time-consuming preparation required before imaging begins. Optical tweezers enable analysis from the very first contact and thus prove useful in immunology. Using optical tweezers not only moved the NK cell to its target, but also increased the natural contact between the two cells. Importantly cell morphological changes were observed immediately after contact with NK cell. This demonstrates the importance of the very first cell-cell interactions and highlights the feasibility of optical tweezers in providing a means to observe it.

Mechanical forces between T cells and APCs may play a role in lymphocyte activation and Anvari *et al*. used optical tweezers to trap polystyrene beads coated with a specific antibody against the TCR, bringing the beads into contact with a

single T cell [261]. Following initial contact, tangential forces were applied to the bead using the optical tweezers and the formation of pseudopodia was observed. From their results it was shown that lymphocytes can generate pseudopodia at different locations within 1 minute of contact with an antibody coated bead. However, by applying tangential forces at the point of bead contact along the cell membrane they noticed that pseudopodia were formed in the direction of the bead, which eventually led to the bead being engulfed by the lymphocyte.

Furthermore, in a series of papers [124,262,263] optical tweezers were used to determine the sensitivity of T-cells to antigen and to determine the minimum number of receptors required for TCR signalling by observing calcium flux. Within these studies it was demonstrated that the leading edge of a T cell is more sensitive than the trailing edge, and that a minimum of approximately 170 anti-CD3 monoclonal-antibody (mAb) were required within the contact area between a bead and T-cell to drive calcium flux [124,262,263].

Whilst the immune synapse has been extensively studied (see above), one limitation is that the high resolution images are difficult to obtain given the dynamic nature of the cell interactions and many images that have been obtained use artificial lipid bi-layers or antibody coated glass slides [264,265]. In 2008 Oddos *et al.* imaged the distribution of TCRs at the immune synapse using optical tweezers firstly to bring the cells into contact and subsequently to orientate the cell pair for high resolution imaging [266].

In a related study, the interaction between HIV-infected and uninfected T cells has been controlled using optical tweezers. Applying cell manipulation in combination with high speed spinning disk confocal microscopy allowed the identification of a virological synapse which allows the transfer of viral material to the un-infected cells [267].

It is clear that there are a number of key studies that have used optical tweezers in areas of immunology. Whilst this has been invaluable, to date there is no current literature whereby optical tweezers are used to quantify the interaction force between

T-cells and DCs. Moreover, whilst some of these studies have directly trapped cells, no one has used optical tweezers to directly trap T-cells and manipulate their interaction with DCs. As highlighted above, recent evidence suggests that the strength and/or duration of interaction between a T-cell and DC may be important in the initiation of TCR signalling and T cell effector function. Therefore, building a system that can manipulate and control the T-cell and DC interaction whilst simultaneously quantifying the interaction strength would be advantageous and provide a useful tool for understanding more about how the strength and duration could influence T-cell function.

1.17 Objectives.

As described above (**Section 1.11**), my overall aim was to build and develop an optical tweezer system that could directly trap T-cells, manipulate their contact with DCs and quantify the subsequent interaction forces.

Therefore, my initial objectives were to

- **Build an optical tweezer system capable of manipulating cells.**
- **Develop optics to minimise cell death/maintain cell viability.**
- **Optimise approaches for quantifying interaction forces.**
- **Control individual T/DC interactions – quantify Ag-specific interaction forces at single cell level.**

The development and optimisation of such a system to fulfil these objectives is described in **Chapter 3**.

Given the significance of the T cell/DC interaction, there are many research questions for which such a system would be useful in measuring such interactions. As such, following on from these objectives, I aimed to apply optical trapping of T cells to 3 specific biological questions, each of which are outlined in brief below and the results of which are described in **Chapters 4, 5 and 6**.

1.17.1 Does L-arginine alter the interaction forces between T-cells and DCs?

L-arginine is a semi-essential amino acid and has been implicated in affecting T-cell responses [268–270] The depletion of L-arginine has been shown to impair T-cell responses to antigen during immune responses and tumour growth [271,272]. This semi essential amino acid is metabolised by the enzymes arginase and Nitric-oxide synthase (NOS) to produce either urea and L-ornithine or nitric oxide (NO) and L-citrulline [273,274]. In turn, expression of these enzymes is regulated by T_H1 and T_H2 cytokines, which competitively control arginase and NOS production in myeloid cells such as macrophages, DCs and granulocytes. For instance, classically activated macrophages, driven by T_H1-derived IFN-γ, increase inducible NOS expression and subsequent NO release, inhibiting IL-4-driven arginase production. Conversely, alternative activation is regulated by T_H2 cytokines IL-4, IL-10 and IL-13 which inhibit inducible nitric oxide synthase (iNOS) activity and induce the production of arginase. L-arginine is metabolised by arginase to L-ornithine and urea and as a result, levels of L-arginine are depleted. On the other hand, iNOS inhibits arginase activity through the generation of a NO intermediate, hydroxyl-L-arginine and therefore L-arginine levels remain the same [275–277].

This has important implications within infections, especially in *Leishmania* infection where alternatively activated macrophages produce arginase, which in turn produces polyamines enhancing parasite replication and growth [278,279]. L-arginine is essential for *Leishmania* growth and *Leishmania* promastigotes cannot be maintained in L-arginine-free media [280,281]. Furthermore, Kropf *et al*. and Munder *et al*. showed that high levels of arginase correlated with uncontrolled replication of *Leishmania* parasites and that *Leishmania* major-specific T-cells were rendered hypo-responsive when L-arginine levels were depleted [282,283].

For a number of years studies have shown that L-arginine is essential for normal T-cell proliferation and function [268,284,285]. One of the main effects of L-arginine depletion is a reduced and progressive reduction of CD3ζ-chain expression [284,286,287].

Although IL-2 production and up-regulation of IL-2 receptor alpha chain is maintained in the absence of L-arginine [288] a study by Rodriguez *et al*. showed that L-arginine depletion impairs T-cell proliferation by arresting the cells in G_0-G_1 phase of the cell cycle through the inability of T-cells to up-regulate cyclin D3 and cyclin-dependent kinase 4, two mediators which regulate the progression of the cell cycle from G_1 to the S phase [270].

Recent work has suggested that L-arginine depletion impairs synapse formation between T-cells and APCs [289]. The main affect associated with this was an increase in phosphocofilin dephosphorylation which resulted in an altered actin-polymerisation, impairing IS formation. As synapse formation correlates with interaction forces, I hypothesise that impaired T-cell activation in the absence of L-arginine correlates with an altered force of interaction between T-cells and DCs

Therefore my objectives for Chapter 4 were:

- **Determine if L-arginine deprivation affects T-cell function?**
- **Assess whether altered T-cell function in absence of L-Arg is associated with changes to interaction force between T-cell and DC.**
- **Finally, given the role that *Leishmania* plays in depleting local levels of L-arginine *in vivo*, determine if *Leishmania* alters the interaction forces between T-cells and DCs.**

1.17.2 Does citrullinated antigen alter the interaction forces between T-cells and DCs?

T-cells play a central role in the pathology of rheumatoid arthritis (RA) and are found in greater number than any other lymphocyte within the RA synovium [290–292]. RA is an autoimmune disease and involves the recognition of self-antigens by autoreactive T and B cells. Significant work has sought to identify a number of joint-specific self-antigens but interest has developed recently in how citrullinated proteins may act as RA auto-antigens [290].

The mechanism by which peptidyl arginine deiminases (PADS) catalzes the reaction in citrullination requires Calcium and has been proposed by Arita *et al.* [293]. Importantly, citrullination of self-antigens has been linked to two autoimmune diseases; Rheumatoid arthritis and Multiple Sclerosis [294–299].

1.17.2.1 Evidence for citrullination in RA.

During clinical RA, autoantibodies are used as a diagnostic marker of the disease. Interestingly antibodies to self-antigens such as anti-keratin, anti-Sa and have been found in patients with RA and these were shown to recognise citrullinated proteins [300–303]. As such, anti citrullinated peptide antibodies (ACPAs) are a clinical marker of RA and can be a direct indicator of the severity and prognosis of the disease [304–308]. Specifically anti-citrullinated cyclic peptide (CCP) antibodies are higher in arthritic synovium which could indicate a local immune response [309–311]. Using a collagen induced arthritis model, Kuhn *et al.* showed that monoclonal antibodies that could bind to citrullinated fibrinogen induced more severe disease. Further to this there was an increased level of citrullinated protein in the lymph nodes and that the presentation of citrullinated antigen within the lymph was generating the antibodies [312].

Importantly the presence of such ACPAs requires a loss of tolerance within a $CD4^+$ T-cell population implicating an important role for T-cell function [313]. Evidence suggests that citrullination of peptides may increase their affinity with MHC binding groove. In a study by Hill *et al.* peptides derived from vimentin that contained citrullinated substitutions within the P4 pocket of MHC bound with a much higher affinity than vimentin peptides that did not contain a citrullinated residue. Immunisation with citrullinated peptides in complete Freunds adjuvant induced a robust T-cell response that was not observed following immunisation with the unmodified peptide, suggesting that the citrullinated vimentin peptide was able to breach self-tolerance [314]. Similarly, immunisation with citrullinated fibrinogen induced an arthritis-like disease in HLA-DR4 mice whereas unmodified fibrinogen did not [315]. Importantly, these studies identified a population of T-cells that reacted

to citrullinated peptides, supporting the idea that there is a lack of tolerance to citrullinated peptides. However, a major stipulation to this conclusion is that the structure of protein antigen can also be changed, which is sufficient to breach tolerance [316]. Therefore, citrullination may denature protein and when presented on surface of APC there is altered interaction, especially with T-cells that have escaped negative selection [317].

Interestingly, autophagy has been linked to the generation of citrullinated peptides recognised by CD4$^+$ T-cells [318]. B-cells starved in culture of foetal calf serum (FCS) and put under stress are more likely to present citrullinated peptide [319]. This is very interesting link given the changes in tissue environment during RA that may induce autophagy by APCs [319], which in turn increases citrullination of self-peptides and potential autoreactivity.

Another interesting link is that genetically predisposed individuals are more than likely to get RA. Specifically MHC alleles that are genetically predisposed to the disease have a positive charge amino acid at the P4 peptide-binding pocket of the MHC. Citrullinated peptides have a neutral citrulline rather than a positive one and as a result it favours binding and could alter the affinity [319].

The idea that citrullination of self-antigens provides a potential mechanism for initiation of RA is a simple and attractive explanation. However, it would be important to understand the biology within cells of the immune system in order to fully understand the role of citrullinated antigen in RA. T-cells have been identified that recognise citrullinated antigen [320]. Furthermore, as APCs can present citrullinated antigen this also implicates a role for APCs and antigen presentation in RA. However, to date it remains unclear if citrullination of antigen alters how individual T-cells recognise antigen and if there is altered interaction forces with an APC, which could influence T-cell function.

Therefore my objectives for **Chapter 5** were:

- **Determine if citrullination of an antigen affects T-cell function.**

- **Assess whether altered T-cell function due to citrullinated antigen is associated with changed in interaction force between naive T-cells and DCs.**

- **Given that recognition of cit-peptides may breach self-tolerance to initiate RA, to determine whether interactions between previously tolerant T-cells and DCs are altered upon re-stimulation with citrullinated antigen.**

1.17.3 Does MKP-II play a role in influencing T-cell function and determining interaction strength with DCs?

As discussed above, the duration, strength and quality/quantity of antigen may influence T cell effector function. As such, specific intracellular signalling pathways may drive distinct T-cell effector functions [118,321–324]. Proximal signalling upon the binding of pMHC to TCR is thought to be involved in tightly regulating a T-cell response. For instance, maximal ITAM phosphorylation proceeds following ligation of TCR to antigenic pMHC, and only minimal phosphorylation proceeds following ligation of TCR to self pMHC [325]. Indeed inappropriate intracellular signalling can result in autoimmune disorders [48]. Previous work has shown that ERK is recruited to the immunological synapse suggesting that ERK is important for the formation of the immunological synapse and thus potentially determining the interaction forces between T-cells and APC [116,326,327] and differences in the responsiveness of naïve and antigen-experienced T-cells may be associated with phosphorylation of MAP-kinases such p38 and ERK [118].

Furthermore, studies have indicated that JNK may play a role in regulating IL-2 gene transcription and IL-2 mRNA stability, as well as affecting T_H1 and T_H2 differentiation. The importance of JNK has also been highlighted in an infection with *Leishmanina major,* where JNK-deficient mice show an enhanced T_H2 response and as a result cannot resolve the infection [328–332]. Unlike JNK, p38 does not affect the production of IL-2 and the proliferation of T-cells [333]. However, p38 seems to play a role in the effector functions of T-cells, with p38 activation being essential for IFN-γ production by T_H1 cells but not IL-4 or IL-5 by T_H2 cells [334]. Conversely, the

ERK activation does not seem to be essential for IL-2 production or proliferation [335]. However, ERK is required for IL-4 receptor function and consequently the differentiation of $CD4^+$ T_H2 cells [336].

In addition to affecting T-cell function, MAP-kinases can also influence the activation of antigen presenting cells. Upon stimulation with lipopolysaccharide (LPS), DCs induce the phosphorylation of MAP-kinases such as ERK, JNK and p38 [337] and pre-treatment of DCs with p38, ERK or JNK inhibitors impairs the up-regulation of CD40, CD80, CD86, HLA-DR and cytokine production, following LPS or TNF-α stimulation [337–343].

MKP-II regulates the dephosphorylation of JNK, p38 and ERK and a lack of MKP-II may enhance and prolong MAP kinase phosphorylation [344–347]. Indeed, this is demonstrated in MKP-II-deficient T-cells, which were shown to be hyper-proliferative with enhanced CD25 expression and IL-2 signalling, as well as an increase in STAT5 phosphorylation [348]. Furthermore, MKP-II deletion in APCs has been shown to influence the phenotype of a T-cell response. In Al-Mutairi *et al*. *Leishmania mexicana* infection of MKP-II deficient mice was shown to down regulate T_H1 responses and induce T_H2 responses. Furthermore, deficiency of MKP-II in macrophages rendered them more susceptible to infection with intracellular parasites and thus mice had a reduced capacity to control lesion development and parasite replication [349]. Similar results were obtained in the context of *Leishmania major* infection [350] and in a recent report by Woods *et al*. which showed that MKP-II deficient mice were more susceptible to *Toxoplasma gondii* infection, correlating with reduced inducible NOS activity [351]. There is therefore clear evidence that MAP-kinases play a role in T-cell activation and MKP-II can influence the functional outcome of activated T-cells.

Given the importance of MAP kinases in mediating synapse formation and establishing the early interactions with an APC, I hypothesised that deficiency of MKP2 would alter T-cell function and that this would be associated with changes in the interaction force between T-cells and DCs.

Therefore my objectives for Chapter 6 were:

- **Determine if MKP-II affects T-cell function.**
- **Assess whether altered T-cell function in absence of MKP-II is associated with changes to interaction force between T-cell and DC.**
- **Determine if MKP-II plays a role in the development and function of DCs.**
- **Establish whether MKP-II-deficient DCs influence functional outcome for T-cells and whether this is associated with altered interaction forces between cells.**

Chapter 2 – Materials and Methods

2.1 Introduction to methods.

This chapter details the materials and methods for all biological experiments carried out within the thesis. **Chapter 3** will detail the construction, development and implementation of the optical tweezer system and how it was used to quantify the interaction forces between T-cells and DCs.

2.2 Materials.

Foetal bovine serum (Biosera, France), L-Glutamine solution (Sigma-Aldrich, UK), Penicillin-Streptomycin solution (Sigma Aldrich, UK), Hanks Balanced Salt Solution (Life Technologies, UK), Phosphate-Buffered Saline (Life Technologies, UK), RPMI Media 1640 (Life Technologies, UK), G418 Geneticin (Life Technologies, UK), Fluorescein isothiocyanate (FITC) Annexin V (BD Biosciences, UK), Propidium Iodide Solution (Sigma-Aldrich, UK), Anti-mouse CD11c PE (e-Bioscience, UK), Anti-mouse MHC-II FITC (e-Bioscience, UK), Anti-mouse CD4 FITC (e-Bioscience, UK), Anti-mouse CD69 PE (e-Bioscience, UK), Ki-67 PerCP-Cy5 (e-Bioscience, UK), Anti-mouse CD16/CD32 FC receptor block (e-Bioscience, UK), Anti-mouse E-alpha 52-68 peptide (e-Bioscience, UK), APC anti-mouse TCR Vβ5.1, 5.2 (Biolegend, UK), PE anti-mouse TCR Vα2 (Biolegend, UK), $CD4^+$ T-cell Isolation Kit (Miltenyl Biotec, UK), Fixation/permeabilization solution kit (BD Biosciences, UK), Triton X-100 (Sigma-Aldrich, UK), Tween-20 (Sigma-Aldrich, UK), EDTA (Sigma-Aldrich, UK), CFSE (Life Technologies, UK), Ovalbumin protein (Sigma-Aldrich, UK) $OVA_{323-339}$ peptide and citrullinated $OVA_{323-339}$ peptide (ProImmune, UK).

2.3 Animals.

All experiments used mice that were between 6-10 weeks of age.

OT-II transgenic mice originally from Charles River were maintained as colony at the Biological Procedure Unit (BPU) of Strathclyde Institute of Pharmacy and Biomedical Sciences (SIPBS). They express an alpha and beta chain TCR that pairs

with CD4 co-receptor and is specific for the Ovalbumin (OVA) $_{323\text{-}339}$ peptide in the context of I-A^{b}. All lymphocyte preparations were prepared from these mice unless otherwise stated.

The MKP-II deficient mice have been described previously [349]. MKP-II $^{-/-}$ and MKP $^{+/+}$ mice on a C57BL/6 background were crossed with OT-II mice to generate OT-II $^{+/+}$ MKP-II $^{+/+}$ (wild type) and OT-II $^{+/+}$ MKP-II $^{-/-}$ (knock out) mice. T-cells from these mice have the MKP-II gene knocked out but express a transgenic TCR that is specific for OVA$_{323\text{-}339}$ peptide. These were kindly gifted by Professor Robin Plevin, University of Strathclyde.

C57BL/6 and BALB/c mice, also obtained from the BPU in SIPBS, were used for all other lymphocyte preparations and the generation of bone marrow derived DCs (unless stated otherwise).

All animal experiments were approved by both a local ethical review board and the UK Home Office.

2.4   Tissue culture.

2.4.1   Preparation of complete media.

The cRPMI medium, prepared in a sterile flow hood, consisted of 500ml RPMI 1640 medium supplemented with L-Glutamine (2 mM), penicillin (100 µg/ml), streptomycin (100 µg/ml) and 10% foetal calf serum.

L-arginine depleted media was the same as above, except that custom RPMI media lacking L-arginine was used (a kind gift from Dr Pascale Kropf, Imperial College, London).

2.4.2   T-cell hybridoma.

The DO11.10-green fluorescent protein (GFP) T cell hybridoma was kindly gifted by David Underhill [352] and used for viability studies. To keep cells at log phase of

growth, every 2-3 days, 5ml complete medium was removed and replaced with fresh Geneticin-supplemented media. Cells were grown in 25 cm^2 sterile flasks (Sigma-Aldrich, UK). Furthermore, this T-cell hybridoma also co-expresses a transgenic TCR specific for $OVA_{323-339}$ peptide in the context of I-A^d.

2.4.3 Preparation of Lymphocytes.

Axillary, brachial, mensenteric, inguinal, lumbar, caudal and popliteal peripheral lymph nodes were harvested from adult OT-II transgenic mice (6-10 weeks). Lymph nodes were collected into cRPMI and homogenised through Nitex mesh to prepare a single cell suspension. After homogenising the lymph node, the lymphocyte suspension was then transferred to a sterile 50ml falcon tube (Sigma-Aldrich, UK), passed through the Nitex mesh once more and pelleted by centrifugation at 300g for 5 minutes. The cell pellet was re-suspended in cRPMI and washed a further 2 times. Viable cells were counted on a Neubauer haemocytometer using an up-right phase contrast microscope before diluting to an appropriate final concentration, as indicated below.

2.4.3.1 Antigen-specific T-cell activation.

For experiments measuring antigen-specific T-cell proliferation and cytokine secretion, $5x10^5$ non-purified OT-II lymphocytes were added to each well of a 24-well plate, pre-seeded with $5x10^5$ OVA-pulsed or un-pulsed DCs (**Section 2.5.2** and **Section 2.5.3**). T-cell/DC co-cultures were incubated for 48 hrs in a humidified incubator at 37°C, 5% CO_2. After incubation, supernatants were removed and pipetted into eppendorfs (Starlab, UK). To ensure no cells were in supernatants, samples were centrifuged at 10,000 RPM for 1 minute; supernatants were removed, pipetted into fresh eppendorfs and stored at -20°C for analysis of cytokine production by ELISA or Luminex (**Section 2.5.3**). Remaining cells were harvested in 1ml of chilled Phosphate buffered saline (PBS), gently scraping the wells and collecting the cell suspension (through Nitex mesh) into Fluorescence-activated cell sorter (FACS) tubes for analysis of cell proliferation by flow cytometry (**Section 2.5.2**).

2.4.3.2 CD4⁺ T-cell purification.

For certain experiments, particularly the optical trapping experiments where single cell experiments were performed, populations of purified CD4$^+$ T-cells were required. Lymphocytes were prepared as described (**Section 2.4.3**) and CD4$^+$ T cells isolated using magnetic-assisted cell sorting, according to the manufacturer's instructions (Miltenyi Biotec, UK).

Briefly, following preparation as described in **Section 2.4.3**, cells were re-suspended in 40µl of magnetic assorted cell sorting (MACS) buffer (PBS, 0.5% FCS, 2nM Ethylenediaminetetraacetic acid (EDTA); de-gassed) per 10^7 total cells. 10µl of a cocktail of biotin-conjugated monoclonal antibodies against non CD4$^+$ T-cells (CD8a, CD11b, CD11c, CD19, CD45R (B220), CD49b (DX5), CD105, anti-MHC class II and Ter-119) was added per 10^7 total cells and incubated for 20 minutes at 4°C. After incubation 30µl of MACS buffer and 20µl of anti-biotin micro-beads per 10^7 cells was added to the sample, mixed well and incubated for 15 minutes at 4°C. After incubation, cells were washed by adding 2ml of MACS buffer per 10^7 cells and centrifuged (300g, 10 minutes). The supernatant was discarded and the cells were re-suspended (up to 10^8) in 500µl of MACS buffer.

Using a LS column the now magnetically labelled cells were separated. The column was prepared by washing 3 times with 3ml MACS buffer and then adding the magnetically labelled and un-labelled cells. Labelled cells will remain in the column and un-labelled CD4$^+$ T-cells will pass through the column. The column was washed a further 4 times with 3ml of MACS buffer to increase cell yield. Purified CD4$^+$ T-cells were centrifuged, washed 3 times and re-suspended cRPMI medium. As can be seen in **Figure 2.1** the percentage of CD4 $^+$ T-cells increased from 65% (pre-purification) to 89% (after purification). The percentage of Vα2 and Vβ5 positive cells increased form 63% (pre-purification) to 87% (after purification). The alpha-chain and beta-chain T-cell receptor pairs with CD4 co-receptor and is specific for chicken ovalbumin 323-339 in the context of I-A b.
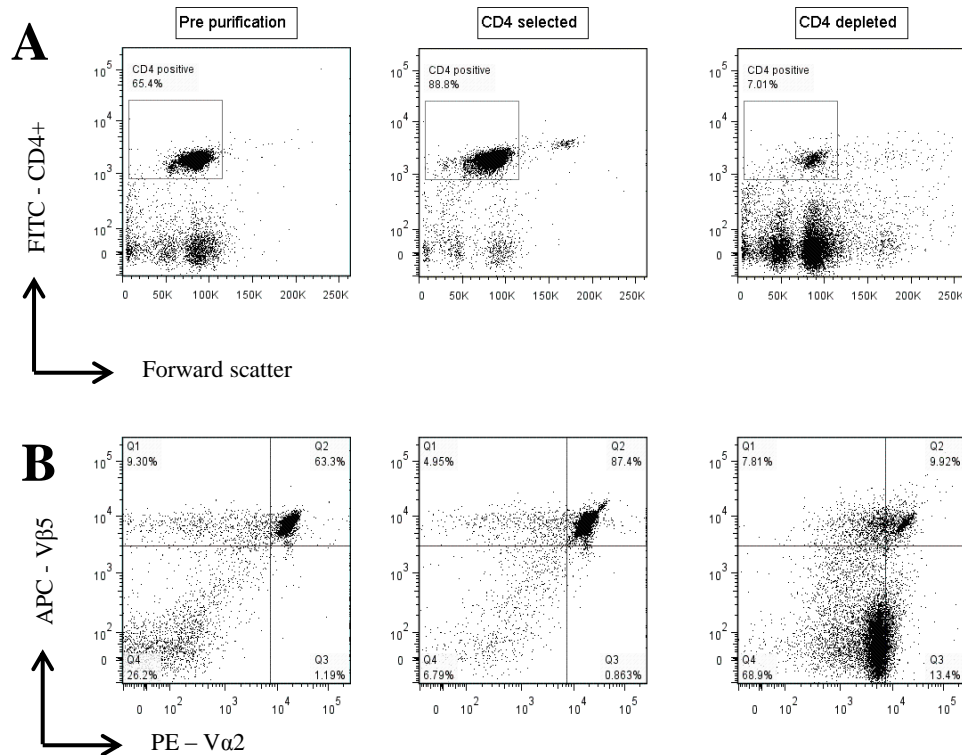
Figure 2.1: **CD4$^+$ purification from lymphocyte preparations.**

Flow cytometry was used to analyse lymphocyte preparations. T-cells of interest were identified using anti-CD4, anti-Vα2, anti-Vβ5 and represented in dot-plots showing **A:** gating of lymphocytes and the % of CD4$^+$ T-cells, **B:** gating of lymphocytes and the % of Vα2 and Vβ5 T-cells, in pre-purification, CD4 selected and CD4 depleted samples as indicated.

2.4.4 Generation of bone marrow derived dendritic cells.

Bone marrow-derived dendritic cells (BMDC) were generated as previously described [353]. The femurs and tibiae of mice were removed and separated from surrounding muscle. The epiphysis of each bone was cut with scissors and the marrow was flushed out with cRPMI using a syringe with a 25 g needle. Cell clumps were disaggregated by vigorous pipetting. Cells were then washed once before seeding 2 x 10^6 viable cells in 10ml cRPMI, supplemented with 10% medium from x63- granulocyte macrophage colony-stimulating factor, in Corning bacteriological

petri dishes (Corning Costar, Amsterdam). Cells were incubated at 37°C for 7 days and fed by replacing half the medium with fresh GM-CSF-supplemented cRPMI on days 3 and 5. On day 7 cells were collected by washing plates gently with chilled PBS, washed, enumerated and used immediately.

2.4.4.1   Stimulation and antigen pulsing of DCs with Ovalbumin.

Viable cultures of bone marrow-derived DCs were plated onto 6 well plates (Corning Costar, Amsterdam) at a concentration of $5x10^6$ and activated with 1µg/ml LPS and/or antigen pulsed with 1 milligram per millilitre (1mg/ml) ovalbumin for 6 hrs (unless otherwise stated) in 2 ml of complete cRPMI medium. Alternatively, DCs were pulsed with OVA-peptide or citrullinated OVA peptide, at 10µg/ml (unless otherwise stated). Following stimulation or antigen pulsing, DCs were washed 3 times in cRPMI medium to remove soluble antigen and re-plated onto microscope chamber slides for optical trapping experiments or tissue culture plates for T-cell functional analysis.

2.5   Flow cytometry.

Aliquots of single cell suspension were prepared and a minimum of $1x10^5$ total cells were added to 12 x 75 millimetre (mm) polystyrene tubes (Falcon BD, UK). Cells were pelleted by centrifugation at 300 g for 5 minutes, the supernatant discarded and cells re-suspended in 50 µl of FACS buffer (1% bovine serum albumin (BSA) in PBS) containing 0.5µg Fc block (anti-mouse CD16/23) and incubated for 10 minutes at 4°C, to reduce non-specific binding by Fc receptors. After incubation the appropriate fluorochrome-conjugated or biotinylated antibodies (**Table 2.1**) were added to the appropriate FACS tube and samples were again incubated at 4 °C in the dark for 15-30 minutes. After incubation cells were washed with 2 ml FACs buffer. Cells were washed a further two times and after final wash cells were re-suspended in 400 µl of FACs buffer and data was acquired using a BD FACS Canto.

Before acquiring any data, forward scatter (FSC) and side scatter (SSC) were adjusted to gate cells of interest on screen. Un-stained samples were used as auto-

fluorescence controls and if needed settings were adjusted to lower the fluorescence intensity within the first decade of log scale on histogram. Un-stained samples were also compared to isotype controls and labelled cells to confirm correct scale. Subsequently, single-colour stained samples (or FACS Calibrite Beads; BD Biosciences) were used to define a compensation matrix. All data was analysed using FlowJo (Treestar Inc, CA, USA).

2.5.1 Measuring antigen up-take and presentation.

Antigen presentation and up-take was measured using EαGFP/YAe system [354]. DCs which internalise EαGFP can be quantified using flow cytometry to determine the proportion of cells which have taken up antigen (based on GFP fluorescence) and presentation of the Eα peptide in the context of MHC class II is detected by staining cells with the YAe antibody, which is specific for this pMHC complex.

Bone marrow-derived DCs were incubated with 100 µg/ml EαGFP for 24 hrs as detailed in **Section 2.4.4.1**. Control wells were incubated with complete RPMI medium only. The following day cells were harvested and stained as in **Section 2.5**, except biotinylated anti-mouse Eα52-68 (1 µg/ml) first added. After incubation cells were washed and Allophycocyanin (APC) streptavidin was added (1ug/ml). Cells were then analysed for antigen up-take and presentation using flow cytometry (**Section 2.5**). Mean fluorescence intensity (MFI) of GFP was a measure of antigen up-take and degradation and MFI of APC was a measurement of antigen presentation.

2.5.2 Measurement of ovalbumin-specific proliferation *in vitro*.

To identify proliferating cells, cell suspensions were first stained as above (**Section 2.5**) using a FITC-conjugated anti-CD4 antibody. After the final wash, cells were fixed and permeabilized by adding 250 µl of fixation/ permeabilization solution per tube and incubated in the dark at 4 °C for 20 minutes. After permeabilization, cells were washed 3 times with BD perm/wash buffer, re-suspended in 50 µl of BD

perm/wash buffer containing PerCP-Cy5 Ki-67 (1:200 dilution) and incubated for 30 minutes in the dark at 4 °C. Ki-67 is a marker present at all stages of the cell cycle, except resting cells, and has been used previously to assess T-cell proliferation [355]. Cells were then washed a further 3 times in BD perm/wash buffer, re-suspended in FACS Flow and analysed using a flow cytometer to quantify the proportion of proliferating (Ki-67-expressing) CD4$^+$ cells **(Section 2.5)**.

2.5.3 Measurement of antigen-specific cytokine production.

Supernatants taken from T-cell/DC co-cultures were analysed for antigen-specific cytokine production using either Enzyme-linked immunosorbent assay (ELISA) or Luminex. The cytokines IL-2, IFN-γ and IL-5 were measured.

2.5.3.1 Luminex.

A Luminex® assay (Invitrogen, UK) was used to measure cytokine production in some experiments. Samples were stained and analysed according to the manufacturer's instructions.

Individual wells of a 96 well opaque plate were pre-wetted with 200 µl of working wash solution before removing using a vacuum manifold. 25 µl of diluted beads with defined spectral properties and conjugated to cytokine-specific capture antibodies were pipetted into each well, along with 200 µl of working wash solution and incubated for 30 seconds in the dark to allow beads to soak before washing. 50 µl of incubation buffer containing 0.05% sodium azide was added to all wells. 100 µl of recombinant cytokine standard was added to designated wells and a 3-fold serial dilution of reconstituted standard was prepared to make standard curve. 50µl of supernatant samples along with 50 µl of assay diluent was added to the wells designated as samples. The plate was covered with aluminium foil to protected from light and incubated for 2 hrs at room temperature on an orbital shaker before 2 wash steps, and incubation with 100 µl of 1X analyte-specific biotinylated detector antibody for 1 hr at room temperature.

After incubation and 2 wash steps, 100 µl of 1X R-Phycoerythrin-conjugated streptavidin was pipetted into all wells and incubated in the dark for a further 30 minutes. A final 3 wash steps were carried out followed by addition of 100 µl of wash buffer to each well. This was placed on an orbital shaker for 3 minutes to re-suspend beads and a further 3 wash steps were carried out. 100 µl of working wash solution was added to each well after final wash and placed on an orbital shaker for 3 minutes to re-suspend beads. The plate was then placed onto a XY platform Luminex 100 instrument and samples were analysed.

2.5.3.2 ELISA.

Sandwich ELISA was used to analyse cytokine concentration from supernatants of T-cell/DC co-cultures. Flat bottomed 96 well plates were coated with 100 µl per well capture antibody in coating buffer (0.1M NaHCO$_3$, pH 8.2), sealed and incubated overnight at 4 °C. After 3 washes with wash buffer (PBS pH 7.0 containing 0.05% Tween-20), non-specific binding sites were blocked for 2 hrs at 37 °C by adding 200 µl per well of 10% FCS diluted in PBS pH 7.4, containing 0.05% Tween-20. After 3 washes with wash buffer, 50 µl of culture supernatant samples was added to the plate. Recombinant cytokine standards with starting concentrations of 20 ng/ml (IFN-γ and IL-5) were added and 2-fold titrations of the standards used to make the standard curve. The plate was incubated for 2 hrs at 37 °C in wash buffer with 10% FCS. Plates were washed 6 times with wash buffer and after final wash 50µl of the appropriate biotinylated anti-cytokine detection mAb was added to each well. Plates were sealed and incubated for 1 hr at 37°C. Plates were washed 6 times again and after final wash, 75 µl Horseradish Peroxidase detection enzyme was added to each well and incubated for 1 hr at 37°C. After incubation, plates were washed 6 times before addition of 100 µl of tetramethylbenzidine (TMB) per well. Plates were left to develop in the dark at room temperature for 15 mins. Plates were read at 630 nm using a micro-plate reader and the levels of cytokine in supernatants calculated.

2.6 Statistical analysis.

Results are represented either as the mean ± standard deviation (SD) or standard error mean (SEM), or as the median ± SD as indicated in each Figure. Data with a normal distribution was analysed using a Student's t test, whilst data that had a skewed distribution was analysed using a Mann Whitney test. Statistical analysis was performed using Origin pro version 9.0.

Table 2.1 Monoclonal antibodies used

Antigen	Clone	Isotype
CD4	RM4-5	Rat IgG2aκ
DO.11.10. TCR	KJ1-26	Mouse IgG2aκ
Class II MHC	M5114.15.2	Rat IgG2bκ
CD11c	N418	Armenian Hamster IgG
CD40	IC10	Rat IgG2aκ
CD69	H1.2F3	Armenian Hamster IgG
Ki-67	SolA15	Rat IgG2aκ
Eα 52-68	YAe	Mouse IgE2b
Vα2	B20.1	Rat IgG2a λ
Vβ5.1, 5.2	MR9-4	Mouse IgG1κ

All antibodies were obtained from e-bioscience and used at a concentration of 1:400, unless stated otherwise.

Chapter 3 - The development of an optical tweezer system to control cell-cell interaction and quantify immune cell interaction forces.

3.1 Aims and objectives.

This chapter details the design and implementation of an optical tweezer system built around a commercial Nikon TE2000u microscope at The Institute of Photonics. The main aim of the system was to directly trap live T cells without compromising their viability and to measure the interaction force between T cells and DCs. When using optical tweezers to measure forces it is common to attach a bead to the cell of interest and trap the bead instead of the cell itself [211,253,356–358]. The system described in this chapter measures forces directly from the trapped cell and therefore removes the need to introduce foreign bodies into the sample. This chapter includes details of the build and design of the system, the system calibration, viability studies of the optically trapped T cells, methods for tracking the position of the trapped cells and approaches for quantifying interaction forces.

The chapter is divided into 3 main sections:

1. Design and implementation of optical tweezer system (**Section 3.2**).

2. Optimising the trapping, tracking, calibration and viability of optically trapped T-cells (**Section 3.3**).

3. Manipulating and quantifying the interaction forces between T-cells and DCs (**Section 3.4**).

The final section, **section 3.4**, demonstrates that the optical trapping system is capable of measuring the interaction forces between T cells and DCs and observing a difference in the force associated with the presence or absence of specific antigen.

3.2 Design and implementation of the optical tweezer system.

The main components of an optical tweezer system are the trapping laser, high numerical aperture (NA) microscope objective, microscope sample slide, beam delivery optics and method for observing the specimen, [185,359]. Often systems are built around a commercial microscope, which provides a means of imaging the

specimen and holding of the microscope sample slide. The next few sections will discuss the design and assembly of the optical tweezer system built for manipulating immune cells, highlighting the important features of the various components required.

3.2.1   The microscope.

The microscope consisted of a two tier turret system, one above the other. The bottom turret held the appropriate filter cube for any fluorescence imaging and the top turret the dichroic mirror used to direct the trapping laser beam into the microscope objective. As shown in **Figure 3.1,** this set-up meant that the trapping laser and the fluorescence source entered the back of the microscope in two separate beam paths and therefore could operate at two different wavelengths. A side port on the microscope allowed a camera to be attached so that an image could be viewed in real time on a computer monitor. Depending on the experiment a QCam colour camera from QImaging or a black and white Dalsa Genie Camera was used. A schematic diagram of the microscope, fluorescence filter cube, dichroic mirror and camera port is also shown in **Figure 3.1**.

A

Turret 2 -
trapping laser

Turret 1 -
Fluorescence

B

Illumination

White light

Sample

Immersion oil

Objective

Laser (1064nm)

1064nm dichroic
mirror

Mercury arc lamp

SEMROCK filter

Side port to
Colour camera
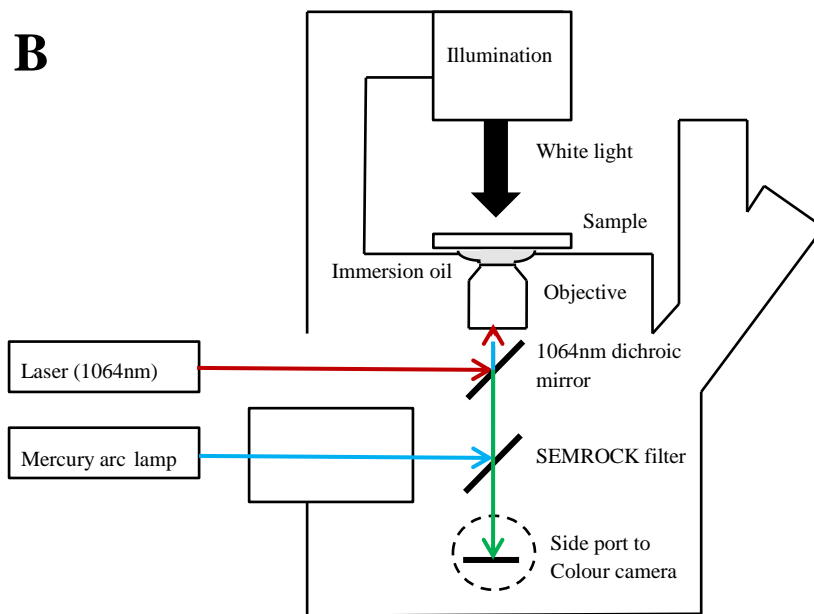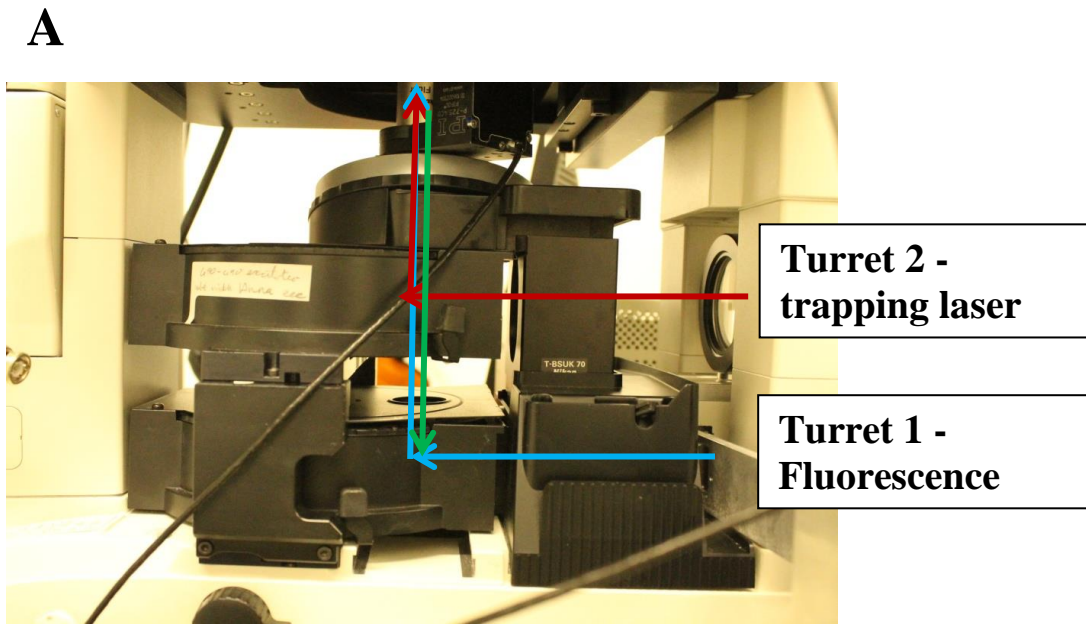
Figure 3.1: <u>**Laser and fluorescence beam path and schematic diagram of microscope.**</u>

A: A picture illustrating the two turret wheels and the pathway of the trapping 1064nm laser (red line), fluorescence excitation light source (blue line) and emission light (green line) with **B:** A schematic diagram of the microscope, showing the two ports for both the fluorescence and 1064nm laser, as indicated.

The dichroic mirror in turret 2 reflects wavelengths above approximately 700 nm and transmits all lower wavelengths. This meant that the trapping laser (wavelength of 1064nm) was reflected at 45^0 to enter the microscope objective, whilst wavelengths in the visible range used for illumination and fluorescence were transmitted, allowing simultaneous trapping of particles and fluorescence imaging. Incorporating fluorescence within the optical tweezer system is further discussed in **Section 3.3.**

A motorised sample stage was used, which allowed the position, speed, acceleration and rate of acceleration of the sample stage to be controlled either with a joystick or a computer, via the COM1 port and a LabVIEW programme. This meant that an optically trapped particle could remain stationary relative to the rest of the sample, whilst the sample was moved using the stage. Further to this, a heated stage was used to maintain samples at an optimum temperature of 37°C.

The choice of objective is important as it determines the overall efficiency of the optical tweezer system both in terms of light and optical trapping efficiency. In order to produce an optical trap the intensity gradient at the focus of the laser beam must be sufficient to overcome the scattering force resulting from the on-axis rays. This relies on using a tightly focusing lens or a lens with a high numerical aperture (NA). Typically oil immersion objectives are used with an NA greater than 1.3. The microscope objective used here was a Nikon Plan Fluor objective with a NA of 1.30 and a magnification of 100x.

Most microscope objectives are designed for imaging visible wavelengths and are not optimal for focusing infrared light [184,213]. To measure the transmittance through a high NA lens a dual objective method is normally used, whereby two identical matched objectives are used with collimated light entering the back of the first objective [184]. The focusses of the two objectives are aligned resulting in collimated light exiting the second and the power measured before and after the objectives meaning the transmittance can be calculated. A review by Svoboda and Block (2004) gives an overview of common objectives used in optical tweezer set-ups and

the relative transmittance in the near-infrared. According to Svoboda and Block, the objective used in this set-up has a transmittance of 61%, meaning that 39% of laser power is lost through the objective [185]. This loss in laser power was assumed throughout all subsequent experiments in this chapter and throughout the thesis.

3.2.2 Laser.

When trapping biological material the choice of wavelength is important since too much absorption can permanently damage the sample. Discussed further in **Chapter 1**, **Section 1.15** the absorption spectrums for water and biological material are at their lowest between 800 -1100 nm, which makes 1064 nm, an ideal wavelength to use in the implementation of the optical tweezer system and for biological experiments.

A 1064 nm, 3W Ventus IR continuous wave laser (Laser Quantum Ltd) was used, providing a cost-effective way of minimising damage and trapping biological cells. The laser power supply unit allows the laser diode current to be adjusted and thus laser power could be easily adjusted without the need to place variable filters in the beam path. The laser calibration graph showing laser power against % of laser diode current can be seen in **Figure 3.2**, and applied current scales linearly with output laser power. However, 25% is the minimum current required to reach laser threshold and for the laser to start lasing.
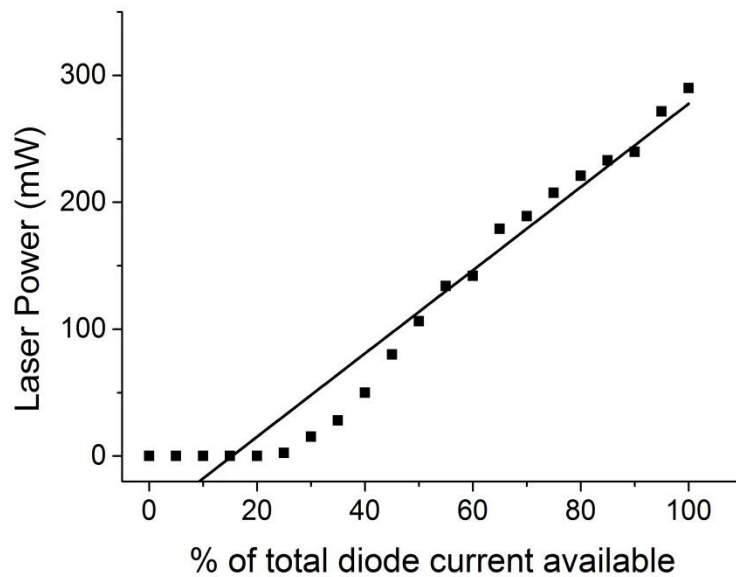
Figure 3.2: <u>**Ventus IR 1064nm laser.**</u>

Calibration of % of the total diode current available against laser power (at sample).

3.2.3 Fluorescence Microscopy.

For experiments looking to assess the viability of trapped T-cells, (**See section 3.3**), I aimed to use a fluorescent marker, propidium iodide to assess necrosis. Therefore, the development of fluorescence microscopy in conjunction with the optical tweezer system had to be implemented and tested.

As discussed in **Section 3.2.1**, the turret can hold multiple filter cubes allowing multiple colours to be imaged. A quad band filter cube (Semrock, USA) was purchased and used in conjunction with a colour camera. The filter set is designed for imaging key fluorophores with four bands for the emitted wavelengths and four bands for the excitation wavelengths. Further information on the excitation/emission spectra of the SEMROCK filter cube can be found at the website link http://www.semrock.com/SetDetails.aspx?id=2929.

Further to this, in order switch easily between fluorescence and white light illumination an automated flipper mount was implemented to block the white light illumination while fluorescence images were taken. This can be seen in **Figure 3.3** below.
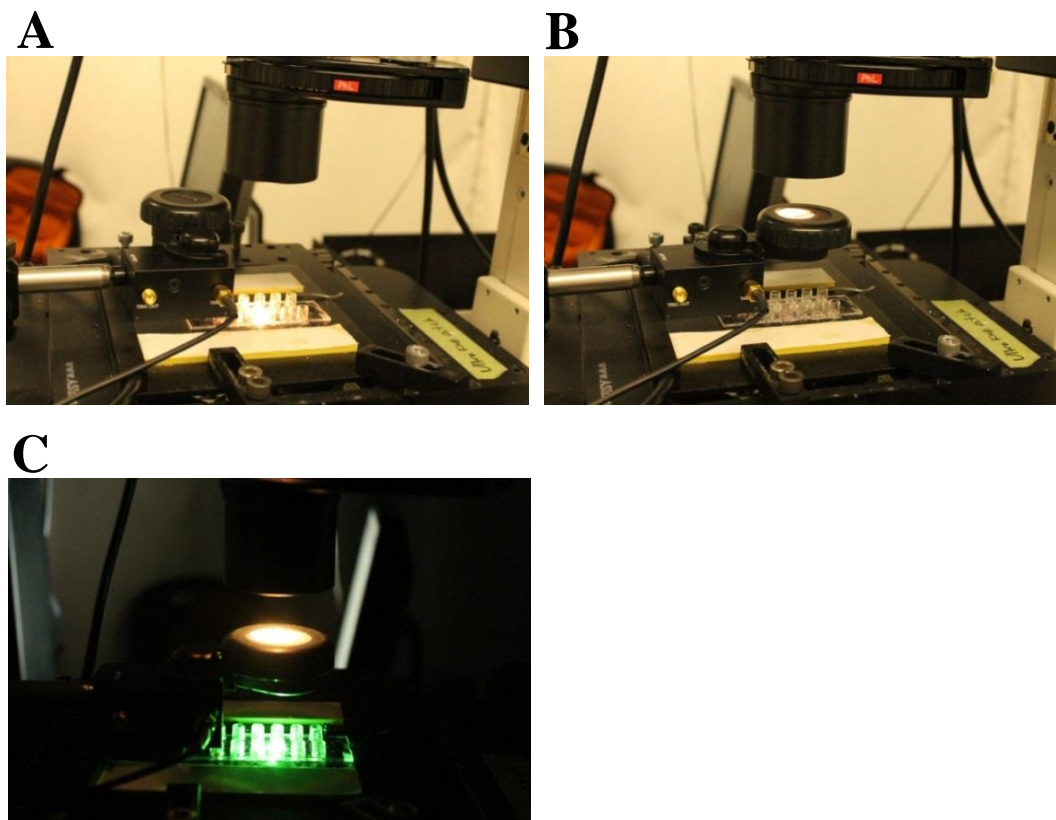
Figure 3.3: <u>**Flipper mount sequence to image in brightfield and fluorescence sequentially.**</u>

A sequence of photographs that show and demonstrate the motorised flipper mount and how it works. **A:** Flipper mount not blocking white light illumination, **B:** Blocking white light illumination, **C:** Blocking white light illumination allowing fluorescence images to be taken.

Overall, the optical system was able to detect multiple colours as can be seen below, in **Figure 3.4**. By implementing the above optimisations multiple colours of beads

within the same sample are detectable. Although they were still distinguishable from one another, some mixtures of beads were more difficult to detect than others. For example, a mixture of APC (ex 650 nm, em 660 nm) and PE (ex 496 nm, em 576 nm) beads were readily distinguished, whereas a mixture of PerCP-Cy5 (ex 482 nm, em 695 nm) and PE beads could be distinguished but not easily. From other combinations it is clear that FITC (ex 495 nm, em 519 nm) and PE were easily identified from each other and therefore these wavelength properties would be ideal for any future combinations of fluorophores used.
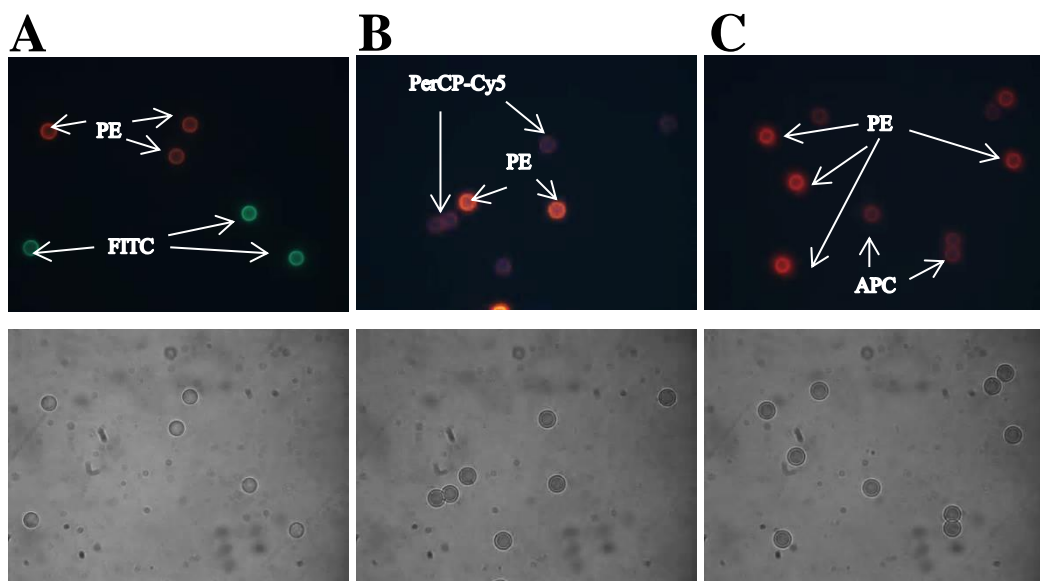
Figure 3.4: <u>**Images demonstrating multiple colour imaging of fluorescent beads.**</u>

A series of images showing florescent 6µm diameter beads with the ability to detect several fluorescent wavelegnths at once using the Semrock filter. **A:** FITC and PE stained beads, **B:** PE and PerCP Cy5 stained beads, **C:** APC and PE stained beads.

3.2.4 Beam delivery system.

3.2.4.1 Spatial light modulator.

There are a number of beam-steering strategies that allow precise control over multiple optical traps. These include the use of mechanical scanners, electro optic deflectors, acousto optic deflectors and, more recently, spatial light modulators (SLM) [185,213] The choice of beam scanners will ultimately depend on how many particles you want to trap at any one time and the area of the sample that you wish to work with. For example mechanical scanners have a large scan angle but are limited by the response time [360,361], whilst optic deflectors are faster but are limited by the distance at which they can scan. Acousto optic deflectors compromise and fall in the middle between distance scanned and speed [233,362]. SLM can also be used steer the laser beam [363,364].

The system built for this project used a Boulder Nonlinear Systems XY series SLM allowing multiple optical traps to be created and moved independently of each other. Nematic spatial light modulators have lower efficiencies than other competitors; however distinct advantages that they do offer include the ability to change the mode of beams; such as a Guassian into a Laguerre-Gaussian beam as well as changing the phase of the beam profile along the axial direction [365].

An SLM is ideal for multiple trapping because all traps can be formed at once from a single optic simplifying the optical alignment. Moreover, the SLM would provide the user with the ability to change the beam profile at the click of a button, which may allow the trapping of a large cell to be optimised more easily, as demonstrated using "Red Tweezers" software by Bowman *et al.,* [366]. Furthermore, the flexibility that a SLM provides in trapping large biological material, which are both static and motile has been demonstrated [367]. The basic structure of a SLM and how the crystals align following the application of a voltage can be seen in **Figure 3.5**.
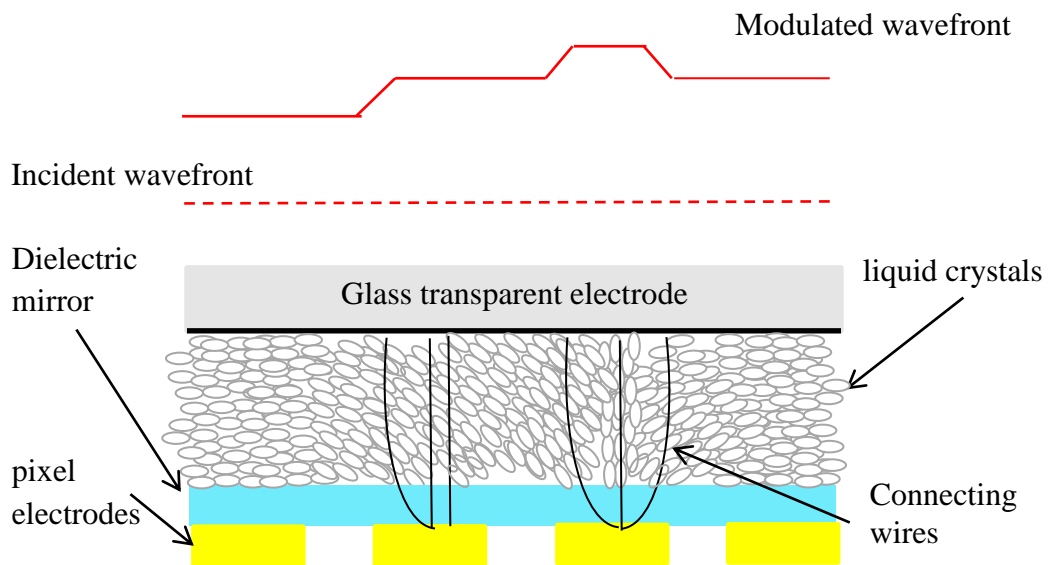
Figure 3.5: <u>**Schematic of liquid crystals orientation and structure of SLM interface.**</u>

Schematic diagrams illustrates SLM interface. Individually addressed pixels (yellow boxes) are at bottom, with a second electrical contact layer (grey box) above the liquid crystals. Upon application of an electrical field the liquid crystals rotate and change the local refractive index and thus change and alter the phase of the incident light beam coming in at that particular pixel area. This is reflected with the light beam now modulated as shown.

3.2.4.2 Beam steering optics.

Two beam expanders were included in the system; the first to ensure that the laser beam was large enough to slightly overfill the SLM and the second to ensure that the beam size was matched to the back aperture of the objective to ensure the maximum power out at the same time making full use of the high NA of the lens. The beam expander used to overfill the SLM is shown in **Figure 3.6**.
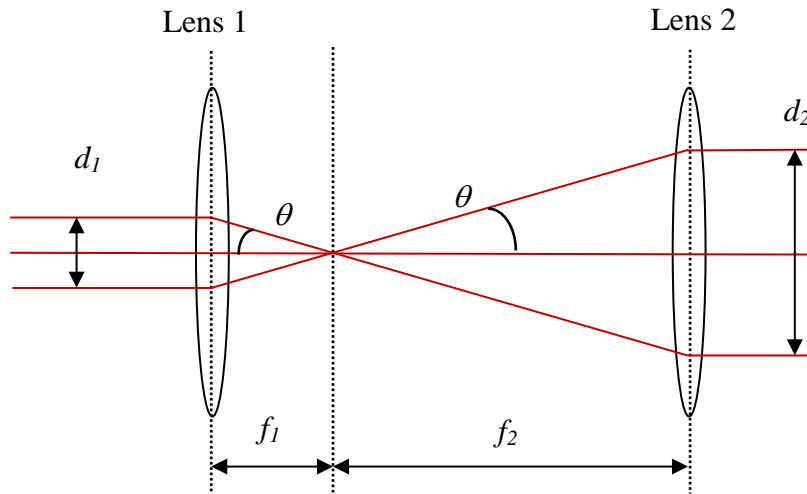
Figure 3.6: <u>**Beam expander.**</u>

A schematic diagram of a beam expander. The laser diameter was expanded 4.2 times from 2.4 mm (d_1) to 10 mm (d_2) using lens 1 (f_1 = 60 mm) and lens 2 (f_2 = 250 mm).

As shown in **Figure 3.6** above, the diameter of the expanded beam, d_2, can be calculated using trigonometry to produce two expressions for the angle, depicted, θ,.

<u>**Equation 3.1**</u>

$$\tan \theta = \frac{(\frac{d_1}{2})}{f_1}$$

<u>**Equation 3.2**</u>

$$\tan \theta, = \frac{(\frac{d_2}{2})}{f_2}$$

The above equations can be equated,

Equation 3.3

$$\frac{d1}{d2} = \frac{f1}{f2}$$

Referring to **Figure 3.9** scan transfer optics were used to allow the laser beam to pivot around the back of the aperture of the microscope objective as the user adjusted mirror M5. Two lenses (L5, L6) were placed in such a way that M5 was re-imaged onto the back aperture of the microscope objective. By adjusting the angle of M5, only the angle of the light entering the back aperture would change and not the position of the laser beam. This resulted in the position of the laser focus moving in the sample x-y plane. A similar arrangement was used to re-image the SLM onto M5 using lenses L3 and L4. Similar arrangements have been used in previous work [218,368]. A schematic diagram of the scan transfer optics used to re-image onto the back aperture of the objective can be seen in **Figure 3.7**.
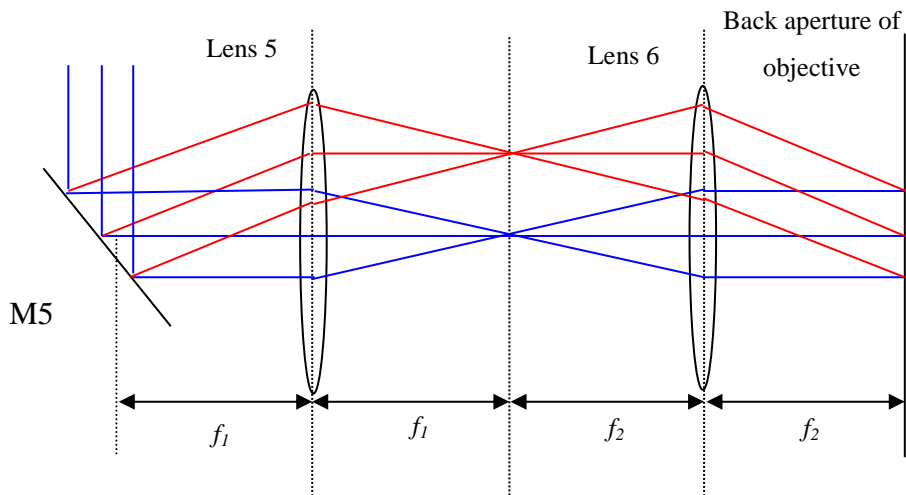
Figure 3.7:   Scan transfer system.

A schematic diagram illustrating a general set-up for a scan transfer system. This ensured that only the angle of the laser beam changed at the back aperture of the objective, as indicated by red lines.

Figure 3.8 shows the final optical trapping set-up, with **Table 3.1** showing the focal lengths of the lenses and the distances between the optics involved in the system. The first beam expander was made up of two lenses L1 and L2 which expanded the beam 4.2 times, from 2.4 mm to 10 mm to overfill the SLM active area. L3 and L4 slightly decreased the beam diameter to match the back aperture of the objective. L3 and L4 act as a scan transfer system to re-image the SLM onto M5, this is then re-imaged onto the back aperture of the microscope objective using a second scan transfer system involving L5 and L6. L1 and L2 were 25 mm in diameter, all other lenses were 50 mm, and coated with an anti-reflection coating for near infrared wavelengths to reduce losses in the system. Finally a photograph of the trapping system is shown in **Figure 3.9**.
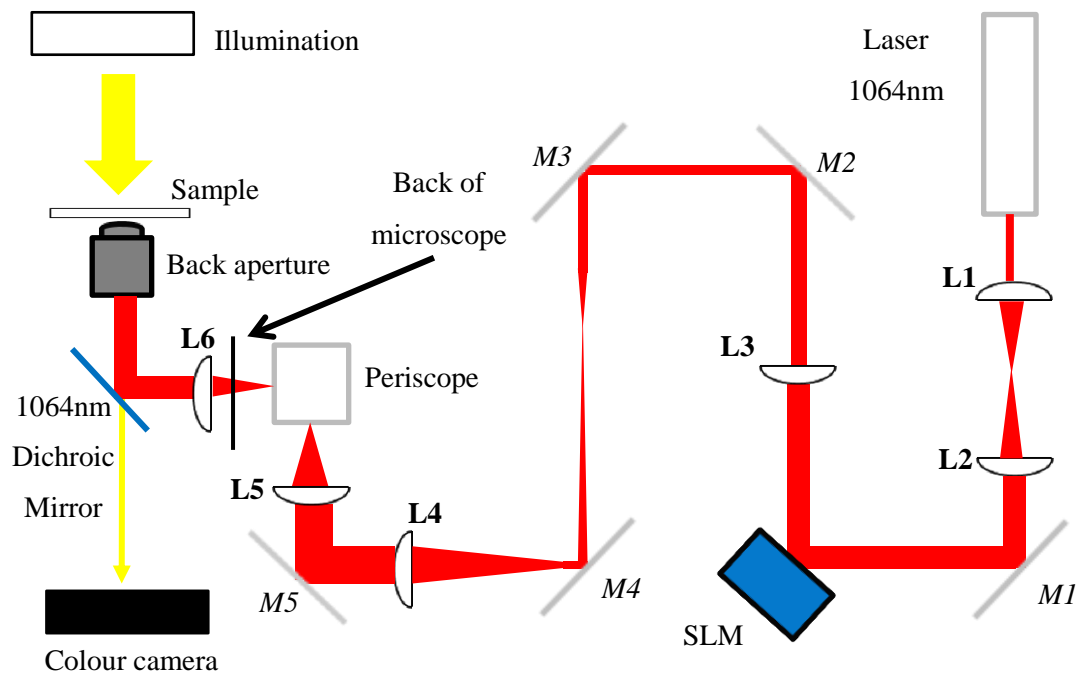
Figure 3.8: <u>**Final optical trapping system set-up.**</u>

A schematic diagram of the optical tweezer system (not to scale). Indicates components of optical tweezer system and highlights the focal points of laser.
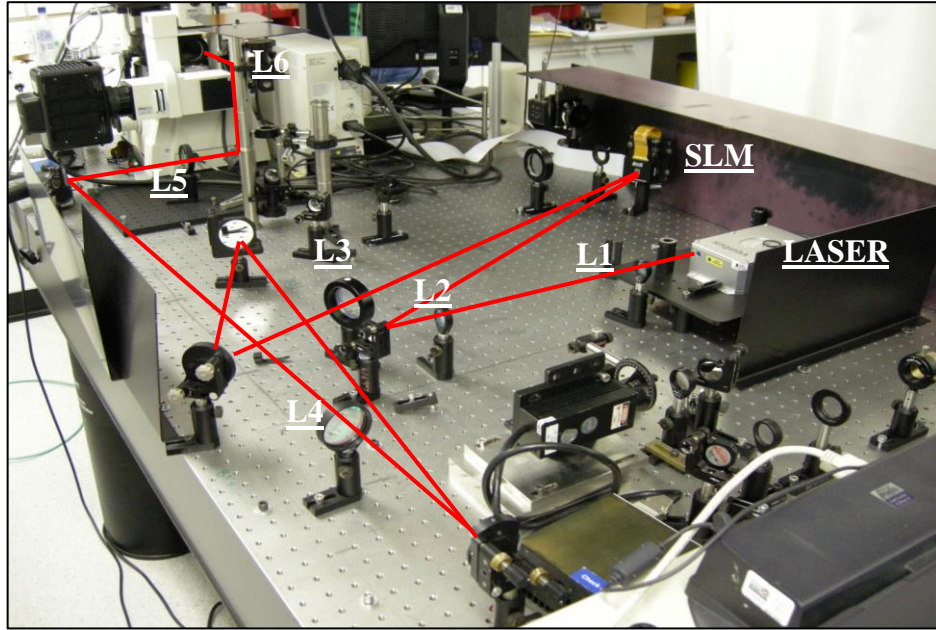
Figure 3.9: <u>**Photograph of final set-up.**</u>

Photograph shows the final optical trapping system that was built at the Institute of photonics and the red line represents the laser beam path.

Table 3.1: <u>**The focal lengths of the various lenses used in the optical trapping system.**</u>

Lens	Focal length (mm)	Distances from……	To…….	Distance (mm)
L1	60	L1	L2	310
L2	250	L2	SLM	1000
L3	750	SLM	L3	750
L4	1000	L3	L4	1750
L5	250	L4	L5	1250
L6	250	L5	L6	500
		L6	Objective	250

3.3 Optimising the trapping, tracking, calibration and viability of optically trapped T-cells.

The main aim of this thesis was to accurately and reliably quantify the interaction forces between immune cells, which relies on accurately calibrating the optical trapping force with respect to the laser beam power, as it is from here that we are able to decipher the cellular interaction force. Therefore the next few sections discuss and show the calibration of the optical tweezers looking at two methods; escape force method and the equipartition theorem [369]. Moreover, optimisations are discussed that were carried out in order to improve both the viability and trapping of T-cells. Finally the last section looks at the viability of trapped T-cells.

3.3.1 Escape force method.

An escape force method can be used to calibrate the optical trapping force whereby an external viscous drag force is applied to the optical trap, the magnitude of which can be increased by increasing the velocity of the microscope stage whilst the trapped object is stationary, until the trapped particle or cell falls out of the trap at which point the trapping force is said to be equal to the external viscous drag force. The viscous drag force, F, for a Newtonian fluid with low Reynolds number is given by Stokes's Law

Equation 3.4

$$F = -6\pi\eta r \boldsymbol{v}$$

where η is the viscosity of surrounding medium (assumed to be that of water, $n = 0.001$ Pa.s), [370] $\boldsymbol{v}$ the stage velocity at the point of release and r the radius of the trapped object, here a T cell.

The optical trap was calibrated using this method at laser powers of 54 mW, 141 mW, 221 mW and 293 mW. For each laser power, an individual T cell was optically trapped and first brought to the surface of the coverslip. The trapped T-cell was next lifted off the coverslip surface by adjusting the focus of microscope to a distance of roughly 9 μm – a distance whereby any additional drags by surface walls can be neglected [187]. The stage velocity, (controlled by a programme written in LabView) was increased until the T-cell was released from the trap. The critical velocity (where the T-cell falls out the trap) was calculated out for 36 individual cells at each power. From this, the average stage velocity at point of release could be determined and applied to **Equation 3.4** to determine the total trapping force at each power. **Figure 3.10** shows that the minimum force of the optical trap was 3.3 pN (relating to a laser beam power at the sample of ~ 54 mW) and the maximum force due to the maximum power available from the laser beam (~ 293 mW at the sample) was 17.6 pN. Importantly this would set a limitation as to the minimum and maximum force of interaction that could be measured. The maximum force stemmed from the maximum laser power available, whilst the minimum force stemmed from the minimum laser power that was sufficient to optically trap T-cells, whilst moving microscope stage. The total force of the trap scaled linearly with laser power as expected [218,371]. This is due to the steepness of the potential well increasing with laser power, and hence a greater external force required for the particle to fall out the trap. **Equation 3.4** relies on knowing the radius of the trapped object and therefore 36 individual cells were measured giving a mean radius of 3μm ± 0.08μm. Importantly this agrees partly with Altan-Bonnet *et al.* who measured the diameter of a naïve T-cell to be 5.6 μm ± 0.5 μm [372]. Despite this method relying on knowing the cell size, the SD error was relatively low and more importantly there was a low SD error in the overall calibration of the optical trap for each power. For single spot trap calibration the overall calibration error was 2.43×10^{-25} whilst the triple spot trap calibration error was 1.76×10^{-18}, the single spot relates to a standard Gaussian beam, details and relevance of the triple spot will be explained in **Section 3.3.2.1**.
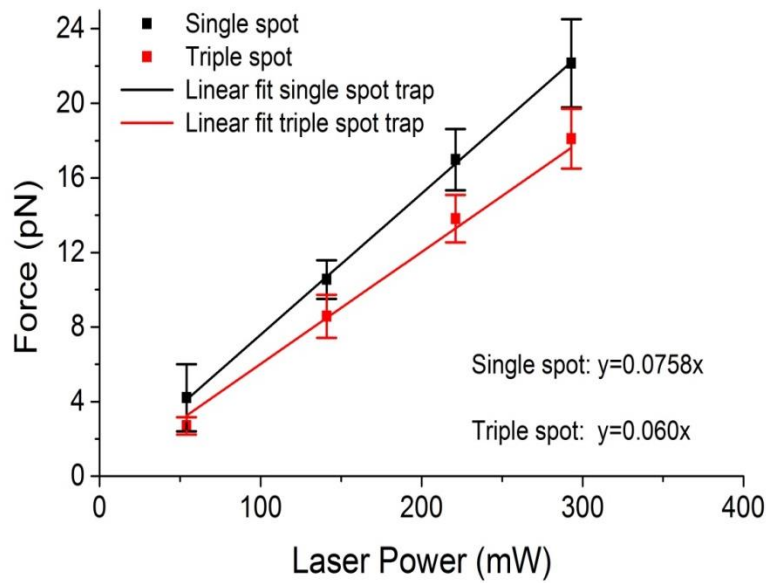
Figure 3.10: <u>**Calibration of the optical trap using the escape force/viscous drag force method.**</u>

Shows the calibration for both a single (black line) and triple (red line) optical traps. Each data point represents the mean force, ± SD, of 36 T-cells. The triple spot trap will be discussed later in **Section 3.3.2.1**

3.3.2 Equipartition theorem.

For small displacements from trap centre, optically trapped particles or cells will behave like a damped harmonic oscillator, where the restoring force is generated by the highly focused laser beam and the damping force is provided by the surrounding medium [185,213,218]. In this regime the trap can be thought of as a weight on a spring and forces modelled using Hooke's law,

<u>Equation 3.5</u>

$$F = -\kappa x$$

where F is the applied force, κ is the stiffness of the spring or spring constant and x is the displacement from equilibrium. There are a number of methods to measure trap stiffness and one of them is to use the theory of Equipartition. The equipartition theorem equates the potential energy in the system to the thermal energy in the system,

Equation 3.6

$$\frac{1}{2}k_BT = \frac{1}{2}k\langle x^2\rangle$$

Where k_B is Boltzmann's constant, T is the absolute temperature, and $\langle x^2\rangle$ is the time-averaged square displacement of the particle from its trapped equilibrium position. Therefore, if one can measure the Brownian motion of a trapped particle over time, it is possible to determine the variance $\langle x^2\rangle$, and thus the stiffness of the optical trap can be calculated. However, accurate tracking of a trapped particle is required in order to determine a precise stiffness calibration.

3.3.2.1 Accurate tracking.

There are a number of tracking algorithms used routinely in optical trapping and fluorescence microscopy and these are reviewed in [226]. They can determine the position of an optically trapped particle over time. One of these is the centre of mass tracking algorithm which has a tracking resolution less than the size of a camera pixel and review in [226,373]. This method can be implemented within LabView and allows determination of a trapped particles position. This was used in the next few experiments. This is an algorithm that works best for simple, circular, bright objects. The centre of mass tracking algorithm is computationally simple, fast and can be used to estimate the distance an object has moved over time. The centre of mass of an object can be calculated using the equation,

<u>Equation 3.7</u>

$$Cx \;=\; \sum_{i=1}^{m} \; \sum_{j=1}^{n} (x_i\, \mathbf{I}_{ij})/ \sum_{i=1}^{m} \; \sum_{j=1}^{n} I_{ij}$$

Where x_i is the coordinate of a pixel on the x axis, and $\mathbf{I}_{ij}$ is the intensity of that pixel. In order to calculate the distance the object had moved, C_x from one image is calculated and then subtracted from the subsequent C_x of another image. This method assumes that the intensities of the object is higher than the background and is susceptible to particle shape changes and orientation between successive images. Furthermore, it is important to exclude as much as the image background as possible so that the bias towards the centroid calculation to the centre of the images is lessened.

However, un-like beads, cells are rarely perfectly spherical and there is a large degree of differing refractive indices, which can cause issues for the centre of mass tracking algorithm.

An optical trap works best for objects that are uniform, roughly spherical and 1-10 µm in diameter. When initially trapping T-cells, a single high refractive index feature of the cell was trapped and this caused the cell to re-orientate or roll within x, y and z planes due to either Brownian motion or an external force such as sample stage motion.

The rolling of a trapped T-cell, associated with the movement of the stage can be seen in **Figure 3.11**. This was quantified by first taking time-stamped images whilst microscope stage was moved. Using Velocity software (PerkinElmer, USA) the threshold for the images was lowered so that only the bright phase point (yellow circle) was highlighted. Once pixel size for the camera was calibrated, the distance the cell moved was determined between each consecutive image. Although the T-cell is technically "trapped" this roll could make calibrating the optical tweezers

using the Equipartition theorem difficult, leading to an under estimation of trap stiffness due to a larger variance in $\langle x^2 \rangle$.
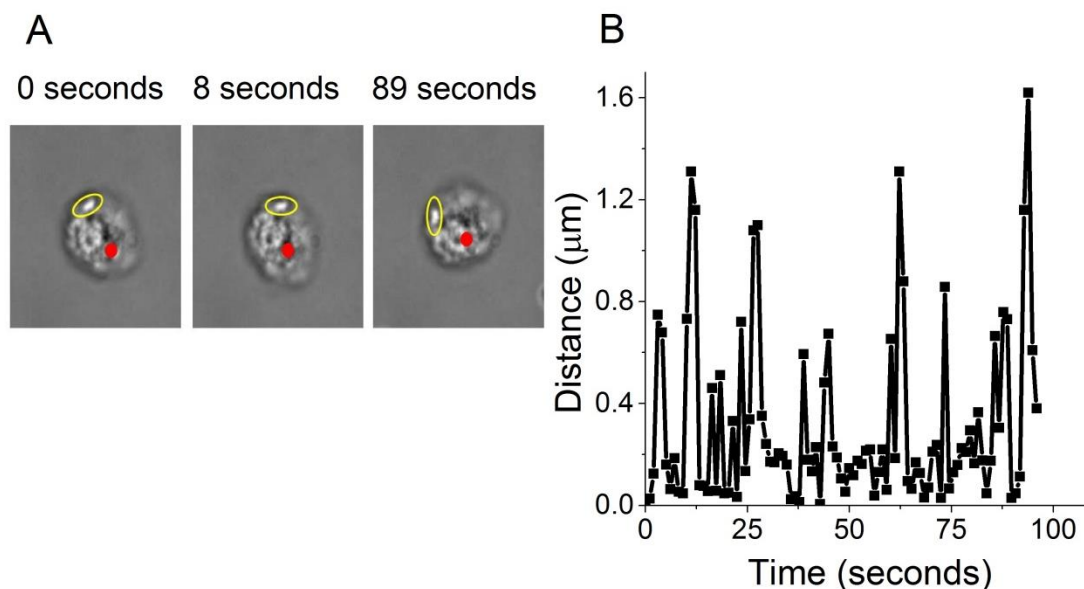
Figure 3.11: <u>**Stability of optically trapped T-cell.**</u>

A: Representative images showing an optically trapped T-cell. Red dots represent the position of the focal point of the laser and the phase-bright point (highlighted in yellow) shows how the cell is rolling whilst moving the stage. The stage was moved 200µm back and forth in the x direction and the feature of high contrast (highlighted yellow in **A**) was tracked using Velocity software (PerkinElmer, USA). **B:** The displacement of the cell feature (as in **A**) as tracked over time as the microscope stage was moved.

As the centre of mass tracking algorithm works best on a dark background and it is important to exclude as much background as possible, a threshold is applied to enhance the contrast between background and the trapped particle of interest, to obtain a suitable image to track. Doing this for a bead is relatively easy but it is difficult to threshold properly for a cell. It is difficult to convert a white light transmission image of an inhomogeneous cell into a suitable image for tracking.

Figure 3.12 highlights the difficulties in obtaining a suitable image for a T-cell, compared to a bead.

	6μm bead	**T-cell**
Before Thresholding		
After Thresholding		
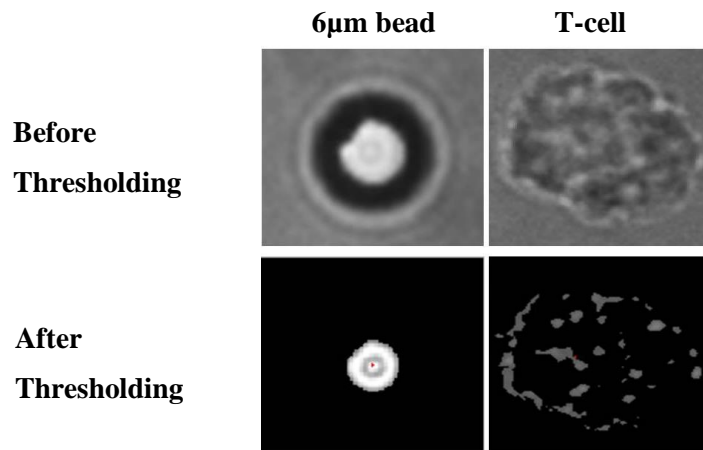
Figure 3.12: <u>**Images highlighting the problems associated with applying a threshold to a transmission image of an un-stained T-cell.**</u>

A bead is homogenous and there is a large contrast between the bead and background and therefore it is easy to threshold and position track. However, in the case of a T-cell there is structure within the cell with varying refractive indices, causing the contrast between the cell and background to be poor and appear non-symmetric, leading to errors in tracking.

Due to problems with tracking the position of a trapped cell, a set of experiments were preformed investigating two routes of improvements. The first experiment was to fluorescently stain a T-cell with 5, 6-carboxy-succinimidyl-fluorescein ester (CFSE) and track the position of the cell from a fluorescence image. The hypothesis was this would provide a cell image that is more homogeneous and thus improve the accuracy of tracking throughout the experiment.

The second approach was using the SLM to produce a novel beam profile to address this issue. A triple spot trap was created using the SLM to generate three beams whose position could be controlled independently of each other. The beams were

placed just inside the cell membrane effectively creating three trapping sites. The hypothesis was if 3 points on the T-cell were optically trapped, then it would remain in focus and the chance of the T-cell drifting or rolling Z would be minimised.

Figure 3.13 shows the improvements made when T-cells were either stained or optically trapped using a triple spot trap.
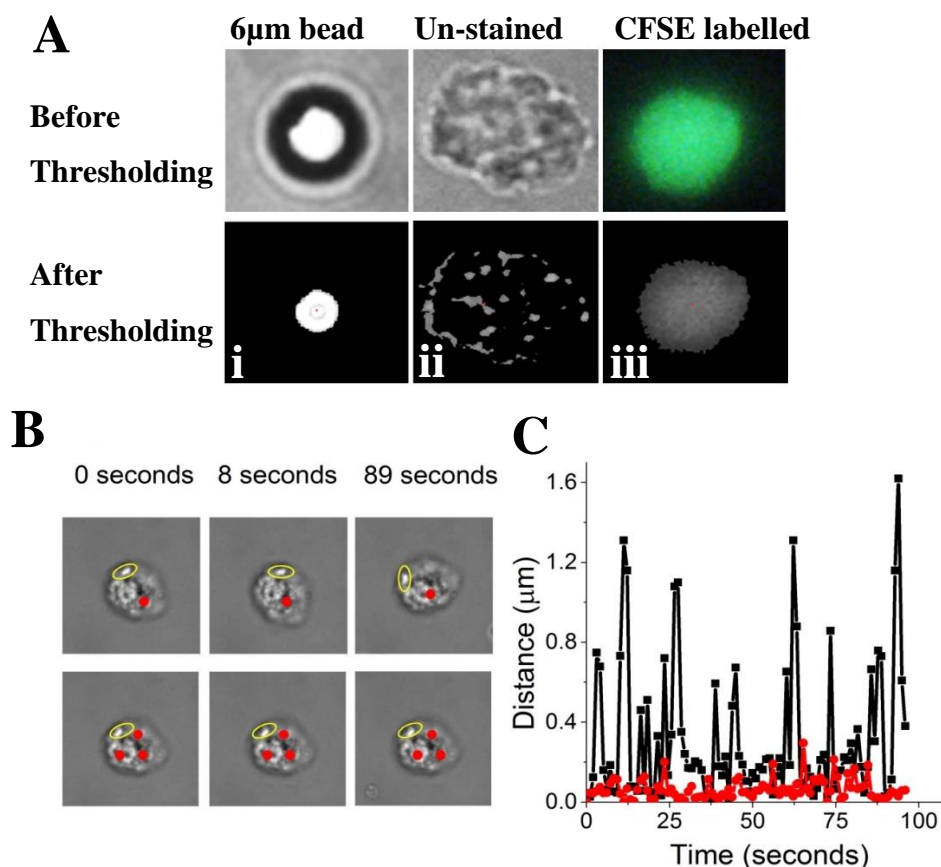
Figure 3.13: Improvements in tracking using CFSE labelled T-cells and triple spot trap.

A: i) A bead which is homogenous and easy to convert to an image of white object on a black background making it simple to track. **ii)** An un-stained T-cell with varying refractive indices, making it hard to achieve a homogenous image suitable for tracking. **iii)** CFSE stained T-cell imaged in fluorescence. The bright florescence signal removes the structure and the cell appears as a homogenous object with a strong contrast between the background and object,

improving the tracking of the optically trapped T-cell. **B:** Representative images showing T-cells trapped with a single (top row) or triple (bottom row) spot trap. Red dots represent the position of each focal point of the laser and the highlighted phase-bright point (yellow dot) shows the region of the cell that was tracked whilst moving the stage. This was tracked using Volocity (PerkinElmer, USA). The stage was moved 200µm back and forth in the x direction. **C:** The position of the trapped T cell versus time when trapped with a single (black line) or triple (red line) spot trap when the sample stage is being moved.

Having established that by fluorescently labelling T-cells a more suitable image could be obtained to accurately track the position the trapped T-cells, and having shown that using a triple spot trap could minimise cell roll which again could improve the accuracy in tracking (**Figure 3.11** and **Figure 3.13**) the centre of mass tracking algorithm was used to track the position of the cell over time and save its x and y coordinates.

Figure 3.14 shows problems associated with cell roll and difficulty in tracking. When optically trapping an unstained T-cell using a single spot trap there is a very large variance in x and y coordinates over time. This could be down to either cell roll or problems in obtaining a suitable image to accurately track a trapped T-cell. Once tracking has started, the bright features which initially had a high contrast compared to the background, are changing throughout the tracking period. This comes from the cells position changing as it rolls within x, y and z planes, and hence this is detected in the centre of mass tracking leading to misleading coordinates in x and y position, (**Figure 3.14**, **panel A**, **red**). By staining a T-cell with CFSE, the image appears homogenous (**Figure 3.14**, **panel A**, **blue**). It is possible that the cell is still rolling but this does not show up in the fluorescent image since the stain is uniform across the whole cell. Furthermore, by using a triple spot trap the issue of obtaining a suitable image to track is resolved. Firstly, the cell roll is minimised and as a result the bright features compared to background do not change. This is due to

the T-cell being fixed at 3 points and therefore cell roll within x, y and z plane is prevented. Overall results show an improved accuracy of tracking for either un-stained T-cells or CFSE stained T-cells, (**Figure 3.14**, **panel B**, **red**, **panel B**, **blue**) when trapped with a triple-spot trap compared to a single-spot trap. This data set also compares well to 6 μm bead of similar size, (**Figure 3.14**, **Panel A**, **Panel B**, **black**).
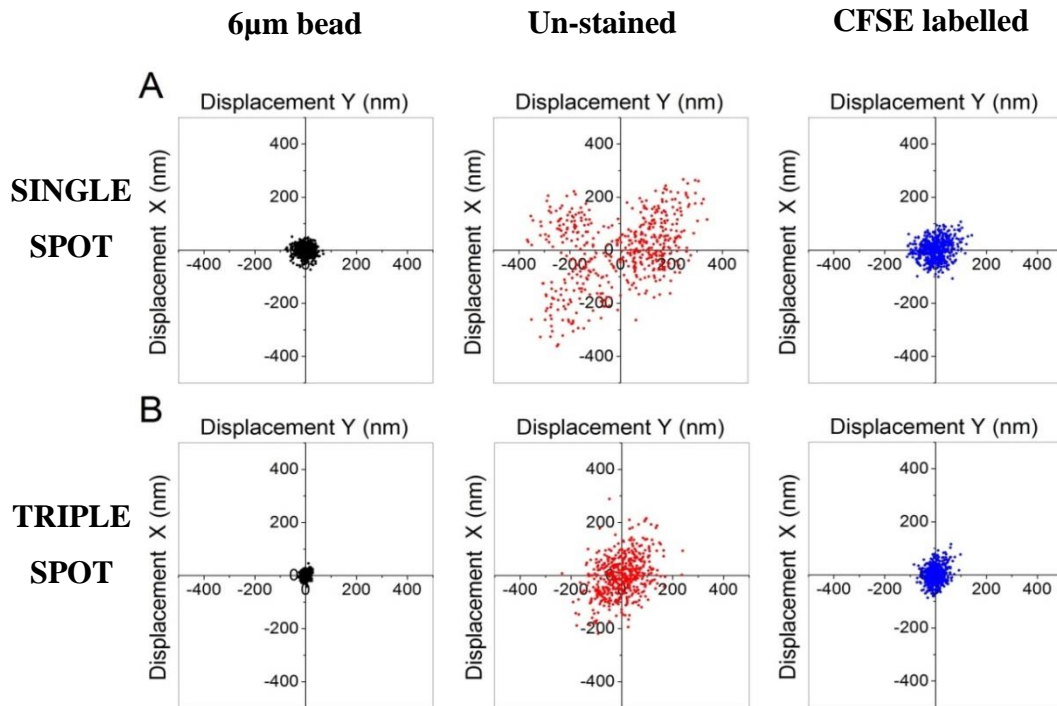
Figure 3.14: <u>Scatter plots comparing single and triple spot traps used to trap stained and un-stained cells.</u>

Scatter plots comparing the postion determined by a centre of mass tracking algorithm of an optically trapped 6μm diameter polystyrene bead (black dots), un-stained T-cell (red dots) and CFSE stained T-cell (blue dots) in **A:** single **B:** triple spot trap. Each dot represents x and y coordinates over time.

Having now shown that labelling a T-cell with CFSE and/or using the triple spot trap improved the accuracy of tracking position using the centre of mass tracking

algorithm, the two improvements were used to determine if trap stiffness calibration was also improved. To achieve this, individual cells or beads were first trapped. Then LabView code written in-house determined the displacement of the trapped particle from the centre of the trap over time, using the centre of mass tracking algorithm (as discussed in **Section 3.3.2.1**). This was converted to a time-averaged square displacement from the centre of the trap $\langle x^2 \rangle$ and applied to **Equation 3.6** to determine stiffness of optical tweezers.

Trap stiffness was determined for 36 individual beads, un-stained T-cells and stained T-cells trapped with a single or triple spot trap at each laser beam power (54 mw, 141 mW, 221 mW and 293 mW respectively). The average stiffness for the measurements was determined from the 36 measurements and a graph of trap stiffness versus power produced. Trap stiffness should be linearly proportional to laser beam power with zero power resulting in zero trapping force.

Indeed as shown in **Figure 3.15**, trapping an un-stained T-cell using a single spot trap results in low value for trap stiffness and large standard deviation when compared to the values obtained for the optically trapped bead.

Using a triple spot trap to minimise cell roll or fluorescently labelling a T-cell with CFSE, the accuracy in tracking was improved (**Figure 3.14**). This meant that the stiffness of the optical trap could be calculated more accurately, with this data set comparing well to a 6 μm bead of similar size.
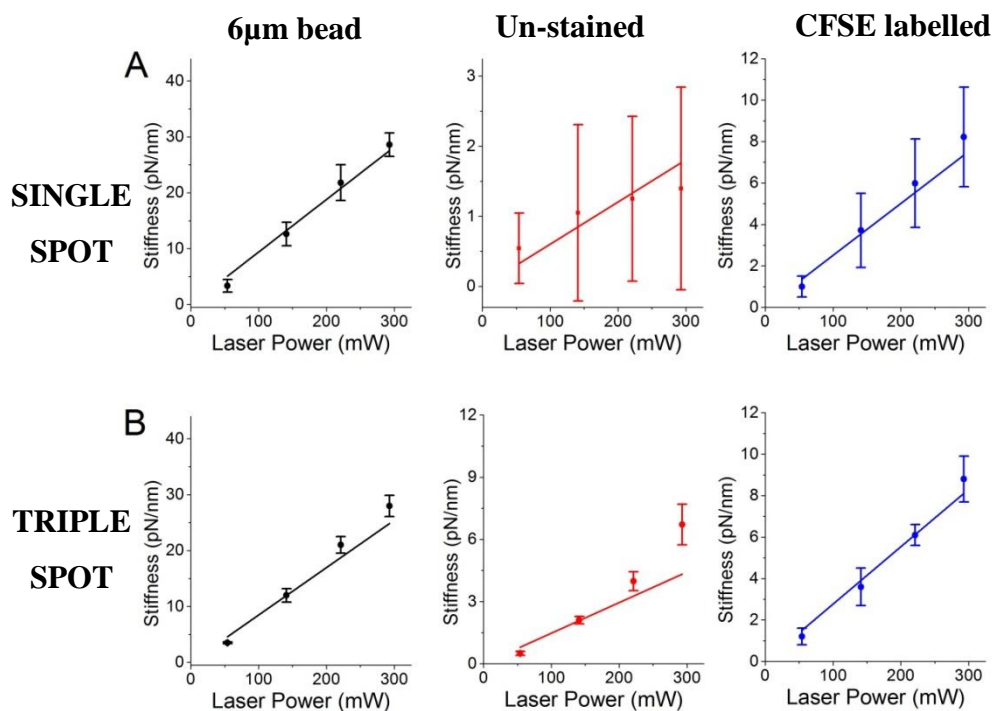
Figure 3.15: <u>**Calibration of optical trap using a centre of mass tracking algorithm.**</u>

Shows calibration plots of trap stiffness versus laser beam power for an optically trapped 6 μm diameter polystyrene bead (black line), un-stained T-cell (red line) and a CFSE stained T-cell (blue line) for **A:** single and **B:** triple spot trap. Data represents the mean trap stiffness ± SD of 36 T-cells or beads for each condition with linear fits going through the origin.

Overall I have presented two methods that would improve the tracking of an optically trapped T-cell meaning that the accuracy in the calibration of the optical tweezer system was improved. From **Figure 3.15** it is clear that both the triple spot trap and fluorescently staining the T-cell reduces error and improves accuracy in measuring the trap strength. Using the fluorescent method, the cell can be tracked at a rate of 35 Hz, much lower than the tracking rate using bright field centre of mass tracking (triple spot) at 1.1 kHz. Furthermore, there can also be problems associated with photobleaching using the fluorescent method. The choice of approach will

ultimately depend on the imaging and trapping system. Not all optical tweezer systems will have a SLM to produce three traps and similarly not all systems will have fluorescence imaging capabilities. Nevertheless, the two approaches presented covers both of these issues.

3.3.3 T-cell viability.

It is now common to trap with a laser beam wavelength between 800nm to 1064nm, often known as the "therapeutic window". Although working with a laser wavelength at 1064nm, the precise mechanisms of photo-damage are not well understood, meaning that cell damage may be caused by a trapping laser and could be cell specific. This is discussed further in **Chapter 1 Section 1.16**. Therefore, it was necessary to conduct a series of viability studies to understand the level of photo-damage and avoid "optucition", a term first coined by Ashkin describing the laser-induced death of specimens [184,185].

Cell viability changes have been widely studied *in vitro* and *in vivo* and many features of a cell undergoing apoptosis or necrotic death well known [374]. I carried out a viability test to determine if the optical tweezer system could optically trap T-cells without compromising their viability using fluorescent viability marker, propidium iodide (ex 535 nm, em 617 nm) as a marker of necrosis. Just prior to trapping experiments propidium iodide (PI) (1 µg/ml) was added to sample.

Initially a high laser power ~400 mW was used to increase the chances of a T-cell becoming necrotic in order to determine the feasibility of using propidium iodide as an indicator of cell death in this system. From **Figure 3.16**, a T-cell which loses its membrane integrity can incorporate propidium iodide and the fluorescence signal can be detected clearly by the colour camera.
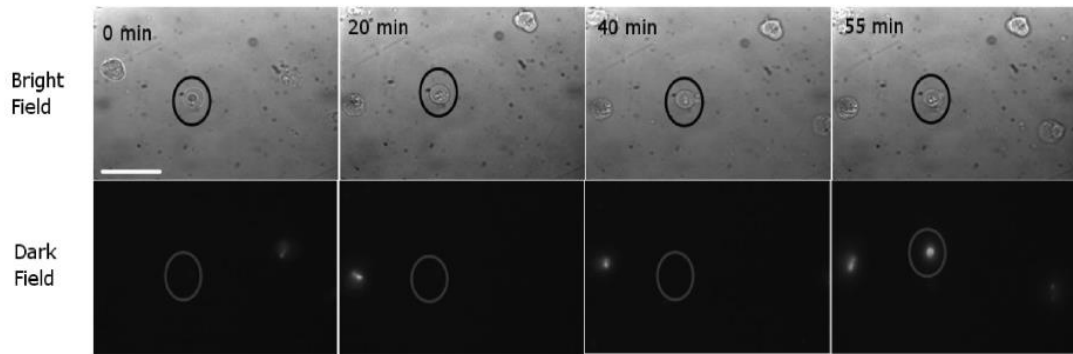
Figure 3.16: <u>**Feasibility of Propidium Iodide as a marker of cell death.**</u>

Shows a T-cell trapped with a high intensity laser beam over time. After approximately 55 mins the T cell's viability is compromised, the membrane breaks down and it becomes propidium iodide positive.

Once the suitability of propidium iodide had been confirmed, lower powers of 180 mW and 30 mW (at the sample) were tested in a single spot trap. Alternatively, the SLM was used to create three laser spots of approximately equal power, positioned just inside the cell membrane with a total power of 180 mW and 30 mW. Once an individual T-cell was trapped using the triple spot trap, the position of each spot was independently adjusted to be within the cell's membrane to allow for variations in cell size. This way, the same laser power was applied to the trapped T-cells within a single and triple spot trap. It was hypothesised that by spreading out the total power of the laser over the cell, the temperature rises that occur during trapping would be less harmful and cell viability would be maintained.

Shown in **Figure 3.17**, the viability of the T-cells was significantly improved using a triple spot trap. Fitting a sigmoid function to lines representing 180 mW gave a mean time to 50% cell death of 70 minutes for a single-spot trap and 83 minutes for the triple-spot trap. The cell death at laser power 30mW was too low to make any comparisons between the different beam profiles. A preliminary test using Annexin V in combination with propidium iodide confirmed that cell death was due to necrosis and not apoptosis. This confirmed that a stress response was being induced

in the trapped T-cells due to the laser beam causing a sudden necrotic death. When using powers of 30mW or less at the sample we can be confident that the cell will remain viable for at least 60 minutes.
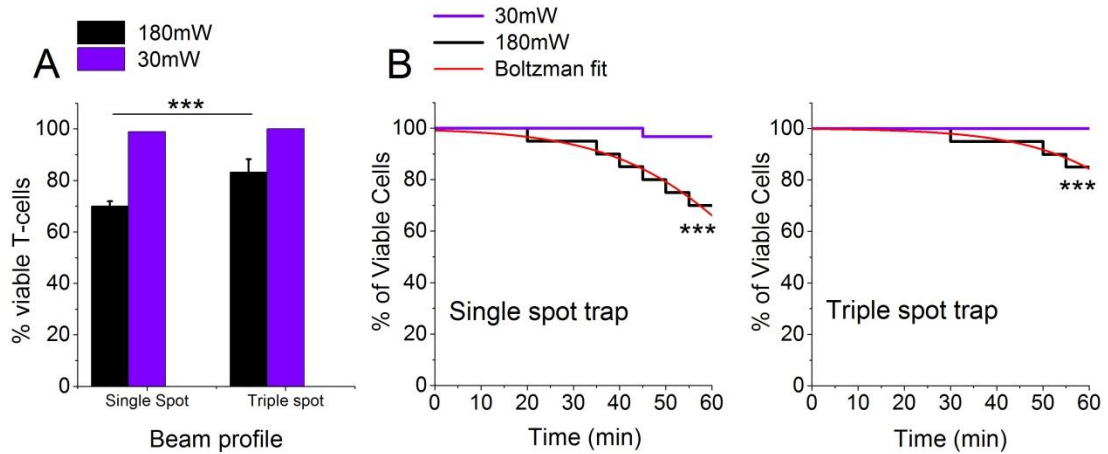
Figure 3.17: <u>Viability of optically trapped T-cells assessed by the uptake of propidium iodide.</u>

T-cells were continuously trapped with a single or triple-spot trap. **A:** Shows the mean % of viable cells (n = 30) continuously trapped for 60 minutes in a single or triple-spot at 30 mW (violet bars) and 180 mW (black bars) measured at sample. **B:** Fitting a sigmoid fit with Boltzmans function to lines representing 180 mW gave a mean time to 50% cell death of 70 minutes for a single-spot trap and 83 minutes for the triple-spot trap. Cell death was significantly reduced when using a triple-spot trap at 180 mW compared to the single spot trap at the same power. n = 30 cells for each condition (*** $p \leq$ 0.0005 by un-paired t-test).

3.4 Manipulating and quantifying the interaction forces between T-cells and DCs.

The optical tweezer system could directly trap T-cells and, by using a novel triple spot trap, precise position and orientation control was possible and cell viability was significantly improved. Therefore, all further experiments carried out, used the "triple spot trap", unless stated otherwise. Furthermore, the force of the tweezers were calibrated whilst trapping T-cells, permitting manipulation and quantification of the interaction forces between ovalbumin (OVA)-specific OT-II T-cells and an antigen presenting DC.

3.4.1 Which calibration method to use?

The choice of method to use for quantifying the force of interaction between T-cells and DC depends on the width of the optical trap, or in other words the distance over which the behaviour of the trap behaves like a spring, where the trap stiffness is linear to the displacement from equlibrium. For distances from the trap centre, where restoring force is proportional to displacement, then the theory of equipartition can be used. If, however, the object is far from the trap centre, where force is no longer proportional to displacement, then the escape force method should be used to give the total force of the optical trap

Shown in **Figure 3.18** is the displacement of an optically trapped 6 μm diameter bead from equilibrium when subjected to different viscous drag forces and trapped using a triple spot trap. A 6 μm bead was first trapped and the speed of the stage was set. The stage was then set to continually move at the set speed, in order to displace the trapped particle from centre of trap and track the displacement using centre of mass tracking (discussed earlier in **Section 3.3.2.1**). This was repeated for increasing stage speeds (as indicated in **Figure 3.18**) until the trapped bead fell out of the trap. The displacement of the bead over time can be seen in **panel A** and in **panel B** the force, calculated using Stoke's Law (**See equation 3.4**), is linearly proportional to this displacement indicating that the optical tweezer system is

behaving like a spring and obeying $F = -kx$, with k the trap stiffness. The maximum displacement of the trapped bead before the applied force was too great and the bead fell out of the optical trap was just below 2 μm.
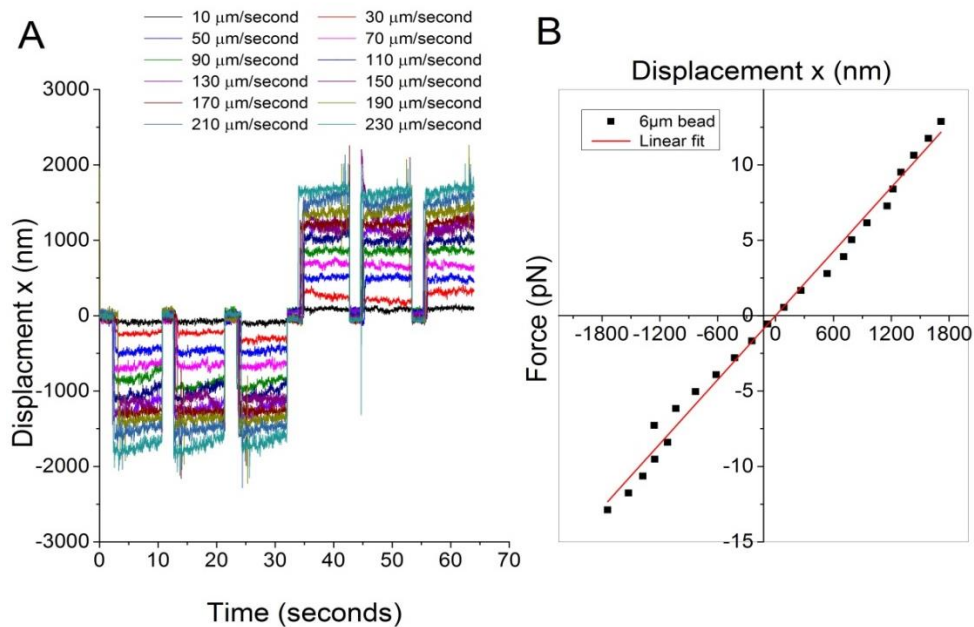
Figure 3.18: <u>**Displacement of 6 μm bead from the optical trap centre.**</u>

The microscope stage was moved to exert an external viscous drag force on the bead and the displacement of the bead from equilibrium due to the external force measured. **A:** Shows the displacement from centre of trap at increasing velocities and therefore increasing viscous drag forces. **B:** Displacement of bead from trap centre (from **A**) vs the applied viscous drag force (determined by **Equation 3.4**, shown earlier).

From **Figure 3.18**, it is clear that an equipartation approach should be used to measure external forces when distances between the cell and the trap centre are less than 2 microns and an escape force method should be used for distances greater than 2 microns where the total trapping force is required. As discussed next in **Section 3.4.2**, after bringing the cells into contact the trap was moved 5 μm from the cell pair

and therefore, the escape force method would be applicable. All interaction force measurements in the subsequent chapters to follow refer to the calibation graph (**Figure 3.10**) using the escape force method.

3.4.2 Quantifying the interaction force between T-cells and DCs.

The key to initiating an effective adaptive immune response is through the recognition of specific antigen displayed on the surface of professional antigen presenting cells by antigen specific T-cells. This is a highly sensitive and a dynamic process [9,23,74].

In the previous sections an optical tweezer system was developed to directly trap T-cells. It was then optimised to improve the stability of trapping and the viability of T-cells. Using optically trapped T-cells, the system was calibrated using two calibration methods with the escape force method being the appropriate method to use for quantifying subsequent interaction forces between T-cells and DC. Next, investigations were carried out into whether the optical tweezer system could be used to quantity the interaction force between T-cells and DC for the first time.

3.4.2.1 Experimental design – Manipulating T-cell and DC interaction.

To quantify the interaction force an experimental method was first developed that allowed T-cells to be trapped whilst precisely controlling T-cell and DC interaction. It was important to ensure that a T-cell was truly naïve and had not previously encountered a DC. Therefore OVA-pulsed (or un-pulsed) DCs were seeded into an Ibidi μ-slide VI $^{0.4}$ flow channel slide. The slide has 6 pairs of chambers that were connected via a flow channel and was used in all experiments looking at the initial contact between T-cells and DCs. The flow channel allowed T-cells to be added to one end of the channel and, due to the flow of medium within the channel, the T-cells would enter the field of view where they could be optically trapped and brought into contact with a DC on the surface of the microscope slide. This approach

minimised the chances of a naïve T-cell encountering a DC before subsequent trapping and force measurements were to follow.

A series of images demonstrates the experimental procedure used in order to manipulate the interaction as well as quantifying the interaction force, as shown in **Figure 3.19**. An individual OT-II OVA-specific T-cell was captured using the triple spot optical trap (**Figure 3.19 – panel i**) and brought into contact with a DC (**Figure 3.19 – panel ii**), directly controlling the initial antigen-specific recognition by naïve T-cells. Immediately after contact, the trapping laser shutter was closed and the cells allowed to interact for a given length of time (**Figure 3.19 – panel iii**). Subsequently, the trap was reinstated 5 μm from the T-cell and the laser power progressively increased until the two cells were separated (**Figure 3.19 – panel iv, v and vi**). The laser power at which the T-cell was pulled away from the DC was recorded and the force applied determined from the earlier calibration plots (**Figure 3.10**). Whilst the calibration of the tweezers was not carried out before each experiment, a power meter was used to measure the power prior to each experiment, to confirm there was no drift in laser power To ensure trap was re-instated 5 μm from T-cell, a mark was placed on computer monitor, indicating where trapping beam was after being blocked. The cells (now in contact) were moved 5 μm from the position of the trapping beam using the motorised microscope stage. If the T-cell migrated towards the beam during cell-cell contact, the stage was used to maintain a distance of 5 μm between the T cell and the focal point of the optical trap.
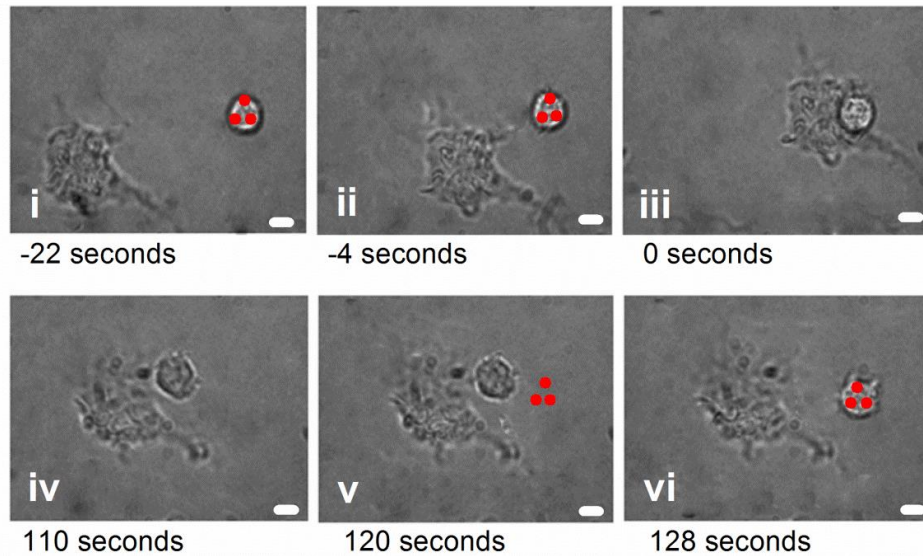
Figure 3.19: <u>**Approach used to determine the interaction forces between antigen-specific T-cells and dendritic cells.**</u>

The optical trap (red spots) was used to bring a T cell into contact with a DC (**i**) As soon as contact was made (**ii**), the trap was blocked and the cells left to interact for a given period of time (**iii - iv**). Subsequently, the trap was re-instated 5 μm from the T-cell (**v**) and power of the laser beam and hence the trap strength increased until the T-cell was pulled away from the dendritic cell and into the trap.

Having now established a technique to control the interactions between T-cells and DC (**Figure 3.19**), I next sought to validate the approach and quantify antigen-dependent interactions. In the absence of antigen, the DC/T-cell interactions were easily disrupted and required a median force of only 3.3 pN (± 1.4 pN) to separate T-cells from DCs (**Figur**e **3.20**, empty symbols). However, disruption of contacts between naïve OVA-specific OT-II T-cells and OVA-pulsed DCs, required a force 2.5 times greater 8.5 pN (± 5.7 pN) (p = 0.001) 30 seconds after initial contact (**Figure 3.20**, filled symbols). Thus, this novel approach is able to accurately quantify the force of interaction between live cells, as well as providing the potential to prematurely attenuate normal T-cell activation. This may allow potential

investigations to be carried out, to investigate the duration of interaction and its effect on T-cell activation.
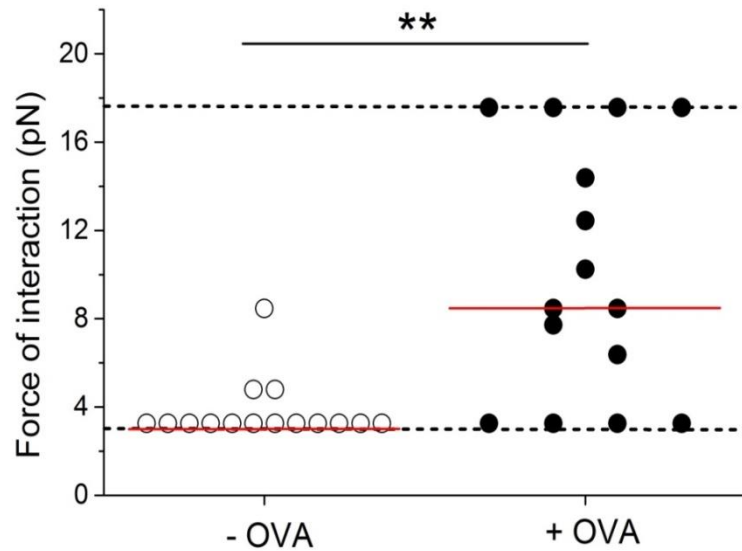
Figure 3.20: <u>Quantification of the interaction force between OVA specific CD4$^+$ T-cells and DC after 30 seconds of interaction.</u>

Bone marrow-derived DCs were pulsed with 1 mg/ml OVA (filled symbols) before addition of OVA-specific OT-II T cells. Control cells remained un-pulsed (empty symbols). The force required to separate T-cells and DCs after 30 seconds of interaction was determined. Data shows the force required to separate individual cell interactions with the median indicated (red line). Dotted lines show the minimum and maximum forces that could be measured (** p ≤ 0.005, by Mann Whitney test).

Finally, the potential of this novel approach in testing therapeutic interventions that may alter the force of interaction between T-cells and DCs was assessed. Stimulation of DCs with lipopolysaccharide (LPS) increases surface expression of MHC Class-II, co-stimulatory and adhesion molecules [11]. Conversely, inhibition of ERK kinase activity represents a potential target for modulating T-cell activation therapeutically [375,376] and may attenuate immune synapse development following

antigen-recognition [327]. Using the optical trapping approach, an increase in the median force from 11.9 pN (± 5.2 pN) to 16.9 pN (± 2.3 pN) was evident 120 seconds after OVA-specific OT-II T-cell recognition of antigen presented by LPS-stimulated DCs relative to interactions with un-stimulated OVA-pulsed DCs (**Figure 3.21**). Conversely, by pre-treating OVA-specific OT-II T cells with the ERK inhibitor FR180204, the force of interaction with antigen-presenting DCs was significantly decreased to just 3.3 pN (± 1.7 pN) (**Figure 3.21**), thus validating the approach to measuring live cell-cell interaction forces. Importantly, this novel system demonstrates the feasibility of this technology in screening pharmacological candidates for attenuating or extenuating T-cell signalling.

Although the system could successfully quantify the interaction forces between T-cells and DC, there was a floor and ceiling affect associated with this measurement. This would limit the range of forces that could be measured. The minimum force of the optical trap was 3.3 pN (relating to a laser beam power at the sample of ~ 54 mW) and the maximum force due to the maximum power available from the laser beam (~ 293 mW at the sample) was 17.6 pN. Each data point at the minimum force represented cells that could be pulled apart immediately after un-blocking laser before starting to incrementally increase the laser power. Furthermore, the data points at the maximum level represented cells that could not be pulled apart, once laser power had been increased to the maximum laser power available. Due to the skewed distribution, data in subsequent chapters are presented as scatter plots (showing the force taken to separate individual cell pairs) along with the median value indicated. In certain experiments, many cells were above or below the limits of detection and, following consultation with a statistician, such skewed data was routinely analysed using a Mann Whitney test. Whilst these limits of detection are present throughout the remaining experiments, they are only indicated in **Figure 3.18** (dotted line in **Figure 3.18**) for simplicity.
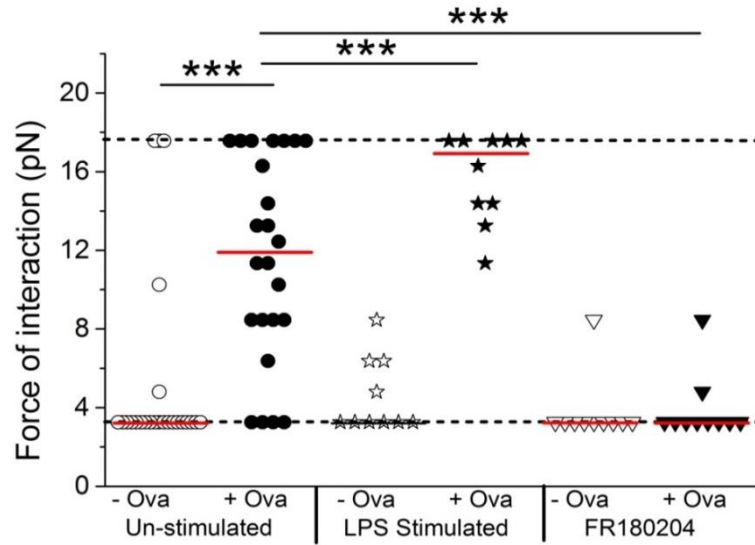
Figure 3.21: <u>Quantification of the interaction force between OVA specific CD4$^+$ T-cells and DC after 120 seconds of interaction.</u>

Bone marrow-derived DCs were pulsed with 1 mg/ml OVA (filled symbols) before addition of OVA-specific OT-II T cells. Control cells remained un-pulsed (empty symbols). The force required to separate T-cells and DCs after 120 seconds of interaction was determined. Cell interaction forces were measured as above, in presence or absence of Ovalbumin antigen, presence or absence of LPS, or when T-cells were pre-treated with 10 µM of ERK-inhibitor FR180204. Data shows the force required to separate individual cell interactions with the median indicated (red line). Dotted lines show the minimum and maximum forces that could be measured. (*** p $\leq$ 0.0005, by Mann Whitney test).

3.5 Summary

This chapter discusses the development and implementation of an optical tweezer system. Once the system was developed it was used to successfully manipulate the interaction between T-cells and DC, whilst quantifying their interaction strength.

Implementing a SLM to optically trap live cells using novel triple-spot trap improved the level of control over the cells, whilst also increasing viability.

Our results fit well with those reported previously [377,378] demonstrating a force of interaction in the piconewton range within two minutes of cell-cell contact. Optical tweezers are therefore ideally suited to this measurement scale and probing the early cellular interaction – as can be seen in **Figure 3.20** and **Figure 3.21**, the maximum force we are able to apply is 17.6 pN with a laser beam power of 292.8 mW at the sample.

The system successfully detected changes in the force of interaction associated with pharmacological inhibitors of cell signalling, and therefore this approach will find wide-ranging applications.

Having achieved my overall aim of developing and building an optical tweezer system that could directly trap T-cells to manipulate their contact with DCs and quantify their subsequent interactions, I was now in a position to apply this approach to a variety of experimental questions. As outlined in the introduction, such an approach provides a unique tool to understand how T-cell/DC interactions are altered by modified peptide antigen, by the local environment or by altered signalling capacity in either cells. In the subsequent chapters, the approach developed above and summarised in **Figure 3.19** to **Figure 3.21** was applied to investigate the role of each of these factors in influencing the interaction forces and related to immune function using a combination of established methods.

Chapter 4 - Manipulating and quantifying immune cell interactions to understand the importance of L-arginine and T-cell function.

4.1 Introduction.

L-arginine is a semi-essential amino acid that plays a central role in regulating an immune response [268–270] . For many years, studies have demonstrated that L-arginine is essential for normal T-cell proliferation and function and in the absence of L-arginine there is impaired proliferation and cytokine production by T-cells [271,272]. As discussed in **Chapter 1**, studies have suggested that the strength and duration of interaction between T-cells and DCs is important for effective T-cell activation [75,148]. However, whether the impaired T-cell function in the absence of L-arginine is associated with an altered interaction between the T-cell and DC remains unknown.

A recent study compared the T-cell/DC interaction *in vivo* to decipher differences in the initiation of T-cell responses under conditions of tolerance or activation. They showed that T-cells initially arrest on APCs in both tolerance and activation conditions. However, this arrest phase was maintained in activation conditions, unlike tolerance conditions where the arrest phase progressed into a transient phase of interaction [36]. This shows the importance of a strong, long term interaction between T-cells and APCs for efficient T-cell clonal expansion *in vivo*. A strong interaction force may be required to help sustain a long term contact between the cells, influenced by the formation of the immunological synapse. The formation of this structure overcomes the relatively low affinity of the TCR and MHC, and interaction forces between T-cells and DCs are determined by its formation [167]. Yet, it has been shown previously that when stimulating T-cells in absence of L-arginine, the immunological synapse fails to form [289]. Therefore, the impaired proliferation and cytokine production of T-cells in the absence of L-arginine may be associated with the inability of T-cells to form a stable contact with a DC for a sufficient length of time. Therefore, the ability to quantify the interaction forces between cells in the absence of L-arginine may allow this hypothesis to be investigated further.

In the previous chapter, I successfully developed an optical tweezer system that could trap cells without compromising viability, allowing direct manipulation of T-cell/DC interactions. Further to this, I demonstrated that the system could be used to

measure the interaction forces between individual cells, quantifying antigen-specific cell-cell contact as well as validating this approach by showing changes in the forces when either using LPS-stimulated DCs or when blocking T-cell signalling (**Chapter 3, Figure 3.20 and 3.21**). These validations suggest that such an approach can be used to determine and test the importance of a number of factors on the force of interaction between T-cells and DCs. As highlighted above, these interactions may be altered in the absence of L-arginine. Therefore, in order to test this hypothesis, I applied optical tweezers to quantify these forces directly. These studies aimed to provide further information on the mechanisms that may be involved in the impairment of T-cell responses upon depletion of L-arginine.

Two areas of particular relevance for the role of L-arginine is in understanding of parasitic diseases, such as *Leishmania*, and in tumor development, where L-arginine plays major roles in determining host defence and resistance [379–382]. T_H2 cytokines can induce high levels of arginase activity in *Leishmania* infection, causing a local depletion of L-arginine, and this correlates with uncontrolled replication of parasites within non-healing BALB/c mice but not in healing CBA mice [282,380]. Furthermore, an increased arginase activity has been described in patients with tumors, resulting in the production of ornithine and polyamines which help sustain rapid cell growth [383]. It is interesting to note that the depletion in L-arginine has been implicated in the development of immunological tolerance induced by tumors [383]. Myeloid-derived suppressor cells are found in tumors as well as the peripheral blood where they can deplete normal levels of L-arginine potentially preventing an immune response to tumors. Thus, understanding more about the role of L-arginine may provide novel therapeutic approaches to treating *Leishmania* but also enhance the efficiency of immunotherapies in treating cancer.

4.2 Results.

4.2.1 Altered T-cell function in the absence of L-arginine.

To examine the effect of L-arginine depletion upon T-cells and DCs, I first sought to refine previous studies to use OT-II OVA-specific T-cells and ovalbumin antigen, rather than stimulating T-cells with anti-CD3 plus anti-CD28 coated micro-beads [270–272,287]. Although some studies have taken advantage of using OT-I and OT-II mice and shown that stimulation of OVA-specific T-cells in the absence of L-arginine resulted in impaired T-cell responses [288,384] these were not looking into the effects of L-arginine on T-cell/DC interaction, and therefore the proposed model system had to be validated.

The first experiment was designed to determine whether the absence of L-arginine results in impaired T-cell proliferation and production of cytokines. Experiments were performed using custom RPMI 1640 media, which contained no L-arginine (subsequently referred to as "depleted media"; a generous gift from Dr Pascale Kropf), or media containing L-arginine (200mg/L) ("control media"). Bone marrow-derived DCs were prepared as previously described (**Chapter 2, Section 2.4.4**), and pulsed overnight with 1 mg/ml of ovalbumin in control media. In this way, differences in cell-cell interactions were only associated with effects on T-cells, and not due to alteration of DC phenotype, or the uptake or presentation of OVA by DC, all of which could potentially be affected by the depletion of L-arginine. Following overnight antigen pulse, and prior to the addition of T-cells, DCs were washed at least 3 times in either depleted media or control media to remove free L-arginine and any remaining soluble OVA antigen. DCs were then plated at 5×10^5 cells per well and used to stimulate OVA-specific OT-II $CD4^+$ T cells for 48hrs. Cells were then analysed for proliferation (by staining for Ki-67, a proliferation marker that is present at all stages of cell cycle except on resting cells) and effector function (by measuring cytokine secretion), as described in **Chapter 2**.

As shown in **Figure 4.1 panel A**, there was a significant decrease in the proliferation of OVA-specific CD4$^+$ T-cells in depleted media compared to control media. The proportion of proliferating T-cells following stimulation with OVA pulsed-DC in control media was around 70%. However, in the absence of L-arginine, OVA-specific CD4$^+$ T cell proliferation was impaired, with only around 10% of cells expressing Ki-67. Overall these results validate that L-arginine depletion reduces the proliferative response of antigen-specific T-cells in agreement with previous reports [270–272,287].

Supernatants from the above cultures were collected and analysed for cytokine production (**Figure 4.1**). A similar pattern to the reduction in T-cell proliferation was observed, with a significant decrease in the OVA-specific production of both IFN-γ (**Panel B**) and IL-2 (**Panel C**) when T cells were stimulated in the absence of L-arginine. Interestingly, antigen-driven IL-2 production was significantly reduced, despite a previous study suggesting that this cytokine is not affected by depletion of L-arginine upon the stimulation of T-cells [271].
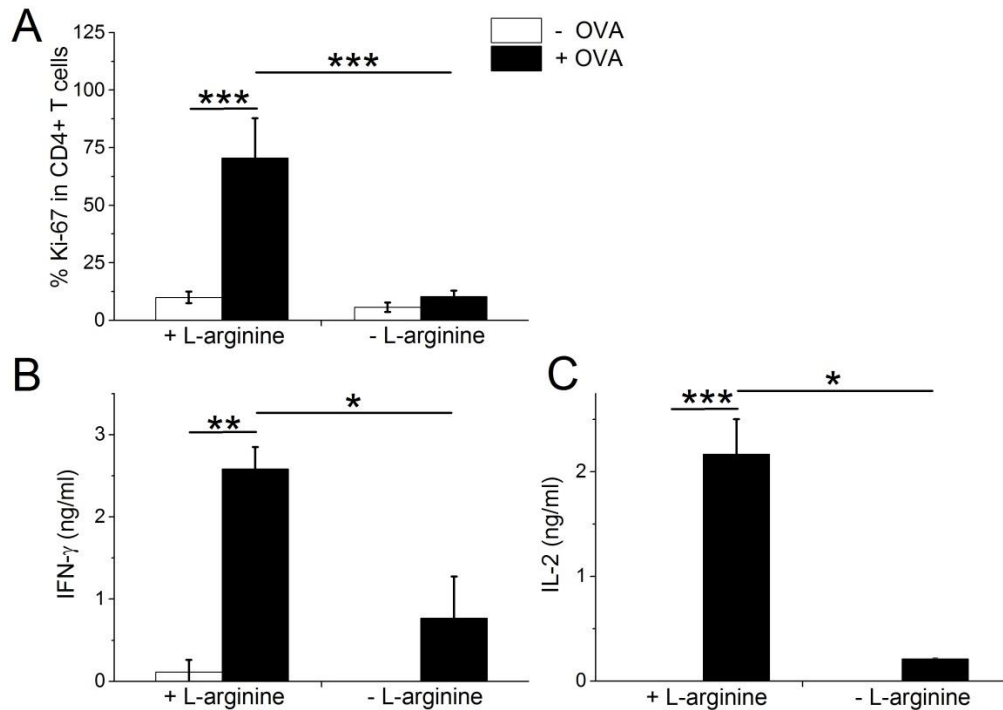
Figure 4.1: <u>Analysing CD4 $^+$ T-cell function in the presence and absence of L-arginine.</u>

T-cells (5 x 10^5) were co-cultured in 24 well plates with un-pulsed DC (5x10^5), (white bars) or antigen-pulsed DC (5 x 10^5), (black bars). Results shown are the mean of **A:** proliferation, quantified by flow cytometry **B:** IFN-γ cytokine production, measured by ELISA **C:** IL-2 cytokine production measured by Luminex. Results are of duplicate cultures of 2 independent experiments ± SD. (* p ≤ 0.05, ** p ≤ 0.005, *** p ≤ 0.0005 by un-paired t-test).

Having shown L-arginine depletion has a profound effect on the proliferative capacity and cytokine production of T-cells, I next wanted to determine whether this was due to a complete failure of antigen-recognition in L-arginine depleted media, subsequently preventing all aspects of T-cell activation – particularly earlier activation signals. To do this I sought to determine whether early activation of T-cells was affected by L-arginine depletion by analysing up-regulation of the early activation marker CD69. The above experiment was repeated and T-cells were

analysed for expression of CD69 (an early-activation marker) at 2, 4, 6 and 24 hrs following antigen recognition. As expected there was a marked up-regulation of CD69 on OVA-specific CD4^{+} T-cells following recognition of antigen in control media, with 64% of antigen-specific cells expressing CD69 by 24 hrs. Interestingly, similar results were observed when T-cells were activated in L-arginine-depleted media, with up to 63% of antigen specific cells expressing CD69 after 24 hrs (**Figure 4.2**).
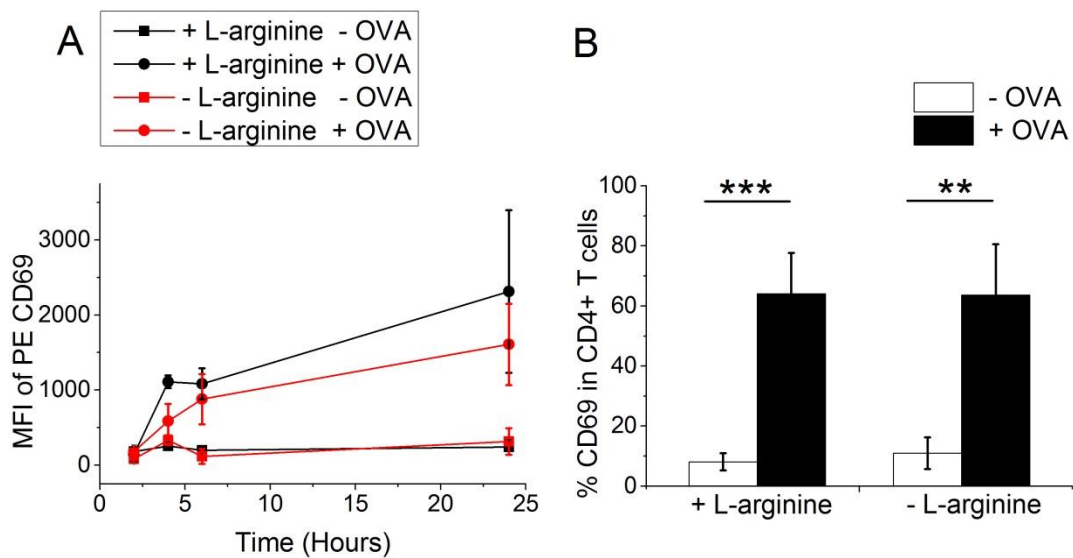
Figure 4.2: <u>**Analysing CD69 up-regulation on CD4 [+] T-cells in the presence and absence of L-arginine.**</u>

T-cells (5 x 10^5) were co-cultured in 12 well plates with un-pulsed DC (5 x 10^5) or antigen-pulsed DC (5 x 10^5). CD69 up-regulation in gated CD4^{+} population was measured by flow cytometry. **A:** MFI of CD69 over time, following culture with antigen-pulsed or un-pulsed DC in the presence or absence of L-arginine, representative of duplicate cultures, of 1 independent experiment ± SD. **B:** Same as above, except mean % of CD69 up-regulation after 24 hr period, representative of duplicate cultures, of 2 independent experiments ± SD. (** p ≤ 0.005, *** p ≤ 0.0005 by un-paired t-test).

Together, these results demonstrate that whilst the absence of L-arginine reduces the ability of T-cells to proliferate or produce cytokines following antigen-recognition, they can still become activated and up-regulate expression of CD69, as previously described [271,380]. *In vivo* imaging has shown that T-cells can interact with DCs transiently, during which time there is up-regulation of CD69 [9,80], whereas a longer interaction is required for proliferation of T-cells and cytokine release [148]. In the absence of L-arginine T-cells coming in contact with antigen bearing DCs demonstrate these early signs of activation, but fail to acquire effector functions and this may be associated with the strength or duration of cell interactions. The optical tweezer system was therefore used to quantify the interaction force between T-cells and DC in depleted media relative to forces in control media.

4.2.2 Quantifying the interaction forces between CD4$^+$ T-cells and DCs in control and L-arginine depleted media.

Having determined that the absence of L-arginine alters the normal response of OVA-specific T-cells to antigen, the next step was to quantify the interaction force between T-cells and DCs in depleted media compared to control media. To date this would be the first time that this has been investigated. The initial force of interaction was measured as described previously (**Chapter 3, section 3.4.2.1**), using the optical tweezers to first manipulate an individual OVA-specific CD4$^+$ T-cell into contact with a DC and then to quantify the force after 2 minutes of interaction. As shown in **Figure 4.3 Panel A**, as expected, the interaction force between T-cells and DCs in control media was significantly increased in the presence of OVA with an increase in the median force of interaction from 3.3 pN ± 1.3 pN (un-pulsed) to 9.9 pN ± 4.8 pN (OVA-pulsed). Interestingly, there was a significant increase in the force of interaction when cells were analysed in L-arginine depleted media, compared to control media. Whilst there remained a clear antigen-dependent force of interaction in the absence of L-arginine (un-pulsed 7.4 pN ± 6 pN; OVA-pulsed 16.9 pN ± 5.3 pN), each of these values was significantly increased relative to the forces measured in their respective control media.

In earlier experiments, T-cells showed normal up-regulation of CD69 in L-arginine depleted media, but an impaired proliferation and function at later time points (**Figures 4.1 – 4.2**). For that reason, I hypothesised that the interaction between T-cells and DCs would be significantly lower after 6 hrs of co-culture in the absence of L-arginine. Previous work has highlighted that this is the minimum length of time T-cells need to interact with an antigen bearing DC *in vivo* in order for naïve CD4$^+$ T-cell clonal expansion [148].

To measure this, the experimental approach was modified slightly. DCs were pulsed with 1 mg/ml of OVA in control media and re-plated in 8 well Ibidi chamber slides at 1 x 10^5 total cells per well, containing depleted media or control media. Purified OVA-specific CD4$^+$ T-cells were added into appropriate chambers at 1 x 10^5 total cells per well. After 6 hrs co-culture, individual cell pairs were identified and the force required to separate a T-cell from a DC was quantified using the optical tweezer system. Interestingly, despite reducing the proliferative and functional capacity of OVA-specific CD4$^+$ T-cells, measuring the cell contact after 6 hrs of T-cell/DC culture showed a similar trend to the initial contact measurements, with an increased force of interaction in the absence of L-arginine, irrespective of antigen recognition (**Figure 4.3**, **Panel B**).

As expected, the interaction forces between T-cells and DCs in control media was significantly increased in the presence of OVA, with an increase in the median force of interaction from 3.3 pN ± 5.2 pN (un-pulsed) to 16.3 pN ± 6.2 pN (OVA-pulsed). In depleted media there was a clear antigen-dependent force of interaction (un-pulsed 12.4 pN ± 6.5 pN; OVA-pulsed 17.6 pN ± 4.9 pN), but each of these values was significantly increased relative to the forces measured in their respective control media. Furthermore many of the cell pairs within the depleted media samples could not be separated due to the interaction force being greater than the maximum force the optical tweezer system could apply. This issue was described earlier in **Section 3.4.2.1** and therefore data is presented with median and statistically analysed using Mann Whitney test. These results suggest a hitherto uncharacterised role for L-arginine in T-cell activation.
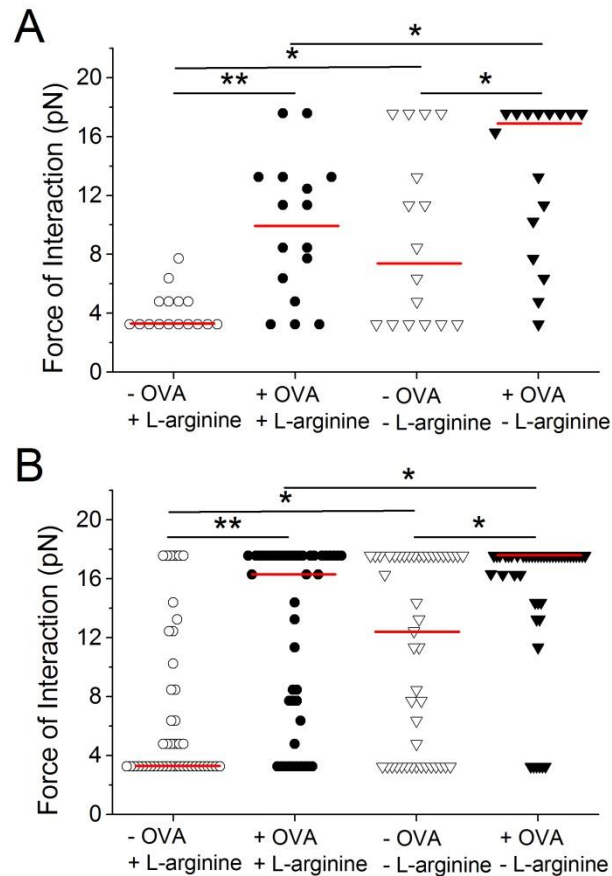
Figure 4.3: Quantification of the interaction force between CD4^{+} T-cells and DCs in the in the presence and absence of L-arginine.

DCs were pulsed with OVA and used to present to OVA-specific OT-II T-cells as desribed in **Chapter 3**. The force required to separate CD4^{+} T-cells and DCs after **A:** 120 seconds of interaction and **B:** 6 hrs of co-culture, was determined using calibrated optical tweezers. Data shows the force required to separate individual cell interactions of 3 independent experiments with the median indicated (red line) ([*] $p \leq 0.05$, [**] $p \leq 0.005$, by Mann Whitney test).

4.2.3 T-cell Ca^{2+} flux in control and L-arginine depleted media.

The results above suggest a higher interaction force between T-cell and DC in L-arginine depleted media relative to control media, irrespective of antigen recognition. Previous work has suggested the importance of calcium signalling within T-cells and its potential role in stopping T-cell migration following antigen recognition [115,133,385]. The next experiment investigated whether CD4$^+$ T-cells differ in their ability to calcium flux (following Phorbol 12-myristate 13-acetate (PMA) stimulation) when deprived of L-arginine. I hypothesised that if the intensity of calcium flux plays a role in inducing a stop signal within T-cells, there would be a greater intensity of calcium flux in T-cells cultured in depleted media than those in control media, accounting for the increased force of interaction observed above. Purified T-cells were stained with PerCP-conjugated anti-CD4 as well as the calcium indicator Fluo-4 AM, before washing and re-suspending in depleted media or control media. PMA was added immediately prior to analysis by flow cytometry, and the MFI of Fluo-4 AM in gated CD4$^+$ T-cells was determined after 1, 15, 30, 45 and 60 minutes. It is clear from **Figure 4.4** that no differences in the MFI of Fluo 4AM were observed in CD4$^+$ T cells, irrespective of whether L-arginine was present in the media or not. These results suggest that differences in the Ca^{2+} flux following antigen recognition are not responsible for the increase in interaction forces observed when T-cells are stimulated in the absence of L-arginine. However, the increase in Ca^{2+} levels in T-cells cultured in either depleted or control media, appears sufficient enough to up-regulate early activation marker CD69, which was not affected in depleted media (**Figure 4.2**), suggesting that T-cells deprived of L-arginine are not completely unresponsive.
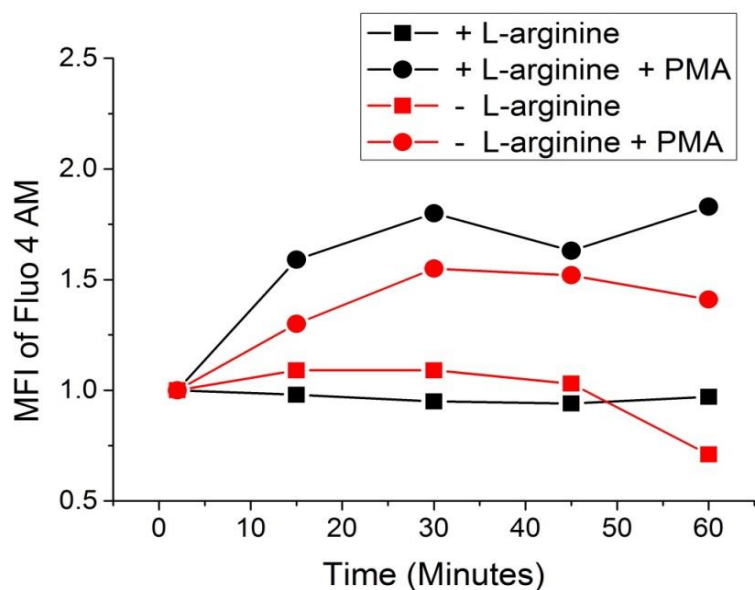
Figure 4.4: <u>**MFI of Fluo 4 AM in CD4$^+$ T-cells in absence or presence of L-arginine.**</u>

Purified CD4$^+$ were labelled with Fluo 4 AM calcium dye. PMA (10 µg/ml) was added into the appropriate samples (as indicated above). At time points 1, 15, 30, 45 and 60 minutes, samples were analysed using flow cytometry to determine the MFI of Fluo 4 AM. Results shown are representative of 3 independent experiments.

4.2.4 Quantifying the interaction forces between CD4$^+$ T-cells and DC deprived of L-arginine for 24hrs.

Within the literature, it has been suggested that there is a marked decrease in CD3ζ expression when T-cells are deprived of L-arginine. The level of expression has been desribed to gradually decrease over time, with only minimal expression of CD3ζ by around 24 hrs. Furthermore, following stimulation with cross linked anti CD3 and anti-CD28, CD3ε and CD3ζ are rapidly down-regulated at the surface and begin to re-express after 24 hrs, but this fails in the absence of L-arginine [271,386]. Having demonstrated profound changes in the force of interaction between DCs and T-cells only transiently deprived of L-arginine, I wanted to detemine the

consequences for CD4$^+$ T-cells cultured in the absence of L-arginine for a longer period of 24 hrs. As previous work has shown a down-regulation of CD3 chain, especially at 24 hrs when depleted of L-arginine, then I hypothesised that this may have further consequences in altering T-cell/DC interaction given the vital role of CD3 in generating an activation signal in T-lymphocytes.

Purified OVA-specific CD4$^+$ T-cells were cultured overnight in either control or depleted media. Subsequently, T-cells were washed, added to OVA-pulsed DCs, and the interaction forces quantified for both when T-cells were first brought into contact with a DC and after a further 6 hrs of co-culture.

From **Figure 4.5**, **Panel A** it is clear that the interaction forces throughout all samples are lower in comparison to the previous experiments (**Figure 4.3**). Despite there being a significant antigen-dependent increase in the interaction force in control media, the median force was increased to only 8.5 pN $\pm$ 4.4 pN (as opposed to 9.9 pN $\pm$ 4.8 pN measured previously) and was not fully restored after a further 6 hrs of co-culture (**Figure 4.5**, **Panel B**). These findings were similar when cells were pre-cultured overnight in depleted media, where the median interaction force was 6.4 pN $\pm$ 5.3 pN after 6 hrs of co-culture with DC - lower compared to 17.6 pN $\pm$ 4.9 pN force of interaction when measuring freshly-purified T-cells (**Figure 4.4**), showing that the incubation period of freshly isolated T-cells may be altering the function of cells.
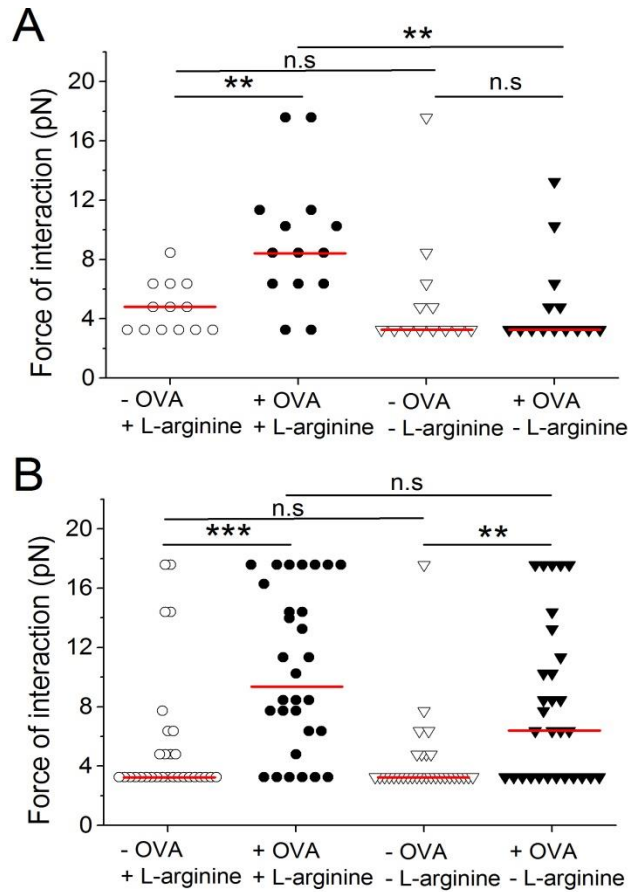
Figure 4.5: <u>Quantification of the interaction force between CD4^{+} T-cells and DCs in depleted or control media.</u>

OVA-specific OT-II T-cells were incubated for 24 hrs in either L-arginine containing media or L-arginine depleted media (as indicated). Following incubation cells were used to interact with un-pulsed or OVA-pulsed DCs. The force required to separate CD4^{+} T-cells and DCs after **A:** 120 seconds and **B:** 6 hrs of interaction was determined using calibrated optical tweezers. Data shows the force required to separate individual cell interactions of 2 independent experiments with the median indicated (red line) ([**] $p \leq 0.005$, ([***] $p \leq 0.0005$ by Mann Whitney test)

4.2.5 Analysing CD3 expression on T-cells deprived of L-arginine for 24 hours.

In **Section 4.2.4** interaction forces between T-cells and DCs were quantified after T-cells had been deprived of L-arginine for a period of 24 hrs. The interaction forces were lower compared to the forces of interaction between T-cells and DCs, partially deprived of L-arginine (**See section 4.2.2**). This altered interaction force could be down to reduced CD3 expression when cells are deprived of L-arginine for a longer period of time.

To confirm whether the lack of L-arginine resulted in decreased expression of CD3 in my setup, $CD4^+$ T-cells were cultured in either control or depleted media for 6 or 24 hrs before analysis by flow cytometry. Although there was a decrease in the expression of CD3 on T-cells after 24 hrs of culture in depleted media, this was also observed with cells incubated in control media (**Figure 4.6**). These results demonstrate that L-arginine depletion lowers expression of CD3 through time. However, within control media the same trend was shown and therefore could be down to another factor independent of L-arginine.
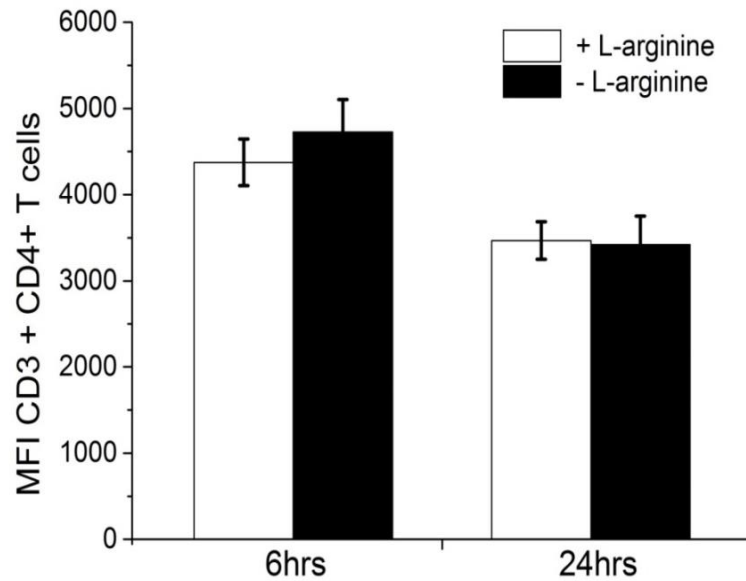
Figure 4.6: <u>CD3 expression on CD4$^+$ T-cells in the presence or absence of L-arginine.</u>

T-cells (5 x 10^5) were cultured in 12 well plates with depleted or control media for a period of 6 and 24 hrs. Cells were harvested and analysed using flow cytometry for the expression of CD3 in gated CD4$^+$ population. Data shows the mean MFI of CD3 expressed on cells $\pm$ SD of duplicate samples of 1 experiment.

Having demonstrated a reduced expression of CD3 by T cells after 24 hrs in culture (**Figure 4.6**), I hypothesised that these cells would be less responsive in expression of the early activation marker CD69. To test this, T-cells were incubated in control or depleted media for 24 hrs before addition of OVA-pulsed DC (or un-pulsed controls). Although there was a marked up-regulation of CD69 on approximately 39% of OVA-specific CD4$^+$ T-cells following antigen-recognition (**Figure 4.7**) this was much reduced relative to the results above using freshly-isolated T-cells (**Figure 4.2**). Similarly, the same trend was shown for T-cells pre-cultured in depleted media, where only 38% of OVA-specific T cells up-regulated CD69 expression in response

to antigen (**Figure 4.7**), much lower than the previous experiment in which around 63% of T-cells responded (**Figure 4.2**).
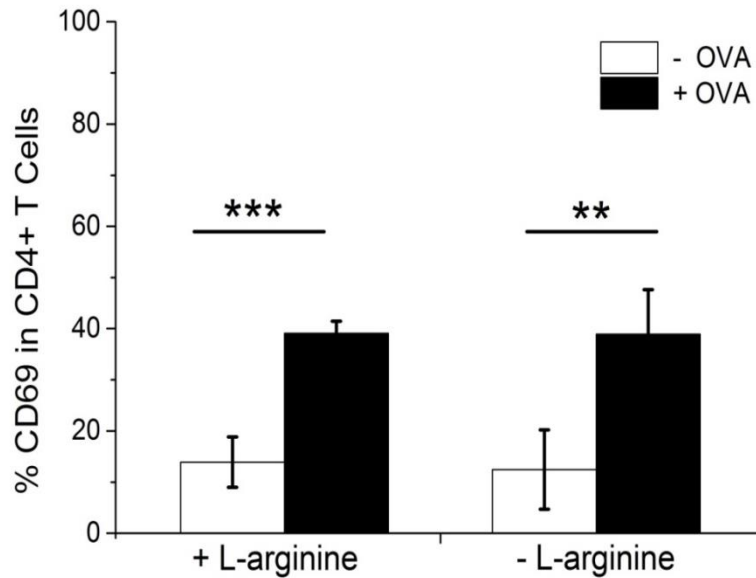
Figure 4.7: <u>**Expression of CD69 on CD4 $^+$ T-cells in the absence or presence of L-arginine after T-cells had been incubated for 24 hrs in depleted or control media.**</u>

T-cells were incubated in control or depleted media for 24 hrs. Following incubation T-cells (5 x 10^5) were then co-cultured in 12 well plates with un-pulsed DCs (5 x 10^5) or antigen-pulsed DCs (5 x 10^5) in control or depleted media. CD69 up-regulation in gated CD4$^+$ population was measured by flow cytometry. **A:** mean % up-regulation of CD69 of duplicate cultures of 2 independent experiments $\pm$ SD. **B:** Same as above, except mean MFI of PE-CD69 up-regulation after 24 hr period. Results shown are of duplicate cultures, of 2 independent experiments $\pm$ SD. (** p $\leq$ 0.005, *** p $\leq$ 0.0005 by un-paired t-test).

These results demonstrate that the T-cells deprived of L-arginine for a period of 24 hrs had reduced interaction forces (**Figure 4.5**) as well as reduced CD69 up-

regulation (**Figure 4.7**), which may be down to reduced CD3 expression (**Figure 4.6**). However, this was the same case for control media as well, suggesting another factor could be affecting the results.

An increase in apoptosis has been suggested to play a role in decreased expression of CD3 [387,388]. However, in studies that demonstrated a decreased expression of CD3 in L-arginine depleted media, this was not associated with decreased cell viability, as determined by Annexin V, propidium iodide and Trypan blue [271,389]. However, unlike my results, expression of CD3 was not decreased in control media.

Therefore, it would be important to determine if reduced CD3 expression was due to L-arginine depletion or another independent factor such as decreased viability. From observations using the microscope the morphology of T-cells showed characteristic cell changes, such as blebbing and shrinkage after 24 hrs of incubation. To determine whether this was the case or if the results were due to lowered CD3 expression I tested the viability of T-cells.

4.2.6   T-cell viability in control and depleted media.

To investigate whether reduced cell viability may account for the lowered interaction force, CD69 up-regulation and down-regulation of CD3 expression, T-cells were incubated for 6 hrs or 24 hrs in control or depleted media and cell viability tested using Annexin V and propidium iodide staining. An increase in both apoptosis/necrosis was evident in T-cells that were cultured for a period of 24 hrs (**Figure 4.8**). Importantly, this was irrespective of whether L-arginine was present in the culture medium or not. These results suggest that the reduced capacity for CD69 up-regulation, the decreased median force of interaction and the down-regulation of CD3 are likely to be associated with a compromised T-cells viability.
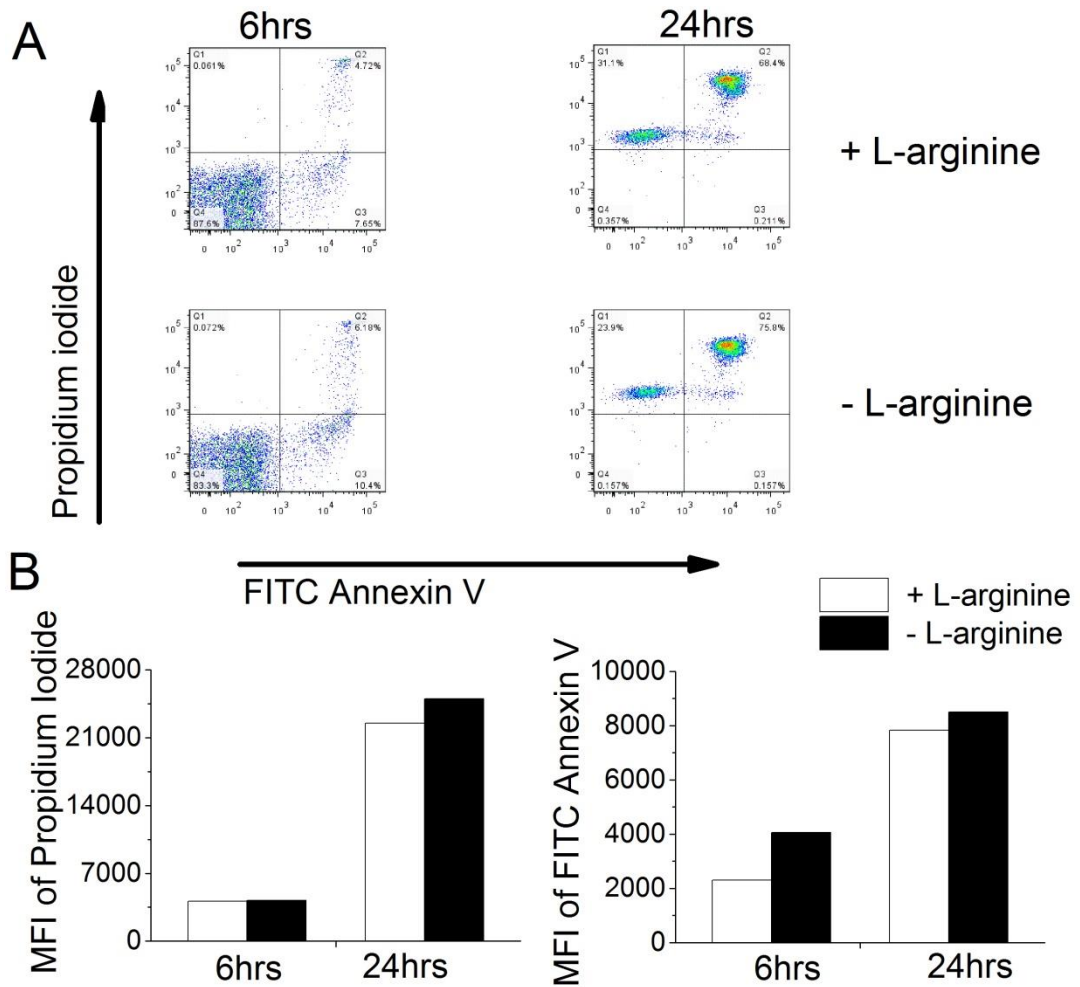
Figure 4.8: <u>Viability of CD4⁺ T-cells in the control and L-arginine depleted media.</u>

CD4$^+$ T-cell were incubated in depleted or control media for the period of time indicated. Cells were stained with Propidium Iodide or FITC Annexin V and analysed using flow cytometry for MFI of the apoptotic and necrotic marker. Results shown are **A:** FACs plots of propidium iodide vs. FITC Annexin V in gated CD4$^+$ T-cells, **B:** MFI of Propidium iodide and FITC Annexin V stained CD4$^+$ T-cells. Results shown are representative of 1 experiment.

4.2.7 Effect of *Leishmania* on T-cell function and interaction with DC.

Leishmania is a parasitic disease, in which L-arginine plays an important role [379–382]. As discussed in more detail in **Chapter 1 Section 1.18.1**, the outcome of infection is dependent on the expression of two inducible enzymes - NO synthase 2 and arginase - both of which share the common substrate, L-arginine. APCs can internalise *Leishmania* parasites, inducing arginase activity and resulting in a local depletion of L-arginine [390]. During non-healing infection, there is a reduction in the concentration of L-arginine within the local environment and this may affect *Leishmania* antigen-specific T-cell responses [380]. Having shown that the interaction force between T-cells and DCs is significantly increased in L-arginine-depleted media compared to control (**Figure 4.3**), I next wanted to determine whether infecting DCs with *Leishmania mexicana* would affect the interaction force between OVA-specific T-cells and OVA-pulsed DCs. I hypothesised that upon internalising *Leishmania*, DCs would produce arginase, resulting in local depletion in L-arginine and an increase in the interaction force between T-cells and DCs.

To test this, DCs were incubated with *Leishmania mexicana* promastigotes for 6 hrs at a 5:1 ratio. Subsequently, DCs were pulsed with OVA and incubated overnight, whilst control cells remained un-pulsed and/or uninfected. Following incubation, DCs were washed; re-plated and OVA-specific T-cells were added before quantifying interaction forces at the 1st time of contact or after 24hrs of co-culture, as well as assessing T cell proliferation after 48 hrs. As expected, T-cells proliferated normally upon recognition of antigen presented by non-infected DCs (**Figure 4.9**). This same trend was also observed in OVA-specific CD4$^+$ T-cells stimulated by *L. mexicana*-infected, OVA-pulsed DCs and was comparable to control. This indicates that infection with *Leishmania mexicana* promastigotes did not affect the antigen-specific proliferative response of CD4$^+$ OVA-specific T-cells.
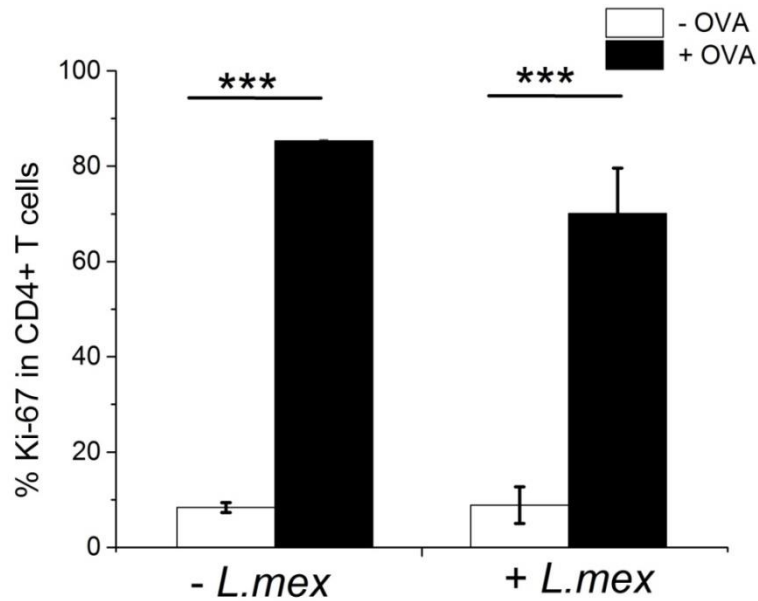
Figure 4.9: <u>Proliferation of CD4⁺ T-cells in the presence or absence of ovalbumin antigen, with/without *Leishmania mexicana* infected DCs.</u>

DCs were infected with *Leishmania mexicana* for 6 hrs (5:1 ratio). Following incubation, DCs were pulsed with 1mg/ml OVA overnight (black bars). Control DCs remained un-pulsed (white bars). After overnight incubation, 5 x 10^5 DCs were re-plated into each well of a 24-well plate and co-cultured with T-cells (5 x 10^5). Proliferation of CD4$^+$ T-cells was assayed 48 hrs later by determining the proportion of Ki-67-stained CD4$^+$ T cells using flow cytometry. Results shown are the mean proliferation of 1 experiment ± SD of triplicate cultures (*** $p \leq 0.0005$ vs un-pulsed by un-paired t-test).

Having demonstrated that parasite-containing DCs are able to stimulate exogenous antigen-specific T cell responses, optical tweezers were used to quantify the interaction forces between T cells and *Leishmania*-containing DCs. The force of interaction was carried out as described above (**Section 4.2.2**), except the time point measured was after 24 hrs of co-culture. Prior to quantifying the force of interaction, DCs containing CFSE labelled parasites were checked and positively identified using fluorescence microscopy. As shown in **Figure 4.10**, a clear increase in the

interaction force between OVA-specific CD4$^+$ T-cells and DCs was evident when DCs were pulsed with OVA. This trend is shown for both the initial contact between T-cell and DC (**Figure 4.10A**), and after a 24 hr co-culture (**Figure 4.10B**).

Interestingly, whilst *L. mexicana* infection had little impact on the force of initial contact, there was an increase in the force of interaction between CD4$^+$ T-cells and *Leishmania*-containing DCs following a 24hr co-culture. In samples without *L.mexicana* there was a clear antigen specific increase in the median interaction force from 3.3 pN ± 5.2 pN (un-pulsed) to 14.4 pN ± 6.4 pN (OVA-pulsed). Within samples where DCs were prior infected with *Leishmania* promastigotes there was an antigen-specific increase in the median interaction force from 12.4 pN ± 6.4 pN (un-pulsed) to 17.6 pN ± 6.3 pN (OVA-pulsed).

This result mirrors the same trend for force measurements, shown in **Figure 4.3**, where there was an increase in interaction force when L-arginine was depleted. Whilst this experiment was only a preliminary test and could not be repeated due to time constraints, this result suggests that *L. mexicana*-containing DCs are depleting L-arginine levels within the sample by inducing production of arginase. Further repeats would have to be carried out in order to validate the findings.

Given that *Leishmania* may cause a local decrease in L-arginine, these data support the findings above and demonstrate that depletion of L-arginine increases the interaction forces between T-cells and DCs. Despite this change in the early activation of T cells, the lack of L-arginine clearly affects the proliferative capacity and cytokine production of T-cells and in further work I would need to determine a potentially un-identified role of L-arginine.

Figure 4.10: <u>Quantification of interaction force between T-cells and OVA pulsed or un-pulsed DC infected with/without *L. mexicana*.</u>

T cells and DCs were prepared as described in **Figure 4.9** (or similar) and the force required to separate CD4^{+} T-cells and DCs quantified using optical tweezers after **A:** 1st contact and **B:** 24 hrs of co-culture. Cell interaction forces were measured between OVA pulsed DC (*L.mexicana* infected/un-infected) or un-pulsed DC (*L.mexicana* infected/un-infected), as indicated. Data shows the force required to separate individual cell interactions of 1 experiment with the median indicated (red line).

4.3 Discussion.

These experiments sought to investigate the role of L-arginine on the effector function of T-cells. Following on from this we sought to understand whether L-arginine plays a role in determining the interaction forces between T-cells and DC, whereby the strength of interaction could determine the function of T-cells.

Previous reports have shown that L-arginine is essential for normal T-cell proliferation and function [268,284,285]. L-arginine depletion inhibits the expression of CD3ζ chain, the main signal-transduction component of the TCR [284,286,287,391]. Furthermore in the absence of L-arginine there is suppression of the cell-cycle progression via inhibition of cyclin D3 [270].

Indeed, the results presented here in **Figure 4.1** support these previous reports and demonstrate that the absence of L-arginine had a profound effect on the proliferative capacity and cytokine production of OT-II CD4$^+$ T-cells following stimulation with OVA-pulsed DCs. Interestingly, **Figure 4.1C** demonstrates an impaired antigen-specific IL-2 secretion in L-arg-depleted media, which is somewhat different from Zea *et al.* (2004) who suggests IL-2 production is not affected by L-arginine depletion [271]. One possible explanation for this discrepancy may be associated with the mechanism of stimulating T cells. Whereas Zea *et al.* stimulated the T-cells with anti-CD3 and anti-CD28, the T cells analysed throughout this chapter were activated with antigen-pulsed DCs, providing a more robust signalling method. Indeed there is evidence to suggest that upon activating T-cells with anti-CD3 there are lower levels of phosphorylated Zap-70 [392]. Furthermore, engagement of anti-CD3 antibody with TCR is much stronger than cognate recognition of pMHC - due to antibody binding with greater affinity to TCR than pMHC [75], and thus may not be an appropriate representation of physiological TCR stimulation. Finally, naïve T-cell activation and subsequent signalling following TCR binding to pMHC ligands is much slower and more sustained than when anti-CD3 antibody is used [113,117,118]. The importance of IL-2 in determining the proliferative capacity of T-cells has been shown and therefore my results fit in well with the proliferation data [393,394]. Although the

differences are quite clear, it should be noted that IL-2 production was from only one set of experimental data and only by repeating the experiment will this result be clarified.

Despite impaired effector function, results indicate that T-cells show at least some level of early activation in the absence of L-arginine, as demonstrated by up-regulation of CD69 following antigen stimulation, and Ca^{2+} flux following PMA addition. This suggests that despite the absence of L-arginine, there is sufficient signalling between T-cells and DCs to drive early activation or perhaps the intracellular levels of L-arginine are sufficient to allow early activation marker expression. Together the results presented in **Figures 4.1, 4.2, 4.3, 4.4,** suggest that L-arginine is having a profound effect on the later stages on T-cell activation but does not seem to be affecting early activation of T-cells. Interestingly this data set is comparable to naïve T-cells that undergo tolerance induction with up-regulation of early activation marker CD69 but no proliferative capacity or cytokine production following *in vitro* re-stimulation [395].

The importance of a stable and strong interaction has been implicated in T-cell activation and there are suggestions that the strength can influence the effector function of T-cells, specifically in determining whether a T-cell will become tolerant to a given antigen or an effector response is induced. As shown in **Chapter 3**, an optical tweezer system was built that could manipulate T-cell and DC interaction as well as quantify the interaction force between cells. This system was employed to determine whether the absence of L-arginine affected the interaction force between T-cells and DCs and quantify this for the first time. The immunological synapse is important for T-cell activation and atomic force microscopy has been used to demonstrate that the formation of the immunological synapse determines the interaction force between T-cells and antigen-presenting cells [155,164,167,396]. Recently a study demonstrated that in the absence of L-arginine, stimulated human T-cells showed lowered dephosphorylation of phosphocofilin and lower cofilin activation, resulting in impairment of immunological synapse formation [289,397,398]. Together the above results suggest that L-arginine depletion may influence the interaction force

between naïve T-cells and DCs, by preventing the formation of the immunological synapse. Indeed L-arginine depletion did alter the interaction forces between T-cells and DCs; however the result was not what I first hypothesised. Based on my results showing that T-cell function was impaired (**Figures 4.1, 4.2, 4.3, 4.4,**) and from the literature whereby IS formation is impaired in L-arginine depleted media, my hypothesis was that the interaction force between T-cells and DCs in depleted media would be significantly lower compared to control. Surprisingly, despite T-cell function being impaired following depletion of L-arginine, the interaction force between T-cells and DCs in depleted media was significantly increased relative to cells in L-arginine control media (**Figure 4.3, Panel A**). This stronger force of interaction was evident irrespective of antigen recognition and the same trend was observed both upon initial contact between T cell and DC and after 6 hrs of co-culture (**Figure 4.3**, **Panel B**).

One possible explanation for these observations is that deprived T-cells may be seeking an alternative source of L-arginine, an amino acid required for efficient T-cell activation. An alternative source may be provided intracellularly by the DC and upon contacting a DC the cells will form a stable conjugate. Whilst there is no evidence within the literature, this hypothesis is supported by **Figure 4.2** showing up-regulation of CD69. Sufficient intracellular L-arginine may be present to drive early activation but not enough for proliferation and cytokine release, in the presence of OVA antigen.

Another explanation could be down to differences in the intensity of Ca^{2+} flux in T-cells following interaction with DC. A Ca^{2+} flux has been implicated in determining the "stop" signal as well as determining the ability of a T-cell to detach from a DC [115,133,385]. Previous work has shown no differences in the intensity of Ca^{2+} flux in L-arginine depleted media [271]. However, in this particular experiment by Zea *et al.* (2004), Ca^{2+} flux was induced by using OKT-3 which binds to CD3 complex. As L-arginine depletes CD3 expression then this method might not be ideal. Using PMA no difference in the Ca^{2+} flux of T-cells was observed irrespective of cells being in control or L-arg-depleted media. However, this would be better carried out using

cell-cell interactions, to give a truer physiological representation of signalling in T-cells, following interaction with a DC. PMA has a structure analogous to diacylglycerol which activates PKC to trigger a Ca^{2+} flux. However, by carrying out the experiment using mixed populations of T-cells and DCs, this would take into consideration the binding of the TCR with its specific ligand, which could be altered by depletion of L-arginine. Indeed increased interaction strength was observed in depleted media. Unfortunately, initial attempts to image Ca^{2+} fluxing of optically trapped T cells proved problematic, possibly due to problems associated with light-induced calcium flux within T-cells, which has been reported before [399–401]. If more time was permitted then one could explore this as a potential explanation, after investigations have been carried out into light-induced calcium flux.

As mentioned previously, L-arginine depletion impairs synapse formation in human T-cells following stimulation [289]. The interaction force between T-cells and DCs correlates with the formation of the IS. The force of interaction increases upon antigen recognition and peaks at roughly 30 minutes of interaction when the IS is fully mature and formed at the cell-cell interface [167]. Taking this into account one would assume that the interaction force would be decreased due to lack of synapse formation resulting from depletion of L-arginine. However, this was not the case and the results indicate that the interaction force between T-cells and DC is significantly higher in depleted media compared to control, irrespective of antigen recognition.

Whilst we don't have evidence to show that the IS is affected in our set-up, if more time was permitted then the IS could perhaps be imaged using confocal microscopy. T-cells and DC co-cultures could be fixed in the presence and absence of L-arginine and stained for markers such as LFA-1 and ICAM-1 to determine whether IS formation is impaired, as in agreement with Feldmeyer *et al.* (2012) [289] Moreover, the optical tweezer system could itself be incorporated around a confocal microscope. This would enable high resolution imaging and one could then look to determine whether there are differences in the IS formation kinetics in control or depleted media. This would be important given the importance of its formation in determining not only the interaction forces between T-cells and DC but also for

promoting T-cell signalling and activation [155,164,167,396,402]. Whilst fluctuations in beam power and the distance the beam was placed away from T-cell when determining interaction force could be controlled, a number of factors could not. These include the viscosity of media and the refractive index of cell. Whilst these may only have a minimal effect, future experiments could look at this to determine what and if these experimental factors affected cell-cell interaction forces.

Furthermore, it would be interesting to see if the increased interaction force between cells in L-arg-depleted media is restored to normal levels upon reconstituting media with L-arginine and if it is possible to restore the proliferative and cytokine release of T-cells following antigen-recognition. This may have therapeutic relevance, in particular for restoring anti-tumor T-cell responses to cancers or perhaps restoring T-cell responses to non-healing *Leishmania* infection.

Previous reports have suggested that expression of the CD3ζ chain shows a gradual decrease in the absence of L-arginine. This decrease was evident after 4 hrs [386]. Indeed, **Figure 4.6** demonstrated that CD3 expression was reduced following a 24hr incubation in depleted media. However, this same trend was also evident in control media. Although T cells cultured *in vitro* without L-arg were still able to up-regulate CD69 following antigen stimulation, this was evidently much lower than the level of expression shown when stimulating freshly-isolated T cells. Upon quantifying the interaction forces between T-cells and DC, although these cells demonstrated an antigen specific increase in interaction force in both depleted and control media, this again was much lower than shown previously, when T-cells were freshly isolated and used immediately.

The CD3 co-receptor is essential for the activation signal during T-cell activation. Perhaps the reduced CD69 up-regulation and force measurement observed could be down to reduced expression of CD3 after 24 hr incubation. However, as this was also evident in control media another factor could be involved other than L-arginine depletion. It is known that an increase in apoptosis can result in decreased expression of CD3ζ [387,388]. Indeed a viability analysis showed T-cells incubated *in*

vitro for 24 hrs had significantly higher levels of apoptosis/necrosis, suggesting that differences observed at later time-points may be associated with lower viability of T-cells. This highlights the caveats of such *in vitro* experiments and suggests that other results within the literature may have to address viability more thoroughly.

In summary the above highlights that L-arginine not only has a profound effect on the function of T-cells but that L-arginine depletion can increase the interaction force between T-cells and DCs. Despite a stronger interaction, the functional outcome of T-cells is impaired. This is significant as it has been proposed that a stable IS-like interaction with APCs supports robust T-cell activation [36,190], whereas my data suggests otherwise. This highlights the complexity in T-cell/DC interaction dynamics on the functional outcome of T-cells.

As mentioned in the introduction, L-arginine plays a crucial role in *Leishmania* infection. It lies at the crossroads of whether there is effective clearance of parasites or whether parasite replication growth and replication is promoted [268,379]. T_H1 cytokines control expression of NOS, whereby the oxidation of L-arginine into NO effectively kills the parasite. On the other hand, T_H2 cytokines promote the production of arginase, depleting local levels of L-arginine with the latter being the production of ornithine which promotes parasite growth [379,390]. Indeed un-controlled replication of *Leishmania* correlates with high levels of arginase in non-healing mice [380].

Given the importance of L-arginine in *Leishmania* infection and the results shown in **Figures 4.1**, **4.2**, **4.3**, and **4.4** suggesting that L-arginine can affect the function of T-cells and their interaction with DCs, a preliminary experiment was conducted to determine the consequence of *Leishmania* upon DC/T cell interactions. Whilst this preliminary experiment analysed only a limited number of cell interactions, the trends in the data can be related back to the force measurements as shown in **Figure 4.3**. *Leishmania* infected DCs showed an increase in interaction strength after 24 hrs of co-culture compared to un-infected DCs, this was irrespective of antigen.

The data presented in **Figure 4.10** suggests that *L.mex* infected DCs are depleting local levels of L-arginine through production of arginase. This could inevitably affect the interaction force between T-cells and DC. It is interesting to note that this experiment was carried out in control media. Therefore, interaction forces between T-cells and DC may not be affected till later time points with sufficient time passing where local levels of L-arginine are depleted low enough by *L.mex* infected DCs. This would indeed explain why interaction forces were not altered for the first time contact. However, it is difficult to come to a solid conclusion due to the low number of cell-cell interaction measured.

In summary, although this is a preliminary experiment, it certainly provides foundations for further work, such as determining T-cell effector function and whether parasites from healing/non-healing infection may influence the interaction dynamics between T-cells and DCs. *L.major* specific CD4^{+} T-cell proliferation and cytokine release is impaired in non-healing mice and T-cell subsets induced by *L.major* infection can differ in the magnitude and quality of their responses in healing and non-healing mice. However, this can be rescued by supplementation of L-arginine or inhibition of arginase [380,382]. An aspect that these studies didn't take into consideration was if *L.major* specific CD4^{+} T-cells, particularly in non-healing mice display a more tolerised phenotype compared to healing mice. This hypothesis is discussed in the next paragraph. Moreover, these studies are unable to determine how the interactions between T-cells and DC differ. As I demonstrated differences in the force of interaction, multiphoton microscopy could be used to image T-cell/DC interactions following infection with *L.major in vivo*.

Another aspect that the above results indicate is the implication that absence of L-arginine could render a naïve T-cell to become tolerant or anergic to its specific antigen. This stems from earlier results investigating T-cell function, which display the characteristics of a naïve, T-cell undergoing tolerance induction. For instance, OVA-specific T-cells from mice fed OVA show a rapid up-regulation of CD69, yet upon *in vitro* re-stimulation with OVA OVA-specific T-cells show a marked decrease in IL-2, IFN-γ and proliferation [395], These results are similar in trend to

those shown in **Figures 4.1**, **4.2**. Interestingly although adaptively tolerant T-cells are still able to form conjugates with APCs, they have impaired IS formation [403]. This would be similar to the study conducted by Feldmeyer *et al.* (2012) [289], who demonstrated impaired IS formation in the absence of L-arginine, demonstrating further evidence for this hypothesis. However, whether IS formation is impaired in the model system used in this chapter would have to be investigated. Furthermore, in the absence of L-arginine T-cells perhaps begin to express higher levels of Cytoxic T-lymphocyte associated antigen 4 (CTLA-4). CTLA-4 prevents T-cells from entering the cell-cycle which is the same trend shown for when T-cells are depleted of L-arginine. Interestingly this binds with higher affinity to its ligand than CD28 [404]. This might perhaps account for the increased interaction force, as measured using the optical tweezers.

Despite reduced capacity for proliferation and cytokine release, *in vivo* imaging has shown that under tolerising and priming induction, tolerant T-cells are able to interact with a DC for a substantial period of time. Within this study Zinselmeyer *et al.* (2005) demonstrate that tolerant T-cells form stable interactions with DCs, forming large clusters around a single DC [144]. Moreover, as described later in **Chapter 5**, the optical tweezer system can also be applied to quantify the interaction force between tolerant T-cells and DCs, with results suggesting that tolerant T-cells interact with a high interaction force with DCs despite a reduced proliferative and cytokine response following *in vitro* re-stimulation with OVA, supporting this hypothesis. This ultimately hints that the state of un-responsiveness in T-cells in the absence of L-arginine could be associated with the polarisation of the naïve $CD4^+$ T-cell towards an anergic or tolerant phenotype.

In summary, the results shown here demonstrate that L-arginine affects T-cell proliferation and function, supporting previous findings. Interestingly, despite studies demonstrating that L-arginine depletion prevents immunological synapse formation, these results suggest that L-arginine depletion causes an increase in the interaction force between T-cells and DC. This ultimately highlights the complexity

in the role that L-arginine plays on T-cell antigen specific responses and suggests that an unknown mechanism may be involved.

Chapter 5 - Manipulating and quantifying immune cell interactions to understand the importance of citrullination on T-cell function.

5.1 Introduction.

Citrullination is a post-translational modification resulting from arginine deamination by the enzymes Petidylarginine deiminase (PAD) in the presence of calcium, whereby the positively charged arginine residue is changed to a neutral citrulline residue. These modifications are essential for basic cell function, but in certain cases they can modify and change the antigenicity of proteins. There are suggestions that citrullination and Anti-citrullinated protein antibodies (ACPAs) play a critical role in the initiation of autoimmune diseases such as RA, in the context of an inflammatory response [405]. Specifically, PAD 4 expression links with clinical signs of RA [406–409] whilst PAD 2 has been detected in synovial fluid of patients with RA and spondyloarthritis [410]. To date several studies have described and identified ACPAs and citrullinated antigens which are associated with RA. These include type I and type II collagens, fibrinogen, vimentin, aspirin, actin-F capping protein and enolase-α [411–417]. The presence of citrullinated proteins can enhance and determine the pathogenic path of RA, as demonstrated in arthritis animal models highlighting the participation of citrullination in the auto-immune response. Hill *et al*. used citrullinated human fibrinogen and upon presentation by APCs, this antigen induced arthritis (characterised by synovial hyperplasia followed by ankylosis) in DR4-IE transgenic mice [314,315]. Furthermore, Lundberg *et al*. showed that citrullinated rat serum albumin antigen resulted in the breakdown of immunological tolerance and disease symptoms of collagen type II induced arthritis were evident much earlier. In addition, they demonstrated that the severity of arthritis correlated with PAD4 expression as well as the level of citrullinated-collagen II [304].

Interestingly detection of ACPAs is possible long before the manifestation of clinical symptoms of RA, suggesting that citrullination of antigen is not only associated with inflammation but also the generation of ACPAs [410]. Furthermore, the presence of such class-switched antibodies requires loss of tolerance within the CD4$^+$ T cell population suggesting that the initial interactions with T-cells may play a crucial role in development of disease [313]. Indeed there are a large number of CD4$^+$ T-cells within synovial tissue and therefore perhaps the production of ACPAs is T-cell

dependent whereby citrullinated peptides presented on the surface of APCs may alter the threshold for T-cell stimulation. Indeed, T-cells reactive to citrullinated peptide have been identified which show an enhanced T_H1 phenotype [320]. Whilst others have suggested that native and citrullinated forms of hen egg lysozyme are differentially recognised by T cells [318] and that such cit-peptides are generated during autophagy in antigen-presenting cells [418].

Further evidence for T-cells playing a role in pathogenesis of RA was the identification of MHC class II genes which were major risk factors for RA, in particular the HLA-DRB1* shared epitope [419–421]. By measuring ACPA levels using a cyclic citrullinated peptide assay, alleles such as DRB1*0401 and *0404 were shown to not only be risk factors for RA, but that ACPA production levels were influenced by the presence of these genes [422,423]. Furthermore, the risk for ACPA-positive RA can be increased by as much as 20-fold in genetically predisposed individuals who have the HLA-DRB1 SE and the PTPN22 gene [424]. Other risk factors include smoking where Klareskog *et al.* observed a correlation with the presence of HLA-DRB1*0401 allele with the presence of anti-citrullinated antibodies in individuals that smoke [425]. Whilst this may provide evidence that smoking could enhance the citrullination of proteins and with it the initiation of RA disease, further environmental or genetic factors may play a role [426].

Together, the above provides strong evidence for MHC-class II dependent T-cell activation and a potential role for antigen presentation in the breakdown of tolerance and initiation of RA. Indeed it has been suggested that antigen-presenting cells, which have a level of autophagy, may take up self-peptides and present them as citrullinated peptides [319,427]. There is evidence to link autophagy with citrullination of self-peptides, where changes in the local environment may affect the APC to induce autophagy and with it increased citrullination of self-peptides [319]. In RA there is increased inflammation and as a result there would be a high level of apoptosis of cells. It has been suggested that abnormal cell death or clearance of apoptotic bodies could be disturbed and as a result there is increased presentation of citrullinated self-peptides [428,429], for example citrullinated vimentin is presented following apoptosis

[427]. Overall citrullination may generate a new set of peptides that could potentially associate with MHC molecules, resulting in the activation of auto-reactive T-cells [430] and the generation of anti-citrullinated peptide antibodies (ACPAs) [405].

Modified citrullinated peptides may alter the affinity for either the MHC binding pockets and/or the specific T-cell receptor, stabilising the complex [431]. The TCR can discriminate between subtle differences in pMHC complexes and although the affinity is within the micro molar range, differing affinities of interaction can have a profound effect on the development, survival and peripheral function of T-cells [54,75,120,432]. HLA-DR molecules share an epitope sequence and have a positively charged P4 peptide binding pocket. However, citrullination removes the positive charged P4 groove and as a result it might enhance the ability to bind to class II molecules [433]. Indeed increased affinity between citrullinated vimentin peptide for DRB1*0401 has been demonstrated by Hill *et al.* [314].

The presentation of modified citrullinated peptides by antigen-presenting cells may change the threshold requirements for T-cell stimulation, potentially altering the interaction dynamics and leading to breakdown of tolerance. However, despite a wealth of data linking citrullination to RA, it remains unclear how autoimmune diseases such as RA are initiated and if modification of a specific antigen alters how an individual T-cell recognises this antigen or how it interacts with an antigen-presenting cell. Understanding more about how citrullination affects the interaction between T-cells and DCs and also its effects on T-cell activation may lead to new therapeutics that could aim to inhibit or promote this to manipulate immune responses. Conversely, understanding more about how tolerised, primed and naïve T-cells would interact upon secondary exposure to antigen may have important consequences for immunotherapeutics and vaccines that aim to manipulate secondary immune responses to antigen.

Therefore, this chapter sought to determine whether citrullination of an antigen would affect T-cell function but also whether it altered the interaction strength between T-cells and DCs, investigating any potential role for this event in the

breakdown of self-tolerance and initiation of RA. Finally I sought to determine the interaction strength between naïve, primed and tolerised T-cells with antigen-presenting DC following secondary exposure to antigen.

5.2 Results.

5.2.1 Altered T-cell function to citrullinated antigen.

T-cells that form stable and longer contacts with APCs *in vivo* can show a more robust T-cell activation [9,76,148]. Although previous work has highlighted that T-cells can respond to citrullinated self-peptides which can alter T-cell function [314,418,434,435], these studies assessed the functional responses of T-cells upon recognition of citrullinated human aggrecan and hen egg lysozyme peptides. In this chapter ovalbumin peptide with a modified, citrullinated C-terminal arginine residue was used. Therefore, the first objective was to validate the proposed model, to determine if OVA-specific OT-II T-cells can also recognise the citrullinated form of ovalbumin; and secondly to examine the effect of citrullinated OVA antigen on T-cell function and determine whether T-cells display altered proliferation or cytokine release. This would be the first time that experiments have been carried out to determine the T-cell function in the context of antigen recognition using citrullinated ovalbumin. To address these aims, DCs were pulsed with the $OVA_{323-339}$ peptide either in its native form or with a citrullinated arginine residue at the C-terminus. In this way, direct comparisons could be made to assess T-cell function following co-culture with DCs presenting OVA antigen in a normal form or OVA antigen that was in a citrullinated form.

DCs were pulsed with 10 μg/ml of OVA peptide (OVAp) or citrullinated OVA peptide (cit-OVA) for 6 hrs, washed and re-plated into 24 well plates at a concentration of 5×10^5 total cells per well and used to stimulate lymphocytes from OT-II mice. Cells were then analysed for proliferation and cytokine secretion, as described in **Chapter 3**. As shown in **Figure 5.1** there was a significant increase in proliferation between unpulsed and OVAp-pulsed samples, demonstrating an antigen-specific response. The proportion of proliferating (Ki-67^{+}) T-cells following stimulation with OVAp pulsed DC was around 72%. Interestingly, in samples where DCs presented the modified cit-OVA peptide, a similar proportion of OVA-specific CD4^{+} T cell proliferated (73% ± 21.1%). These results suggest that whilst citrullination of this peptide may not enhance the (already high) proliferative

response of T-cells, the modified peptide is still presented by DCs and is recognised by the OT-II T-cells sufficiently to drive antigen-specific proliferation.
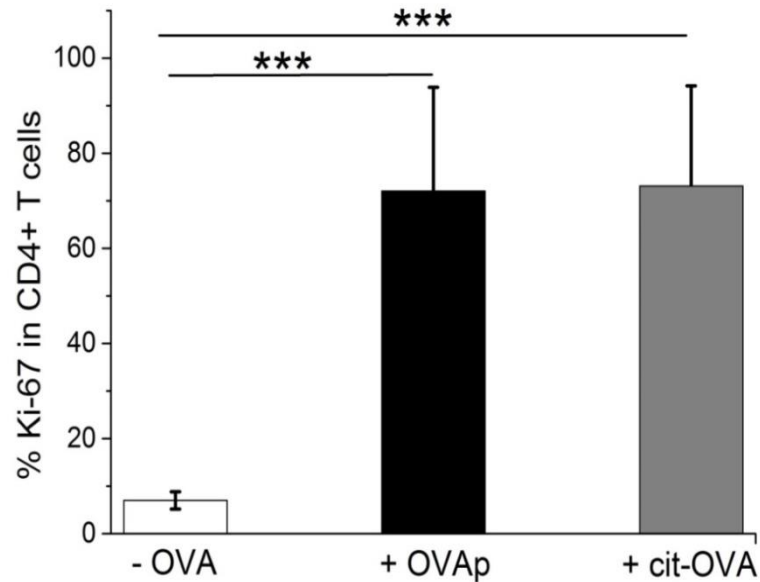
Figure 5.1: <u>**Proliferation of OVA-specific CD4$^+$ T-cells upon recognition of cit-OVA.**</u>

OVA-specific OT-II T-cells (5 x 10^5) were co-cultured in 24 well plates with 5 x 10^5 un-pulsed (white bar) or OVAp-pulsed DC (black bar) or cit-OVA pulsed (grey bar) dendritic cells. Proliferation of CD4$^+$ T-cells was assayed 48 hrs later by identifying Ki-67$^+$ CD4$^+$ T cells using flow cytometry. Results shown are the mean proliferation of triplicate cultures of 5 independent experiments $\pm$ SD. (*** p $\leq$ 0.0005 by un-paired t-test).

Supernatants from the above cultures were collected and analysed for cytokine production (**Figure 5.2**). As expected, a significant increase in OVA-specific production of both IFN-γ and IL-5 was evident when T-cells were co-cultured with DC presenting OVAp. However, interestingly this OVA-specific cytokine production was increased when T-cells were stimulated with cit-OVA-pulsed DCs, with a moderate increase in IL-5 and significantly more IFN-γ production in

response to cit-OVA relative to native peptide. Together, these results demonstrate that OVA-specific OT-II T-cells recognise the modified, citrullinated form of OVA$_{323-339}$ and suggest that citrullination may enhance the activation of T-cells, which may be associated with an increased interaction between T-cells and DCs.
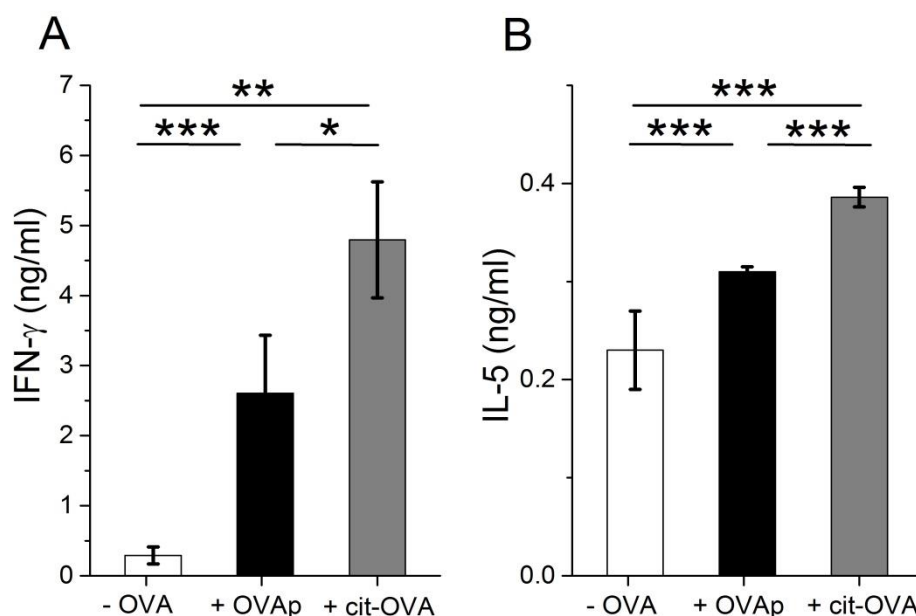
Figure 5.2: <u>**Cytokine production by OVA-specific CD4$^+$ T-cells upon recognition of cit-OVA.**</u>

OVA-specific OT-II T-cells (5 x 10^5) were co-cultured with DCs (5 x 10^5) as described in **Figure 5.1**. **A:** IFN-γ and **B:** IL-5 cytokine production was measured by ELISA of culture supernatants after 48 hrs. Results shown are the mean ($\pm$ SD) of triplicate samples and are representative of 3 independent experiments. (* p $\leq$ 0.05, ** p $\leq$ 0.005, *** p $\leq$ 0.0005 by un-paired t-test).

5.2.2 Quantifying the interaction force upon CD4$^+$ T-cell recognition of citrullinated antigen.

As discussed above, citrullinated antigens have been linked to RA where this process can produce novel self-peptides and has the potential to breakdown tolerance.

Specifically, citrullination of peptide residues have been shown to increase peptide-MHC affinity leading to enhanced $CD4^+$ T-cell activation [314]. Therefore, given that the results above demonstrated an increased cytokine production in response to cit-OVA, it was hypothesised that there would be an increased interaction force between T-cells and DCs presenting citrullinated OVA compared with native antigen.

Dendritic cells were pulsed with either native or citrullinated forms of $OVA_{323-339}$ peptide and used to present to purified $CD4^+$ OT-II T cells. The force of initial interaction was measured (as described in **Chapter 3)**, using the optical tweezer system. As shown in **Figure 5.3**, the interaction force between T-cells and DCs pulsed with OVAp was significantly increased, with a median increase from 3.3 pN ± 4.3 pN (un-pulsed) to 10.2 pN ± 5.8 pN (OVAp pulsed). Interestingly, even though there was a clear antigen-specific increase in the interaction force between T-cells and cit-OVA-pulsed DCs (un-pulsed, 3.3 pN; cit-OVA pulsed, 8.5 pN ± 6.6 pN) this was not significantly different to the median interaction force of T cells recognising native OVAp. Whilst this further confirmed that the OVA-specific OT-II T cells were able to recognise cit-OVA, these findings suggest that the initial interactions between T cells and DCs are not altered by citrullination of antigen, contrary to the initial hypothesis.

Figure 5.3: <u>Quantification of the initial force of interaction between OVA-specific CD4^{+} T-cells and DCs upon recognition of cit-OVA.</u>

DCs were pulsed with OVAp or cit-OVA as described above and used to present to OVA-specific OT-II T cells as described in **Chapter 3**. The force required to separate T-cells and DCs after 120 seconds of interaction was then determined using calibrated optical tweezers. Data shows the force required to separate individual cell interactions of 5 independent experiments with the median indicated (red line) ([**] $p \leq 0.005$, [***] $p \leq 0.0005$, by Mann Whitney test).

The importance of a long term interaction for successful proliferation and cytokine production in T-cells has been demonstrated previously [148]. Given that cit-OVA was sufficient to enhance T cell effector function (**Figure 5.2**), without any detectable change in the initial force of interaction, I next determined the interaction forces between T-cells and DCs after 6 hrs of interaction and hypothesised that there would be a higher interaction force between T-cells and DCs that are presenting citrullinated OVA.

As shown in **Figure 5.4**, the interaction force between T-cells and DC pulsed with OVAp was significantly increased, with a median increase from 3.3 pN ± 5.3 pN (unpulsed) to 12.4 pN ± 6.4 pN (OVAp pulsed). As observed above, there was also a clear antigen-specific increase in the interaction force between DC and T cells recognising cit-OVA (un-pulsed, 3.3 pN ± 5.3 pN; cit-OVA pulsed, 17.6 pN ± 4.7 pN). Interestingly, this force of interaction was significantly higher when T cells were stimulated for 6 hrs with the citrullinated form of the antigen relative to T cells recognising native OVAp. Indeed, many of the cell pairs in cit-OVA pulsed cultures had reached a force of interaction greater than the upper limit of the optical tweezer system. Together these data suggest that the altered pMHC:TCR interaction associated with citrullinated antigen has important consequences on the T-cell interaction with an antigen-presenting cell. Overall, the increase in the interaction forces between T-cells and DCs may explain the increased cytokine production observed in **Figure 5.2**.
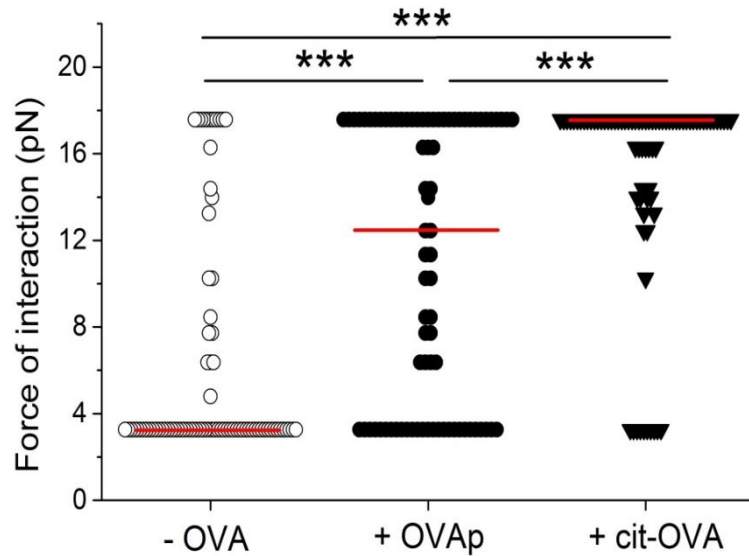
Figure 5.4: <u>Quantification of force between CD4^{+} T-cells and DCs antigen pulsed with/without OVAp or cit-OVA after 6 hr co-culture.</u>

DCs were pulsed with OVAp or cit-OVA as described above and used to present to OVA-specific OT-II T cells as described in **Chapter 4**. The force required to separate T-cells and DCs after 6 hrs of interaction was then determined using calibrated optical tweezers. Data shows the force required to separate individual cell interactions of 4 independent experiments with the median indicated (red line) n = 80 individual cell measurements for each condition. ([**]p≤ 0.005, [***] p ≤ 0.0005, by Mann Whitney test).

5.2.3 The effect of antigen dose on T-cell effector function.

The strength of TCR stimulation can be influenced by a combination of pMHC density (antigen dose/concentration), pMHC potency (affinity and half-life of TCR/pMHC interactions) and finally the duration of T-cell/APC contacts (stability). These can have important consequences for either immunogenic and tolerogenic responses [75,121]. Specifically, higher amounts of pMHC is mirrored by the generation of a larger memory population and the magnitude of CD8^{+} cytotoxic function correlates with the dose of antigen [81,83–85]. It is clear that the density of pMHC can have a profound effect on T-cell function. However, a greater affinity of interaction

between T-cells with DCs can lower the threshold for antigen detection and T-cell activation [75,436]. Therefore, in situations where there is higher affinity between T-cells and DCs, TCRs may sense a lower pMHC dose and as a result lower antigen doses could be required for effective TCR stimulation. Recently there have been proposals that the TCR can sense the strength of interaction and can play a key role in initiating TCR signalling [104] and others have suggested that citrullinated peptides may bind with higher affinity to MHC [314]. As shown above, cit-OVA resulted in increased T-cell IFN-γ cytokine release (**Figure 5.2**) and the interaction forces between T-cells and DCs pulsed with citrullinated antigen was significantly higher than samples recognising native ovalbumin (**Figure 5.4**).

Therefore, as affinity may lower the threshold for T-cell activation and given that the results above demonstrated an increased cytokine production with an increased interaction force in response to cit-OVA, it was hypothesised that lower doses of cit-OVA would be required to effectively activate T-cells, compared to native antigen. To investigate this, DCs were antigen pulsed with titrating doses of either OVAp or cit-OVA peptide. Following overnight antigen pulse, purified OVA-specific CD4$^+$ T-cells were added and co-cultured for 48 hrs. Cells were analysed for proliferation (staining for Ki-67) and effector function (by measuring cytokine secretion using Luminex) as described in **Chapter 2**, **Sections 2.5.1** and **2.5.2**.

As shown in **Figure 5.5** the proliferative capacity of T-cells correlated with titrating doses of OVAp and cit-OVA. For OVAp the proportion of proliferating CD4$^+$ T-cells decreased from 27% (10 µg/ml) to 12% (0.1 µg/ml), whilst cit-OVA samples decreased from 28% (10 µg/ml) to 15% (0.1 µg/ml) respectively. As in agreement with earlier experiments **(Figure 5.1)** a similar proportion of OVA-specific CD4$^+$ T cell proliferated in samples where DCs were presenting cit-OVA, compared to native antigen.

Interestingly, OVA-specific cytokine production was increased when T-cells were co-cultured with cit-OVA-pulsed DCs at antigen doses 5 µg/ml and 1 µg/ml, with a significant increase in IL-2 (1 µg/ml) and IFN-γ (5 µg/ml and 1 µg/ml) relative to

native peptide. Together, these results demonstrate and confirm that OVA-specific OT-II T-cells recognise the modified, citrullinated form of $OVA_{323-339}$ and suggest that citrullination may enhance the activation of T-cells, with recognition of cit-OVA by T cells resulting in an increased force of interaction and thus lowering the threshold for robust T-cell activation. It should be noted supernatants were also tested for the cytokines IL-10, IL-6, IL-12, IL-17 and IL-4 using Luminex, but all measurements were below the limits of detection. Furthermore, unlike previous data the results below are presented as SEM due to only being able to quantify duplicate cultures or 1 experiment.
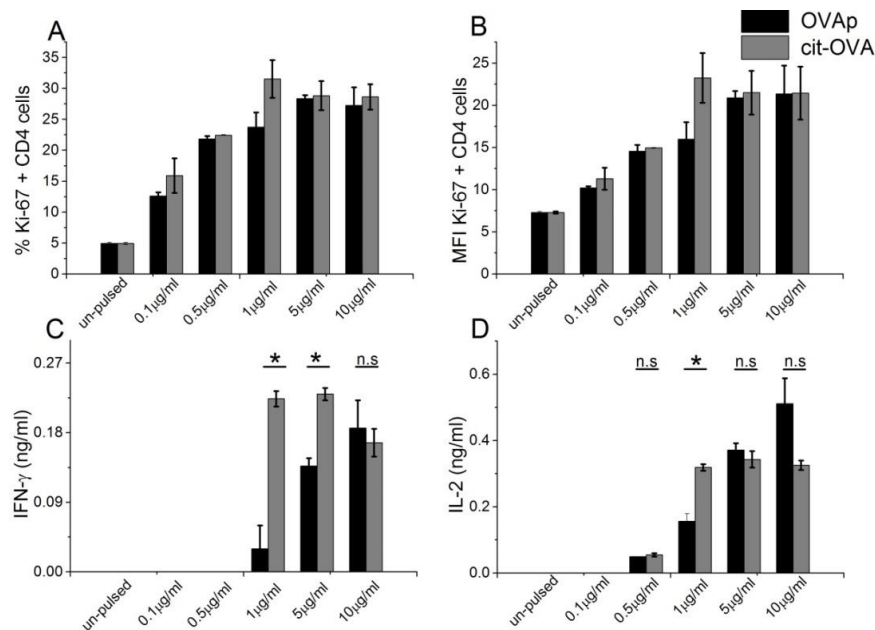
Figure 5.5: <u>**Determining the effect of antigen dose on function of T-cells.**</u>

OVA-specific T-cells (5×10^5) were co-cultured in 24 well plates with 5×10^5 un-pulsed (white bar), OVAp-pulsed (black bar) or cit-OVA pulsed (5×10^5) (grey bar) DCs. Data shows **A:** percentage of proliferating $CD4^+$ gated T-cells **B:** MFI of Ki-67 positive $CD4^+$ T-cells, after 48 co-culture, **C:** IFN-γ and **D:** IL-2 cytokine production, measured by Luminex of culture supernatants after 48 hr co-culture. Results shown are the mean proliferation and cytokine production of duplicate samples ± SEM, representative of 1 independent experiment (* p≤ 0.05, ** p ≤ 0.005 by un-paired t-test).

5.2.3.1 The effect of antigen dose on interaction forces between T-cells and DCs.

A stronger adhesion between T-cells and DCs may overcome the threshold required for effective TCR stimulation at lower doses of antigen. Therefore following on from the experiments above, I next determined the interaction forces between T-cells and DCs antigen pulsed with varying concentrations of either native or citrullinated peptide antigens. Due to time constraints it was only possible to conduct one repeat of this experiment. It was therefore decided that a 6hr co-culture between T-cells and DC (OVAp) and T-cells and DC (cit-OVA) was carried out, to maximise the number of cell pairs measured and as this was the time point where significant differences in interaction force was detected (**Figure 5.4**).

As shown in **Figure 5.6,** the interactions between T cells and DCs presenting OVAp or cit-OVA demonstrate a dose-dependent force, with 0.1 ug/ml of peptide generating only 8.5 pN ± 5.3 pN of force relative to 14.4 pN ± 5.8 pN at 10 µg/ml of OVAp. Interestingly, in samples where DCs were pulsed with cit-OVA, the median force of interaction was higher across a range of peptide concentrations from 0.1 µg/ml (11.3 pN ± 4.7 pN) to 10 µg/ml (17.6 pN ± 3.8 pN) compared with samples in which DCs were pulsed with native OVAp. Whilst these results weren't significant in this preliminary experiment, this trend was similar to the force measurements comparing the two OVA peptides earlier, (**Figure 5.4**).
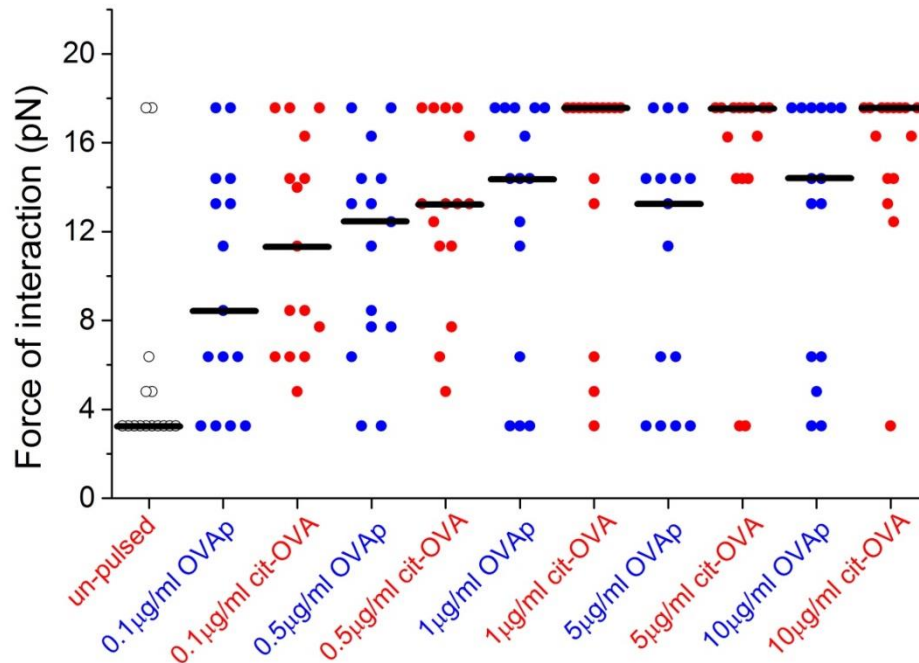
Figure 5.6: <u>**Quantifying the interaction force between T-cells and DCs pulsed with titrating doses of OVAp or cit-OVA.**</u>

DCs were pulsed with increasing concentrations of OVAp or cit-OVA and co-cultured with CD4$^+$ T-cells for 6 hrs. After co-culture the force required to separate individual cell-cell pairs was determined as described in **Figure 5.4** and in **Chapter 4**, **Section 4.2.2**. Data shows the force required to separate individual cell interactions of 1 experiment with the median indicated (black line).

The above results suggest that citrullination of antigen increases the interaction force between T-cells and DCs and, associated with this higher interaction force there is a more robust T-cell effector response. Furthermore, although not conclusive, citrullination may lower the threshold required for effective TCR stimulation at lower doses of antigen. This is demonstrated by an increase in cytokine production at lower doses of citrullinated peptide compared to native antigen. Furthermore, preliminary data quantifying the interaction forces at various doses of OVAp or cit-

OVA also suggests that an increase in interaction strength may reduce the threshold for effective T cell activation.

5.2.4 Quantifying the interaction forces between naïve, primed and tolerised T-cells with DCs.

As described above the loss of self-tolerance in autoimmunity may be associated with post-translational modifications such as citrullination [431]. The above studies have demonstrated that naïve OVA-specific T cells are capable of recognising the citrullinated form of this peptide. However, it is unclear whether loss of self-tolerance in autoimmunity represents the recognition of novel citrullinated antigens by naïve T cells or whether previously self-tolerant T cells recognising modified self-antigens change in phenotype and become aberrantly activated. Therefore using the optical tweezer system I next sought to investigate the nature of the interactions of naïve, primed and tolerised populations of T-cells with DCs upon secondary exposure to antigen. Until now studies have only been able to image such interactions and have suggested differences in the dynamics of cell contact *in vivo* and quantifying T cell velocity, migration and clustering [145]. Directly quantifying these forces may enable a potential mechanism for the loss of self-tolerance to be investigated and determine for the first time whether the interaction strength plays a role in the breach of self-tolerance that may be associated with recognition of citrullinated antigens.

5.2.4.1 Induction of tolerance and priming.

In order to make comparisons between naïve, primed and tolerised T-cells, I first had to generate populations characteristic of naïve, primed and tolerised T-cells. An established model of oral tolerance induction was used by feeding OT-II TCR transgenic mice OVA dissolved in drinking water at a concentration of 50 mg/ml for 10 days [145]. Another group of OT-II mice were primed by immunisation with a single dose of 100 µg OVA emulsified in Complete Freunds' adjuvant (CFA), whilst naive mice were fed saline only. Eleven days later mice were sacrificed and cells of

the peripheral lymph nodes and mesenteric lymph nodes analysed for lymphocyte phenotype to ensure the tolerising and priming regimes had generated the expected cell phenotypes using flow cytometry. The remaining cells were used for optical tweezer experiments. See **Figure 5.7** for experimental schedule.
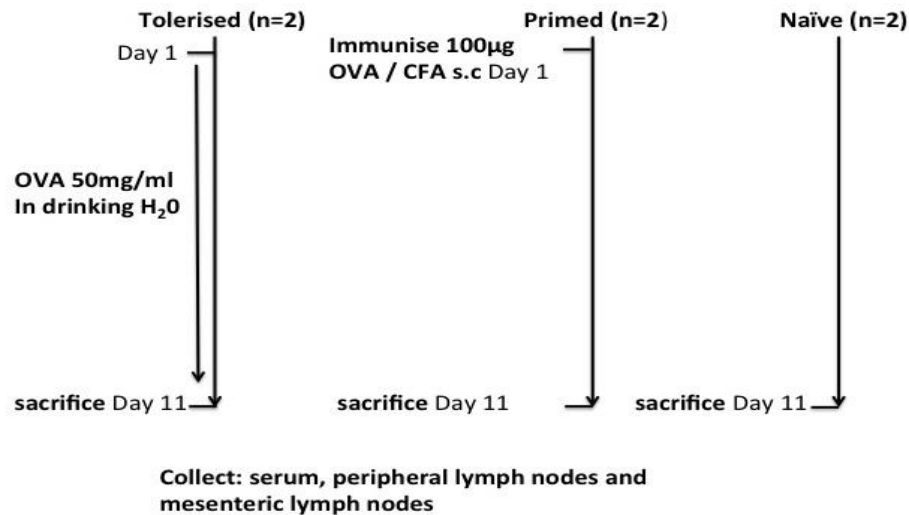
Figure 5.7: <u>**Experimental schedule for tolerance induction.**</u>

OT-II mice were fed OVA in drinking water at 50 mg/ml for 10 days or immunised subcutaneously with 100 μg OVA emulsified in complete freund's adjuvant (CFA). The generation of tolerant or primed population of T-cells was assessed 10 days later.

As demonstrated previously [90,437], orally tolerising mice with antigen generates OVA-specific T-cells with an increased CD25 expression, compared to naïve or primed controls. Indeed analysis of T-cells isolated from the lymph nodes of tolerised mice showed a phenotype which is consistent with tolerance (**Figure 5.8**). Moreover, OVA-fed mice showed increased expression of transcription factor Foxp3 by CD4$^+$CD25$^+$ cells, as well as elevated levels of CTLA-4 and the inhibitory surface molecule PD-1 [437–439]. These results demonstrate that we were able to generate populations of phenotypically distinct cells, displaying characteristics of primed or

tolerised T cells. Importantly, cells from these mice could then be used to determine the interaction forces upon secondary exposure to antigen.
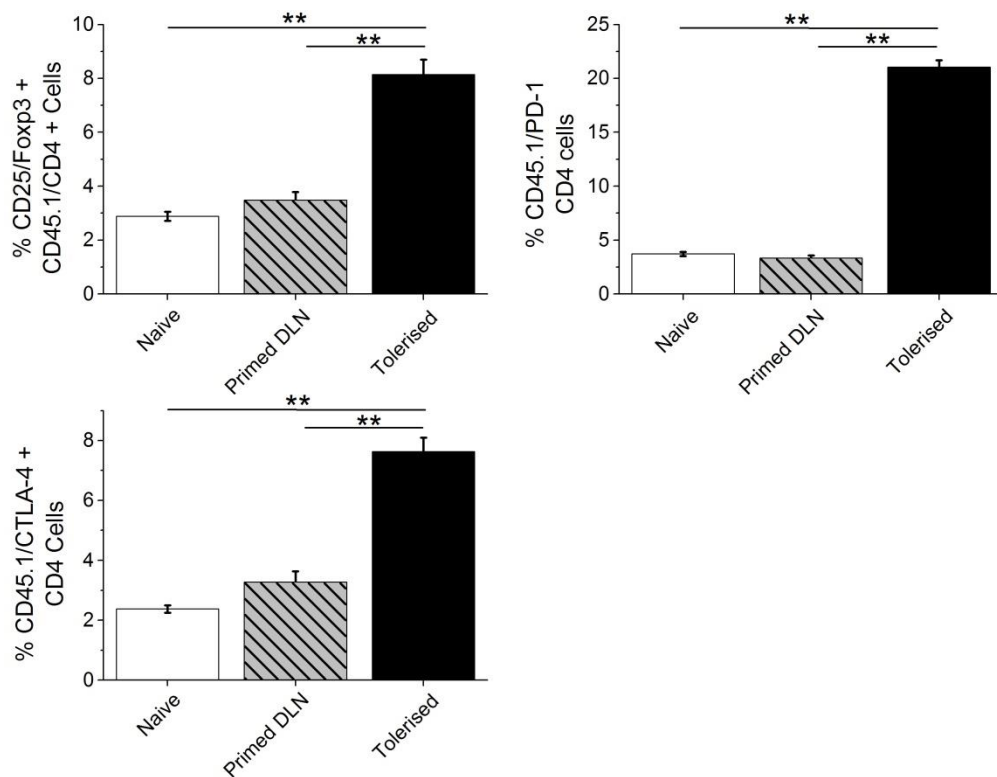
Figure 5.8: <u>**Phenotype of primed, tolerised and naïve T-cells.**</u>

OT-II mice were tolerised by feeding OVA dissolved in drinking water at a concentration of 50 mg/ml for 10 days. Control mice were primed by immunisation with a single dose of OVA/CFA at 100 µg/ml, whilst naive mice were fed saline only (**See Figure 5.7**). Mice were sacrificed and T cells analysed by flow cytometry for the expression of the indicated markers. Data shown is the % of indicated markers gated on CD4$^+$ T-cells for naïve (white bars) primed draining lymph node (DLN) (stripe bars) and tolerised (black bar). (** p ≤ 0.005 by un-paired t-test).

5.2.4.2 Comparison of interaction forces between naïve, primed and tolerised T-cells with DCs.

Having demonstrated that OVA-specific T cells could be induced towards a tolerant or primed phenotype *in vivo*, these cells were then analysed using the optical tweezer system to quantify the interaction forces between these populations of T-cells (naïve, primed or tolerised) and DCs. The initial force of interaction was measured as above (**Section 5.2.2**) and described in detail in **Chapter 3**.

As shown in **Figure 5.9A**, the interaction force between naïve T-cells and DCs was significantly increased recognising OVAp, with an increase in the median force of interaction from 3.3 pN ± 4.3 pN (unpulsed) to 9.4 pN ± 4.5 pN (OVAp pulsed). Interestingly the force of interaction between either primed or tolerised T-cells and OVA-presenting DCs was significantly lower than forces generated by naïve T-cells recognising antigen (**Figure 5.9**, **panels B, C**). Although there is slight evidence to suggest that some CD4$^+$ T-cells are interacting with a high interaction force in both primed and tolerised conditions, the vast majority of interactions could be pulled apart at the lowest interaction force measured. This suggests that naïve T-cells require a stronger interaction to accumulate sufficient signalling for T-cell activation. It also suggests that tolerised or primed T-cells are more efficient at scanning the surface of a DC and perhaps do not require a stable contact, supporting the data from *in vivo* imaging of similar cell populations [145].
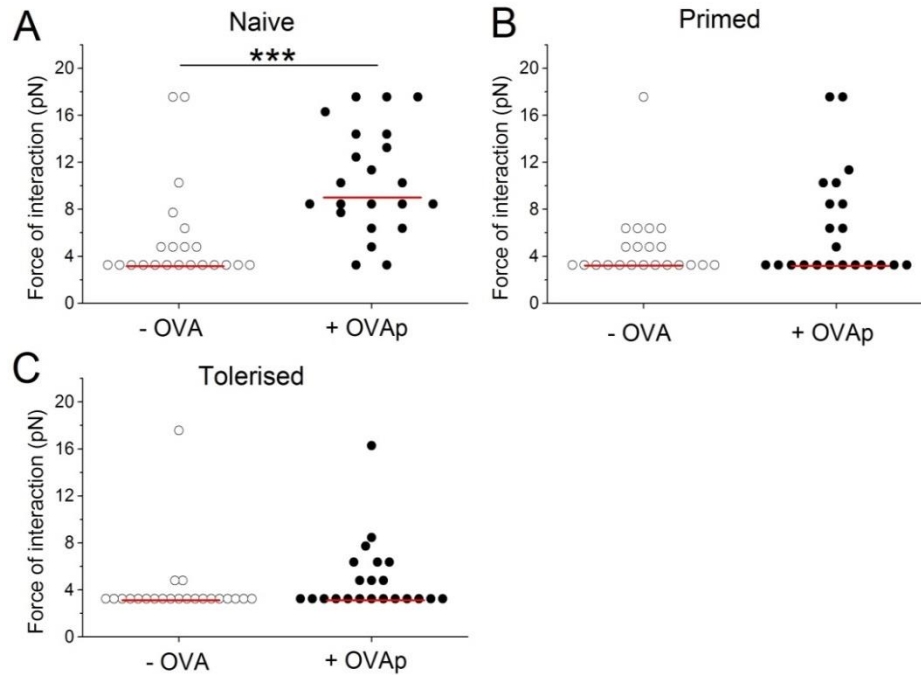
Figure 5.9: **Quantification of the interaction force between naïve, primed or tolerised CD4$^+$ T-cells with DCs.**

DCs were pulsed with OVAp as described above and used to present to either naïve, primed or tolerised OVA-specific OT-II T cells as described in **Chapter 3**. The force required to separate T-cells and DCs after 120 seconds of interaction was then determined using calibrated optical tweezers. Data shows the force required to separate individual cell interactions of 3 independent experiments with the median indicated (red line). (*** p $\leq$ 0.0005, by Mann Whitney test).

It has previously been shown that the duration of interaction between T-cells and DCs can often last longer than 12 hrs during activation, but that transient contacts may lead to tolerance. Therefore, having shown that both tolerised and primed CD4$^+$ T-cells generate a significantly lower interaction force with DCs than naïve T-cells, I next sought to investigate the interactions between these cells at different time points of co-culture. OVA-pulsed DCs were again used to present to either naïve, primed or tolerised OVA-specific OT-II T-cells and forces measured after 4 hrs (**Figure**

5.10) or 24 hrs (**Figure 5.11**) of incubation. As shown in previous experiments, naïve T cells showed a significant increase in interaction force with DC upon recognition of antigen, increasing from 3.3 pN ± 5.5 pN (un-pulsed) to 10.2 pN ± 5.8 pN (OVAp pulsed) (**Figure 5.10A**). Interestingly the interaction forces between a primed T-cell and DC showed a very different trend from the first contact, demonstrating a significant increase in interaction force from 4.8 pN ± 6.6 pN (un-pulsed) to 17.6 pN ± 5.4 pN after 4hrs and 17.6 ± 5.5 pN after 24 hrs (**Figures 5.10B & 5.11B**). This same result was observed when looking into the interaction forces between a tolerised T-cell and DC (**Figure 5.10C & 5.11C**). Interestingly, the median interaction forces for primed and tolerised T-cells were somewhat higher than naïve T-cells after 4 hrs (10.2 pN, naïve; 17.6 pN primed; 17.6 pN, tolerised). Further statistical analysis showed a small significant increase ($p = 0.04$) in interaction force between naïve and primed T-cells. However, further analysis may be required as many of the cell measurements had reached the maximum threshold of the optical tweezer system.
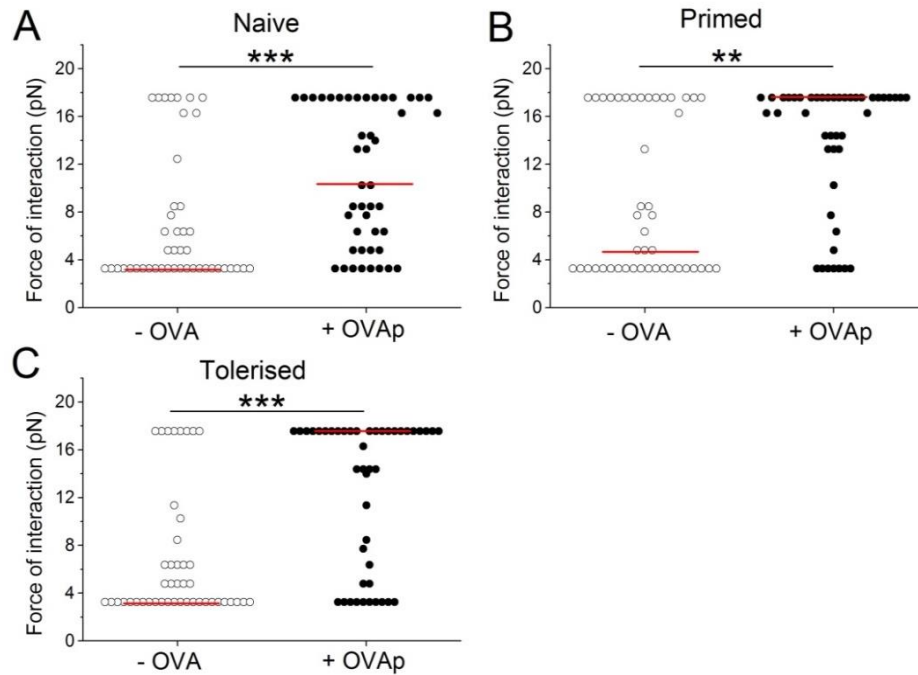
Figure 5.10: <u>Quantification of the interaction force between naïve, primed or tolerised CD4$^+$ T-cells with DCs after 4 hrs.</u>

DCs were pulsed with OVAp as described above and used to present to OVA-specific OT-II T cells (naïve, primed or tolerised) as described in **Chapter 4**. The force required to separate T-cells and DCs after 4 hrs of interaction was then determined using calibrated optical tweezers. Data shows the force required to separate individual cell interactions of 3 independent experiments with the median indicated (red line) (** p$\leq$ 0.005, *** p $\leq$ 0.0005, by Mann Whitney test).
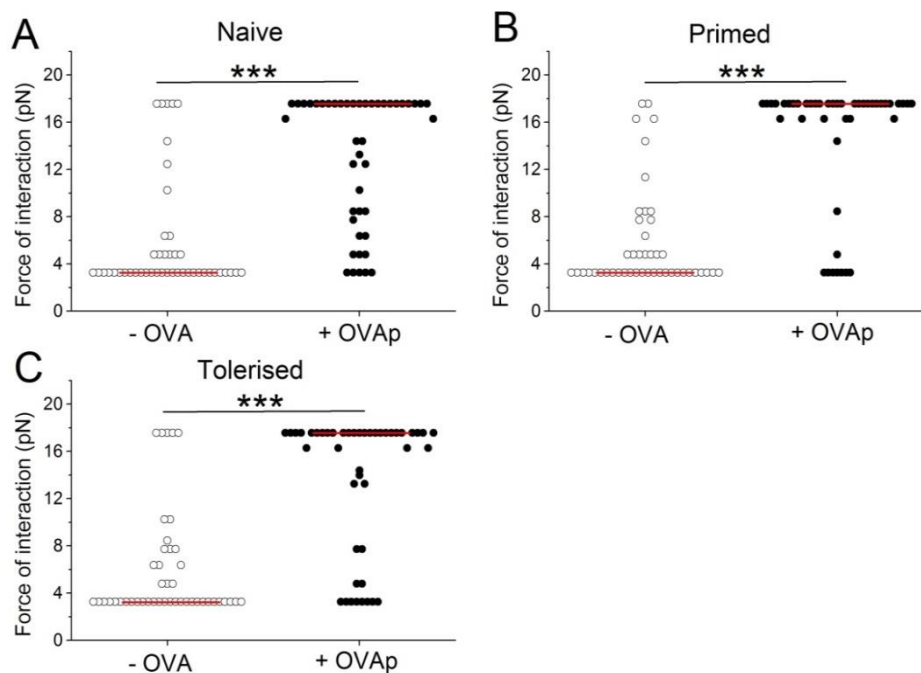
Figure 5.11: <u>Quantification of the interaction force between naïve, primed or tolerised CD4⁺ T-cells with DCs after 24 hrs.</u>

Forces of interaction were determined as in **Figure 5.10**, except after 24 hrs of interaction. Data shows the force required to separate individual cell interactions of 3 independent experiments with the median indicated (red line) (*** $p \leq 0.0005$, by Mann Whitney test).

Overall the results suggests that upon early initial interaction, tolerant and primed T-cells do not bind with strong affinity to DCs pulsed with OVAp. However, at later stages of activation, the forces of interaction between antigen-experienced T cells and an antigen-presenting DC are significantly higher than those of naïve T cells, irrespective of whether a T-cell is primed or tolerised. Certainly *in vivo* imaging has revealed that tolerant and primed T-cells are able to form large sustained clusters with DCs [144,145]. Yet despite this, these studies have been limited to certain imaging time-windows and may miss important initial interactions which may influence the function of T-cells. For the first time we were able to quantify the interaction force between tolerant and primed T-cells potentially revealing that the initial strength of

interaction could determine the function of tolerant vs primed vs naïve T-cells, perhaps playing a role in the maintenance of peripheral tolerance.

5.2.4.3 Comparison of interaction forces between naïve, primed and tolerised T-cells with DCs presenting OVAp or cit-OVA.

Having demonstrated that tolerised and primed OVA-specific T-cells show different kinetics in the strengthening of interaction forces upon secondary exposure to antigen when compared to naïve T-cells recognising antigen for the first time, and having demonstrated that recognition of cit-OVA results in enhanced T-cell functions associated with increased interactions, I next aimed to determine whether recognition of citrullinated antigen may enhance the activation of previously tolerant T cells. If mice are tolerised with native ovalbumin but their T-cells restimulated with the citrullinated form of OVA, then I hypothesised that there would be a stronger interaction force suggesting that tolerance is broken as a result of citrullination.

The following data set was obtained in parallel with the data presented in **Figures 5.9 to 5.11**. However, the data below shows the quantification of interaction force with DCs presenting cit-OVA antigen in order to compare the interaction forces between T-cells (naïve, primed and tolerised) with DCs presenting either native antigen or citrullinated antigen. As shown in **Figure 5.12**, **panel A**, the initial interaction force between naïve T-cells and DCs was significantly increased upon first recognition of cit-OVA, with an increase in the median force of interaction from 3.3 pN ± 4.3 pN (un-pulsed) to 14.2 pN ± 6.1 pN (cit-OVA pulsed). The median force of interaction between T-cells and DCs (cit-OVA) was slightly higher when compared to DCs (OVAp), supporting earlier findings (**Figure 5.3**).

Interestingly, recognition of citrullinated OVA by tolerised or primed T cells did not result in any significant increase in the initial interaction forces with DCs. As shown in **Figure 5.12B** & **C,** the interaction force between T-cells (primed and tolerised) and DC (cit-OVA pulsed) was broadly similar to T-cells recognising native OVAp. Interestingly, the median force of interaction between tolerant cells recognising cit-OVA was slightly elevated when compared to tolerant cells stimulated by native

antigen (3.3 pN ± 0.6 pN OVAp; 5.6 pN ± 5.5 pN cit-OVA). As shown in **Figure 5.12**, **panel C** it is evident that more T-cell/DC interactions (cit-OVA pulsed) were stronger, with some cell pairs reaching the maximum force that could not be quantified. This was not observed in T-cell/DC interactions (OVAp pulsed) where all cell interactions were below maximum threshold. This subtle trend suggests that citrullination may increase the interaction force, and may suggest an association with recognition of citrullinated antigen and altered responses by tolerant T cells. However, as the number of individual contacts measured for cit-OVA samples was low, any interpretation of this trend should be approached with caution and no significant differences were detected in these preliminary experiments. By carrying out more quantification in interaction force, the result could be clarified and more accurate interpretation could be conducted.
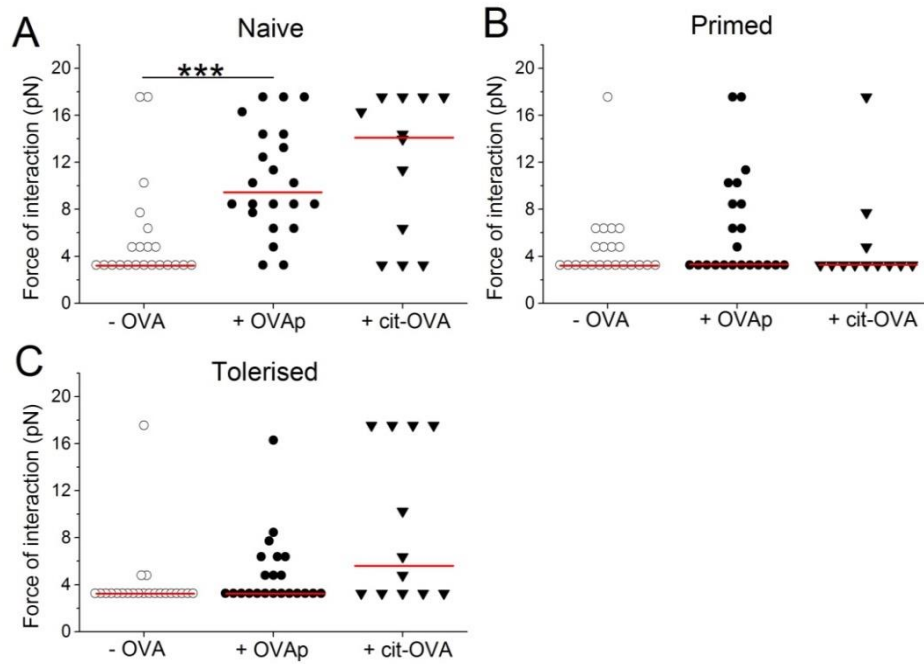
Figure 5.12: <u>**Quantification of the interaction force between CD4$^+$ T-cells and DC.**</u>

Force of interaction was determined after 120 seconds between T-cells and DCs as in **Figure 5.9**, with addition of cit-OVA sample. Data shows the force required to separate individual cell interactions of 2 independent experiments (cit-OVA samples) and 3 independent experiments (- OVA and OVAp samples) with the median indicated (red line) (*** p ≤ 0.0005, by Mann Whitney test).

As shown in **Figure 5.10** and **Figure 5.11**, the interaction forces of tolerised or primed T-cells increased significantly after co-culture for 4 or 24 hrs. We therefore quantified the interaction forces in cit-OVA stimulated samples, at later time points. A significant increase in interaction force between naïve T-cells and DCs was observed, from 3.3 pN ± 5.5 pN (un-pulsed) to 17.6 pN pN ± 5.5 pN (cit-OVA pulsed) (**Figure 5.13**, **panel A**). This was significantly higher than naïve T-cells and DCs (OVAp pulsed) which was in agreement with data shown earlier (**Figure 5.4**). Moreover, as shown in **Figure 5.13**, **panel B** and **C**, both primed and tolerised T-

cells interacted very strongly with DCs pulsed with cit-OVA after 4 hrs of co-culture. In primed T-cells, the median interaction force with DCs was increased from 4.8 pN ± 6.6 pN (un-pulsed) to 17.6 pN ± 5.9 pN (cit-OVA pulsed). In tolerised T-cells a similar trend was found, with a significant increase in interaction force between T-cells and DCs (cit-OVA pulsed) compared to T-cells and DCs (un-pulsed). These interactions were further strengthened after 24 hrs, with all T cell phenotypes showing very strong interactions upon recognition of either native or citrullinated antigen (**Figure 5.14**), confirming earlier experiments.
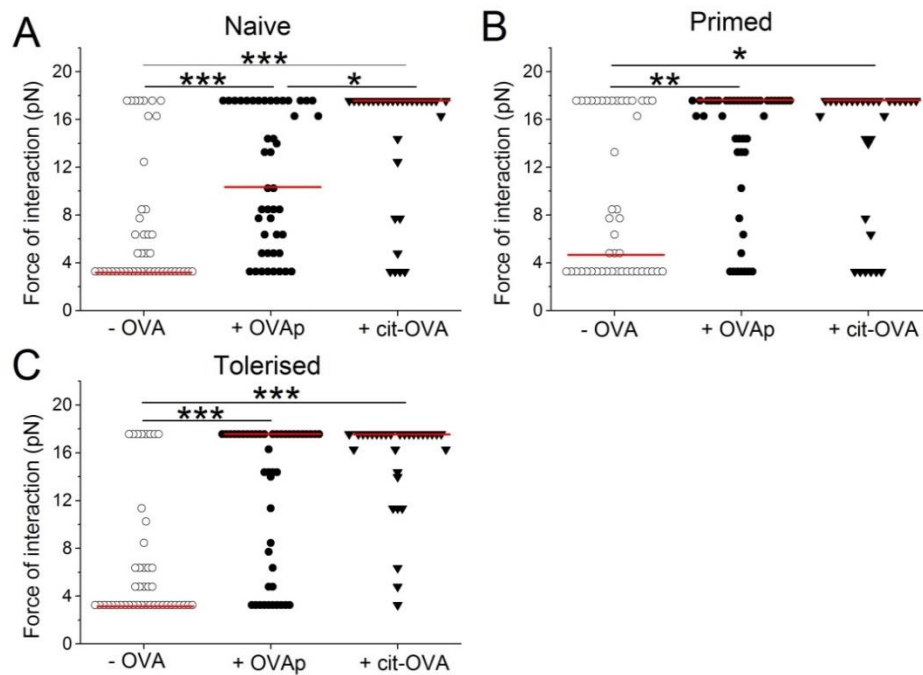
Figure 5.13: <u>Quantification of the interaction force between CD4^{+} T-cells and DC after 4 hrs.</u>

Forces of interaction were determined as in **Figure 5.10**, with addition of cit-OVA sample. Data shows the force required to separate individual cell interaction of 2 independent experiments (cit-OVA samples) and 3 independent experiments (- OVA and OVAp samples) with the median indicated (red line) ([*] $p \leq 0.05$, ([**] $p \leq 0.005$, [***] $p \leq 0.0005$ by Mann Whitney test).
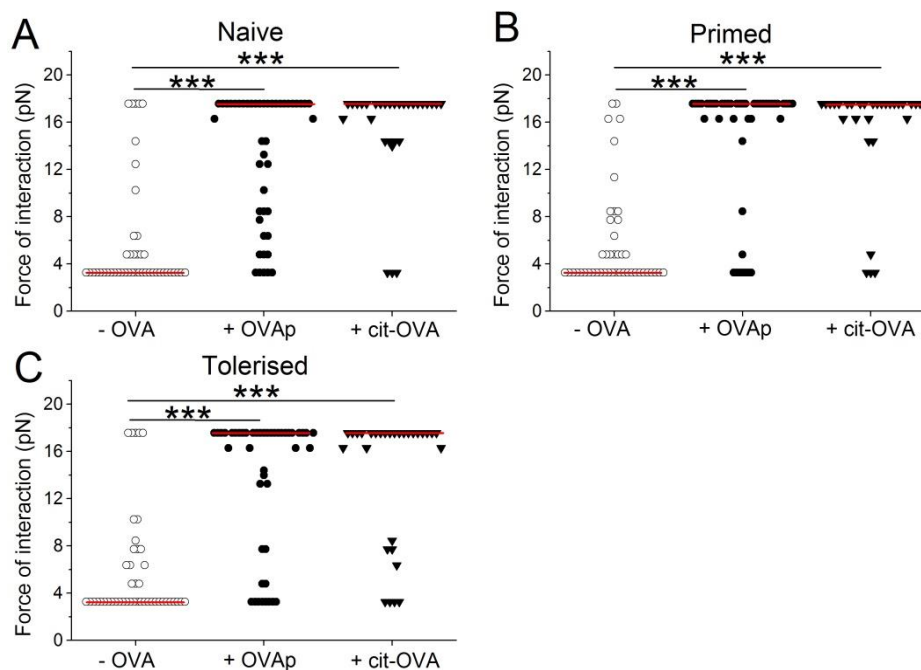
Figure 5.14: <u>Quantification of the interaction force between CD4^{+} T-cells and DC after 24 hrs.</u>

Forces of interaction were determined as in **Figure 5.11**, with addition of cit-OVA sample. Data shows the force required to separate individual cell interaction of 2 independent experiments (cit-OVA samples) and 3 independent experiments (- OVA and OVAp samples) with the median indicated (red line) ([***] $p \leq 0.0005$ by Mann Whitney test).

Overall the data presented above further demonstrates that recognition of citrullinated forms of antigen increases the interaction strength between naive T-cells and DCs. Whilst citrullination of antigen may increase the initial interaction force between tolerised T-cells and DCs, the low number of measurements meant that differences did not reach significance. Unfortunately, whether recognition of citrullinated antigen increases the interaction forces between tolerised or primed T-cells with DCs at later time points remains unknown. This is due to many of the cell pairs being above the maximum force available with the current optical tweezer setup, suggesting other techniques may be helpful in further interpreting the data.

5.3 Discussion.

Anti-citrullinated protein antibodies are highly specific for RA and the presence of citrullination can be a measure of disease severity; [427,433,440,441]; more so citrullinated proteins can increase the immunogenicity of RA disease with evidence suggesting that citrullination of proteins can break natural tolerance leading to immune attack of tissue within the joint [304,314,418,435,442–444]. However, the generation of ACPAs requires a breakdown of self-tolerance within the CD4^{+} T cell population, highlighting a potential role of T-cells. Moreover, further evidence strongly associates a role for antigen presentation in RA. Specifically individuals who possess the HLA-DRB1[*] shared epitope are more likely to develop RA disease [405]. Together, the above evidence strongly suggests a role for MHC-class II dependent T-cell activation in RA. TCR interactions with peptide complexes are highly specific with evidence showing that TCR can discriminate between subtle differences in the peptide:MHC complex. Despite binding affinities in the micro-molar range, differences in the affinity of TCR with peptide MHC complexes is critical for the development, survival and peripheral function of T-cells and can govern the magnitude of *in vivo* CD4^{+} and CD8^{+} T-cell responses to various antigens [65,115,445]. There is evidence to suggest that APCs can present self-proteins as a citrullinated peptide, breaking down tolerance and leading to immune response [318,319,446,447]. Therefore, as TCR can discriminate between subtle changes in peptide MHC, citrullination may play a key role in the initiation of RA whereby tolerance to joint-derived antigens is broken. Indeed citrullinated vimentin peptide binds with higher affinity for DRB1 [*]0401 than non-citrullinated vimentin [314]. Yet, it remains unclear if, or how, citrullinated antigen changes the interaction between T-cells and DCs and whether T-cell's effector function is changed and is sufficient to breach tolerance. Therefore I sought to determine whether citrullinated antigen changed the interactions between T-cells and DCs to further understand the pathology of disease.

Furthermore, the use of multi-photon imaging has revealed subtle differences in the interactions between tolerised, primed and naïve T-cells upon secondary exposure to antigen [145]. However, to date this technology has only been able to measure

parameters such as T cell migration, velocity or clustering with APCs. Therefore I also sought to quantify the interaction force between DCs and naive, primed or tolerised T-cells. Measuring how strongly the cells interact may reveal a potential mechanism underlying the maintenance of peripheral tolerance. Finally, I examined whether citrullinated antigen alters the interaction of tolerised T-cells with DCs to investigate whether the citrullination of antigen is sufficient to breach tolerance in the context of autoimmunity.

Results in **Figure 5.1** showed that T-cells recognised a citrullinated form of OVA presented on the surface of DCs and proliferated with the same magnitude as its native antigen (OVAp). Interestingly, **Figure 5.2** demonstrated that T-cells recognising citrullinated antigen had an enhanced T_H1 phenotype and that this was associated with T-cells interacting with cit-OVA with greater force relative to native antigen (**Figure 5.4**). This increase in force of interaction was evident across a range of cit-OVA doses compared to native antigen (**Figure 5.6**). Due to this increased affinity, the threshold for full T-cell activation may be lowered – as demonstrated by significantly higher IFN-γ production at lower doses of cit-OVA relative to OVAp (**Figure 5.5**). However, it is clear from this figure that the proliferative responses of T-cells at the highest dose of OVAp or cit-OVA were much lower than the proliferative capacity of T-cells stimulated with the same dose of antigen shown earlier (**Figure 5.1**). As this preliminary experiment was representative of 1 experiment it would be important to delineate this result further by repeating.

There is evidence to show that citrullination of antigen changes T-cell function. Specifically, work has shown a cohort of T-cells that selectively respond to citrullinated forms of hen egg lysozyme (HEL) bound to MHC molecule [418]. Furthermore, this study also showed that when DCs and peritoneal macrophages were pulsed with the native lysozyme protein, some of these cells presented a citrullinated form of HEL, resulting in the activation of citrullinated specific T-cells. A subsequent study used a defined peptide sequence from the cartilage proteoglycan aggrecan (P4D) previously shown to activate CD4$^+$ T-cells from DR4-IE transgenic mice. Using this peptide two new peptides were synthesised; one had aspartic acid

substituted by arginine (P4R) whilst the other had a citrullinated substitution at the same position (P4cit). Interestingly, they found that DR4-IE transgenic mice immunized with these peptides and assessed 10 days later showed altered T-cell responses. The P4D peptide induced a strong proliferative response with IFN-γ production [314,434]. Whilst the P4R peptide did not induce T-cell proliferation or cytokine production, the P4cit induced significant proliferation and IFN-γ production. Finally, Law *et al.* (2012) characterised T-cell auto-reactivity towards unmodified and citrullinated self-epitopes in RA patients and healthy controls. They found that the proliferation and cytokine production was very similar. However, citrullinated aggrecan was the most immunogenic with the production of pro-inflammatory cytokines such as TNF [435]. The above literature suggests that citrullinated peptides induce distinct T-cell responses and this is further confirmed in this chapter using an ovalbumin-based model. However, my work goes further and also attempts to define why T-cell responses directed against citrullinated antigens may be enhanced. Within this chapter and as shown in **Figures 5.3, 5.4** and **5.6** a potential mechanism was identified, suggesting that citrullination of peptide increases the interaction between T-cells and DCs, which may be sufficient to affect T-cell responses. These findings have wider implications, for example a study by Lundberg *et al.* (2004) compared the immune response to citrullinated rat serum albumin and to unmodified rat serum albumin, as well as induced arthritis by immunisation with citrullinated rat collagen type II or unmodified collagen type II. They showed that citrullination of non-immunogenic antigen Rat serum albumin (RSA) induced an antibody response against citrullinated protein as well as cross-reactivity to an unmodified protein. Furthermore, the proliferative responses to cit-RSA immunised rats demonstrated a significantly stronger response than cells from animals immunised with the unmodified protein [304]. Again, these enhanced responses may be down to altered T-cell/APC interactions in the context of citrullinated antigen within induction of RA. As the optical tweezer system demonstrated an enhanced interaction force due to citrullinated antigen, then this evidence strengthens the case for perhaps using multi-photon imaging to view cell-

cell interactions under collagen-induced arthritis with a citrullinated or native form of collagen type II peptide.

Multiphoton imaging has shown that tolerant T-cells are able to form stable contacts with DCs in a manner similar to activation. The main difference is that tolerant T-cells form a greater number of shorter lived, smaller clusters with DCs during tolerance induction, whilst under priming conditions there is the formation of large, stable clusters with DCs [144,145,448]. Furthermore, under tolerising conditions T-cells are able to regain migration quicker compared to priming conditions. Whilst it is important to appreciate the differences in the dynamics of T-cell/DC interaction during induction of tolerance and priming, it is important to understand the behaviour of T-cells during secondary exposure to antigen as this event may be associated with the loss of self-tolerance in RA and other autoimmune conditions. Moreover, it would be important to determine if T-cell/DC interaction is changed dependent if T-cells are naïve, primed or tolerised. This would help in the design of therapies to manipulate immune function.

Therefore we used the optical tweezer system to determine the interaction forces between naïve, primed and tolerised T-cells upon secondary exposure to OVA peptide. Tolerised and primed T-cells initially interacted with only very low forces (compared to naïve T-cells with DCs), but these interactions stabilised at later time points (**Figure 5.9**, **5.10** & **5.11**). Interestingly, primed T-cells have a decreased threshold for activation and require less co-stimulation to develop a robust effector response [448]. Therefore, primed and tolerised T-cells that have been previously exposed to antigen, may only require a short, low affinity interaction upon secondary antigen exposure. This is the case in memory T cells, which have a low dependence on co-stimulation and accelerated antigen responsiveness in comparison to naïve T-cells. Furthermore, tolerised T-cells may maintain tolerant to antigen as they interact initially with less force and thus there isn't sufficient TCR stimulation to activate the T-cell.

Observations in the samples at later time points also showed the formation of large clusters between T-cells and DCs. These were more evident in tolerised and primed samples than in samples containing naïve T cells (data not shown). An attempt was conducted to quantify this, as shown previously [449] although these results were inconclusive and more time was required to optimise this assay. A reason for this observation could be that T-cells can sense antigen dose. Antigen dose can govern the interactive behaviour with DCs [81,115] and evidence shows that T-cells can survey the amount of antigen present through multiple short interactions with DCs, with up-regulation of CD69 and the latter forming stable interactions with DCs quicker, at higher doses of antigen [9,80,190]. Perhaps tolerised T-cells are able to effectively recognise the antigen initially, but through time accumulate signals to assess the amount of antigen present. If there is a high level of antigen then they form large stable clusters with DCs and in doing so would prevent naïve T-cells getting access to p-MHC complexes. There is evidence to suggest that T-cells compete for p-MHC sites on APCs [450]. This data is also supported by *in vivo* evidence showing that T-cells are able to form stable contacts with DCs and form large clusters after 8 hrs of antigen challenge [128,144]. However, the data shown in **Figures 5.9**, **5.10** and **5.11** highlights the importance of the initial interactions between T-cells and DCs and that whilst studies using multiphoton imaging to determine the dynamics of interaction under tolerising, priming and naïve conditions *in vivo* have developed some important hypotheses, such imaging approaches might be missing very early events after antigen challenge.

We next determined whether secondary exposure to citrullinated OVAp would increase the strength between tolerised and primed T-cells to OVA. This would determine whether citrullination of antigen is sufficient to perhaps change the interaction dynamics between T-cells and DCs and thus alter effector function, perhaps breaching tolerance. From the data presented in **Figure 5.12**, **5.13** and **5.14** the force measurements followed the same trends as in **Figure 5.9** to **Figure 5.11**. However, for initial interactions, recognition of citrullinated antigen appeared to slightly elevate the interaction strength between tolerised T-cells and DCs, suggesting that indeed a citrullinated residue may be sufficient to breach tolerance.

However, as cell numbers were low and only based on two independent experiments further experiments would be needed to clarify this further. Moreover, improvements to the optical tweezer system would need to be applied in order to measure cell-cell interactions at later stages as many of the cell interactions were above the maximum threshold of the system. Further work could also antigen pulse with lower doses of antigen (**shown in Figure 5.6**). Here, at lower doses of antigen many of the cell pairs could be pulled apart, despite a 6 hr co-culture.

Multiphoton imaging could also be used to image T-cell/DC interactions upon secondary exposure to citrullinated antigen or native antigen. Native OVA could be used to tolerise and prime OT-II mice and the OVA-specific T-cells from tolerised, primed or naïve T-cells adoptively transferred into naive recipients. These recipient mice would then be challenged with either native or citrullinated antigen and the cellular interactions in the draining lymph node imaged using multiphoton microscopy to determine if there are any differences in the interaction dynamics. This approach was used by Rush *et al*. (2009) to determine the interaction dynamics between tolerised, primed and naïve T-cells upon secondary exposure to OVA [145]. They revealed that tolerised, naïve and primed T-cells display different dynamics of interaction with DCs upon secondary antigen exposure. Therefore, it would be interesting to determine whether upon secondary exposure to cit-OVA, tolerised T-cells display interaction dynamics more characteristic of naïve or primed T-cells, perhaps suggesting that tolerance is broken. However, it would be important to try and image cell-cell interactions as early as possible as the data in this chapter highlights the importance of the initial interactions between T-cells and DCs.

The above data suggests a role for citrullination of antigen in increasing the interaction forces between T-cells and DCs and with it a more robust T-cell effector response. My work quantified, for the first time, the interaction forces between naïve, primed and tolerised T-cells with DCs. It was found that tolerised and primed T-cells interacted initially with only a low force, but that this interaction force increased over time. Whilst this potentially implies that the affinity of TCR and pMHC may play a role in maintaining peripheral tolerance to an antigen, it also

reveals the importance of carrying out experiments at a single cell level and looking at the very first interactions between T-cells and DCs. Using multiphoton imaging to look at the dynamics of interaction between T-cells and DCs within lymph nodes has drawbacks. Often these experiments require a large number of $CD4^+$ or $CD8^+$ T-cells to be adoptively transferred into a recipient and after antigen challenge it is possible that the initial interactions between T-cells/DCs that are so essential to T cell function may be outside of the imaging volume. This can affect the outcome of T-cell activation and vary the dynamics of interaction due to intraclonal T-cell competition [450–452]. Moreover, the data not only highlights the importance of the initial interactions between T-cells and DCs at a single cell level but it also shows that citrullinated antigen can affect T-cell activation. This would have wider implications in designing therapeutics to prevent or promote citrullination to manipulate immune responses, particularly in treating RA where this plays a key role.

It is interesting to note that despite a citrullinated residue within the OVA peptide, OT-II T-cells specific for $OVA_{329-339}$ were still able to recognise and activate. More importantly is that T-cells responding to citrullinated antigen showed an enhanced effector response, which clearly shows that citrullinated-antigen, plays an important role in determining T-cell recognition and function. Overall the data highlights the importance of understanding the interactions between individual cells and that change in the strength and/or duration of interaction between a T-cell and APC can dramatically alter the functional outcome of T-cells. Further studies will be required to determine if similar interaction is observed *in vivo* as well as determine how citrullinated antigen reverse established tolerance to self-antigens. It is clear that the optical tweezers have revealed novel insights and through refinements it would further provide a useful tool to explore fundamental questions in the context of citrullination and RA.

Chapter 6 - Manipulating and quantifying immune cell interactions to understand the importance of MKP-II on T-cell function.

6.1 Introduction.

T-cells are the major players in the development of an adaptive immune response. Following activation they will proliferate and differentiate into effector cells that will help protect against pathogens such as bacteria, fungi and viruses. However, cells must be activated under the right conditions and must not activate in an inappropriate way, leading to a potential breakdown in tolerance and development of autoimmune disease. Over a number of years the signalling cascade in both T-cells and DCs has been investigated, demonstrating the importance of signalling and a subsequent T-cell response.

In **Chapter 3**, I demonstrated that pre-treatment of T-cells with the ERK inhibitor, FR180204 significantly reduced the force of interaction, abrogating T-cell/DC interactions. Previous work has shown that ERK is recruited to the immunological synapse and thus may play a role in altering the interaction forces between T-cells and DCs [116,326,327]. Moreover, inappropriate intracellular signalling can result in autoimmune disorders and differences in the responsiveness of naïve and antigen experienced T-cells is associated with changes in the phosphorylation of MAP-kinases such as p38 and ERK [118]. Furthermore, as discussed further in **Chapter 1**, MAP-kinases can play a role in determining the effector function of T-cells. Specifically, JNK can influence IL-2 production and T_H1 and T_H2 differentiation. p38 can affect T_H1 effector responses, specifically IFN-γ production. Finally ERK is required for effective IL-4 receptor function and T_H2 differentiation. These highlight the importance of intracellular signalling, in particular the role of MAP-kinases in affecting T-cell function.

Likewise MAP-kinases can also affect the maturation process of antigen presenting cells. A variety of studies using MAP-kinase inhibitors have demonstrated that DCs have impaired up-regulation of co-stimulatory function – essential for T-cell activation (**See Chapter 1**).

Whilst the differentiation and activation of T-cells is regulated by the MAP kinases, these are in turn regulated by MKP-II [344,346,349,350,453,454]. Indeed, this is demonstrated

in a study by Huang *et al.* where MKP-II-deficient T-cells were shown to be hyper-proliferative with enhanced CD25 expression and IL-2 signalling, as well as an increased STAT5 phosphorylation [348].

Given this evidence, and the influence that intracellular signalling has on the development of a T-cell response, it is important to investigate the influence of signalling molecules on T-cell interactions as understanding these may lead to new targeted therapeutics for intervention in cancer, autoimmune disease and persistent infections.

From the evidence presented above, MAP-kinases are emerging as key therapeutic targets in the context of immune regulation. Several studies have used inhibitors in experimental models of inflammatory diseases [455–457] whereby an immune response could be manipulated through inhibition of certain MAP-kinases within both T-cells and DCs. However, what is not clear is how deletion of MKP-II (which negatively controls the phosphorylation of MAP-kinases) can influence T-cell function and in particular how this alters the interaction between T-cells and DCs.

As described in **Chapter 1**, T-cell effector function is determined by interactions with a DC [88,89,121,458,459] and dysregulation of MAP-kinase or MKP-II activity within cells may therefore influence this interaction following antigen recognition. Specifically, a lack of MKP-II may enhance or prolong phosphorylation of ERK, especially at the synapse, increasing the strength of interaction between T-cell/DC. This links with reports that suggest ERK is active at the synapse and plays a role in microtubule-organising centre (MTOC) polarisation. Therefore, the hyper-proliferative response of MKP-II (or DUSP-4)-deficient T-cells [348] may actually be a result of altered interaction forces between T-cells and DCs, due to prolonged MAP-kinase production. Moreover, as highlighted above, activation of DCs is regulated by MAP-kinase activity and may influence T-cell effector function by regulating antigen-presentation and cell interactions.

In **Chapter 3**, I demonstrated that upon treatment with an ERK inhibitor, the interaction between a T-cell and DC was ablated completely, implicating ERK in

synapse formation and determining the interaction strength between T-cells and DCs. I therefore hypothesised that a failure to dephosphorylate ERK in MKP-II-deficient T-cells would prolong cell conjugate formation. Thus, the interaction force between MKP-II-deficient T-cells and DCs would not only be stronger initially, but also be maintained for longer. Therefore, within this chapter I aimed to investigate the effect of MKP-II deletion in T-cells or DCs on the activation of T-cells. Using optical tweezers I sought to measure the interaction force and determine whether any differences in T cell function were associated with a stronger force, potentially explaining the hyper-proliferative response described for MKP-II-deficient T-cells.

6.2 Results.

6.2.1 MKP-II and T-cell function.

Given the potential role of MKP-II in affecting T-cell function my first objective was to determine whether MKP-II knockout T-cells would display un-controlled T-cell activation through higher production of cytokines and increased proliferative capacity. To do this, MKP-II-sufficient (MKP-II$^{+/+}$) or MKP-II-deficient (MKP-II$^{-/-}$) mice were back-crossed onto the OT-II TCR transgenic background. This created mice in which the majority of T-cells expressed a TCR specific for OVA$_{323-339}$ peptide, but lacked this important MAP kinase phosphatase.

I first examined whether these MKP-II-deficient OT-II T-cells showed an increased capacity for proliferation or effector function upon antigen stimulation. Whilst T-cells from a different MKP-II-deficient mouse have shown to be hyper-proliferative, differences in the knockout strategy could influence results and it was therefore necessary to validate these findings in our system [460].

DCs derived from wild-type mice were prepared as previously described, and used to stimulate lymphocytes from MKP-II-sufficient or MKP-II-deficient OT-II mice. Cells were co-cultured for 48hrs and were analysed for proliferation (by staining with Ki-67) and effector function (by measuring cytokine secretion), as described in **Chapter 2**.

As shown in **Figure 6.1**, there was a significant increase in T-cell proliferation in OVA-pulsed samples, demonstrating an antigen-specific response. However, this was irrespective of whether T-cells were isolated from MKP-II$^{+/+}$or MKP-II$^{-/-}$ OT-II mice. The proportion of proliferating T-cells in the presence of antigen was 80% for wild-type OT-II T cells and although T-cells from knockout animals showed a slightly elevated proliferative response (with 88% of cells showing cell division), this was not significant.

Supernatants from the above cultures were collected and analysed for cytokine production (**Figure 6.2**). A similar pattern to the T-cell proliferation (**Figure 6.1**)

was observed, with a significant increase in the production of IFN-γ and IL-5 when T cells were stimulated with OVA antigen, but again there were no differences in the capacity of MKP-sufficient and MKP-deficient T-cells to secrete either cytokine.
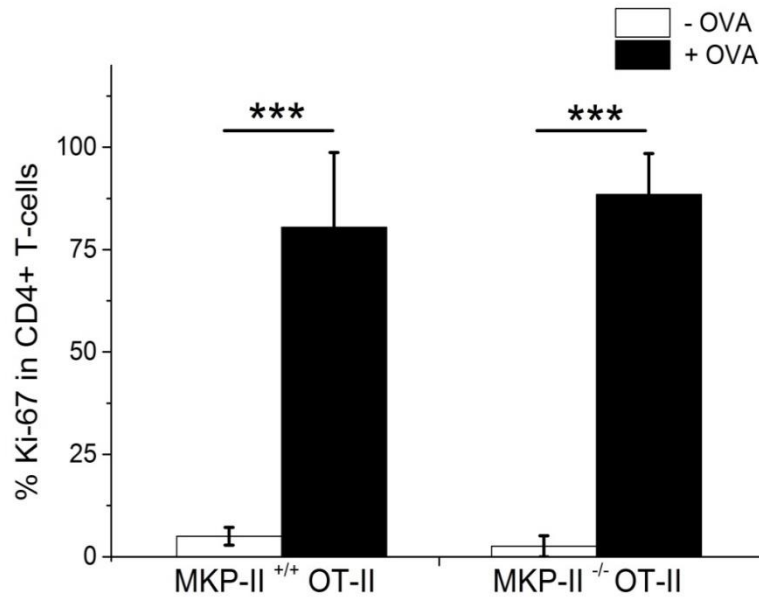
Figure 6.1: <u>**Analysing the proliferation of MKP-II $^{+/+}$ and MKP-II $^{-/-}$ CD4$^+$ T-cells.**</u>

Wild type or MKP-II-deficient T-cells (5×10^5) were co-cultured in 24 well plates with 5×10^5 un-pulsed (white bars) or antigen-pulsed (black bars) DC. Proliferation of CD4$^+$ T-cells was assayed 48 hrs later using flow cytometry and staining for proliferation marker Ki-67. Results shown are the mean % proliferation (± SD) of CD4$^+$ lymphocytes in triplicate cultures of 2 independent experiments. (*** p ≤ 0.0005 by un-paired t-test).
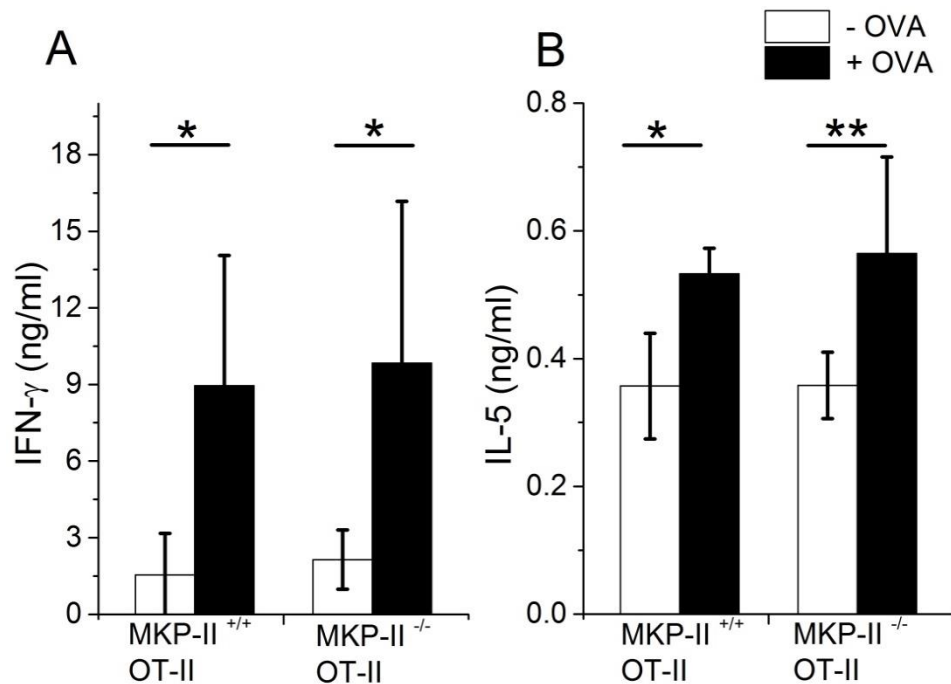
Figure 6.2: <u>Analysing cytokine release of MKP-II [+/+] and MKP-II [-/-] CD4^{+}</u>
<u>T-cells.</u>

Cells were stimulated as in **Figure 6.1** and cytokine production was measured
by ELISA of culture supernatants after 48 hrs. Results shown are the mean
concentration (± SD) of IFN-γ (**A**) and IL-5 (**B**) in triplicate cultures of 2
independent experiments. ([*] $p \leq 0.05$, [**] $p \leq 0.005$ by un-paired t-test).

Together this demonstrates that MKP-II deletion does not increase the proliferative
capacity or cytokine production of T-cells. These results were somewhat surprising
as I had first hypothesised that the activation would be higher in MKP-II^{-/-} T-cells,
and these findings contradict the report by Huang *et al*. (2012), where MKP-II-
deficient (or DUSP-4-deficient) T-cells were hyper-proliferate upon stimulation [348].
Differences in the method used to quantify the proliferation or the method of
stimulation used to activate T-cells may account for this. However, these findings
do show that knockout T cells can activate efficiently and as such I next wanted to
determine whether the interaction forces between DC and T cell were affected by
MKP-II deficiency.

6.2.2 MKP-II and T-cell/DC interaction force.

Although no functional differences were evident during the early stages of MKP-II$^{+/+}$ and MKP$^{-/-}$ T-cell activation, it remained possible that the interaction forces were altered in MKP-II-deficient T cells. The results in **Chapter 3** demonstrated that inhibition of ERK signalling within T-cells significantly decreased their force of interaction with antigen-presenting DCs. As MKP-II negatively regulates ERK by de-phosphorylation, I hypothesised that there would be a stronger interaction force, especially at later time points when MKP-II activity may become more important in regulating ERK phosphorylation.

Interaction forces between MKP-II-sufficient or MKP-II-deficient OT-II T cells and antigen-pulsed DCs were measured at various times of co-culture, as previously described (**Chapter 4**). As shown in **Figure 6.3**, after 30 minutes of co-culture, the interaction force between wild-type T-cells and DCs was significantly increased by the presence of OVA, with an increase in the median force of interaction from 4 pN ± 5.7 pN (un-pulsed) to 13.8 pN ± 6.1 pN (OVA-pulsed). Whilst there was still a clear antigen-dependent force of interaction between MKP-II-deficient T cells and DCs (un-pulsed 3.3 pN ± 5.9 pN; OVA-pulsed 12.8 pN ± 5.8 pN), there were no clear significant differences detected to wild type, using the measurement tool available. By implementing a higher laser power, higher forces could be measured to solve this problem (later discussed in **Section 7.3.1**). As MKP-II may act upon MAP-kinase activity at later time points after initial T-cell signalling, the force of interaction between T-cells and DCs was next quantified at later time points. The same trend was shown throughout all time points (3 hrs, 6 hrs and 24 hrs) where there was clear antigen-specific increase in the interaction force, but no difference detected between MKP-II$^{+/+}$ and MKP$^{-/-}$ T-cells
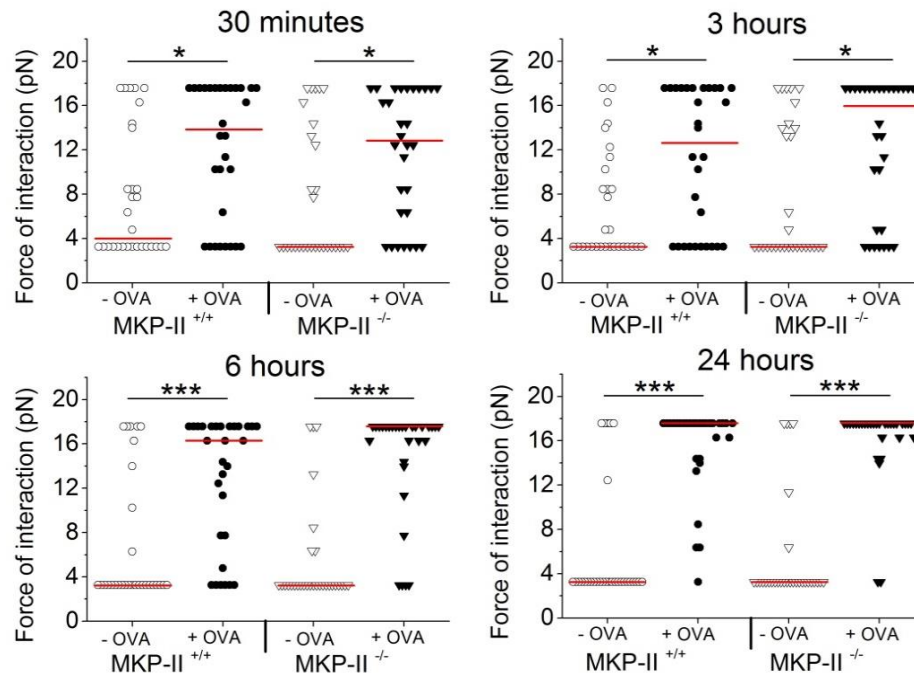
Figure 6.3: <u>Quantification of the interaction forces between DCs and MKP-II $^{+/+}$ and MKP-II $^{-/-}$ CD4$^+$ T-cells.</u>

DCs were pulsed with OVA as described in **Chapter 4**, **Section 4.2.2** and used to present to OVA-specific MKP-II$^{+/+}$ or MKP-II$^{-/-}$ T-cells as described in **Chapter 4**. Data shows the force required to separate individual cell interactions of 2 independent experiments with the median indicated (* p ≤ 0.05, *** p ≤ 0.0005 by Mann Whitney test).

It is interesting that whereas at the 30 minute time point, many of the cell pairs could be pulled apart but after a 24 hr co-culture many of the cell pairs could not be separated. This was due to the interaction force being greater than the maximum force of the optical tweezers. Testing the significance with a non-parametric Mann-Whitney test, there is a significant increase in the interaction force between T-cells and DCs when comparing 30 minutes and 24 hrs of co-culture for both wild type (p= 0.02) and knockout samples (p = 0.0005) within + OVA samples. Thus, although these findings suggest that there are few differences in the interaction forces of MKP-II$^{-/-}$ T cells over 24 hrs, they demonstrate that the optical tweezer system could

178

be used to detect differences in the interaction force over time. This could be important if testing therapeutics that seek to alter the kinetics of T-cell/DC interactions and potentially provides a tool to explore this dynamic interaction further. However, the issue with the ceiling effect as discussed in **Chapter 3, Section 3.4.2.1** would have to be addressed. Using a higher powered laser source or combining the optical tweezer system with Atomic Force Microscopy to measure higher interaction forces could address this.

6.2.3 Activation, up-take and presentation of MKP-II$^{+/+}$ and MKP-II$^{-/-}$ DCs.

Having determined that T-cells lacking MKP-II show no obvious defect in proliferation or function and that they interact with antigen-presenting DCs with a force similar to that of wild-type T cells, I next wanted to investigate whether expression of MKP-II by DCs might play any role in immune activation.

As discussed in the introduction, inhibiting MAP-kinases in DCs can affect the maturation following LPS or TNF-α stimulation. Depending on which MAP-kinase is inhibited, the expression of co-stimulatory markers can be reduced following stimulation [461]. As MKP-II negatively regulates MAP-kinases, understanding more about MKP-II in DC function, as well the subsequent effect on T-cell function, would be important. It may reveal novel targets for the therapeutic intervention in modulating an immune response.

It is well known that the strength of TCR and pMHC interactions sets a minimum dose requirement for the initiation of T-cell activation [462]. Therefore, I first assessed whether MKP-II deficiency would affect the activation of DCs or uptake and presentation of antigen. DCs derived from the bone marrow of wild type or MKP-II$^{-/-}$ mice were plated in a 24 well plate (5 x 10^5 total cells per well), and LPS-stimulated. Following 24 hr incubation, DCs were then analysed for MHC-II and CD40 expression. As shown in **Figure 6.4,** there was a clear up-regulation of both

MHC-II and CD40 upon LPS stimulation. Importantly, there was no difference in the ability of MKP-II$^{-/-}$ DCs to activate relative to wild type DCs.
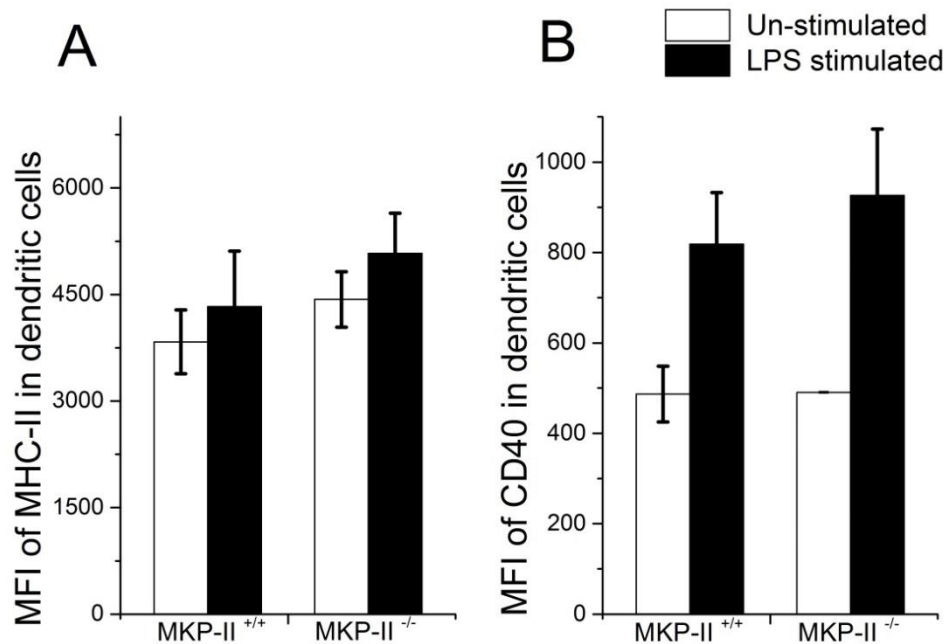
Figure 6.4: <u>**MHC-II and CD40 up-regulation on MKP $^{+/+}$ and MKP $^{-/-}$ DCs.**</u>

Bone-marrow derived DCs from wild type or MKP-II-deficient mice (as labelled) were stimulated with 1μg/ml of LPS (black bars), control cells remained un-stimulated (white bars). DCs were incubated for 24 hrs, after which MHC-II and CD40 expression was anaylsed on CD11c-gated viable cells by flow cytometry. Data shows the mean fluorescence intensity of FITC-MHC-II and APC-CD40 of 1 experiment of duplicate culyures ± SD.

Subsequently, the uptake and presentation of antigen was determined in MKP-II$^{+/+}$ and MKP-II$^{-/-}$ DCs using EαGFP. When EαGFP is taken up by DCs, it is degraded and the Eα peptide:MHC complex can be detected by staining cells with a monoclonal YAe antibody, which is specific for the MHC-II:Eα complex. This allows assessment of antigen uptake (by quantifying GFP-containing cells), in combination with measuring antigen-presentation (using the YAe antibody) [449] [354].

From **Figure 6.5** it is clear there were no differences in the uptake of antigen (based on MFI of GFP) between MKP^{+/+} and MKP^{-/-} DCs. However, a small but significant decrease in the level of antigen presentation was evident in MKP-II^{-/-} DCs. This was true whether DCs were either un-stimulated or LPS-stimulated. However, as this was from one preliminary experiment it would have to be repeated to clarify and therefore should be interpreted with caution.
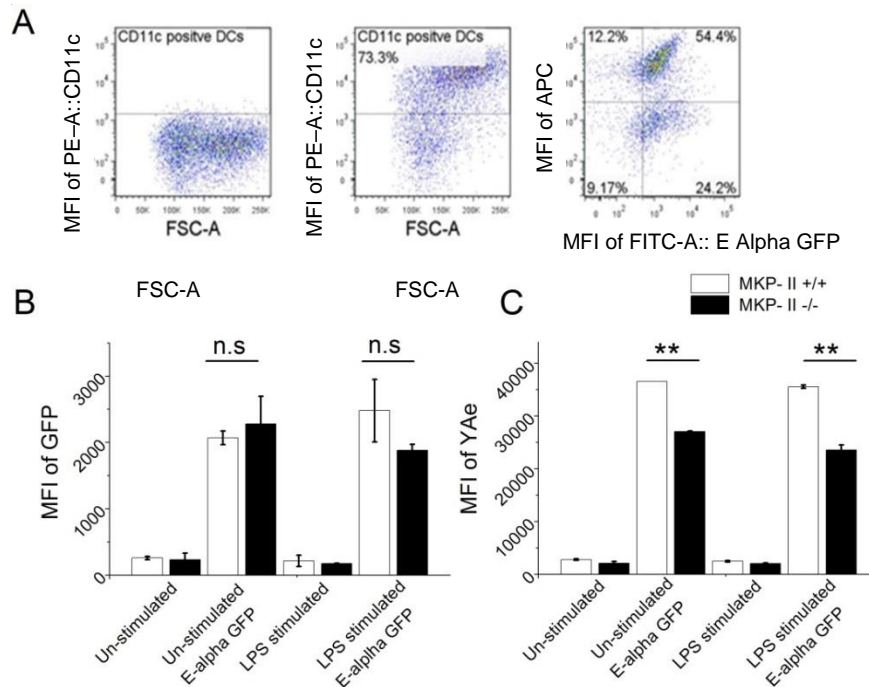
Figure 6.5: <u>**Measurement of antigen up-take and presentation of wild type and knock out DCs by EαGFP/YAe system.**</u>

Bone-marrow derived DCs (5×10^5/ml) from wild type (white bars) or MKP-II-deficient (black bars) were incubated in media. DCs were either un-stimulated or stimulated with 1 μg/ml of LPS, and incubated with or without 100 μg/ml of EαGFP for 24 hrs, as labelled. **A:** Shows an example of gating strategy. Cells were analysed on forward scatter and CD11c positive DCs were gated based on isotype controls. Cells above gate were CD11c positive (73.3% as shown), with MFI of GFP and YAe levels being carried out on CD11c positive DCs, The bar graphs show the MFI of GFP (**B**) and MFI or YAe (**C**)

in different groups, as labelled.   Results shown are expressed as mean ± SD of triplicate cultures in 1 experiment.   (** p ≤ 0.005 by un-paired t-test).

Whilst this apparent difference may represent a reduced capacity for antigen-presentation in MKP-II$^{-/-}$ DCs, further analysis of these data also indicated a reduced proportion of CD11c-expressing cells in cultures derived from MKP$^{-/-}$ animals. In wild-type DCs the mean proportion of CD11c^{+} cells within triplicate samples was 87% (un-stimulated) and 87.5% (LPS stimulated).   This was significantly higher than cultures from knockout animals where between 73% (LPS stimulated) and 73% (un-stimulated) of cells were CD11c-expressing, as shown in **Figure 6.6**.   This indicates that the lower antigen-presentation in knockout DCs evident in **Figure 6.5** may reflect fundamental differences in the generation of functional DCs in the absence of MKP-II.   It also indicates that MKP-II may play a role in the development of DCs from bone-marrow.
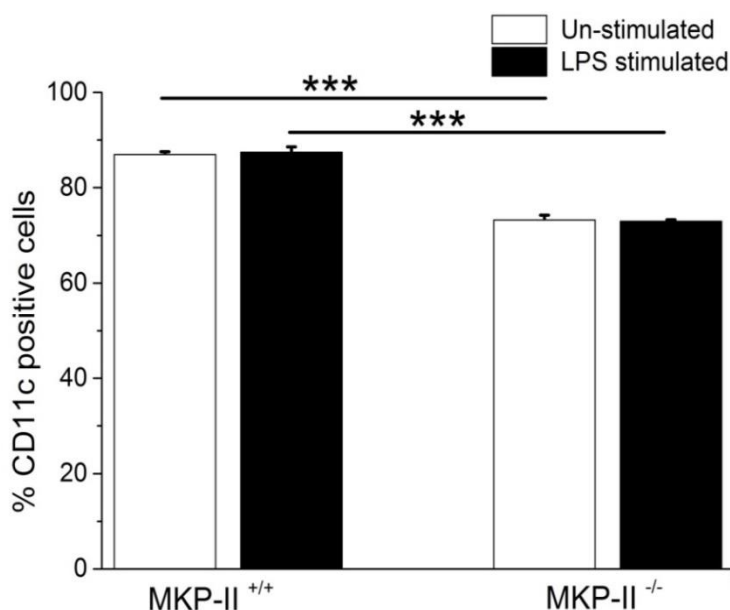
Figure 6.6: <u>% of CD11c positive DCs in wild type and knockout DC.</u>

Flow cytometry was used to determine the mean % of CD11c positive DCs in either wild type or knockout DCs. Results shown are expressed as mean ± SD of triplicate cultures of 1 experiment. ([***] p ≤ 0.0005 vs MKP-II knockout by un-paired t-test).

6.2.4 T-cell function and MKP-II [+/+] and MKP-II [-/-] DCs.

As DCs derived from MKP^{-/-} mice may show differential functionality compared with wild-type DCs, I next sought to determine whether such differences might affect the proliferative and effector function of T-cells. I hypothesised that T-cells activated by DCs generated from MKP^{-/-} mice would be hypo-proliferative and have lowered cytokine production compared with T cells co-cultured with wild type DCs. Indeed in a study by Schroeder *et al.* (2013), infection with *L. major* found that naïve MKP-II deficient macrophages were more susceptible to infection compared to wild-type macrophages and this resulted in a generalised T-cell hypo-responsiveness [350]. Furthermore, as shown in **Figure 6.5**, a lower amount of antigen presentation could affect the robustness of T-cell activation as the interaction dynamics with DCs and the level of T-cell activation are highly dose-dependent [81].

As described previously, OVA-specific OT-II T-cells were co-cultured with OVA-pulsed DCs generated from either MKP$^{+/+}$ or MKP-II$^{-/-}$ mice, for 48 hrs (control cells remained un-pulsed) and were analysed for proliferation (by staining with Ki-67) and effector function (by measuring cytokine secretion). As shown in **Figure 6.7A**, and as expected, the proportion of proliferating T-cells co-cultured with MKP-II-sufficient DCs increased from 4% (un-pulsed) to 83% (OVA-pulsed). The proportion of proliferating T-cells stimulated with MKP-II-deficient DCs increased from 5% (un-pulsed) to 89% (OVA-pulsed) and this was not significantly decreased relative to proliferation of T-cells stimulated by wild-type DCs as was expected. A similar pattern was observed with cytokine production, with a significant increase in the OVA-specific production of IFN-γ and IL-5 when T cells were stimulated with OVA antigen, but again there were no differences between samples that were co-cultured with MKP-sufficient and MKP-deficient denditic cells (**Figure 6.7B&C**).
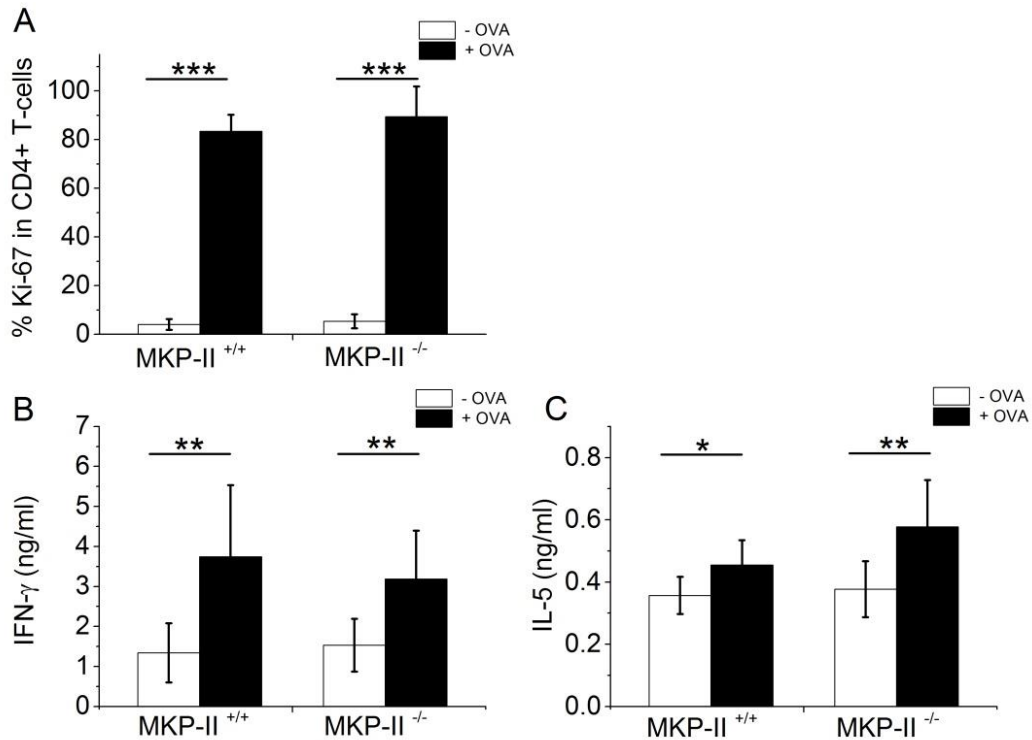
Figure 6.7: Proliferation and cytokine production of T-cells co-cultured with MKP-II $^{+/+}$ or MKP-II $^{-/-}$ DCs.

T-cells (5 x 10^5) were co-cultured in 24 well plates with un-pulsed DC (5 x 10^5), (white bars) or antigen-pulsed DC (5 x 10^5), (black bars) from MKP-II $^{+/+}$ or MKP-II $^{-/-}$ mice, as labelled. **A:** Proliferation of CD4$^+$ T-cells was assayed 48 hrs later using Ki-67. Cytokine production was measured by ELISA of culture supernatants after 48 hrs, **B:** IFN-γ **C:** IL-5. Results shown are the mean % proliferation and mean cytokine production of triplicate cultures of 3 independent experiments ± SD. (* p ≤ 0.05, ** p ≤ 0.005, *** p ≤ 0.0005 by un-paired t-test).

6.2.5 Measuring the force of interaction between T-cells and wild type and MKP knockout DCs.

Having investigated the functional responsiveness of MKP-II$^{-/-}$ DCs and their ability to drive T cell activation, I finally sought to determine the consequences for the T-

cell/DC interactions. MKP-II$^{+/+}$ and MKP-II$^{-/-}$ DCs were pulsed with OVA and used to present to purified MKP-II sufficient OVA-specific OT-II T-cells. Interaction forces between T-cells and MKP-II sufficient and MKP-II deficient DCs were then quantified after 30 minutes, 3 hrs, 6 hrs and 24 hrs using the optical tweezers, as previously described (**Chapter 4**).

As shown in **Figure 6.8**, and as expected, the interaction force between T-cells and wild-type DCs was significantly increased in the presence of OVA with an increase in the median force of interaction from 3.4 pN ± 6.3 pN (un-pulsed) to 12.4 pN ± 6.1 pN (OVA-pulsed). Similarly, a clear antigen-dependent interaction occurred between T-cells and MKP-II$^{-/-}$ DCs (un-pulsed 3.4 pN ± 6.4 pN; OVA-pulsed 16.3 pN ± 6.2 pN) and whilst this suggested a modest increase in the interaction force, this was not significantly different to the interaction forces with wild-type DCs, using the measurement tool available. This same trend was shown throughout all time points (3 hrs, 6 hrs and 24 hrs).
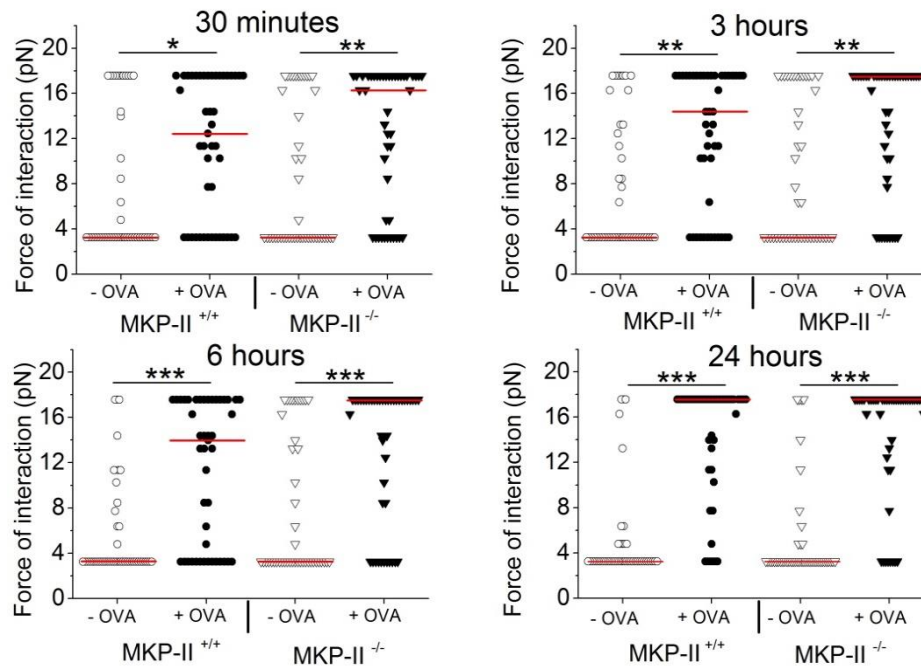
Figure 6.8 <u>**Quantification of the interaction force between T-cells and MKP-II$^{+/+}$ or MKP-II$^{-/-}$ DCs.**</u>

MKP-II sufficient (MKP-II $^{+/+}$) or MKP-II deficient (MKP-II $^{-/-}$) DCs were pulsed with OVA as described in **Chapter 4**, **Section 4.2.2** and used to present to OVA-specific MKP-II suffcent T-cells as described in **Chapter 4**. Data shows the force required to separate individual cell interactions of 3 independent experiments with the median indicated (* p $\leq$ 0.05, ** p $\leq$ 0.005 *** p $\leq$ 0.0005 by Mann Whitney test).

As mentioned in **Section 6.1** MAP-kinases negatively controlled by MKP-II can influence the maturation and cytokine profile of DCs. This can potentially influence the functional outcome of T-cells and perhaps influence the differentiation into either T_H1 or T_H2 cells. We aimed to determine whether DCs deficient in MKP-II functionally were the same and whether the activation of T-cells was affected. Optical tweezers allowed quantification of the interaction force between these cells for the first time. These results demonstrate that MKP-II deficiency within DCs does

not significantly alter their antigen-dependent interaction force with T-cells. However, future work using a higher laser power to measure higher forces of interaction would be required, as many of the cell pairs had reached the maximum threshold (discussed earlier in **Section 3.4.2.1**).

6.3 Discussion.

These experiments sought to investigate the role of MKP-II on the effector function of T-cells. Investigations were carried out to assess whether T-cells lacking MKP-II had altered interaction forces with DCs, compared to control T-cells and if lack of MKP-II affected T-cell function. Furthermore, investigations were carried out to determine if DCs from mice lacking MKP-II,were able to effectively interact with and activate normal T-cells.

As mentioned in the introduction, MAP kinases are regulated by dual-specificity phosphatases, which are capable of dephosphorylating tyrosine and threonine residues of activated MAP kinases [346,347,463]. The role of dual-specificity phosphatases such as MKP-1, DUSP2 and MKP-5 has been investigated and shown to have an impact on cytokine secretion, regulation of innate and adaptive immune responses as well as susceptibility to sepsis and resistance to autoimmune disease [464–466]. MKP-II is highly expressed in T-cells and a previous report has suggested a role for this in the regulation of T-cell activation. MKP-II^{-/-} T-cells were described to be hyper-proliferative, showing enhanced CD25 expression, IL-2 signalling and STAT5 phosphorylation [348,467]. However, using a different MKP-II-deficient mouse strain, I revealed differing results suggesting that no significant difference was observed in the proliferative capacity or effector function of T-cells from MKP-II knockout mice or wild type mice. Using plate bound anti-CD3 and anti-CD28 to stimulate CD4^{+} T-cells Huang *et al.* (2012) showed that following stimulation, MKP-II-deficient T-cells proliferated more due to increased IL-2 production and induction of the high affinity subunit of the IL-2 receptor (CD25). Furthermore, the experiments above are a refinement of this as I am looking at antigen-dependent activation, whereas they may be looking at subset differences. Using cell-cell contact may also give a truer representation of T-cell activation, compared to using anti-CD3 and anti-CD28 to stimulate T-cells. The discrepancy with my results could be associated with the different methods of stimulating the T-cells and also the type of analysis used to determine proliferation. Whilst the Ki-67 marker used here can give a measure of the proportion of cells entering cell-cycle, using CFSE (as used by Huang *et al.*),

provides quantification of the number of cell divisions throughout a given period. As Ki-67 is present at all stages of the cell cycle apart from resting cells, differences in my data may not be detectable using this proliferation marker. Therefore, perhaps future work could take advantage of CFSE to quantify the rate of proliferation in MKP-II $^{+/+}$ and MKP-II $^{-/-}$ T-cells. Moreover, the T-cell's response, in the experiments may be at threshold following co-culture with DCs antigen pulsed with 1mg/ml of OVA. Perhaps using lower doses of OVA antigen would reveal subtle differences in T-cell function. Huang *et al.* (2012) also investigated cognate antigen stimulation and whether this could also induce hyper proliferation of MKP-II deficient T-cells. The draining lymph node from OVA/CFA-immunized MKP-II $^{-/-}$ or WT mice were re-stimulated with 0, 1 and 10 μg/ml of OVA. Thymidine incorporation resulted in a 2 − 3 fold increase in the proliferation of MKP-II T-cells relative to WT at all concentrations. Therefore, future work could be to antigen pulse DCs with various concentrations of OVA and co-culture with either MKP-II $^{+/+}$ or MKP-II $^{-/-}$ T-cells. Or the MKP-II-deficient and MKP-II sufficient mice could be immunized with OVA/CFA, sacrificed and cells from the draining lymph node perhaps re-stimulated *in vitro* with OVA to determine proliferation. This would enable direct comparisons to be made with this study as the experimental protocol would be the same. This set-up would also allow forces of interaction to be compared following re-stimulation with OVA antigen *in vitro*.

There are suggestions that the MAP-kinase ERK plays a role in immunological synapse formation. Studies have shown that active ERK accumulates at the synapse and is important in microtubule organising centre (MTOC) polarisation in T-cells upon interaction with APCs [116,326,468–470]. Importantly, MKP-II has been shown to dephosphorylate and inactivate ERK and JNK *in vitro* [453]. This suggests that deletion of MKP-II would cause constitutively active ERK to extend the synapse, and at the interface between T-cells/DC could be enhanced and potentially the interaction force would be stronger.

Evidence for a potential role of ERK in determining interaction strength was presented in **Chapter 3**, **Section 3.7.3**. There was a significantly decreased

interaction force between T-cells and DCs following pre-treatment of T-cells with an ERK inhibitor. Therefore I hypothesised that if there was no regulation by MKP-II, perhaps there would be a significantly stronger interaction force overtime due to an enhanced and prolonged phosphorylation of MAP-kinases, specifically ERK which may play a role in synapse formation. From the force measurement data there was no difference in the interaction force between T-cells (MKP-II $^{+/+}$) or T-cells (MKP-II $^{-/-}$) and DC, detected using the measurement tool available. These results were somewhat surprising and contradicted my first hypothesis that MKP-II deficiency may increase the strength of interaction between T-cells and DC. However, these measurements complement the proliferation and cytokine production, where no differences were observed between MKP-II $^{+/+}$ and MKP-II $^{-/-}$ T-cells. Despite the lack of MKP-II in T-cells, the phosphorylation of MAP-kinases such as ERK, JNK and p38 actually might not be enhanced following stimulation. Indeed in the study using DUSP-4 deficient mice, the phosphorylation of ERK, JNK and p38 was not increased in DUSP4 $^{-/-}$ T-cells compared to WT T-cells, following stimulation with plate bound anti-CD3 [348]. Whilst MKP-II has been shown to dephosphorylate ERK and JNK *in vitro*, there are findings that contradict this [349,453,471]. Therefore, future work could use Western blot analysis to compare the phosphorylation of MAP-kinases following co-culture with either T-cells (MKP-II $^{+/+}$ or MKP-II $^{-/-}$) and DC (un-pulsed or OVA-pulsed). This would provide valuable information as to whether any MAP-kinase phosphorylation is enhanced and prolonged in MKP-II $^{-/-}$ T-cells in my system, which may affect subsequent immune response.

Antigen presenting cells such as DCs can stimulate naïve T-cells in a primary immune response. There are suggestions that T_H responses can be regulated by different DC subsets and that different DC subsets can be generated by different stimuli such as gene expression and cytokine secretion. However, recent studies have implicated MAP-kinases in the phenotypic maturation, cytokine secretion and functional maturation of DCs, all of which could influence functional outcome of T_H responses. Therefore, I sought to understand the role of MKP-II on DC functions and if the functional outcome of T-cells was altered following an antigen-specific response.

MKP-II $^{+/+}$ and MKP-II $^{-/-}$ DCs functionally responded equally following LPS stimulation. Inhibiting p38 prevents the maturation of DCs and expression of co-stimulatory markers such as CD40, whilst inhibiting ERK or JNK has partial affects [337,339]. This indicates that ERK, p38 and JNK may independently regulate the phenotypic maturation of DCs such as CD40 expression. Therefore as MKP-II may negatively control the phosphorylation of MAP kinases, the initial maturation of DCs may not be affected following LPS stimulation as shown in **Figure 6.4**. However, an enhanced and prolonged MAP-kinase signalling of p38 and JNK has been demonstrated in macrophages from MKP-II $^{-/-}$ mice previously [349]. Future work could therefore determine whether MKP-II $^{-/-}$ DCs would remain in a mature state for a longer period of time, with perhaps an enhanced and prolonged MAP kinase signalling influencing this.

Al-Mutairi *et al.* (2010) also revealed that there was enhanced cytokine production of IL-6, IL-12 and TNF-α. Furthermore, cytokine release can correlate with MAP-kinase phosphorylation with evidence showing a role for p38 in IL-6, IL- TNF-α expression. Although JNK is less defined, a cell type specific involvement has been implicated [472–474]. Therefore, another future experiment may look to determine whether cytokine production of knockout DCs is altered following LPS stimulation and as a result this may determine the differentiation of naïve T-cells into T_H1 or T_H2 phenotype.

The data presented in **Figure 6.5** and **Figure 6.6** suggests that knockout DCs had a lower level of antigen presentation, suggesting that the level of presentation of OVA in other experiments could potentially be lower in MKP-II deficient DCs compared to wild type cells. T-cells are highly sensitive and around 1-400 pMHC complexes on the surface of APCs are sufficient to fully activate a T-cell [53,55,475]. The amount of antigen present on the surface of APCs can determine the interaction dynamics as well as the level of T-cell activation and subsequent function. Indeed a lowered presentation of OVA antigen in MKP-II $^{-/-}$ DCs may be affecting the proliferation of T-cells, as shown in **Figure 6.7**. However, there was variation between each week for this result shown in **Figure 6.7**. This could perhaps be down to variance in the

maturation of CD11c positive DCs in each experiment; differences in the presentation and/or uptake of antigen or differences in the maturation of DCs, all of which may influence T-cell functional outcome.

As the experiments measuring antigen presentation and maturation of DCs were only single, preliminary experiments, it would be important to clarify the effect MKP-II has on the function of DCs. This would then pin-point exactly what could be causing the variation in T-cell function per individual experiment and whether there are any differences in the DC phenotype and/or function per individual experiment.

Cytokine data again also showed variation. There are however hints that the cytokine production of T-cells co-cultured with MKP-II $^{-/-}$ DCs is more phenotypically T_H2 than T_H1. IFN-γ production in 2 experiments (of 3) was significantly lower in supernatants from co-cultures of T-cells and MKP-II deficient DCs, compared to co-cultures of T-cells and MKP-sufficient DCs. Whilst only 1 experiment showed significantly higher production of IL-5 the other 2 experiments showed a similar trend, although results were not significant. This would be in agreement with Al-Mutairi *et al.* (2010), which demonstrated that *Leishmania mexicana* infection caused a down-regulation of T_H1 responses and a concomitant up-regulation of T_H2 responses in MKP-II $^{-/-}$ mice, compared to MKP-II $^{+/+}$ mice [349]. However, in another study, infection with *Leishmania major* did not alter T_H1/T_H2 responses of MKP-II$^{-/-}$ mice, compared to MKP-II $^{+/+}$ mice and instead suggested that infection enhanced Arginase-1 in MKP-II-deficient mice resulting in T-cell hypo-responsiveness [350].

Overall although there was a trend towards T_H2/IL-5, this was not significant over triplicate experiments and only significant in one of them.

As mentioned in the introduction the strength of TCR and pMHC determines the amount of antigen needed for initiation of T-cell signalling, where low doses of peptide can compensate for weaker TCR/pMHC interactions. The affinity and dose can influence the functional outcome on T-cell, for example development of memory, cytokine production and proliferation [121,122,462]. Therefore as there was a

suggestion that the amount of antigen presentation by MKP-II-deficient DCs was lower than wild type cells, I sought to investigate whether this would influence the interaction force between T-cells and DCs.

From the force measurement data there were no significant differences detected in the force of interaction between T-cells and DC from wild type or knock out DCs using the measurement tool available . This suggests that the optical tweezer system might not be sensitive enough to detect varying doses of antigen. However, it is difficult to come to this conclusion as the experiment determining the level of antigen presentation was from 1 preliminary experiment and would need further investigation to clarify.

Another reason for detecting no differences in the interaction force could be that enough pMHC complexes are present to initiate synapse formation and strong interaction between T-cell and DC. It has been shown that T-cell activation requires as few as 100-300 MHC-antigen complexes and that as few as 300-400 TCRs are sufficient to initiate a Ca^{2+} signal [124,262]. The results show a decrease in the antigen presentation in MKP-II deficient DCs. However, it could be that sufficient MHC-II antigen complexes are still present in order to initiate a positive signal for T-cell activation with a sufficient interaction force still occurring. Perhaps by antigen pulsing MKP-II [+/+] DCs or MKP-II [-/-] DCs with titrated doses of OVA we may start to reveal subtle differences in the interaction force. However, interestingly T-cells can form stable interactions more quickly with DCs expressing low amounts of peptide [77].

This chapter sought to determine whether MKP-II plays a role in the strength of interaction between T-cells and DCs. From my data, no differences were observed in the interaction forces, irrespective of MKP-II deletion in either DCs or T-cells. The data presented shows that MKP-II [-/-] OVA-specific T-cell activate to the same extent as MKP-II [+/+] OVA-specific T-cells, in terms of proliferation and cytokine production. However, whether ERK, JNK or p38 in knockout T-cells or DCs show enhanced phosphorylation following OVA stimulation, LPS stimulation or T-cell/DC

co-cultures remains unknown and would have to be investigated. Preliminary data does however suggest that MKP-II $^{-/-}$ DCs may influence the proliferation and effector function of OT-II OVA specific T-cells. Differences in the development and antigen presentation of knockout DCs may account for this, although this data is preliminary and should be interpreted with caution. Nonetheless, it highlights the complexity of MAP-kinase role in T-cell development and DC function and the role that MKP-II may play in immune function.

Chapter 7 – General Discussion.

7.1 Development of optical tweezer system.

The overall aim of the present study was to develop an optical tweezer system that could directly trap T-cells and subsequently quantify the interaction force between T-cells and DCs.

Several papers have reported that the interaction between T-cells and DCs is very dynamic. This has led to the hypothesis that either the duration [9,36,74,76,77,80,126,147–149,188–190] or the strength of contact [104,169–172,175,191–194] or a combination of both can determine the robustness of T-cell activation and effector function. Parameters such as affinity of pMHC/TCR contact, pMHC dose, time/duration of interaction, and the force of interaction may also influence T-cell effector function [66–75]. Recent reports also propose that the TCR can mechanosense, where upon sufficient application of force the TCR will initiate signalling. Together these studies highlight the importance of T-cell/DC interaction as well as the importance of directly quantifying the strength of their interaction – an aspect which may determine T-cell fate [104,105,171].

Moreover, despite numerous *in vitro* and *in vivo* imaging experiments examining the dynamics of the T-cell/DC interaction, direct visualisation of these cells has provided only limited information about how strongly the T-cells and DCs are interacting with each other at early stages following antigen recognition. Given that the strength of this interaction has been proposed to initiate TCR signalling and determine T cell fate, it represents an important parameter to quantify in order to address a wide range of immunological questions. This may have wider reaching applications in understanding more about the generation of T-cell antigen-specific immune response and have important consequences for the generation and maintenance of peripheral tolerance; prevention and/or initiation of autoimmune diseases; and responses to food antigens and allergens.

Optical tweezers are a tool that has been used to manipulate immune cells, specifically looking into the sensitivity and the minimum number of TCRs required to initiate T-cell signalling using coated latex beads [124,261–263]. However, to date the results presented in this thesis are the first application of optical tweezers in

manipulating T-cell and DC interactions and quantifying their subsequent interaction force. This opens up the possibility of using optical manipulation to investigate how the **duration** of interaction and **force** of interaction can influence T-cell effector function and may give greater insight into the complex T-cell/DC interaction.

Indeed it is possible to optically trap biological material without compromising the viability. However, viability can vary between cell types and parameters such as laser power, laser wavelength and the length of trapping time can affect it [184,239–241]. Therefore it was important to develop an experimental approach to directly trap T-cells and quantify the interaction with DCs without compromising cell viability. Moreover, T-cells are much larger than the focal spot size of the laser beam focused with a high N.A objective lens and, therefore, difficulties such as cell roll and calibrating the optical tweezers can arise (**see chapter 3**). In order to address both of these challenges, I optimised the system to create a novel beam profile termed "triple spot trap" that improved the direct trapping of T-cells two-fold, first, improving the viability of trapped cells and secondly improving the stability of trapped T-cells. Others have trapped particles using different laser modes [218]. One such approach is the Laguerre-Gaussian mode and this has been used to trap and rotate Chinese hamster chromosomes [476] and more recently the trapping and rotation of red blood cells [477]. A further development is the use of Bessel light beams and this has been used to trap objects laterally in two dimensions as demonstrated by Arlt *et al*. in 2001. This would allow trapped objects to be stacked along the centre of the laser beam [478]. There is a general agreement that to minimise cell death a laser wavelength in the near infrared is appropriate and that both the time of trapping and laser power are important factors that can affect cell viability [184]. Here within this thesis I expanded this and compared the benefits to cell viability when using a triple spot trap rather than the conventional single spot trap. Whilst others have used different laser modes to trap particles (as described above), this is the first time that comparisons between different trapping configurations have been made in order to determine the effect on cell viability. We show that a triple spot trap improves cell viability, highlighting that a single spot trap may not be the best option to trap biological cells with. Moreover, as each spot within the triple spot trap are

independently controlled it would be possible to apply the same beam profile to trap other biological cells that may be smaller or larger than T-cells.

In order to use the system to quantify the interactions between T-cells and DCs, the force of the new optical tweezers had to be calibrated. I compared two methods to calibrate the system, the equipartition theorem and the escape force method. I demonstrated that the choice of calibration is determined by the width of the optical trap where the trap would still behave like a spring, where the trap stiffness is linear to the displacement from equilibrium. Through experimental comparisons it was found that the escape force method was applicable for quantifying the interaction forces as the trap was moved at a distance from the cell pair where it no longer behaved like a spring. Importantly the escape force method has previously been used by Andersson *et al*. in 2007 to successfully quantify the interaction forces between human bone cells and medical implants [187].

As a proof-of-concept approach, the antigen-specific interaction forces between T-cells and DCs were measured and the new triple-spot optical tweezers were demonstrated to successfully detect an increase in force when T cells recognised antigen. In addition, the potential value of such a system in determining how the interaction forces between T cells and DCs are changed by immunomodulators was investigated to determine the limits of such an approach (**see chapter 3**). Here, changes in the interaction force between the cells were detected following treatment with either LPS or an ERK inhibitor, demonstrating that optical tweezers may provide a useful approach across a wide range of applications in immunology where the crucial T-cell/DC interaction plays a role, such as the development of vaccines and treatment of auto-immune diseases.

Therefore, the primary aim of this thesis was successfully achieved whereby an optical tweezer system had been developed that could trap T-cells to manipulate their interaction with DCs whilst quantifying their interaction. Throughout the development of the tweezer system we utilised a novel triple spot trap to improve the viability of T-cells and improve the trapping of the large cells. For the first time we

successfully trapped T-cells without the need to attach beads to act as handles whilst quantifying the interaction force with dendritic cells. Whilst this thesis concentrates on quantifying the interaction forces between T-cells and DCs, the optical tweezer system presented here could be used to quantify interaction forces between other cell types. A recent review article [168] highlights and discusses the importance of forces and the ability of cells to sense force and transmit signals that impact on cellular responses.

7.2 Applications of optical tweezer system.

Having developed and validated an optical tweezer system and shown proof-of concept that the approach could quantify the interaction forces between T-cells and DCs, I next sought to use the system to investigate a number of important topics in which these interactions may play a role. From the literature cell signalling pathways [118,324], amino acid bioavailability [268,269] and post-transcriptional modification of antigens [313,314,318,320] can all influence T-cell effector functions and I therefore aimed to determine whether this was a direct result of altered interaction strength between T-cells and DCs.

7.2.1 L-arginine.

We firstly investigated the role of L-arginine (**See Chapter 4**). The data presented within **Chapter 4** supports the hypothesis that in the absence of L-arginine T-cell proliferation and cytokine function is impaired [268–272,283,287,289,386]. Finally, to fulfil the main aim of this chapter which was to determine whether altered interaction forces between T-cells and DCs were responsible for the impairment of T-cell activation, the optical tweezer system was used to quantify cell interaction for the first time. Using the system we were able to quantify the interaction forces between T-cell/DC in the absence of L-arginine. Surprisingly, despite impaired activation the strength of interaction (measured using optical tweezers) between T-cells and DCs were significantly higher; irrespective of antigen or not in L-arginine depleted media.

This was somewhat surprising since IS formation is impaired in the absence of L-arginine [289].

A preliminary experiment using the optical tweezer system to quantify the interaction forces between T-cells and DCs (infected with/without *Leishmania*) showed similar force measurements to L-arginine depleted media, especially for the 24 hr time point. *Leishmania* has been known to deplete levels of L-arginine locally through arginase production [379,380]. Therefore, the high interaction force could be associated with depleted levels of L-arginine within the sample but this result would have to be repeated to clarify. It may be possible to use mass spectrometry to measure and detect the levels of L-arginine in samples before and after 24 hr co-culture to determine if the L-arginine levels have indeed been lowered by presence of *Leishmania*.

Another interesting idea is that in the absence of L-arginine T-cells may become tolerant or anergic to OVA antigen. They express characteristics of T-cells undergoing tolerance with up-regulation of early activation marker CD69 but no proliferative capacity or cytokine production [395] Moreover, tolerant T-cells are still able to form conjugates with APCs, yet have impaired IS formation [403]. This links well with the study showing that in L-arginine depleted media, IS formation at T-cell/DC interface is impaired [289]. Within this thesis we have shown using the optical tweezers that cells are able to form conjugates, albeit with a stronger interaction force in L-arginine depleted samples, implying that those T-cells could be tolerant.

Therefore, L-arginine may have important consequences in induction of tolerance but also in rendering T-cells anergic during infection or disease. Future experiments could determine the expression of CTLA-4 vs CD28 expression in L-arginine depleted media compared to control media. Interestingly expression of CTLA-4 blocks T-cell activation and binds with higher affinity than CD28, which could be a reason why force measurements are so strong in sample depleted of L-arginine. Furthermore, CTLA-4 prevents T-cells from entering cell-cycle [404,479,480] which would link in well with a report showing L-arginine depletion arrests T-cell cycle

progression [270]. Therefore, future experiments could also measure the expression of CTLA-4 and CD28 in combination with propidium iodide for cell-cycle analysis in depleted and control media to answer this.

Further afield, understanding more about L-arginine could have implications in cancer patients. It has been shown that several tumour lines from lung carcinoma and breast carcinoma express levels of arginase [481,482]. T-cell responses to tumours could be rendered anergic and tolerant to tumor antigens which may be a mechanism for tumor evasion [288,383,483]. Indeed within humans a study found that in patients with metastatic renal cell carcinoma there was a 6-10 fold increase in arginase levels observed in peripheral blood mononuclear cells as well as down-regulation of CD3ζ chain [484]. Tumours don't stop growing and there is continued destruction of tissue causing the infiltration of arginase producing cells to promote collagen production and healing of tissue damage. This would eventually deplete local levels of L-arginine leading to the T-cell anergy, inhibiting T-cell anti-tumor responses [483].

Overall L-arginine could have therapeutic applications in infection with parasites and also in the treatment of cancer. It seems to be that L-arginine affects a number of parameters involved in T-cell activation such as proliferation, cytokine production and cell-cycle progression. Also there are hints that L-arginine could play an important role in T-cell anergy and tolerance. Therefore, it may be possible to therapeutically use L-arginine to restore local levels of L-arginine in the context of disease and infection in order to rescue protective T-cell responses.

7.2.2   Citrullination.

We next investigated the role of citrullination (**See Chapter 5**). The data presented in **Chapter 5** showed that at a later time point of 4 hrs, the OVA-specific OT-II T-cells not only recognised the modified antigen, but that recognition of cit-OVA was associated with an increased force of interaction between cells compared to the time point 120 seconds. Furthermore, T-cell effector function, as measured by IFN-γ release and IL-5, was significantly enhanced following recognition of cit-OVA. The preliminary results presented demonstrated that at lower doses of antigen there was

elevated IFN-γ release in OT-II T-cells interacting with DCs presenting cit-OVA than OVAp. An enhanced interaction force may compensate for lower doses of antigen and as such the optical tweezer system was used to quantify the force of interaction between T-cells and DCs presenting titrating doses of either cit-OVA or OVA-p. There was a slightly increased median interaction force between T-cells and DC presenting cit-OVA, compared to DCs presenting OVA-p. Whilst this trend was observed throughout, it would be important to clarify this result by repeating the experiment.

Nevertheless, the optical tweezer system detected changes in the force of interaction between cells following cit-antigen recognition for the first time. The novel data that would not have been possible to obtain without the optical tweezer system suggested that naïve OT-II T-cells differentially recognise native and citrullinated forms of antigen and that the increase in force of interaction associated with proliferation and enhanced cytokine production may explain how post-translational modification of antigen could alter immune function, potentially breaching self-tolerance.

Further studies could determine whether similar responses occur *in vivo*, as well as to delineate the mechanisms by which citrullinated antigens can reverse established tolerance to self-antigens. It would also be interesting to use *in vivo* multi-photon imaging to determine if the interaction dynamics between T-cells and DCs are altered when citrullinated antigen is presented compared to native antigen.

We next compared the interaction forces between naïve, primed and tolerised T-cells with DCs. Interestingly the data showed that both primed and tolerised T-cells showed a significant decrease in interaction strength, compared to naïve T-cells. This was irrespective of whether antigen was OVA peptide or citrullinated OVA peptide. This trend was observed when cells were first brought into contact with a DC, however at later time points the force of interaction then increased after 4 hrs and 24 hrs of co-culture. It is interesting to note that primed T-cells have a decreased threshold for activation and therefore a strong interaction may not be required for effective response. This may also be the case for tolerised T-cells whereby a low

initial interaction force with DC could be a requirement to maintain peripheral tolerance. Later time points showed similar force trends to naïve T-cells. There is evidence to show that upon secondary exposure to antigen tolerised and primed T-cells do form large stable clusters with DCs [145].

Together, along with my results, this suggests that the initial interaction between T-cells and DCs and the relevant force of interaction could be a determining factor as to the maintenance of tolerance and activation of naïve T-cells. Differences in the initial interaction forces may explain why tolerant T-cells vs naïve T-cells have different functional outcomes following *in vitro* re-stimulation with OVA. Quantifying the interaction force between tolerant and primed T-cells with DCs at later time points showed a different trend with interaction strength being comparable to that of naïve T-cells. However, clustering of tolerised and primed T-cells with DCs has been observed in previous studies [144] despite functional responses of these T-cells being lower following stimulation with OVA.

It could be suggested that this may be a mechanism as to how peripheral tolerance is maintained. Tolerised T-cells could simply block pMHC complexes being exposed to naïve T-cells and this links in well with studies showing that T-cells compete for available pMHC complexes on the surface of antigen presenting cells [450]. Future studies could use *in vivo* imaging to see the interaction dynamics of T-cells and DCs following secondary exposure to antigen in tolerised, primed and naïve mice. As tolerised, primed and naïve T-cells display differing dynamics of interaction with DC upon secondary exposure to antigen [145] future experiments could carry out the same protocol but in the context of secondary exposure to citrullinated OVA peptide. This perhaps might reveal changed interaction dynamics that are more associated with naïve T-cells than tolerised T-cells. If any changes were observed then it would imply that tolerance has been breached due to the presence of a post translocational modification.

The data presented in this thesis suggests that citrullination can alter the effector function of T-cells and interaction force with DCs. Moreover, for the first time we

demonstrated that tolerised, primed and naïve T-cells interact differently with DCs. *In vivo* imaging may be missing the crucial early/first time interactions between T-cells and DCs and our results reveal the importance of the initial interactions whereby tolerised, primed and naïve T-cells interacted with altered interaction force, but not at later time points. The next step in this experiment would determine whether similar T-cell interactions and responses occur *in vivo* but carrying out *in vivo* imaging at earlier time points.

7.2.3 MKP-II.

We next investigated the role of MKP-II (**See Chapter 6**). The data presented showed that despite MKP-II deletion in T-cells, the proliferation, cytokine production and forces of interaction with DC were not altered. This was not in agreement with a study demonstrating that DUSP-4 knockout T-cells were hyper proliferative [348]. Furthermore, we had previously shown that inhibition of ERK, which is recruited to the IS, significantly lowered interaction forces between T-cells and DC (**See chapter 3**). Therefore, as MKP-II negatively controls the phosphorylation of ERK then one would hypothesise that with no control over ERK phosphorylation then the interaction forces would be significantly increased. The data suggests otherwise. Within this chapter we also generated DCs from wild type and MKP-II knockout mice. Whilst a lot of this data was preliminary it suggested that the development of DCs was altered. There were fewer CD11c positive DCs in BMDC cultures from knockout mice, compared to control mice. Furthermore, the antigen presentation of DCs was significantly lower, although this may be down to the fact that there were less functional DCs present in knockout samples. Finally the effector function of T-cells was also affected by knockout DCs. However, these results varied between each week although there were hints that T-cells were more phenotypically T_H2 than T_H1. Importantly if this was the case then this has wider applications in parasitic infections such as *Leishmania* whereby the T_H1 or T_H2 response can influence the clearance or persistence of infection. As this was a preliminary experiment it would firstly be important to grasp exactly how MKP-II is altering DC function. This would be in terms of the number of DCs generated from

the knockout mouse compared to control; the activation of DCs following LPS stimulation; and finally the presentation and up-take of antigen. Future work would also use western blotting to determine when, if any, MAP-kinases are up-regulated due to the lack of MKP-II with a comparison made to knockout T-cells. Although no observable effects were shown in terms of force, proliferation and cytokine release it could be that T-cell responses are maximal, as a high antigen dose was used.

Overall the preliminary experiment highlighted the role of MKP-II in T-cell function. For the first time we quantified the interaction forces between T-cells and DCs and determine whether MKP-II directly affected this. Whilst the data suggested that MKP-II may alter the function of DCs and the effector response of naïve T-cells, that firstly would have to be clarified. Nevertheless it highlights the possible role of MKP-II being used therapeutically to alter or bias the immune response towards a certain effector response and fulfils the main aim of investigating whether MKP-II alters interaction forces between T-cell/DC

7.3 Future outlook.

Optical tweezers is a fast developing field and the ability to select and non-invasively control biological cells is of great interest. Immune cells, especially T-cells and DCs are constantly communicating and interacting, therefore, optical tweezers are undoubtedly an ideal tool to control T-cells and manipulate interaction with DCs. Whilst it is clear that the system described within this thesis has proved valuable there a number of developments that could be carried out to further the experiments and push the potential of optical tweezers in immunology further. The major limitations with the optical tweezer system were the minimum and maximum threshold in quantifying the interaction force; the lack of high-resolution imaging; and finally the throughput of data. Whilst previous reports using AFM have demonstrated interaction force between T-cells and DCs reaching a maximum of tens of nano-newton's after several minutes/hours of interaction [167,169], the optical tweezers used here could measure only within the Piconewton range. This limited the ability to quantify the interaction forces between T-cells and DCs, (especially at

later times of interactions) where many of the cell pairs could not be successfully pulled apart and quantified (**eg. see Figure 6.3**). Therefore, it would be important to address this so that one could quantify interaction forces over a wider range (**discussed later in Section 7.3.1**). Furthermore, by combining the optical tweezer system with high resolution imaging, one could correlate force measurements with the formation of the immunological synapse or perhaps key molecules such a PKCθ, which are important for activation of T-cells. By combining both, one could determine the dynamic nature of the immunological synapse and how this correlates with forces of interaction. Moreover, it would allow investigations to be carried out to determine what effect manipulation has on the development of IS and whether a strong interaction is required for IS formation. For example, Oddos *et al*. used optical tweezers to bring T-cells into contact with B-cells and orientate the cell pair to image the immunological synapse at high resolution [266]. Finally the throughput of data could be improved. Whilst carrying out experiments at a single cell level would perhaps reveal insights that may not be visible at a population level, it may be possible to make changes to the experimental set-up or sample preparation to still allow single cell interactions but at a higher number. As well as improving the throughput of data these set-ups would also allow the user to isolate T-cells after tweezing experiments for further *in vitro* analysis. The ways in which the optical tweezer could be improved to help with the above issues are discussed below in more detail.

7.3.1 Higher force.

The maximum force could be improved simply by using a laser source with a higher power. The laser used in the set-up was a Ventus 3W continuous wave 1064 nm laser from Laser Quantum. Other commercial options that could be used would be the Opus 1064 nm laser from Laser Quantum or the Matrix continuous wave 1064 nm laser from Coherent. With the same spatial mode as the Ventus these lasers are available commercially with powers up to 10 W, and thus if incorporated in the set-up there is the potential to more than double the maximum interaction force that can be measured between T-cells and DCs [371]. However, higher laser powers will

generate more heating as shown in a report by Peterman *et al*., (2003) [485] which may decrease cell viability. Due to this optical tweezer used in cell biology generally use laser powers ranging from 25 mW to 2 W in specimen plane [184]. However, the experimental approach shown in this thesis traps T-cells for only a brief time before quantifying the interaction force, and therefore using a high laser power might not be an issue. It may also be possible to improve trapping efficiency by using different beam modes such as a Laguerre-Gaussian Laser mode as shown by Simpson *et al*. [486] They showed that axial trapping efficiency was improved by a factor of two when using a Laguerre-Gaussian to trap particle sizes (1µm, 2µm, 5µm) compared to a TEM_{00} laser mode. Furthermore, improving spherical aberrations would help to [487]. Addressing one or both of these above may allow the user to trap T-cells with a lower laser power and thus having a positive effect on viability. Also due to improvements in trapping efficiency higher forces could potentially be quantified. Furthermore, it is accepted that overfilling the objective is needed to optimise optical trapping [488]. However, a recent report by Mahamdeh *et al*. demonstrated that the highest trapping efficiency (as measured by trapping stiffness) was achieved by slightly under-filling the objective [489]. Therefore, by going back to measure the "optimal" beam expansion through the objective, trapping efficiency could be improved for the set-up shown in this thesis.

A higher refractive index mismatch between a trapped particle and its surrounding medium increases the gradient forces and hence the trapping efficiency. However, as the strong scattering forces increase more than the gradient forces when the mismatch is increased, an upper limit of refractive index mismatch exists [490,491]. To overcome this upper limit it is possible to coat the particles with an anti-reflection layer to lower the effect of the scattering force. Indeed using silica-coated polystyrene beads Bormuth *et al*. demonstrated an improvement in trapping efficiency [490]. However, this was exploited further by Jannasch *et al*. whereby high-refractive index anatase titania microspheres coated with an anti-reflection layer of amorphous titania were used [492]. Using the escape force method they found that the trap stiffness was increased 4-fold compared to silica beads and 2-fold compared to polystyrene beads and they estimated that the maximum force of the optical tweezer

could range up to 1 nN with the coated titania microspheres, demonstrating the application of a nanonewton range optical trap. It may be possible to coat the optimised bead with anti-CD3 antibody to measure the interaction forces at a much higher range. Albeit this is taking away the first aim of directly trapping T-cells but it does address the issue of the maximum threshold that could be measured in our system. Anti-CD3 coated beads have successfully been trapped using optical tweezers and brought in contact with a T-cells to determine its sensitivity to antigen and the number of receptors required to initiate TCR signalling [124,262,263]. Moreover, Jannasch *et al.* also estimates that a low N.A objective would be sufficient to trap coated particles. Certainly it is possible to trap T-cells using a low N.A objective as shown in [493]. This would help in improving the throughput of data (**Discussed in next section**) since the low N.A. would increase the field of view allowing multiple particles to be trapped at once.

7.3.2 Increasing throughput of data.

Carrying out work at a single cell level may reveal mechanisms that might not be apparent at a population level. Furthermore, it would perhaps solve the controversy surrounding T-cell/DC interaction dynamics where studies have shown conflicting results – thought to be due to intraclonal T-cell competition [451,452].

However, experiments such as testing new therapeutics that aim to attenuate or intensify immune cell interactions may require a higher throughput of data. There are a number of methods that could improve the throughput of the optical tweezer system developed in this system. Optical tweezers can be configured to trap multiple particles at once by rapidly scanning a single beam at two trap positions, splitting the beam in the optical path and recombined later before entering the microscope or using computer generated holograms [494–496]. In the case of holographic optical tweezers the number of traps created is limited by the field of view and laser beam power available. As optical tweezers use a high N.A this can be a limiting factor. However, it is possible to trap T-cells using a low N.A lens increasing the field of view to over 1.273 mm x 1.273 mm [493]. Therefore, this could be used in

combination with multiple trapping techniques to increase throughput of experimental data acquired.

Another way to increase the throughput of experiments could be to combine the optical tweezer system with microfluidics. The figure below illustrates some microfluidic devices that have been developed by Skelley *et al*. and Eriksson *et al*. [497,498].
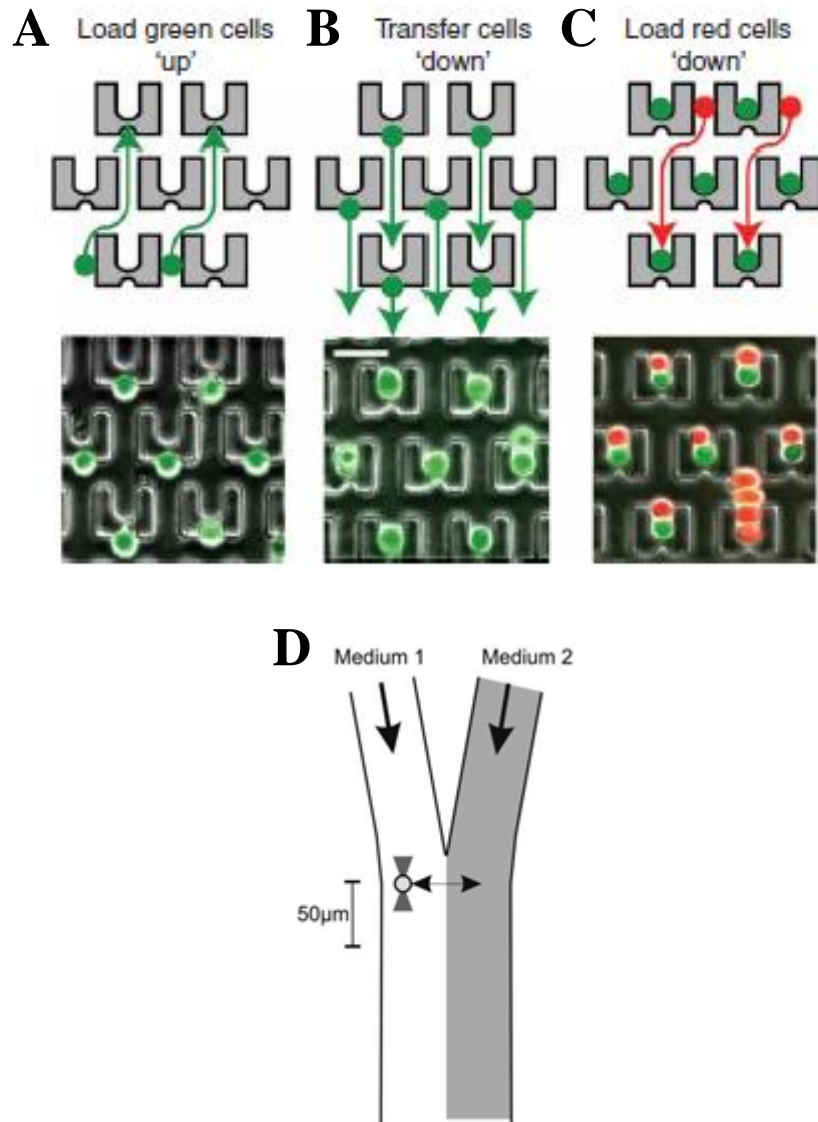
Figure 7.1   <u>**Microfluidic devices that can be combined with optical tweezers.**</u>

The schematic diagram above shows microfluidic devices developed byEriksson *et al.* and Skelley *et al.* [497,498]. **A** and **B** show a way of loading T-cells (green dots), **C:** followed by loading of DCs (red dots) to form cell interactions. Using a SLM, multiple traps could be made close to the cell interactions and then the interaction forces quantified for each cell pair at the same time. **D:** Shows a microfluidic device that allows two media to be kept separate and by using optical tweezers, a T-cell could be manipulated between the two media. These microfluidic devices may be used to increase throughput of data as well as investigate the effects of different media on cell interaction.

The microfluidic device in **Figure 7.1** could be used with the optical tweezer system developed in my thesis. T-cells could potentially be flushed into this system followed by DCs. Cell pairs within the wells could be identified and using holographic optical tweezers it could be possible to investigate a number of cell-cell interactions at once with an array of optical traps. Moreover, this method of loading separate cell populations into the device would ensure that the controlled T-cell and DC interaction is guaranteed to be the first time contact and that T-cells have not transiently interacted with a DC presenting antigen. Whilst my experimental approach to control T-cell/DC interaction was optimised to maximise the chance of first time contact between cell pairs, this was not fully guaranteed. To achieve this one could exploit the size differences between T-cells and DCs and make the chamber size equivalent to a T-cell but too small for a DC (**See Figure 7.1**). After loading the T-cells, DCs could then be loaded. The optical tweezer could then be used to remove a T-cell from the "chambers" and subsequently brought into contact with a DC – ensuring first time contact.

Moreover, another microfluidic device shown in **Figure 7.1D**, developed by Eriksson *et al.* may improve the throughput of data as well as guarantee first time contact. In this study, optical tweezers were used to trap yeast cells and move into different media with different osmolality to observe changes in cell volume. In my set-up T-cells and DCs could be washed down through the different compartments and using the optical tweezer a T-cell could be trapped and brought into contact with a DC on the other side. Interestingly this set-up could not only improve the throughput of force quantifications between T-cells and DCs, but could have further applications in investigating L-arginine depletion on T-cell function. By being able to flush media containing L-arginine or no L-arginine it would be possible to manipulate T-cells using the optical tweezer system between the two different media. This would help in determining a precise time that T-cells show impaired function upon depletion of L-arginine. Furthermore, it would also help in understanding if supplementing L-arginine back into depleted media alters interaction forces between T-cells and DCs. It may be that as the T-cell no longer "seeks" a source of L-arginine then interactions forces would be lower after supplementation. Certainly

using the microfluidic device shown in **Figure 7.1** would allow a more precise way of supplementing T-cells with L-arginine.

7.3.3 Microfluidic devices – the end point is not the trapping.

Another improvement to the system could ensure that the end point of experiments is not the optical tweezers but instead further experiments could be carried out either *in vitro* or *in vivo*. Whilst sample preparations and throughput of data could be improved using microfluidic devices (**Figure 7.1**) they may also be useful to separate cells of interest to carry out further experiments after tweezing experiments. For example using a microfluidic device similar to that described in Skelley *et al*.[498], it would be possible to collect cells after using optical tweezers to controllably initiate T cell activation. After quantifying individual cell interactions the function of T-cells could then be analysed in *in vitro* or *in vivo* assays. From this it would be possible to directly link how the amount of force between a T-cell and DC relates to the level of T-cell activation by assessing proliferation and effector cell function. This would have important consequences for investigating whether strength of interaction influences the effector outcome of naïve T-cells and whether factors such as quality, quantity and duration of T-cell/DC interaction determined the T-cell functional outcome. This would have importance in understanding whether an effective immune response is initiated or a state of anergy is induced, factors that could improve the design of vaccines, suppression of autoimmunity and restoring immune tolerance.

7.3.4 Imaging system.

The optical tweezer system was built into a commercial microscope that had a fluorescence mercury arc lamp. In preliminary experiments the optical tweezer system were used to first manipulate Fluo-4 labelled OT-II T-cells into contact with DCs and then fluorescence imaging used to determine the intensity of Ca^{2+} flux. This has a distinct advantage over conventional methods of imaging Ca^{2+} flux which

rely on mixing cells together and acquiring time-stamped images to measure Fluo-4 intensity over time. In such an approach, the user cannot be completely certain that a T-cell coming into the field of view has not previously encountered an antigen-presenting DC. Furthermore, rare events such as subtle differences in Ca^{2+} intensity could be missed at a population level as one usually tracks the number of cells and averages the values of Ca^{2+}. Optical tweezers allow users to carry out experiments at a single cell level and through better experimental design (**Figure 6.1**) one can ensure that cells have not been in contact until interaction is initiated with optical tweezers.

Whilst my preliminary results initially suggested a Ca^{2+} flux was induced in T-cells brought into contact with DCs presenting OVA, further investigation suggested that T-cells could Ca^{2+} flux after exposure to excitation wavelengths of light from the mercury arc lamp. This has been reported before in other cell types and is termed "light-induced calcium flux" [399]. In future this could be re-visited to determine precisely the mechanism of light-induced Ca^{2+} flux within T-cells but due to time constraints this was not investigated further. Moreover, further optimisation of such an approach could have wider applications as one could then correlate the intensity of Ca^{2+} flux with the force of interaction. It has been suggested that the intensity of Ca^{2+} flux can regulate the interactive behaviour between T-cells and DCs [115,135,499] and a report by Husson *et al.* has used a biomembrane force probe to relate mechanical forces between a T-cell and APC with Ca^{2+} flux and show that the TCR can mechanosense. However, within this study a "model" APC bead coated with anti-CD3 was used and no investigations were carried out to determine how the probe affected the viability of T-cell and if it compromised dynamic receptor scanning between T-cell and target APC. Therefore, if optimisations on the optical tweezer system for measuring Ca^{2+} were carried out then it would be a distinct advantage over this work as it would give a truer representation of cell-cell contact as well as maintain cell viability and dynamic receptor scanning between T-cell/DC.

Whilst the optical tweezer system was built into wide-field fluorescence microscope, which would be sufficient to detect a Ca^{2+} flux, there would be difficulty in imaging

the formation of the immunological synapse using this method due to out-of-focus light degrading quality and resolution of image [119]. Using imaging techniques such as confocal or STED microscopy would improve upon image quality. Typically, objects that are less than 200-350 nm apart can be resolved with wide-field fluorescence microscopy. However, typically confocal laser scanning can have a lateral resolution of 180-250 nm, whilst STED can has a lateral resolution of 60 nm [500].

Certainly it is possible to combine optical tweezers with confocal microscopy. This was demonstrated by Gregory *et al*. who combined a commercially available spinning disk confocal assembly with an optical tweezer system. They used this combination of techniques to manipulate $CD4^+$ T-cells and HIV-infected $CD4^+$ T-cells to image a virological synapse [267]. Furthermore Oddos *et al*. has combined a commercially available laser scanning confocal microscope with optical tweezers and used the optical tweezers to re-orientate the cell pair and image the IS at high resolution [266]. More recently, optical tweezers have been combined with STED fluorescence microscopy to track individual proteins trans-locating on DNA and assess the force kinetics on these proteins along DNA [501]. Therefore it could be a possibility to combine the optical tweezer set-up in this thesis with either confocal or STED microscopy.

The results presented in **Chapter 4** would be complemented by such a design improvement. For example, optical tweezer data showed that interaction forces between T-cells and DCs were significantly higher in L-arginine depleted media compared to control media. By using confocal microscopy to image IS formation, in combination with the optical tweezers to quantify the interaction forces, one could correlate force measurements with IS formation. These are important parameters to measure given that the IS can determine the interaction force between T-cells and DCs [167] as well as previous work highlighting that IS formation is impaired in L-arginine depleted media [289].

Moreover, as discussed previously *in vivo* imaging has highlighted the complexity of T-cell/DC interaction dynamics [9], however, what is not known is how this correlates with IS formation. Whether IS formation is as dynamic as the interactions and whether IS formation influences the stability of T-cell/DC interaction is unknown. *In vivo* imaging of IS has been limited by the number of GFP-tagged proteins relevant to IS formation and hence the lack of bright fluorescence signal required to view the IS. Optical tweezers could be used to answer such questions *in vitro* by firstly allowing T-cell/DC interaction to be controlled and manipulated and secondly how varying these interactions affects the formation of the immunological synapse. After such questions have been answered *in* vitro then perhaps *in vivo* studies could then be carried out. Although quantifying the force of interaction and correlating this with IS formation has been conducted before using AFM, this study was limited in the precise control of T-cell/DC interaction [167,502]. Using optical tweezers in combination with high resolution imaging one could determine if synapse formation forms with T-cells that have previously encountered a DC presenting antigen. This would determine whether IS formation is as versatile as T-cell/DC interactions observed *in vivo*.

7.4 Conclusion.

In summary I have presented a thesis that involved the development of an optical tweezer system and - for the first time - used such an approach to measure and quantify the interaction forces between live T-cells and DCs. Using this system, several immunological investigations were performed to assess the role of MKP-II, L-arginine-deprivation or citrullinated antigen in altering the interaction forces and effector functions of T cells. The data presented here shows that optical tweezers are useful and an ideal tool to investigate T-cell activation at the single-cell level, providing precise control of how and when a T cell becomes activated as well as providing the capacity to quantify the strength of interaction. Previous reports have attempted to understand differences in intracellular signalling and T-cell function at a single-cell level [503]. However, these relied on mixing both sets of immune cells and

taking snapshots at specific time points. Optical tweezers provide a significant advantage over this by being able to monitor the activation of T-cells at a single-cell level, whilst also controlling the length of interaction between T-cells and DCs and quantifying the interaction strength – a parameter that can influence T-cell function. Furthermore, whilst the body of work presented in this thesis uses optical tweezers to control T-cell/DC interaction, it could be used by other cell biologists. Certainly it could be used to investigate how other cellular responses are affected by forces [168]. Furthermore, Lab of chip devices have been used to manipulate cells and investigate biological topics such as stem cell responses [504], chemical biology [505] and single cell analysis [506]. Therefore, through further technology; optics improvement; and combining the technology with microfluidics, would help to deliver a system that is suitable for not only quantifying interaction forces but also new ways of probing cell interactions – especially the complex T-cell/DC interaction. Overall these studies demonstrate the potential of such an approach in answering important biological questions in immunology and cell biology and may provide novel insights for therapeutic intervention.

REFERENCES

1. Parkin, J. & Cohen, B. An overview of the immune system. *Lancet* **357,** 1777–1789 (2001).

2. Abbas, A. K. & Janeway, C. A. Immunology : Improving on nature in the twenty-first century. *Cell* **100,** 129–138 (2000).

3. Guermonprez, P., Valladeau, J., Zitvogel, L., Théry, C. & Amigorena, S. Antigen presentation and T cell stimulation by dendritic cells. *Annu. Rev. Immunol.* **20,** 621–667 (2002).

4. Zhu, J., Yamane, H. & Paul, W. E. Differentiation of effector CD4 T cell populations. *Annu. Rev. Immunol.* **28,** 445–489 (2010).

5. Dittel, B. N. CD4 T-cells: Balancing the coming and going of autoimmune mediated inflammtion in CNS. *Brain Behav. Immun.* **22,** 421–430 (2008).

6. Arstila, T. P. *et al.* A Direct Estimate of the Human T Cell Receptor Diversity. *Science (80-.).* **286,** 958–961 (1999).

7. Bonilla, F. a & Oettgen, H. C. Adaptive immunity. *J. Allergy Clin. Immunol.* **125,** S33–S40 (2010).

8. Smith-Garvin, J. E., Koretzky, G. A. & Jordan, M. S. T cell activation. *Annu. Rev. Immunol.* **27,** 591–619 (2009).

9. Bousso, P. T-cell activation by dendritic cells in the lymph node: lessons from the movies. *Nat. Rev. Immunol.* **8,** 675–684 (2008).

10. Mellman, I. & Steinman, R. M. Dendritic Cells : Specialized and regulated antigen processing machines. *Cell* **106,** 255–258 (2001).

11. Banchereau, J. & Steinman, R. M. Dendritic cells and the control of immunity. *Nature* **392,** 245–252 (1998).

12. Savina, A. & Amigorena, S. Phagocytosis and antigen presentation in dendritic cells. *Immunol. Rev.* **219,** 143–156 (2007).

13. Ganguly, D., Haak, S., Sisirak, V. & Reizis, B. The role of dendritic cells in autoimmunity. *Nat. Rev. Immunol.* **13,** 566–577 (2013).

14. Steinman, R. M., Adams, J. C. & Cohn, Z. A. Identification of a novel cells type in peripheral lymphoid organs of mice. *J. Exp. Med.* **141,** 804–820 (1975).

15. Steinman, R. M. & Cohn, Z. A. Identification of a novel cell type in peripheral lymphoid organs of mice. *J. Exp. Med.* **139,** 380 – 397 (1974).

16. Steinman, R. M. & Cohn, Z. A. Identification of a novel cell type in peripheral lymphoid organs of mice. *J. Exp. Med.* **137,** 1142–1162 (1973).

17. Lipscomb, M. F. & Masten, B. J. Dendritic cells: immune regulators in health and disease. *Physiol. Rev.* **82,** 97–130 (2002).

18. Sakuta, H. *et al.* The Tissue Distribution of the B7-2 Costimulator in Mice: Abundant Expression on Dendritic Cells In Situ and During Maturation In Vitro. *J. Exp. Med.* **180,** 1849 – 1860 (1994).

19. Caux, C. *et al.* B70/B7-2 Is identical to CD86 and is the major functional ligand for CD28 expressed on Human dendritic cells. *J. Exp. Med.* **180,** 1841 –1847 (1994).

20. Kapsenberg, M. L. Dendritic-cell control of pathogen-driven T-cell polarization. *Nat. Rev. Immunol.* **3,** 984–993 (2003).

21. Currie, J., Castro, M., Lythe, G., Palmer, E. & Molina-París, C. A stochastic T cell response criterion. *J. R. Soc.* **9,** 2856–2870 (2012).

22. Yewdell, J. W. & Dolan, B. P. Cross-dressers turn on T cells. *Nature* **332,** 581 –582 (2011).

23. Lanzavecchia, A., Lezzi, G. & Viola, A. From TCR engagement to T cell activation: a kinetic view of T cell behavior. *Cell* **96,** 1–4 (1999).

24. Larsen, C. P., Knechtle, S. J., Adams, A., Pearson, T. & Kirk, a D. A new look at blockade of T-cell costimulation: a therapeutic strategy for long-term maintenance immunosuppression. *Am. J. Transplant.* **6,** 876–83 (2006).

25. Bronstein-Sitton, N. T-cell signalling and activation. *Pathways* 8–12 (2006).

26. Hermiston, M. L., Xu, Z., Majeti, R. & Weiss, A. Reciprocal regulation of lymphocyte activation by tyrosine kinases and phosphatases. *J. Clin. Invest.* **109,** 9–14 (2002).

27. Thaventhiran, T. *et al.* T-cell co-inhibitory receptors-functions and signalling mechanisms. *J. Clin. Cell. Immunol.* **01,** 1 – 12 (2012).

28. Kabourdis, P. S. Lipid rafts in T cell receptor signalling. *Mol. Membr. Biol.* **23,** 49–57 (2006).

29. Brownlie, R. J. & Zamoyska, R. T cell receptor signalling networks: branched, diversified and bounded. *Nat. Rev. Immunol.* **13,** 257–269 (2013).

30. Wang, H. *et al.* ZAP-70: an essential kinase in T-cell signaling. *Cold Spring Harb. Perspect. Biol.* **2,** a002279 (2010).

31. Chan, A. C., Iwashima, M., Turck, C. W. & Weiss, A. ZAP-70: a 70 kd protein-tyrosine kinase that associates with the TCR zeta chain. *Cell* **71,** 649–662 (1992).

32. Zhang, W., Sloan-Lancaster, J., Kitchen, J., Trible, R. P. & Samelson, L. E. LAT: the ZAP-70 tyrosine kinase substrate that links T cell receptor to cellular activation. *Cell* **92,** 83–92 (1998).

33. Weiss, A., Koretzky, G., Schatzman, R. C. & Kadlecek, T. Functional activation of the T-cell antigen receptor induces tyrosine phosphorylation of phospholipase C-gamma 1. *Proc. Natl. Acad. Sci. U. S. A.* **88,** 5484–5488 (1991).

34. Zhang, J. *et al.* p38 mitogen-activated protein kinase mediates signal integration of TCR/CD28 costimulation in primary murine T cells. *J. Immunol.* **162,** 3819–3829 (1999).

35. DeSilva, D. R. *et al.* Inhibition of mitogen-activated protein kinase kinase blocks T cell proliferation but does not induce or prevent anergy. *J. Immunol.* **160,** 4175–4181 (1998).

36. Katzman, S. D. *et al.* Duration of antigen receptor signaling determines T-cell tolerance or activation. *Proc. Natl. Acad. Sci. U. S. A.* **107,** 18085–18090 (2010).

37. Ma, J. *et al.* Regulation of macrophage activation. *Cell. Mol. Life Sci.* **60,** 2334–2346 (2003).

38. Zheng, W. & Flavell, R. a. The transcription factor GATA-3 is necessary and sufficient for Th2 cytokine gene expression in CD4 T cells. *Cell* **89,** 587–96 (1997).

39. Ivanov, I. I. *et al.* The orphan nuclear receptor RORgammat directs the differentiation program of proinflammatory IL-17+ T helper cells. *Cell* **126,** 1121–1133 (2006).

40. Harrington, L. E., Mangan, P. R. & Weaver, C. T. Expanding the effector CD4 T-cell repertoire: the Th17 lineage. *Curr. Opin. Immunol.* **18,** 349–356 (2006).

41. Weaver, C. T., Harrington, L. E., Mangan, P. R., Gavrieli, M. & Murphy, K. M. Th17: an effector CD4 T cell lineage with regulatory T cell ties. *Immunity* **24,** 677–688 (2006).

42. Chatenoud, L., Salomon, B. & Bluestone, J. A. Suppressor T cells--they're back and critical for regulation of autoimmunity! *Immunol. Rev.* **182,** 149–163 (2001).

43. Fu, S. *et al.* TGF-beta induces Foxp3 + T-regulatory cells from CD4 + CD25 - precursors. *Am. J. Transplant.* **4,** 1614–1627 (2004).

44. Nurieva, R. I., Liu, X. & Dong, C. Molecular mechanisms of T-cell tolerance. *Immunol. Rev.* **241,** 133–144 (2011).

45. Matzinger, P. Tolerance, danger, and the extended family. *Annu. Rev. Immunol.* **12,** 991–1045 (1994).

46. Sakaguchi, S., Yamaguchi, T., Nomura, T. & Ono, M. Regulatory T cells and immune tolerance. *Cell* **133,** 775–787 (2008).

47. Bilate, A. M. & Lafaille, J. J. Induced CD4+Foxp3+ regulatory T cells in immune tolerance. *Annu. Rev. Immunol.* **30,** 733–758 (2012).

48. Van der Merwe, P. A. & Dushek, O. Mechanisms for T cell receptor triggering. *Nat. Rev. Immunol.* **11,** 47–55 (2011).

49. Van der Merwe, P. A. The TCR triggering puzzle. *Immunity* **14,** 665–668 (2001).

50. Sykulev, Y., Joo, M., Vturina, I., Tsomides, T. J. & Eisen, H. N. Evidence that a single peptide-MHC complex on a target cell can elicit a cytolytic T cell response. *Immunity* **4,** 565–571 (1996).

51. Irvine, D. J., Purbhoo, M. A., Krogsgaard, M. & Davis, M. M. Direct observation of ligand recognition by T cells. *Nature* **419,** 845–849 (2002).

52. Purbhoo, M. a, Irvine, D. J., Huppa, J. B. & Davis, M. M. T cell killing does not require the formation of a stable mature immunological synapse. *Nat. Immunol.* **5,** 524–30 (2004).

53. Kimachi, K., Croft, M. & Grey, H. M. The minimal number of antigen-major histocompatibility complex class II complexes required for activation of naive and primed T cells. *Eur. J. Immunol.* **27,** 3310–3317 (1997).

54. Krogsgaard, M. & Davis, M. M. How T cells "see" antigen. *Nat. Immunol.* **6,** 239–245 (2005).

55.   Harding, C. V & Unanue, E. R. Quantification of antigen-presenting cell MHC class II/peptide complexes necessary for T-cell stimulation. *Lett. to Nat.* **346,** 574–576 (1990).

56.   Goldrath, A. W. & Bevan, M. J. Low-affinity ligands for the TCR drive proliferation of mature CD8+ T cells in lymphopenic hosts. *Immunity* **11,** 183–190 (1999).

57.   Ernst, B., Lee, D. S., Chang, J. M., Sprent, J. & Surh, C. D. The peptide ligands mediating positive selection in the thymus control T cell survival and homeostatic proliferation in the periphery. *Immunity* **11,** 173–181 (1999).

58.   Viret, C., Wong, F. S & Janeway, C. a. Designing and maintaining the mature TCR repertoire: the continuum of self-peptide:self-MHC complex recognition. *Immunity* **10,** 559–168 (1999).

59.   Palmer, E. & Naeher, D. Affinity threshold for thymic selection through a T-cell receptor-co-receptor zipper. *Nat. Rev. Immunol.* **9,** 207–213 (2009).

60.   Starr, T. K., Jameson, S. C. & Hogquist, K. a. Positive and negative selection of T cells. *Annu. Rev. Immunol.* **21,** 139–176 (2003).

61.   Marrack, P., Scott-Browne, J. P., Dai, S., Gapin, L. & Kappler, J. W. Evolutionarily conserved amino acids that control TCR-MHC interaction. *Annu. Rev. Immunol.* **26,** 171–203 (2008).

62.   Rudolph, M. G., Stanfield, R. L. & Wilson, I. a. How TCRs bind MHCs, peptides, and coreceptors. *Annu. Rev. Immunol.* **24,** 419–466 (2006).

63.   Garcia, K. C., Adams, J. J., Feng, D. & Ely, L. K. The molecular basis of TCR germline bias for MHC is surprisingly simple. *Nat. Immunol.* **10,** 143–147 (2009).

64.   Choudhuri, K. & van der Merwe, P. A. Molecular mechanisms involved in T cell receptor triggering. *Semin. Immunol.* **19,** 255–261 (2007).

65.   Morris, G. P. & Allen, P. M. How the TCR balances sensitivity and specificity for the recognition of self and pathogens. *Nat. Immunol.* **13,** 121–128 (2012).

66.   Tian, S., Maile, R., Collins, E. J. & Frelinger, J. a. CD8+ T Cell Activation Is Governed by TCR-Peptide/MHC Affinity, Not Dissociation Rate. *J. Immunol.* **179,** 2952–2960 (2007).

67.   Krogsgaard, M. *et al.* Evidence that structural rearrangements and/or flexibility during TCR binding can contribute to T cell activation. *Mol. Cell* **12,** 1367–1378 (2003).

68. McKeithan, T. W. Kinetic proofreading in T-cell receptor signal transduction. *Proc. Natl. Acad. Sci. U. S. A.* **92,** 5042–5046 (1995).

69. Holler, P. D. & Kranz, D. M. Quantitative analysis of the contribution of TCR/pepMHC affinity and CD8 to T cell activation. *Immunity* **18,** 255–264 (2003).

70. Stone, J. D., Chervin, A. S. & Kranz, D. M. T-cell receptor binding affinities and kinetics: impact on T-cell activity and specificity. *Immunology* **126,** 165–176 (2009).

71. Germain, R. N. Computational analysis of T cell receptor signaling and ligand discrimination--past, present, and future. *FEBS Lett.* **584,** 4814–4822 (2010).

72. Mcmahan, R. H. *et al.* Relating TCR-peptide-MHC affinity to immunogenicity for the design of tumor vaccines. *J. Clin. Invest.* **116,** 2543–2551 (2006).

73. Kalergis, A. M. *et al.* Efficient T cell activation requires an optimal dwell-time of interaction between the TCR and the pMHC complex. *Nat. Immunol.* **2,** 229–234 (2001).

74. Shaw, A. S. How T cells "find" the right dendritic cell. *Nat. Immunol.* **9,** 229–230 (2008).

75. Corse, E., Gottschalk, R. A. & Allison, J. P. Strength of TCR-peptide/MHC interactions and in vivo T cell responses. *J. Immunol.* **186,** 5039–5045 (2011).

76. Celli, S., Garcia, Z., Beuneu, H. & Bousso, P. Decoding the dynamics of T cell-dendritic cell interactions in vivo. *Immunol. Rev.* **221,** 182–187 (2008).

77. Henrickson, S. E. *et al.* T cell sensing of antigen dose governs interactive behavior with dendritic cells and sets a threshold for T cell activation. *Nat. Immunol.* **9,** 282–291 (2008).

78. Obst, R., van Santen, H.-M., Mathis, D. & Benoist, C. Antigen persistence is required throughout the expansion phase of a CD4(+) T cell response. *J. Exp. Med.* **201,** 1555–1565 (2005).

79. Bousso, P. & Robey, E. Dynamics of CD8+ T cell priming by dendritic cells in intact lymph nodes. *Nat. Immunol.* **4,** 579–585 (2003).

80. Mempel, T. R., Henrickson, S. E. & Von Andrian, U. H. T-cell priming by dendritic cells in lymph nodes occurs in three distinct phases. *Nzature* **427,** 154–159 (2004).

81.   Henrickson, S. E. *et al.* T cell sensing of antigen dose governs interactive behavior with dendritic cells and sets a threshold for T cell activation. *Nat. Immunol.* **9,** 282–291 (2008).

82.   Valitutti, S., Muller, S., Cella, M., Padovan, E. & Lanzavecchia, A. Serial triggering of many T-cell receptors by a few peptide-MHC complexes. *Lett. to Nat.* **375,** 148–151 (1995).

83.   Wherry, E. J., Puorro, K. a, Porgador, A. & Eisenlohr, L. C. The induction of virus-specific CTL as a function of increasing epitope expression: responses rise steadily until excessively high levels of epitope are attained. *J. Immunol.* **163,** 3735–3745 (1999).

84.   Wherry, E. J., McElhaugh, M. J. & Eisenlohr, L. C. Generation of CD8+ T Cell Memory in Response to Low, High, and Excessive Levels of Epitope. *J. Immunol.* **168,** 4455–4461 (2002).

85.   Leignadier, J. & Labrecque, N. Epitope density influences CD8+ memory T cell differentiation. *PLoS One* **5,** e13740 (2010).

86.   Obar, J. J. & Lefranc, L. Memory CD8 + T cell differentiation. *Ann. New York Acad. Sci.* **1183,** 251–266 (2010).

87.   Constant, S., Pfeiffer, C., Woodard, A., Pasqualini, T. & Bottomly, K. Extent of T Cell Receptor Ligation Can Determine the Functional Differentiation of Naive CD4 + T Cells. *J. Exp. Med.* **182,** 1591–1596 (1995).

88.   Jorritsma, P. J., Brogdon, J. L. & Bottomly, K. Role of TCR-Induced Extracellular Signal-Regulated Kinase Activation in the Regulation of Early IL-4 Expression in Naive CD4+ T Cells. *J. Immunol.* **170,** 2427–2434 (2003).

89.   Yamane, H., Zhu, J. & Paul, W. E. Independent roles for IL-2 and GATA-3 in stimulating naive CD4+ T cells to generate a Th2-inducing cytokine environment. *J. Exp. Med.* **202,** 793–804 (2005).

90.   Thorstenson, K. M. & Khoruts, A. Generation of Anergic and Potentially Immunoregulatory CD25+CD4 T Cells In Vivo After Induction of Peripheral Tolerance with Intravenous or Oral Antigen. *J. Immunol.* **167,** 188–195 (2001).

91.   Kretschmer, K. *et al.* Inducing and expanding regulatory T cell populations by foreign antigen. *Nat. Immunol.* **6,** 1219–1227 (2005).

92.   Gottschalk, R. A., Corse, E. & Allison, J. P. TCR ligand density and affinity determine peripheral induction of Foxp3 in vivo. *J. Exp. Med.* **207,** 1701–1711 (2010).

93.   Turner, M. S., Kane, L. P. & Morel, P. a. Dominant role of antigen dose in CD4+Foxp3+ regulatory T cell induction and expansion. *J. Immunol.* **183,** 4895–4903 (2009).

94.   Madrenas, J. & Germain, R. N. Variant TCR ligands: new insights into the molecular basis of antigen-dependent signal transduction and T-cell activation. *Semin. Immunol.* **8,** 83–101 (1996).

95.   Qi, S., Krogsgaard, M., Davis, M. M. & Chakraborty, A. K. Molecular flexibility can influence the stimulatory ability of receptor-ligand interactions at cell-cell junctions. *Proc. Natl. Acad. Sci. U. S. A.* **103,** 4416–4421 (2006).

96.   Sloan-Lancaster, J. & Allen, P. M. Significance of T-cell stimulation by altered peptide ligands in T cell biology. *Curr. Opin. Immunol.* **7,** 103–109 (1995).

97.   Alam, S. M. *et al.* T-cell receptor affinity and thymocyte positive selection. *Lett. to Nat.* **381,** 616–620 (1996).

98.   Evavold, B. D. & Allen, P. M. Separation of IL-4 production from Th cell proliferation by an altered T cell receptor ligand. *Science (80-.).* **252,** 1308–1310 (1991).

99.   Sloan-Lancaster, J., Evavold, B. D. & Allen, P. M. Induction of T-cell anergy by altered T-cell receptor ligand on live antigen-presenting cells. *Lett. to Nat.* **363,** 156–159 (1993).

100. Daniels, M. A. *et al.* Thymic selection threshold defined by compartmentalization of Ras/MAPK signalling. *Nature* **444,** 724–729 (2006).

101. Sloan-Lancaster, J., Shaw, a S., Rothbard, J. B. & Allen, P. M. Partial T cell signaling: altered phospho-zeta and lack of zap70 recruitment in APL-induced T cell anergy. *Cell* **79,** 913–922 (1994).

102. Kersh, B. E. N., Kersh, G. J. & Allen, P. M. Partially phosphorylated T cell receptor zeta molecules can inhibit T cell activation. *J. Exp. Med.* **190,** 1627–1636 (1999).

103. Kersh, E. N., Shaw, A. S. & Allen, P. M. Fidelity of T Cell Activation Through Multistep T Cell Receptor Phosphorylation. *Science (80-.).* **281,** 572–575 (1998).

104. Zhengyu, M. & Finkel, T. H. T cell receptor triggering by force. *Trends Immunol.* **31,** 1–6 (2009).

105. Kim, S. T. *et al.* The alphabeta T cell receptor is an anisotropic mechanosensor. *J. Biol. Chem.* **284,** 31028–31037 (2009).

106. Minguet, S., Swamy, M., Alarcón, B., Luescher, I. F. & Schamel, W. W. a. Full activation of the T cell receptor requires both clustering and conformational changes at CD3. *Immunity* **26,** 43–54 (2007).

107. Xu, C. *et al.* Regulation of T cell receptor activation by dynamic membrane binding of the CD3epsilon cytoplasmic tyrosine-based motif. *Cell* **135,** 702–713 (2008).

108. Sun, Z. J., Kim, K. S., Wagner, G. & Reinherz, E. L. Mechanisms contributing to T cell receptor signaling and assembly revealed by the solution structure of an ectodomain fragment of the CD3 epsilon gamma heterodimer. *Cell* **105,** 913–923 (2001).

109. Aivazian, D. & Stern, L. J. Phosphorylation of T cell receptor zeta is regulated by a lipid dependent folding transition. *Nat. Struct. Biol.* **7,** 1023–1026 (2000).

110. Martínez-Martín, N. *et al.* Cooperativity between T cell receptor complexes revealed by conformational mutants of CD3epsilon. *Sci. Signal.* **2,** ra43 (2009).

111. Fischer, U. B. *et al.* MHC class II deprivation impairs CD4 T cell motility and responsiveness to antigen-bearing dendritic cells in vivo. *Proc. Natl. Acad. Sci. U. S. A.* **104,** 7181–7186 (2007).

112. Wülfing, C. *et al.* Kinetics and extent of T cell activation as measured with the calcium signal. *J. Exp. Med.* **185,** 1815–1825 (1997).

113. Rosette, C. *et al.* The impact of duration versus extent of TCR occupancy on T cell activation: a revision of the kinetic proofreading model. *Immunity* **15,** 59–70 (2001).

114. Chen, J.-L. *et al.* Ca2+ release from the endoplasmic reticulum of NY-ESO-1-specific T cells is modulated by the affinity of TCR and by the use of the CD8 coreceptor. *J. Immunol.* **184,** 1829–1839 (2010).

115. Skokos, D. *et al.* Peptide-MHC potency governs dynamic interactions between T cells and dendritic cells in lymph nodes. *Nat. Immunol.* **8,** 835–844 (2007).

116. Yachi, P. P., Ampudia, J., Zal, T. & Gascoigne, N. R. J. Altered peptide ligands induce delayed CD8-T cell receptor interaction--a role for CD8 in distinguishing antigen quality. *Immunity* **25,** 203–211 (2006).

117. Frauwirth, K. A. *et al.* The CD28 signaling pathway regulates glucose metabolism. *Immunity* **16,** 769–777 (2002).

118. Adachi, K. & Davis, M. M. T-cell receptor ligation induces distinct signaling pathways in naive vs. antigen-experienced T cells. *Proc. Natl. Acad. Sci. U. S. A.* **108,** 1549–1554 (2011).

119. Huppa, J. B. & Davis, M. M. T-cell antigen recognition and the immunological synapse. *Nat. Rev. Immunol.* **3,** 973–983 (2003).

120. Davis, M. M. *et al.* Ligand recognition by αβ T-cell receptors. *Annu. Rev. Immunol.* **16,** 523–544 (1998).

121. Corse, E., Gottschalk, R. A., Krogsgaard, M. & Allison, J. P. Attenuated T cell responses to a high-potency ligand in vivo. *PLoS Biol.* **8,** 1–12 (2010).

122. Zehn, D., Lee, S. Y. & Bevan, M. J. Complete but curtailed T-cell response to very low-affinity antigen. *Nature* **458,** 211–214 (2009).

123. Donnadieu, E., Bismuth, G. & Trautmann, A. Antigen recognition by helper T cells elicits a sequence of distinct changes of their shape and intracellular calcium. *Curr. Biol.* **4,** 584–595 (1994).

124. Negulescu, P. a, Krasieva, T. B., Khan, A., Kerschbaum, H. H. & Cahalan, M. D. Polarity of T cell shape, motility, and sensitivity to antigen. *Immunity* **4,** 421–430 (1996).

125. Berry, R. M. & Berg, H. C. Absence of a barrier to backwards rotation of the bacterial flagellar motor demonstrated with optical tweezers. *Proc. Natl. Acad. Sci. U. S. A.* **94,** 14433–14437 (1997).

126. Gunzer, M. *et al.* Antigen presentation in extracellular matrix: interactions of T cells with dendritic cells are dynamic, short lived, and sequential. *Immunity* **13,** 323–232 (2000).

127. Bousso, P., Bhakta, N. R., Lewis, R. S. & Robey, E. Dynamics of thymocyte-stromal cell interactions visualized by two-photon microscopy. *Science (80-.).* **296,** 323–232 (2002).

128. Miller, M. J., Wei, S. H., Parker, I. & Cahalan, M. D. Two-photon imaging of lymphocyte motility and antigen response in intact lymph node. *Science (80-.).* **296,** 1869–1873 (2002).

129. Miller, M. J., Wei, S. H., Cahalan, M. D. & Parker, I. Autonomous T cell trafficking examined in vivo with intravital two-photon microscopy. *Proc. Natl. Acad. Sci. U. S. A.* **100,** 2604–2609 (2003).

130. Celli, S. & Bousso, P. Intravital Two-Photon Imaging of T-Cell Priming and Tolerance in the Lymph Node. *Methods Mol. Biol.* **380,** 355–363 (2007).

131. Miller, M. J., Hejazi, A. S., Wei, S. H., Cahalan, M. D. & Parker, I. T cell repertoire scanning is promoted by dynamic dendritic cell behavior and random T cell motility in the lymph node. *Proc. Natl. Acad. Sci. U. S. A.* **101,** 998–1003 (2004).

132. Asperti-Boursin, F., Real, E., Bismuth, G., Trautmann, A. & Donnadieu, E. CCR7 ligands control basal T cell motility within lymph node slices in a phosphoinositide 3-kinase-independent manner. *J. Exp. Med.* **204,** 1167–1179 (2007).

133. Wei, S. H. *et al.* Ca2+ Signals in CD4+ T Cells during early contacts with antigen-bearing dendritic Cells in lymph node. *J. Immunol.* **179,** 1586–1594 (2007).

134. Miller, M. J., Safrina, O., Parker, I. & Cahalan, M. D. Imaging the single cell dynamics of CD4+ T cell activation by dendritic cells in lymph nodes. *J. Exp. Med.* **200,** 847–856 (2004).

135. Bhakta, N. R., Oh, D. Y. & Lewis, R. S. Calcium oscillations regulate thymocyte motility during positive selection in the three-dimensional thymic environment. *Nat. Immunol.* **6,** 143–151 (2005).

136. Yeh, J.-H., Sidhu, S. S. & Chan, A. C. Regulation of a late phase of T cell polarity and effector functions by Crtam. *Cell* **132,** 846–859 (2008).

137. Dustin, M. L. T-cell activation through immunological synapses and kinapses. *Immunol. Rev.* **221,** 77–89 (2008).

138. Schrum, a. G. & Turka, L. a. The proliferative capacity of individual naive CD4+T-cells is amplified by prolonged T-cell antigen receptor triggering. *J. Exp. Med.* **196,** 793–803 (2002).

139. Iezzi, G., Karjalainen, K. & Lanzavecchia, a. The duration of antigenic stimulation determines the fate of naive and effector T cells. *Immunity* **8,** 89–95 (1998).

140. Curtsinger, J. M., Johnson, C. M. & Mescher, M. F. CD8 T Cell Clonal Expansion and Development of Effector Function Require Prolonged Exposure to Antigen, Costimulation, and Signal 3 Cytokine. *J. Immunol.* **171,** 5165–5171 (2003).

141. Costello, P. S., Gallagher, M. & Cantrell, D. A. Sustained and dynamic inositol lipid metabolism inside and outside the immunological synapse. *Nat. Immunol.* **3,** 1082–1089 (2002).

142. Harriague, J. & Bismuth, G. Imaging antigen-induced PI3K activation in T cells. *Nat. Immunol.* **3,** 1090–1096 (2002).

143. Hugues, S., Boissonnas, A., Amigorena, S. & Fetler, L. The dynamics of dendritic cell-T cell interactions in priming and tolerance. *Curr. Opin. Immunol.* **18,** 491–495 (2006).

144. Zinselmeyer, B. H. *et al.* In situ characterization of CD4+ T cell behavior in mucosal and systemic lymphoid tissues during the induction of oral priming and tolerance. *J. Exp. Med.* **201,** 1815–1823 (2005).

145. Rush, C. M. *et al.* Characterization of CD4+ T-cell-dendritic cell interactions during secondary antigen exposure in tolerance and priming. *Ixmmunology* **128,** 463–471 (2009).

146. Hugues, S. *et al.* Distinct T cell dynamics in lymph nodes during the induction of tolerance and immunity. *Nat. Immunol.* **5,** 1235–1242 (2004).

147. Shakhar, G. *et al.* Stable T cell-dendritic cell interactions precede the development of both tolerance and immunity in vivo. *Nat. Immunol.* **6,** 707–714 (2005).

148. Celli, S., Lemaître, F. & Bousso, P. Real-time manipulation of T cell-dendritic cell interactions in vivo reveals the importance of prolonged contacts for CD4+ T cell activation. *Immunity* **27,** 625–634 (2007).

149. Stoll, S., Delon, J., Brotz, T. M. & Germain, R. N. Dynamic imaging of T cell-dendritic cell interactions in lymph nodes. *Science (80-.).* **296,** 1873–1876 (2002).

150. Odoardi, F. *et al.* Instant effect of soluble antigen on effector T cells in peripheral immune organs during immunotherapy of autoimmune encephalomyelitis. *Proc. Natl. Acad. Sci. U. S. A.* **104,** 920–925 (2007).

151. Sims, T. N. *et al.* Opposing effects of PKC theta and WASp on symmetry breaking and relocation of the immunological synapse. *Cell* **129,** 773–785 (2007).

152. Tadokoro, C. E. *et al.* Regulatory T cells inhibit stable contacts between CD4+ T cells and dendritic cells in vivo. *J. Exp. Med.* **203,** 505–511 (2006).

153. Tang, Q. *et al.* Visualizing regulatory T cell control of autoimmune responses in nonobese diabetic mice. *Nat. Immunol.* **7,** 83–92 (2006).

154. Monks, C. R. F., Freiberg, B. A., Kupfer, H., Sciaky, N. & Kupfer, A. Three-dimensional segregation of supramolecular activation clusters in T cells. *Nature* **395,** 82 – 86 (1998).

155. Alarcón, B., Mestre, D. & Martínez-Martín, N. The immunological synapse: a cause or consequence of T-cell receptor triggering? *Immunology* **133,** 420–425 (2011).

156. Brossard, C. *et al.* Multifocal structure of the T cell - dendritic cell synapse. *Eur. J. Immunol.* **35,** 1741–1753 (2005).

157. Griffiths, G. M., Tsun, A. & Stinchcombe, J. C. The immunological synapse: a focal point for endocytosis and exocytosis. *J. Cell Biol.* **189,** 399–406 (2010).

158. Lasserre, R. & Alcover, A. Cytoskeletal cross-talk in the control of T cell antigen receptor signaling. *FEBS Lett.* **584,** 4845–4850 (2010).

159. Padhan, K. & Varma, R. Immunological synapse: a multi-protein signalling cellular apparatus for controlling gene expression. *Immunology* **129,** 322–328 (2010).

160. Dustin, M. L., Chakraborty, A. K. & Shaw, A. S. Understanding the structure and function of the immunological synapse. *Cold Spring Harb. Perspect. Biol.* **2,** a002311 (2010).

161. Saito, T. & Bastista, F. D. *Immunological Synapse.* 1121–1133 (2010).

162. Friedman, R. S., Beemiller, P., Sorensen, C. M., Jacobelli, J. & Krummel, M. F. Real-time analysis of T cell receptors in naive cells in vitro and in vivo reveals flexibility in synapse and signaling dynamics. *J. Exp. Med.* **207,** 2733–2749 (2010).

163. Beemiller, P., Jacobelli, J. & Krummel, M. F. Integration of the movement of signaling microclusters with cellular motility in immunological synapses. *Nat. Immunol.* **13,** 1–10 (2012).

164. Dustin, M. L. A dynamic view of the immunological synapse. *Semin. Immunol.* **17,** 400–410 (2005).

165. Biggs, M. J. P., Milone, M. C., Santos, L. C., Gondarenko, A. & Wind, S. J. High-resolution imaging of the immunological synapse and T-cell receptor microclustering through microfabricated substrates. *J. R. Soc.* **8,** 1462–1471 (2011).

166. Cullinan, P., Sperling, A. I. & Burkhardt, J. K. The distal pole complex: a novel membrane domain distal to the immunological synapse. *Immunol. Rev.* **189,** 111–122 (2002).

167. Hosseini, B. H. *et al.* Immune synapse formation determines interaction forces between T cells and antigen-presenting cells measured by atomic force microscopy. *Proc. Natl. Acad. Sci. U. S. A.* **106,** 17852–17857 (2009).

168. Janmey, P. A. & Mcculloch, C. A. Cell Mechanics : Integrating Cell Responses to Mechanical Stimuli. *Annu. Rev. Biomed. Eng.* **9,** 1–34 (2007).

169. Lim, T. S., Mortellaro, A., Lim, C. T., Hämmerling, G. J. & Ricciardi-Castagnoli, P. Mechanical interactions between dendritic cells and T cells correlate with T cell responsiveness. *J. Immunol.* **187,** 258–265 (2011).

170. Judokusumo, E., Tabdanov, E., Kumari, S., Dustin, M. L. & Kam, L. C. Mechanosensing in T lymphocyte activation. *Biophys. J.* **102,** 5959–5963 (2012).

171. Husson, J., Chemin, K., Bohineust, A., Hivroz, C. & Henry, N. Force Generation upon T Cell Receptor Engagement. *PLoS One* **6,** 1–13 (2011).

172. Li, Y.-C. *et al.* Cutting Edge: mechanical forces acting on T cells immobilized via the TCR complex can trigger TCR signaling. *J. Immunol.* **184,** 5959–5963 (2010).

173. Zhengyu, M., Janmey, P. a & Finkel, T. H. The receptor deformation model of TCR triggering. *FASEB J.* **22,** 1002–1008 (2008).

174. Carpentier, B., Pierobon, P., Hivroz, C. & Henry, N. T-cell artificial focal triggering tools: linking surface interactions with cell response. *PLoS One* **4,** e4784 (2009).

175. Henry, N. & Hivroz, C. Early T-cell activation biophysics. *HFSP J.* **3,** 401–411 (2009).

176. Müller, D. J., Helenius, J., Alsteens, D. & Dufrêne, Y. F. Force probing surfaces of living cells to molecular resolution. *Nat. Chem. Biol.* **5,** 383–390 (2009).

177. Evans, E., Ritchie, K. & Merkel, R. Sensitive force technique to probe molecular adhesion and structural linkages at biological interfaces. *Biophys. J.* **68,** 2580–2587 (1995).

178. Zhang, H. & Liu, K.-K. Optical tweezers for single cells. *J. R. Soc.* **5,** 827–841 (2008).

179. Addae-Mensah, K. a & Wikswo, J. P. Measurement techniques for cellular biomechanics in vitro. *Exp. Biol. Med.* **233,** 792–809 (2008).

180. Swank, D. M. *et al.* Alternative exon-encoded regions of Drosophila myosin heavy chain modulate ATPase rates and actin sliding velocity. *J. Biol. Chem.* **276,** 15117–15124 (2001).

181. Neuman, K. C. & Nagy, A. Single-molecule force spectroscopy : optical tweezers , magnetic tweezers and atomic force microscopy. *Nat. Methods* **5,** 491–505 (2008).

182. Radmacher, M., Fritz, M., Kacher, C. M., Cleveland, J. P. & Hansma, P. K. Measuring the Viscoelastic Properties of Human Platelets with the Atomic Force Microscope. *Biophys. J.* **70,** 556–567 (1996).

183. Radmacher, M., Tillmann, R. W. & Gaub, H. E. Imaging viscoelasticity by force modulation with the atomic force microscope. *Biophys. J.* **64,** 735–742 (1993).

184. Neuman, K. C., Chadd, E. H., Liou, G. F., Bergman, K. & Block, S. M. Characterization of photodamage to Escherichia coli in optical traps. *Biophys. J.* **77,** 2856–2863 (1999).

185. Neuman, K. C. & Block, S. M. Optical trapping. *Rev. Sci. Instrum.* **75,** 2787–2809 (2004).

186. Maklygin, A. Y. *et al.* Measurement of interaction forces between red blood cells in aggregates by optical tweezers. *Quantum Electron.* **42,** 500–504 (2012).

187. Andersson, M. *et al.* Using optical tweezers for measuring the interaction forces between human bone cells and implant surfaces : System design and force calibration. *Rev. Sci. Instrum.* **78,** 074302 (2007).

188. Benvenuti, F. *et al.* Dendritic Cell Maturation Controls Adhesion, Synapse Formation, and the Duration of the Interactions with Naive T Lymphocytes. *J. Immunol.* **172,** 292–301 (2004).

189. Friedl, P. & Gunzer, M. Interaction of T cells with APCs: the serial encounter model. *Trends Immunol.* **22,** 187–191 (2001).

190. Hommel, M. On the dynamics of T-cell activation in lymph nodes. *Immunol. Cell Biol.* **82,** 62–66 (2004).

191. James, J. R. & Vale, R. D. Biophysical mechanism of T-cell receptor triggering in a reconstituted system. *Nature* **487,** 64–69 (2012).

192. Sackmann, E. Quantal concept of T-cell activation: adhesion domains as immunological synapses. *New J. Phys.* **13,** 065013 (2011).

193. Bridgeman, J. S., Sewell, A. K., Miles, J. J., Price, D. a & Cole, D. K. Structural and biophysical determinants of αβ T-cell antigen recognition. *Immunology* **135,** 9–18 (2011).

194. Ma, Z., Discher, D. E. & Finkel, T. H. Mechanical force in T cell receptor signal initiation. *Front. Immunol.* **3,** 1–3 (2012).

195. Jonás, A. & Zemánek, P. Light at work: the use of optical forces for particle manipulation, sorting, and analysis. *Electrophoresis* **29,** 4813–51 (2008).

196. Block, S. M. Making light work with optical tweezers. *Nature* **360,** 493–495 (1992).

197. Ashkin, A., Dziedzic, J. M. & Chu, S. Observation of a single-beam gradient-force optical trap for dielectric particles in air. *Opt. Lett.* **22,** 288–290 (1986).

198. Ashkin, A. Optical Levitation by Radiation Pressure. *Appl. Phys. Lett.* **19,** 283–285 (1971).

199. Ashkin, A. & Dziedzic, J. M. Stability of optical levitation by radiation pressure. *Appl. Phys. Lett.* **24,** 586–588 (1974).

200. Ashkin, A. Acceleration and trapping of particles by radiation perssure. *Phys. Rev. Lett.* **24,** 156–159 (1970).

201. Uhlin, B. E. & Axner, O. A Sticky Chain Model of the Elongation and Unfolding of Escherichia coli P Pili under Stress. *Biophys. J.* **90,** 1521–1534 (2006).

202. Berg, H. C. & Turner, L. Torque Generated by the Flagellar Motor of Escherichia coil. *Biophys. J.* **65,** 2201–2216 (1993).

203. Block, S. M., Blair, D. F. & Berg, H. C. Compliance of bacterial polyhooks measured with optical tweezers. *Cytometry* **12,** 492–496 (1991).

204. Block, S. M. & Svoboda, K. Analysis of high resolution recordings of motor movement. *Biophys. J.* **68,** 230–241 (1995).

205. Felgner, H., Frank, R. & Schliwa, M. Flexural rigidity of microtubules measured with the use of optical tweezers. *J. Cell Sci.* **109,** 509–516 (1996).

206. Kuo, S. C. & Sheetz, M. P. Force of single kinesin molecules measured with optical tweezers. *Science (80-.).* **260,** 232–4 (1993).

207. Veigel, C., Bartoo, M. L., White, D. C., Sparrow, J. C. & Molloy, J. E. The stiffness of rabbit skeletal actomyosin cross-bridges determined with an optical tweezers transducer. *Biophys. J.* **75,** 1424–1438 (1998).

208. Knight, A. E., Veigel, C., Chambers, C. & Molloy, J. E. Analysis of single-molecule mechanical recordings : application to acto-myosin interactions. *Biophys. Mol. Biol.* **77,** 45–72 (2001).

209. Block, S. M., Asbury, C. L., Shaevitz, J. W. & Lang, M. J. Probing the kinesin reaction cycle with a 2D optical force clamp. *Proc. Natl. Acad. Sci. U. S. A.* **100,** 2351–2356 (2003).

210. Asbury, C. L., Fehr, A. N. & Block, S. M. Kinesin moves by an asymmetric hand-over-hand mechanism. *Science (80-.).* **302,** 2130–2134 (2003).

211. Wang, M. D., Yin, H., Landick, R., Gelles, J. & Block, S. M. Stretching DNA with Optical Tweezers. *Biophys. J.* **72,** 1335 – 1346 (1997).

212. Rief, M. & Grubmüller, H. Force spectroscopy of single biomolecules. *Chemphyschem* **3,** 255–261 (2002).

213. Svoboda, K. & Block, S. M. Biological applications of optical forces. *Annu. Rev. Biophys. Biomol. Struct.* **23,** 247–85 (1994).

214. Stevenson, D. J., Gunn-Moore, F. & Dholakia, K. Light forces the pace: optical manipulation for biophotonics. *J. Biomed. Opt.* **15,** 041503 (2010).

215. Ashkin, A., Dziedzic, J. M. & Yamane, T. Optical trapping and manipulation of single cells using infrared laser beams. *Nature* **330,** 769–771 (1987).

216. Ashkin, A. Forces of a single-beam gradient laser trap on a dielectric sphere in the ray optics regime. *Biophys. J.* **55,** 1–27 (1992).

217. Ashkin, A. History of Optical Trapping and Manipulation of Small-Neutral Particle, Atoms, and Molecules. *J. Sel. Top. Quantum Electron.* **6,** 841–856 (2000).

218. Molloy, J. E. & Padgett, M. J. Lights, action: Optical tweezers. *Contemp. Phys.* **43,** 241–258 (2002).

219. Dholakia, K., Spalding, G. & Macdonald, M. Optical tweezers : the next generation. *Phys. World* **15,** 31–35 (2002).

220. Grier, D. G. A revolution in optical manipulation. *Nature* **424,** 810–816 (2003).

221. Kuo, S. C. Using optics to measure biological forces and mechanics. *Traffic* **2,** 757–763 (2001).

222. Lang, M. J. & Block, S. M. Resource Letter: LBOT-1: Laser-based optical tweezers. *Am. J. Phys.* **71,** 201–215 (2003).

223. McGloin, D. Optical tweezers: 20 years on. *Philos. Trans. R. Soc.* **364,** 3521–3537 (2006).

224. Keen, S., Leach, J., Gibson, G. & Padgett, M. J. Comparison of a high-speed camera and a quadrant detector for measuring displacements in optical tweezers. *J. Opt.* **9,** S264–S266 (2007).

225. Thompson, R. E., Larson, D. R. & Webb, W. W. Precise nanometer localization analysis for individual fluorescent probes. *Biophys. J.* **82,** 2775–2783 (2002).

226. Cheezum, M. K., Walker, W. F. & Guilford, W. H. Quantitative comparison of algorithms for tracking single fluorescent particles. *Biophys. J.* **81,** 2378–2388 (2001).

227. Keller, M., Schilling, J. & Sackmann, E. Oscillatory magnetic bead rheometer for complex fluid microrheometry. *Rev. Sci. Instrum.* **72,** 3626–3634 (2001).

228. Gosse, C. & Croquette, V. Magnetic tweezers: micromanipulation and force measurement at the molecular level. *Biophys. J.* **82,** 3314–3329 (2002).

229. Otto, O., Gutsche, C., Kremer, F. & Keyser, U. F. Optical tweezers with 2.5 kHz bandwidth video detection for single-colloid electrophoresis. *Rev. Sci. Instrum.* **79,** 023710 (2008).

230. Appleyard, D. C., Vandermeulen, K. Y., Lee, H. & Lang, M. J. Optical trapping for undergraduates. *Am. J. Phys.* **75,** 5–14 (2006).

231. Lang, M. J., Fordyce, P. M., Engh, A. M., Neuman, K. C. & Block, S. M. Simultaneous , coincident optical trapping and single-molecule fluorescence. *Nat. Methods* **1,** 1–7 (2004).

232. D'Helon, C., Dearden, E. W., Rubinsztein-Dunlop, H. & Heckenberg, N. R. Measurement of the optical force and trapping range of a single-beam gradient optical trap for micron-sized latex spheres. *J. Mod. Opt.* **41,** 595–601 (1994).

233. Simmons, R. M., Finer, J. T., Chu, S. & A, S. J. Quantitative Measurements of Force and Displacement Using an Optical Trap. *Biophys. J.* **70,** 1813 – 1822 (1996).

234. Romano, G., Sacconi, L., Capitanio, M. & Pavone, F. S. Force and torque measurements using magnetic micro beads for single molecule biophysics. *Opt. Commun.* **215,** 323–331 (2003).

235. Neil, A. T. O. & Padgett, M. J. Axial and lateral trapping efficiency of Laguerre-Gaussian modes in inverted optical tweezers. *Opt. Commun.* **193,** 45–50 (2001).

236. Xin-Cheng, Y., Zhao-Lin, L., Hong-Lian, G., Bing-Ying, C. & Dao-Zhong, Z. Effect of spherical aberration on optical trapping forces for rayleigh particels. *Chinese Phys. Lett.* **3,** 432–434 (2001).

237. Ke, P. C. & Gu, M. Characterization of trapping force in the presence of spherical aberration. *J. Mod. Opt.* **45,** 2159–2168 (1998).

238. Boulnois, J.-L. Photophysical processes in recent medical laser developments: A review. *Lasers Med. Sci.* **1,** 47–66 (1985).

239. Liu, Y., Sonek, G. J., Berns, M. W. & Tromberg, B. J. Physiological monitoring of optically trapped cells: assessing the effects of confinement by 1064-nm laser tweezers using microfluorometry. *Biophys. J.* **71,** 2158–2167 (1996).

240. Liu, Y. *et al.* Evidence for localized cell heating induced by infrared optical tweezers. *Biophys. J.* **68,** 2137–2144 (1995).

241. Rasmussen, M. B., Oddershede, L. B. & Siegumfeldt, H. Optical tweezers cause physiological damage to Escherichia coli and Listeria bacteria. *Appl. Environ. Microbiol.* **74,** 2158–2167 (2008).

242. Sasaki, K., Koshioka, M., Misawa, H., Kitamura, N. & Masuhara, H. Optical trapping of a metal particle and a water droplet by a scanning laser beam. *Appl. Phys. Lett.* **60,** 807 (1992).

243. Misawa, H., Sasaki, K., Koshioka, M., Kitamura, N. & Masuhara, H. Multibeam laser manipulation and fixation of microparticles. *Appl. Phys. Lett.* **60,** 310 (1992).

244. Finer, J. T., Simmons, R. M. & Spudich, J. A. Single myosin molecule mechanics: pcionewton forces and nanometre steps. *Nature* **368,** 113–119 (1994).

245. Ericsson, M., Hanstorp, D., Hagberg, P., Enger, J. & Nystrom, T. Sorting Out Bacterial Viability with Optical Tweezers Sorting Out Bacterial Viability with Optical Tweezers. *J. Bacteriol.* **182,** 5551–5555 (2000).

246. Lang, M. J., Fordyce, P. M. & Block, S. M. Combined optical trapping and single-molecule fluorescence. *J. Biol.* **2,** 2:6 (2003).

247. Sato, S. & Inaba, H. Optical trapping and manipulation of microscopic particles and biological cells by laser beams. *Opt. Quantum Electron.* **28,** 1–16 (1996).

248. Macdonald, M. P., Spalding, G. C. & Dholakia, K. Microfluidic sorting in an optical lattice. *Nature* **426,** 421–424 (2003).

249. Enger, J., Goksör, M., Ramser, K., Hagberg, P. & Hanstorp, D. Optical tweezers applied to a microfluidic system. *Lab Chip* **4,** 196–200 (2004).

250. Terray, A., Oakey, J. & Marr, D. W. M. Microfluidic control using colloidal devices. *Science (80-.).* **296,** 1841–1844 (2002).

251. Garnier, N., Grigoriev, R. & Schatz, M. Optical Manipulation of Microscale Fluid Flow. *Phys. Rev. Lett.* **91,** 054501 (2003).

252. Wakamoto, Y., Umehara, S., Matsumura, K., Inoue, I. & Yasuda, K. Development of non-destructive, non-contact single-cell based differential cell assay using on-chip microcultivation and optical tweezers. *Sensors and Actuators* **96,** 693–700 (2003).

253. Svoboda, K., Schmidt, C. F., Schnapp, B. J. & Block, S. M. Direct observation of kinesin stepping by optical trapping interferometry. *Nature* **365,** 721–727 (1993).

254. Veigel, C. & Schmidt, C. F. Moving into the cell: single-molecule studies of molecular motors in complex environments. *Nat. Rev. Mol. Cell Biol.* **12,** 163–176 (2011).

255. Bustamante, C., Bryant, Z. & Smith, S. B. Ten years of tension: single-molecule DNA mechanics. *Nature* **421,** 432–427 (2003).

256. Abbondanzieri, E. A., Greenleaf, W. J., Shaevitz, J. W., Landick, R. & Block, S. M. Direct observation of base-pair stepping by RNA polymerase. *Nature* **438,** 460–465 (2005).

257. Seol, Y., Li, J., Nelson, P. C., Perkins, T. T. & Betterton, M. D. Elasticity of short DNA molecules: theory and experiment for contour lengths of 0.6-7 microm. *Biophys. J.* **93,** 4360–4373 (2007).

258. Molloy, J. E., Dholakia, K. & Padgett, M. J. Preface: Optical tweezers in a new light. *J. Mod. Opt.* **50,** 1501–1507 (2003).

259. Misawa, H. & Juodkazis, S. Photophysics and photochemistry of a laser manipulated microparticle. *Prog. Polym. Sci.* **24,** 665–697 (1999).

260. Seeger, S. *et al.* Application of laser optical tweezers in immunology and molecular genetics. *Cytometry* **12,** 497–504 (1991).

261. Anvari, B., Torres, J. H. & McIntyre, B. W. Regulation of pseudopodia localization in lymphocytes through application of mechanical forces by optical tweezers. *J. Biomed. Opt.* **9,** 865–872 (2004).

262. Wei, X., Tromberg, B. J. & Cahalan, M. D. Mapping the sensitivity of T cells with an optical trap: polarity and minimal number of receptors for Ca(2+) signaling. *Proc. Natl. Acad. Sci. U. S. A.* **96,** 8471–8476 (1999).

263. Wei, X. *et al.* Perillyl alcohol inhibits TCR-mediated [Ca(2+)](i) signaling, alters cell shape and motility, and induces apoptosis in T lymphocytes. *Cell. Immunol.* **201,** 6–13 (2000).

264. Bunnell, S. C. *et al.* T cell receptor ligation induces the formation of dynamically regulated signaling assemblies. *J. Cell Biol.* **158,** 1263–1275 (2002).

265. Groves, J. T. & Dustin, M. L. Supported planar bilayers in studies on immune cell adhesion and communication. *J. Immunol. Methods* **278,** 19–32 (2003).

266. Oddos, S. *et al.* High-speed high-resolution imaging of intercellular immune synapses using optical tweezers. *Biophys. J.* **95,** L66–L68 (2008).

267. McNerney, G. P., Hubner, W., Chen, B. K. & Huser, T. Manipulating CD4+ T cells by optical tweezers for the initiation of cell-cell transfer of HIV-1. *J. Biophotonics* **3,** 5421–5427 (2011).

268. Bronte, V. & Zanovello, P. Regulation of immune responses by L-arginine metabolism. *Nat. Rev. Immunol.* **5,** 641–654 (2005).

269. Popovic, P. J., Zeh, H. J. & Ochoa, J. B. Arginine and Immunity. *J. Nutr.* **137,** 1681–1686 (2007).

270. Rodriguez, P. C., Quiceno, D. G. & Augusto, C. O. L-arginine availability regulates T-lymphocyte cell-cycle progression. *Blood* **109,** 1568–1573 (2007).

271. Zea, A. H. *et al.* L-Arginine modulates CD3zeta expression and T cell function in activated human T lymphocytes. *Cell. Immunol.* **232,** 21–31 (2004).

272. Choi, B. S. *et al.* Differential impact of L-arginine deprivation on the activation and effector functions of T cells and macrophages. *J. Leukoc. Biol.* **85,** 268–277 (2009).

273. Wu, G. & Morris, S. M. Arginine metabolism: nitric oxide and beyond. *Biochem. J.* **336,** 1–17 (1998).

274. Bogdan, C. Nitric oxide and the immune response. *Nat. Immunol.* **2,** 907–916 (2001).

275. Munder, M. *et al.* Th1/Th2-regulated expression of arginase isoforms in murine macrophages and dendritic cells. *J. Immunol.* **163,** 3771–3777 (1999).

276. Waddington, S. N., Mosley, K., Cook, H. T., Tam, F. W. & Cattell, V. Arginase AI is upregulated in acute immune complex-induced inflammation. *Biochem. Biophys. Res. Commun.* **247,** 84–87 (1998).

277. Munder, M., Eichmann, K. & Modolell, M. Alternative metabolic states in murine macrophages reflected by the nitric oxide synthase/arginase balance: Competitive regulation by CD4+ T-cells correlates with Th1/Th2 phenotype. *J. Immunol.* **160,** 5347–5354 (1998).

278. Noël, W., Raes, G., Hassanzadeh Ghassabeh, G., De Baetselier, P. & Beschin, A. Alternatively activated macrophages during parasite infections. *Trends Parasitol.* **20,** 126–133 (2004).

279. Kreider, T., Anthony, R. M., Urban, J. F. & Gause, W. C. Alternatively activated macrophages in helminth infections. *Curr. Opin. Immunol.* **19,** 448–453 (2007).

280. Krassner, S. M. & Flory, B. Essential amino acid in culture of Leishmania Taratolae. *J. Parasitol.* **57,** 917–920 (1971).

281. Steiger, R. F. & Steiger, E. Cultivation of Leishmania donovani and Leishmania braziliensis in defined media: Nutrional Requirments. *J. Protozool.* **24,** 437–441 (1977).

282. Kropf, P. *et al.* Arginase and polyamine synthesis are key factors in the regulation of experimental leishmaniasis in vivo. *FASEB J.* **19,** 1000–1002 (2005).

283. Munder, M., Choi, B.-S., Rogers, M. & Kropf, P. L-arginine deprivation impairs Leishmania major-specific T-cell responses. *Eur. J. Immunol.* **39,** 2161–2172 (2009).

284. Rodriguez, P. C. *et al.* L-Arginine Consumption by Macrophages Modulates the Expression of CD3 Chain in T Lymphocytes. *J. Immunol.* **171,** 1232–1239 (2003).

285. Bronte, V. *et al.* IL-4-Induced Arginase 1 Suppresses Alloreactive T Cells in Tumor-Bearing Mice. *J. Immunol.* **170,** 270–278 (2003).

286. Makarenkova, V. P., Bansal, V., Matta, B. M., Perez, L. a. & Ochoa, J. B. CD11b+/Gr-1+ Myeloid Suppressor Cells Cause T Cell Dysfunction after Traumatic Stress. *J. Immunol.* **176,** 2085–2094 (2006).

287. Taheri, F. *et al.* L-Arginine Regulates the Expression of the T-Cell Receptor ζ Chain (CD3 ζ) in Jurkat Cells. *Clin. Cancer Res.* **7,** 58–65 (2001).

288. Rodriguez, P. C. *et al.* Arginase I production in the tumor microenvironment by mature myeloid Cells Inhibits T-cell receptor expression and antigen-specific T-cell responses. *Cancer Res.* **64,** 5839–5849 (2004).

289. Feldmeyer, N. *et al.* Arginine deficiency leads to impaired cofilin dephosphorylation in activated human T lymphocytes. *Int. Immunol.* **24,** 303–313 (2012).

290. Cope, A. P. T cells in rheumatoid arthritis. *Arthritis Res. Ther.* **10,** 1–10 (2008).

291. Cope, A. P., Schulze-Koops, H. & Aringer, M. The central role of T cells in rheumatoid arthritis. *Clin. Exp. Rheumatol.* **25,** S4–S11 (2007).

292. Isomaki, P., Luukkainen, R., Lassila, O., Toivanen, P. & J, P. Synovial fluid T cells from patients with rheumatoid arthritis are refractory to the T helper type 2 di ff erentiation-inducing e ff ects of interleukin-4. *Immunology* **96,** 358–364 (1999).

293. Arita, K. *et al.* Structural basis for Ca(2+)-induced activation of human PAD4. *Nat. Struct. Mol. Biol.* **11,** 777–783 (2004).

294. György, B., Tóth, E., Tarcsa, E., Falus, A. & Buzás, E. I. Citrullination: a posttranslational modification in health and disease. *Int. J. Biochem. Cell Biol.* **38,** 1662–1677 (2006).

295. Pritzker, L. B., Joshi, S., Harauz, G. & Moscarello, M. a. Deimination of myelin basic protein. 2. Effect of methylation of MBP on its deimination by peptidylarginine deiminase. *Biochemistry* **39,** 5382–5388 (2000).

296. Van Gaalen, F., Ioan-Facsinay, A., Huizinga, T. W. J. & Toes, R. E. M. The devil in the details: The emerging role of anticitrulline autoimmunity in rheumatoid arthritis. *J. Immunol.* **175,** 5575–5580 (2005).

297. Zhou, Z. & Ménard, H.-A. Autoantigenic posttranslational modifications of proteins: does it apply to rheumatoid arthritis? *Curr. Opin. Rheumatol.* **14,** 250–3 (2002).

298. Suzuki, A., Yamada, R. & Yamamoto, K. Citrullination by Peptidylarginine Deiminase in Rheumatoid Arthritis. *Ann. N. Y. Acad. Sci.* **1108,** 323–339 (2007).

299. Kidd, B. A. *et al.* Epitope spreading to citrullinated antigens in mouse models of autoimmune arthritis and demyelination. *Arthritis Res. Ther.* **10,** R119 (2008).

300. Schellekens, G. a, de Jong, B. a, van den Hoogen, F. H., van de Putte, L. B. & van Venrooij, W. J. Citrulline is an essential constituent of antigenic determinants recognized by rheumatoid arthritis-specific autoantibodies. *J. Clin. Invest.* **101,** 273–281 (1998).

301. Young, B. J., Mallya, R. K., Leslie, R. D., Clark, C. J. & Hamblin, T. J. Anti-keratin antibodies in rheumatoid arthritis. *Br. Med. J.* **2,** 97–99 (1979).

302. Mallya, R. K. *et al.* Anti-keratin antibodies in rheumatoid arthritis: frequency and correlation with other features of the disease. *Clin. Exp. Immunol.* **51,** 17–20 (1983).

303. Sebbag, M. *et al.* The antiperinuclear factor and the so-called antikeratin antibodies are the same rheumatoid arthritis-specific autoantibodies. *J. Clin. Invest.* **95,** 2672–2679 (1995).

304. Lundberg, K. *et al.* Citrullinated proteins have increased immunogenicity and arthritogenicity and their presence in arthritic joints correlates with disease severity. *Arthritis Res. Ther.* **7,** R458–R467 (2004).

305. Nijenhuis, S., Zendman, A. J. W., Vossenaar, E. R., Pruijn, G. J. M. & VanVenrooij, W. J. Autoantibodies to citrullinated proteins in rheumatoid arthritis: clinical performance and biochemical aspects of an RA-specific marker. *J. Clin. Chem.* **350,** 17–34 (2004).

306. Sebbag, M. *et al.* Clinical and pathophysiological significance of the autoimmune response to citrullinated proteins in rheumatoid arthritis. *Joint, bone, spine* **71,** 493–502 (2004).

307. Vincent, C., Nogueira, L., Clavel, C., Sebbag, M. & Serre, G. Autoantibodies to citrullinated proteins: ACPA. *Autoimmunity* **38,** 17–24 (2005).

308. Sebbag, M. *et al.* Epitopes of human fibrin recognized by the rheumatoid arthritis-specific autoantibodies to citrullinated proteins. *Eur. J. Immunol.* **36,** 2250–2263 (2006).

309. Masson-Bessière, C. *et al.* In the rheumatoid pannus, anti-filaggrin autoantibodies are produced by local plasma cells and constitute a higher proportion of IgG than in synovial fluid and serum. *Clin. Exp. Immunol.* **119,** 544–552 (2000).

310. Reparon-Schuijt, C. C. *et al.* Secretion of anti-citrulline-containing peptide antibody by B lymphocytes in rheumatoid arthritis. *Arthritis Rheum.* **44,** 41–47 (2001).

311. Verpoort, K. N. *et al.* Isotype distribution of anti-cyclic citrullinated peptide antibodies in undifferentiated arthritis and rheumatoid arthritis reflects an ongoing immune response. *Arthritis Rheum.* **54,** 3799–3808 (2006).

312. Kuhn, K. A. *et al.* Antibodies against citrullinated proteins enhance tissue injury in experimental autoimmune arthritis. *J. Clin. Invest.* **116,** 961–973 (2006).

313. Holmdahl, R., Malmström, V. & Burkhardt, H. Autoimmune priming, tissue attack and chronic inflammation - the three stages of rheumatoid arthritis. *Eur. J. Immunol.* **44,** 1593–1599 (2014).

314. Hill, J. A. *et al.* Cutting Edge: The conversion of arginine to citrulline allows for a high-affinity peptide interaction with the Rheumatoid Arthritis-associated HLA-DRB1*0401 MHC class II molecule. *J. Immunol.* **171,** 538–541 (2003).

315. Hill, J. A. *et al.* Arthritis induced by posttranslationally modified (citrullinated) fibrinogen in DR4-IE transgenic mice. *J. Exp. Med.* **205,** 967–979 (2008).

316. Gavin, A. L. *et al.* Adjuvant-enhanced antibody responses in the absence of toll-like receptor signaling. *Science (80-.).* **314,** 1936–1938 (2006).

317. Tarcsa, E. *et al.* Protein Unfolding by Peptidylarginine Deiminase: Substrate specificity and structural relationships of the natural substrates trichohyalin and filaggrin. *J. Biol. Chem.* **271,** 30709–30716 (1996).

318. Ireland, J. M. & Unanue, E. R. Autophagy in antigen-presenting cells results in presentation of citrullinated peptides to CD4 T cells. *J. Exp. Med.* **208,** 2625–2632 (2011).

319. Ireland, J. M. & Unanue, E. R. Processing of proteins in autophagy vesicles of antigen-presenting cells generates citrullinated peptides recognized by the immune system. *Autophagy* **8,** 429–430 (2012).

320. James, E. A. *et al.* Citrulline-specific Th1 cells are increased in rheumatoid arthritis and their frequency is influenced by disease duration and therapy. *Arthritis Rheumatol.* **66,** 1712–1722 (2014).

321. Oers, N. S. C. Van. T cell receptor-mediated signs and signals governing T cell development. *Semin. Immunol.* **11,** 227–237 (1999).

322. Im, S. & Rao, A. Molecules Activation and Deactivation of Gene Expression by Ca 2 + / Calcineurin-NFAT-mediated Signaling. *Mol. Cells* **18,** 1–9 (2004).

323. Serfling, E. *et al.* NFAT and NF-kappaB factors-the distant relatives. *Int. J. Biochem. Cell Biol.* **36,** 1166–1170 (2004).

324. Cantrell, D. T-cell antigen receptor signal transduction pathways. *Annu. Rev. Immunol.* **14,** 259–274 (1996).

325. Mukhopadhyay, H., Cordoba, S.-P., Maini, P. K., van der Merwe, P. A. & Dushek, O. Systems model of T cell receptor proximal signaling reveals emergent ultrasensitivity. *PLoS Comput. Biol.* **9,** e1003004 (2013).

326. Giurisato, E. *et al.* The mitogen-activated protein kinase scaffold KSR1 is required for recruitment of extracellular signal-regulated kinase to the immunological synapse. *Mol. Cell. Biol.* **29,** 1554–1564 (2009).

327. Filbert, E. L., Le Borgne, M., Lin, J., Heuser, J. E. & Shaw, A. S. Stathmin regulates microtubule dynamics and microtubule organizing center polarization in activated T cells. *J. Immunol.* **188,** 5421–5427 (2012).

328. Yang, D. D. *et al.* Differentiation of CD4+ T cells to Th1 cells requires MAP kinase JNK2. *Immunity* **9,** 575–585 (1998).

329. Sabapathy, K. *et al.* JNK2 is required for efficient T-cell activation and apoptosis but not for normal lymphocyte development. *Curr. Biol.* **9,** 116–125 (1999).

330. Matsuda, S., Moriguchi, T., Koyasu, S. & Nishida, E. T Lymphocyte Activation Signals for Interleukin-2 Production Involve Activation of MKK6-

p38 and MKK7-SAPK/JNK Signaling Pathways Sensitive to Cyclosporin A. *J. Biol. Chem.* **273,** 12378–12382 (1998).

331.   Chen, C.-Y., Gatto-Konczak, F. Del, Wu, Z. & Karin, M. Stabilization of Interleukin-2 mRNA by the c-Jun NH2-Terminal Kinase Pathway. *Science (80-.).* **280,** 1945–1949 (1998).

332.   Constant, S. L. *et al.* JNK1 is required for T cell-mediated immunity against Leishmania major infection. *J. Immunol.* **165,** 2671–2676 (2000).

333.   Rincón, M. *et al.* Interferon-gamma expression by Th1 effector T cells mediated by the p38 MAP kinase signaling pathway. *EMBO J.* **17,** 2817–2829 (1998).

334.   Dodeller, F. & Schulze-Koops, H. The p38 mitogen-activated protein kinase signaling cascade in CD4 T cells. *Arthritis Res. Ther.* **8,** 2817–2829 (2006).

335.   Alberola-ila, J., Hogquist, K. A., Swan, K. A., Bevan, M. J. & Perlmutter, R. M. Positive and negative selection invoke distinct signaling pathways. *J. Exp. Med.* **184,** 9–18 (1996).

336.   Yamashita, M. *et al.* T cell antigen receptor-mediated activation of the Ras/mitogen-activated protein kinase pathway controls interleukin 4 receptor function and type-2 helper T cell differentiation. *Proc. Natl. Acad. Sci. U. S. A.* **96,** 1024–1029 (1999).

337.   Arrighi, J., Rebsamen, M., Rousset, F., Kindler, V. & Hauser, C. A critical role for p38 mitogen-activated kinase in the maturation of human blood-derived dendritic cells induced by lipopolysaccharide, TNF-α, and contact sensitizers. *J. Immunol.* **166,** 3837–3845 (2001).

338.   Bennett, B. L. *et al.* SP600125, an anthrapyrazolone inhibitor of Jun N-terminal kinase. *Proc. Natl. Acad. Sci. U. S. A.* **98,** 13681–13686 (2001).

339.   Yu, Q., Kovacs, C., Yue, F. Y. & Ostrowski, M. a. The Role of the p38 Mitogen-Activated Protein Kinase, Extracellular Signal-Regulated Kinase, and Phosphoinositide-3-OH Kinase Signal Transduction Pathways in CD40 Ligand-Induced Dendritic Cell Activation and Expansion of Virus-Specific CD8+ T Cell Memory. *J. Immunol.* **172,** 6047–6056 (2004).

340.   Rissoan, M. Reciprocal Control of T Helper Cell and Dendritic Cell Differentiation. *Science (80-.).* **283,** 1183–1186 (1999).

341.   Agrawal, S. *et al.* Cutting Edge: different toll-like receptor agonists instruct dendritic cells to induce distinct Th responses via differential modulation of

extracellular signal-regulated kinase-mitogen-activated protein kinase and c-Fos. *J. Immunol.* **171,** 4984–4989 (2003).

342. Nakahara, T. *et al.* Role of c-Jun N-terminal kinase on lipopolysaccharide induced maturation of human monocyte-derived dendritic cells. *Int. Immunol.* **16,** 1701–1709 (2004).

343. Sato, K., Nagayama, H., Tadokoro, K., Juji, T. & Takahashi, T. A. Extracellular signal-regulated kinase, stress-activated proteins kinase/c-jun N-terminal kinase and p38mapk are invloved in IL-10-mediated selective repression of TNF-α-induced activation and maturation of humna peripheral blood monocyte-derived dendritic. *J. Immunol.* **162,** 3865–3872 (1999).

344. Chen, P. *et al.* Discordance between the binding affinity of mitogen-activated protein kinase subfamily members for MAP kinase phosphatase-2 and their ability to activate the phosphatase catalytically. *J. Biol. Chem.* **276,** 29440–29449 (2001).

345. Solski, P. a. The Mitogen-activated Protein Kinase Phosphatases PAC1, MKP-1, and MKP-2 Have Unique Substrate Specificities and Reduced Activity in Vivo toward the ERK2 sevenmaker Mutation. *J. Biol. Chem.* **271,** 6497–6501 (1996).

346. Kondoh, K. & Nishida, E. Regulation of MAP kinases by MAP kinase phosphatases. *Biochim. Biophys. Acta* **1773,** 1227–1237 (2007).

347. Camps, M., Nichols, A. & Arkinstall, S. Dual specificity phosphatases: a gene family for control of MAP kinase function. *FASEB J.* **14,** 1227–1237 (2000).

348. Huang, C.-Y. *et al.* DUSP4 deficiency enhances CD25 expression and CD4+ T-cell proliferation without impeding T-cell development. *Eur. J. Immunol.* **42,** 476–488 (2012).

349. Al-Mutairi, M. S. *et al.* MAP kinase phosphatase-2 plays a critical role in response to infection by Leishmania mexicana. *PLoS Pathog.* **6,** e1001192 (2010).

350. Schroeder, J., McGachy, H. A., Woods, S., Plevin, R. & Alexander, J. T cell hypo-responsiveness against Leishmania major in MAP kinase phosphatase (MKP) 2 deficient C57BL/6 mice does not alter the healer disease phenotype. *PLoS Negl. Trop. Dis.* **7,** e2064 (2013).

351. Woods, S. *et al.* MAP kinase phosphatase-2 plays a key role in the control of infection with Toxoplasma gondii by modulating iNOS and arginase-1 activities in mice. *PLoS Pathog.* **9,** e1003535 (2013).

352. Underhill, D. M., Bassetti, M., Rudensky, A. & Aderem, A. Dynamic interactions of macrophages with T cells during antigen presentation. *J. Exp. Med.* **190,** 1909–1914 (1999).

353. Lutz, M. B. *et al.* An advanced culture method for generating large quantities of highly pure dendritic cells from mouse bone marrow. *J. Immunol. Methods* **223,** 77–92 (1999).

354. Ghimire, T. R., Benson, R. A., Garside, P. & Brewer, J. M. Alum increases antigen uptake, reduces antigen degradation and sustains antigen presentation by DCs in vitro. *Immunol. Lett.* **147,** 55–62 (2012).

355. Soares, A. *et al.* Novel application of Ki67 to quantify antigen-specific in vitro lymphoproliferation. *J. Immunol. Methods* **362,** 43–50 (2010).

356. Huang, W., Anvari, B., Torres, J. H., LeBaron, R. G. & Athanasiou, K. a. Temporal effects of cell adhesion on mechanical characteristics of the single chondrocyte. *J. Orthop. Res.* **21,** 88–95 (2003).

357. Kusumi, A. & Sako, Y. Cell surface organization by the membrane skeleton. *Curr. Opin. Cell Biol.* **8,** 566 – 574 (1996).

358. Stark, R., Heckl, W. M., Bhm, M. & Psl, H. Cut out or poke in the key to the world of single genes: laser micromanipulation as a valuable tool on the look-out for the origin of disease. *Genet. Anal. Biomol. Eng.* **14,** 1 – 8 (1997).

359. Smith, S. P. *et al.* Inexpensive optical tweezers for undergraduate laboratories. *Am. J. Phys.* **67,** 26–35 (1999).

360. Florin, E.-L., Pralle, A., Hober, J. K. H. & Stelzer, H. . Photonic force microscope based on optical tweezers and two-photon excitation for biological applications. *J. Struct. Biol.* **119,** 202 –211 (1997).

361. Fällman, E. & Axner, O. Design for fully steerable dual-trap optical tweezers. *Appl. Opt.* **36,** 2107–2113 (1997).

362. Singer, W., Bernet, S., Hecker, N., Ritsch-marte, M. & Physik, È. M. Three-dimensional force calibration of optical tweezers. *J. Mod. Opt.* **47,** 2921 – 2931 (2000).

363. Curtis, J. E., Koss, B. A. & Grier, D. G. Dynamic holographic optical tweezers. *Opt. Commun.* **207,** 169–175 (2002).

364. Mogensen, P. C. & Gluckstad, J. Dynamic array generation and pattern formation for optical tweezers. *Opt. Commun.* **175,** 75–81 (2000).

365. Martin-Badosa, E. *et al.* Design strategies for optimizing holographic optical tweezers setups. *Pure Pllie Opt.* **9,** S267 – S277 (2007).

366. Bowman, R. W. *et al.* "Red Tweezers": Fast, customisable hologram generation for optical tweezers. *Comput. Phys. Commun.* **185,** 268–273 (2014).

367. Thalhammer, G., Steiger, R., Bernet, S. & Ritsch-Marte, M. Optical macro-tweezers: trapping of highly motile micro-organisms. *J. Opt.* **13,** 044024 (2011).

368. Van der Horst, A. & Forde, N. R. Calibration of dynamic holographic optical tweezers for force measurements on biomaterials. *Opt. Express* **16,** 20987–21003 (2008).

369. Capitanio, M. *et al.* Calibration of optical tweezers with differential interference contrast signals. *Rev. Sci. Instrum.* **73,** 1687–1696 (2002).

370. Kestin, J., Sokolov, M. & Wakeham, W. A. Viscosity of liquid water in the range -8°C to 150°C. *J. Phys. Chem. Ref. Data* **7,** 941–948 (1978).

371. Williams, M. C. in *Biophys. Textb. online* 1–14 (2002).

372. Altan-Bonnet, G. & Germain, R. N. Modeling T cell antigen discrimination based on feedback control of digital ERK responses. *PLoS Biol.* **3,** 1925 – 1938 (2005).

373. Udrea, D. D., Bryanston-cross, P. J., Lee, W. K. & Funes-Gallanzi, M. Two sub-pixel processing algorithms for high accuracy particle centre estimation in low seeding density particle image velocimetry. *Opt. Laser Technol.* **28,** 389–396 (1996).

374. Frigault, M. M., Lacoste, J., Swift, J. L. & Brown, C. M. Live-cell microscopy - tips and tools. *J. Cell Sci.* **122,** 753–767 (2009).

375. Dumont, F. J., Staruch, M. J., Fischer, P., DaSilva, C. & Camacho, R. Inhibition of T cell activation by pharmacologic disruption of the MEK1/ERK MAP kinase or calcineurin signaling pathways results in differential modulation of cytokine production. *J. Immunol.* **160,** 2579–2589 (1998).

376. Koike, T. *et al.* A novel ERK-dependent signaling process that regulates interleukin-2 expression in a late phase of T cell activation. *J. Biol. Chem.* **278,** 15685–15692 (2003).

377. Hoffmann, S. *et al.* Single cell force spectroscopy of T cells recognizing a myelin-derived peptide on antigen presenting cells. *Immunol. Lett.* **136,** 13–20 (2011).

378. Ng, G. *et al.* Receptor-independent, direct membrane binding leads to cell surface lipid sorting and Syk kinase activation in dendritic cells. *Immunity* **29,** 807–818 (2008).

379. Wanasen, N. & Soong, L. L-arginine metabolism and its impact in host immunity against Leishmania infection. *Immunol. Res.* **41,** 15–25 (2008).

380. Munder, M., Choi, B.-S., Rogers, M. & Kropf, P. L-arginine deprivation impairs Leishmania major-specific T-cell responses. *Eur. J. Immunol.* **39,** 2161–2172 (2009).

381. Stempin, C. C., Dulgerian, L. R., Garrido, V. V. & Cerban, F. M. Arginase in parasitic infections: macrophage activation, immunosuppression, and intracellular signals. *J. Biomed. Biotechnol.* **2010,** 1–10 (2009).

382. Modolell, M. *et al.* Local suppression of T cell responses by arginase-induced L-arginine depletion in nonhealing leishmaniasis. *PLoS Negl. Trop. Dis.* **3,** 480–491 (2009).

383. Rodríguez, P. C. & Ochoa, A. C. Arginine availability regulates T-cell function in cancer. *Tumor Induc. Immune Suppr.* 219–233 (2008).

384. Kusmartsev, S., Nefedova, Y., Yoder, D. & Gabrilovich, D. I. Antigen-specific inhibition of CD8+ T cell response by immature myeloid cells in cancer Is mediated by reactive oxygen species. *J. Immunol.* **172,** 989–999 (2004).

385. Dustin, M. L., Bromley, S. K., Kan, Z., Peterson, D. A. & Unanue, E. R. Antigen receptor engagement delivers a stop signal to migrating T lymphocytes. *Proc. Natl. Acad. Sci. U. S. A.* **94,** 3909–3913 (1997).

386. Rodriguez, P. C. *et al.* Regulation of T cell receptor CD3zeta chain expression by L-arginine. *J. Biol. Chem.* **277,** 21123–21129 (2002).

387. Chen, X. *et al.* Impaired expression of the CD3-zeta chain in peripheral blood T cells of patients with chronic myeloid leukaemia results in an increased susceptibility to apoptosis. *Br. J. Haematol.* **111,** 817–825 (2000).

388. Combadière, B. *et al.* Qualitative and quantitative contributions of the T cell receptor zeta chain to mature T cell apoptosis. *J. Exp. Med.* **183,** 2109–2117 (1996).

389. Taheri, F. *et al.* l-Arginine regulates the expression of the T-cell receptor ζ chain (CD3 ζ) in Jurkat Cells. *Clin. Cancer Res.* **7,** 958–965 (2001).

390. Liu, D. & Uzonna, J. E. The early interaction of Leishmania with macrophages and dendritic cells and its influence on the host immune response. *Front. Cell. Infect. Microbiol.* **2,** 83 (2012).

391. Baniyash, M. TCR zeta-chain downregulation: curtailing an excessive inflammatory immune response. *Nat. Rev. Immunol.* **4,** 675–687 (2004).

392. Watson, A. R. O. & Lee, W. T. Defective T cell receptor-mediated singal transduction in memroy CD4 T lymphcytes exposed to superantigen or anti-T cell receptor antibodies. *Cell. Immunol.* **242,** 80–90 (2006).

393. Smith, K. A. Interleukin-2: Inception , Impact , and Implications. *Science (80-.).* **240,** 1169–1176 (1988).

394. Cantrell, D. A. & Smith, K. A. The interleukin-2 T-cell system: a new cell growth model. *Science (80-.).* **224,** 1312–1316 (1984).

395. Sun, J., Dirden-Kramer, B., Ito, K., Ernst, P. B. & Van Houten, N. Antigen-specific T cell activation and proliferation during oral tolerance induction. *J. Immunol.* **162,** 5868–5875 (1999).

396. Grakoui, A. *et al.* The Immunological Synapse: A Molecular Machine Controlling T Cell Activation. *Science (80-.).* **285,** 221–227 (1999).

397. Eibert, S. M. *et al.* Cofilin peptide homologs interfere with immunological synapse formation and T cell activation. *Proc. Natl. Acad. Sci. U. S. A.* **101,** 1957–1962 (2004).

398. Condeelis, J. How is actin polymerization nucleated in vivo? *Trends Cell Biol.* **11,** 288–293 (2001).

399. McDonald, A., Harris, J., Macmillan, D., Dempster, J. & McConnell, G. Light-induced Ca(2+) transients observed in widefield epi-fluorescence microscopy of excitable cells. *Biomed. Opt. Express* **3,** 1266–1273 (2012).

400. Smith, N. I. *et al.* Photostimulation of two types of Ca 2+ waves in rat pheochromocytoma PC12 cells by ultrashort pulsed near-infrared laser irradiation. *Laser Phys. Lett.* **3,** 154–161 (2006).

401. Iwanaga, S., Smith, N. I., Fujita, K. & Kawata, S. Slow Ca(2+) wave stimulation using low repetition rate femtosecond pulsed irradiation. *Opt. Express* **14,** 717–725 (2006).

402. Fooksman, D. R. *et al.* Functional anatomy of T cell activation and synapse formation. *Annu. Rev. Immunol.* **28,** 79–105 (2010).

403. Choi, S. & Schwartz, R. H. Impairment of immunological synapse formation in adaptively tolerant T cells. *J. Immunol.* **187,** 805–816 (2011).

404. Macián, F., Im, S.-H., García-Cózar, F. J. & Rao, A. T-cell anergy. *Curr. Opin. Immunol.* **16,** 209–216 (2004).

405. Luban, S. & Li, Z.-G. Citrullinated peptide and its relevance to rheumatoid arthritis: an update. *Int. J. Rheum. Dis.* **13,** 284–287 (2010).

406. Chang, X. *et al.* Localization of peptidylarginine deiminase 4 (PADI4) and citrullinated protein in synovial tissue of rheumatoid arthritis. *Rheumatology* **44,** 40–50 (2004).

407. Vossenaar, E. R., Zendman, A. J. W., van Venrooij, W. J. & Pruijn, G. J. M. PAD, a growing family of citrullinating enzymes: genes, features and involvement in disease. *BioEssays* **25,** 1106–1118 (2003).

408. Nielen, M. M. J. *et al.* Specific autoantibodies precede the symptoms of rheumatoid arthritis: a study of serial measurements in blood donors. *Arthritis Rheum.* **50,** 380–386 (2004).

409. Majka, D. S. *et al.* The duration of pre-clinical Rheumatoid Athritis-related autoantibody positivity increases in subjects with older age at time of disease diagnosis. *Ann. Rheum. Dis.* **67,** 801–807 (2008).

410. Kinloch, A. *et al.* Synovial fluid is a site of citrullination of autoantigens in inflammatory arthritis. *Arthritis Rheum.* **58,** 2287–2295 (2008).

411. Suzuki, A. *et al.* Anti-citrullinated collagen type I antibody is a target of autoimmunity in rheumatoid arthritis. *Biochem. Biophys. Res. Commun.* **333,** 418–426 (2005).

412. Masson-Bessiere, C. *et al.* The major synovial targets of the Rheumatoid Arthritis-specific antifilaggrin autoantibodies are deiminated forms of the - and -chains of fibrin. *J. Immunol.* **166,** 4177–4184 (2001).

413. Vossenaar, E. R. *et al.* Rheumatoid arthritis specific anti-Sa antibodies target citrullinated vimentin. *Arthritis Res. Ther.* **6,** R142 − R150 (2004).

414. Cook, A. D., Gray, R., Ramshaw, J., Mackay, I. R. & Rowley, M. J. Antibodies against the CB10 fragment of type II collagen in rheumatoid arthritis. *Arthritis Res. Ther.* **6,** R477–R483 (2004).

415. Tilleman, K. *et al.* Synovial detection and autoantibody reactivity of processed citrullinated isoforms of vimentin in inflammatory arthritides. *Rheumatology* **47,** 597–604 (2008).

416. Matsuo, K. *et al.* Identification of novel citrullinated autoantigens of synovium in rheumatoid arthritis using a proteomic approach. *Arthritis Res. Ther.* **8,** R175 (2006).

417. Kinloch, A. *et al.* Identification of citrullinated alpha-enolase as a candidate autoantigen in rheumatoid arthritis. *Arthritis Res. Ther.* **7,** R1421–R1429 (2005).

418. Ireland, J., Herzog, J. & Unanue, E. R. Cutting edge: unique T cells that recognize citrullinated peptides are a feature of protein immunization. *J. Immunol.* **177,** 2625–2632 (2006).

419. Wordsworth, B. P. *et al.* HLA-DR4 subtype frequencies in rheumatoid arthritis indicate that DRB1 is the major susceptibility locus within the HLA class II region. *Proc. Natl. Acad. Sci. U. S. A.* **86,** 10049–10053 (1989).

420. Gregersen, P. K., Silver, J. & Winchester, R. J. The shared epitope hypothesis - An approach to understanding the molecular genetics of susceptibility to Rheumatoid Arthritis. *Arthritis Rheum.* **30,** 1205 – 1213 (1987).

421. Klareskog, L., Rönnelid, J., Lundberg, K., Padyukov, L. & Alfredsson, L. Immunity to citrullinated proteins in rheumatoid arthritis. *Annu. Rev. Immunol.* **26,** 651–675 (2008).

422. Huizinga, T. W. J. *et al.* Refining the complex rheumatoid arthritis phenotype based on specificity of the HLA-DRB1 shared epitope for antibodies to citrullinated proteins. *Arthritis Rheum.* **52,** 3433–3438 (2005).

423. Annette, H. M. *et al.* The HLA-DRB1 shared epitope alleles are primarily a risk factor for anti-cyclic citrullinated peptide antibodies and are not an independent risk factor for development of rheumatoid arthritis. *Arthritis Rheum.* **54,** 1117–1121 (2006).

424. Kallberg, H. *et al.* Gene-gene and gene-environment interactions involving HLA-DRB1, PTPN22, and smoking in two subsets of rheumatoid arthritis. *Am. J. Hum. Genet.* **80,** 867–875 (2007).

425. Klareskog, L. *et al.* A new model for an etiology of rheumatoid arthritis: smoking may trigger HLA-DR (shared epitope)-restricted immune reactions to autoantigens modified by citrullination. *Arthritis Rheum.* **54,** 38–46 (2006).

426. Olivares Martínez, E., Hernández Ramírez, D. F., Núñez-Álvarez, C. a & Cabiedes, J. Citrullinated proteins in rheumatoid arthritis. *Reumatol. Clin.* **7,** 68–71 (2011).

427. Venrooij, W. J. Van & Pruijn, G. J. M. Citrullination : a small change for a protein with great consequences for rheumatoid arthritis. *Arthritis Res.* **2,** 249 – 251 (2000).

428. Asaga, H., Yamada, M. & Senshu, T. Selective deimination of vimentin in calcium ionophore-induced apoptosis of mouse peritoneal macrophages. *Biochem. Biophys. Res. Commun.* **243,** 641–646 (1998).

429. Mizoguchi, M. *et al.* Deimination of 70-kD nuclear protein during epidermal apoptotic events In Vitro. *J. Histochem. Cytochem.* **46,** 1303–1309 (1998).

430. Migliorini, P., Pratesi, F., Tommasi, C. & Anzilotti, C. The immune response to citrullinated antigens in autoimmune diseases. *Autoimmun. Rev.* **4,** 561–564 (2005).

431. Wegner, N. *et al.* Autoimmunity to specific citrullinated proteins gives the first clues to the etiology of rheumatoid arthritis. *Immunol. Rev.* **233,** 34–54 (2010).

432. Donermeyer, D. L., Weber, K. S., Kranz, D. M. & Allen, P. M. The study of high-affinity TCRs reveals duality in T-cell recognition of antigen: specificity and degeneracy. *J. Immunol.* **177,** 6911–6919 (2006).

433. Anderton, S. M. Post-translational modifications of self antigens: implications for autoimmunity. *Curr. Opin. Immunol.* **16,** 753–758 (2004).

434. Hill, J. A., Wang, D., Jevnikar, A. M., Cairns, E. & Bell, D. A. The relationship between predicted peptide – MHC class II affinity and T-cell activation in a HLA-DR β 1 * 0401 transgenic mouse model. *Arthritis Res. Ther.* **5,** (2002).

435. Law, S. C. *et al.* T-cell autoreactivity to citrullinated autoantigenic peptides in rheumatoid arthritis patients carrying HLA-DRB1 shared epitope alleles. *Arthritis Res. Ther.* **5,** R118 (2012).

436. Manz, B. N., Jackson, B. L., Petit, R. S., Dustin, M. L. & Groves, J. T-cell triggering thresholds are modulated by the number of antigen within individual T-cell receptor clusters. *Proc. Natl. Acad. Sci. U. S. A.* **108,** 9089– 9094 (2011).

437. Zhang, X., Izikson, L., Liu, L. & Weiner, H. L. Activation of CD25+CD4+ Regulatory T Cells by Oral Antigen Administration. *J. Immunol.* **167,** 4245–4253 (2001).

438. Ise, W. *et al.* Orally tolerized T cells can form conjugates with APCs but are defective in immunological synapse formation. *J. Immunol.* **175,** 829–838 (2001).

439. Chen, Y., Ma, Y. & Chen, Y. Roles of cytotoxic T-lymphocyte-associated antigen-4 in the inductive phase of oral tolerance. *Immunology* **105,** 171–180 (2002).

440. Cerqueira, C. F., Klareskog, L. & Jakobsson, P.-J. Neutralization of anticitrullinated protein antibodies in rheumatoid arthritis - a way to go? *Basic Clin. Pharmacol. Toxicol.* **114,** 13–17 (2014).

441. Yamada, R. Peptidylarginine deiminase type 4, anticitrullinated peptide antibodies, and rheumatoid arthritis. *Autoimmun. Rev.* **4,** 201–206 (2005).

442. Tranquill, L. R. *et al.* Enhanced T cell responsiveness to citrulline-containing myelin basic protein in multiple sclerosis patients. *Mult. Scler.* **6,** 220–225 (2000).

443. Snir, O. *et al.* Identification and functional characterization of T cells reactive to citrullinated vimentin in HLA-DRB1*0401-positive humanized mice and rheumatoid arthritis patients. *Arthritis Rheum.* **63,** 2873–83 (2011).

444. Hida, S., Miura, N. N., Adachi, Y. & Ohno, N. Influence of arginine deimination on antigenicity of fibrinogen. *Jzzzournal Autoimmun.* **23,** 141–50 (2004).

445. Corse, E., Gottschalk, R. a & Allison, J. P. Strength of TCR-peptide/MHC interactions and in vivo T cell responses. *J. Immunol.* **186,** 5039–5045 (2011).

446. Suri, A., Lovitch, S. B. & Unanue, E. R. The wide diversity and complexity of peptides bound to class II MHC molecules. *Curr. Opin. Immunol.* **18,** 70–77 (2006).

447. Rimer, J. Presentation of citrullinated peptides derived from unmodified protein by antigen presenting. 1–36 (2010).

448. Garside, P. & Brewer, J. M. Real-time imaging of the cellular interactions underlying tolerance, priming, and responses to infection. *Immunol. Rev.* **221,** 130–146 (2008).

449. Millington, O. R. *et al.* Malaria impairs T cell clustering and immune priming despite normal signal 1 from dendritic cells. *PLoS Pathog.* **3,** 1380–7 (2007).

450. Garcia, Z. *et al.* Competition for antigen determines the stability of T cell – dendritic cell interactions during clonal expansion. *Proc. Natl. Acad. Sci. U. S. A.* **104,** 4553–4558 (2007).

451. Badovinac, V. P., Haring, J. S. & Harty, J. T. Initial TCR-transgenic precursor frequency dictates critical aspects of the CD8 T cell response to infection. *Immunity* **26,** 827–841 (2007).

452. Marzo, A. L. *et al.* Initial T cell frequency dictates memory CD8+ T cell lineage commitment. *Nat. Immunol.* **6,** 793–799 (2005).

453. Chu, Y., Solski, P. A., Khosravi-Far, R., Der, C. J. & Kelly, K. The mitogen-activated Protein Kinase Phosphatases PAC1, MKP-1, and MKP-2 Have Unique Substrate Specificities and Reduced Activity in Vivo toward the ERK2 sevenmaker Mutation. *J. Biol. Chem.* **271,** 6497–6501 (1996).

454. Caunt, C. J. & Keyse, S. M. Dual-specificity MAP kinase phosphatases (MKPs): shaping the outcome of MAP kinase signalling. *FEBS J.* **280,** 489–504 (2013).

455. Duan, W., Chan, J. H. P., Wong, C. H., Leung, B. P. & Wong, W. S. F. Anti-inflammatory effects of mitogen-activated protein kinase kinase inhibitor U0126 in an asthma mouse model. *J. Immunol.* **172,** 7053–7059 (2004).

456. Escott, K. J. *et al.* Effect of the p38 kinase inhibitor SB203580 , on allergic airway in ⁻ ammation in the rat. *Br. J. Pharmacol.* **131,** 173–176 (2000).

457. Uchi, H., Koga, T., Urabe, K., Moroi, Y. & Furue, M. CX-659S, a diaminouracil derivative, indirectly inhibits the function of Langerhans cells by blocking the MEK1/2-Erk1/2 pathway in keratinocytes. *J. Invest. Dermatol.* **120,** 983–989 (2003).

458. Tao, X., Grant, C., Constant, S. & Bottomly, K. Induction of IL-4-producing CD4+ T cells by antigenic peptides altered for TCR binding. *J. Immunol.* **185,** 4237–4244 (1997).

459. Milner, J. D., Fazilleau, N., McHeyzer-Williams, M. & Paul, W. Cutting edge: lack of high affinity competition for peptide in polyclonal CD4+ responses unmasks IL-4 production. *J. Immunol.* **184,** 6569–6573 (2010).

460. Rincón, M., Flavell, R. a & Davis, R. J. Signal transduction by MAP kinases in T lymphocytes. *Oncogene* **20,** 2490–7 (2001).

461. Nakahara, T., Moroi, Y., Uchi, H. & Furue, M. Differential role of MAPK signaling in human dendritic cell maturation and Th1/Th2 engagement. *J. Dermatol. Sci.* **42,** 5807–5814 (2006).

462. Hemmer, B., Stefanova, I., Vergelli, M., Germain, R. N. & Martin, R. Relationships among TCR ligand potency, thresholds for effector function elicitation, and the quality of early signaling events in human T cells. *J. Immunol.* **160,** 5807–5814 (1998).

463. Alberola-Ila, J. & Hernández-Hoyos, G. The Ras/MAPK cascade and the control of positive selection. *Immunol. Rev.* **191,** 79–96 (2003).

464. Chi, H. *et al.* Dynamic regulation of pro- and anti-inflammatory cytokines by MAPK phosphatase 1 (MKP-1) in innate immune responses. *Proc. Natl. Acad. Sci. U. S. A.* **103,** 2274–2279 (2006).

465. Jeffrey, K. L. *et al.* Positive regulation of immune cell function and inflammatory responses by phosphatase PAC-1. *Nat. Immunol.* **7,** 274–283 (2006).

466. Zhang, Y. *et al.* Regulation of innate and adaptive immune responses by MAP kinase phosphatase 5. *Lett. to Nat.* **430,** 793–797 (2004).

467. Jeffrey, K. L., Camps, M., Rommel, C. & Mackay, C. R. Targeting dual-specificity phosphatases: manipulating MAP kinase signalling and immune responses. *Nat. Rev. Drug Discov.* **6,** 391–403 (2007).

468. Lilic, M., Kulig, K., Messaoudi, I., Remus, K. & Jankovi, M. CD8 + T cell cytolytic activity independent of mitogen-activated protein kinase / extracellular regulatory kinase signaling (MAP kinase / ERK). *Eur. J. Immunol.* **29,** 3971–3977 (1999).

469. Chen, X. *et al.* CD28-stimulated ERK2 phosphorylation is required for polarization of the microtubule organizing center and granules in YTS NK cells. *Proc. Natl. Acad. Sci. U. S. A.* **103,** 10346–10351 (2006).

470. Nejmeddine, M. *et al.* HTLV-1 – Tax and ICAM-1 act on T-cell signal pathways to polarize the microtubule-organizing center at the virological synapse. *Blood* **114,** 1016–1025 (2009).

471. Ramesh, S. *et al.* TGF beta-mediated BIM expression and apoptosis are regulated through SMAD3-dependent expression of the MAPK phosphatase MKP2. *EMBO Rep.* **9,** 990–997 (2008).

472. Al-Mutairi, M. S. *et al.* IL-6 expression induced by adenosine A2b receptor stimulation in U373 MG cells depends on p38 mitogen activated kinase and protein kinase C. *Neurochem. Int.* **46,** 501–512 (2005).

473. Guo, X., Gerl, R. E. & Schrader, J. W. Defining the involvement of p38alpha MAPK in the production of anti- and proinflammatory cytokines using an SB 203580-resistant form of the kinase. *J. Biol. Chem.* **278,** 22237–22242 (2003).

474. Krause, A. *et al.* Stress-activated Protein Kinase/Jun N-terminal Kinase Is Required for Interleukin (IL)-1-induced IL-6 and IL-8 Gene Expression in the Human Epidermal Carcinoma Cell Line KB. *J. Biol. Chem.* **273,** 23681–23689 (1998).

475. Demotz, S., Grey, H. M. & Setre, A. The minimal number of class II MHC-Antigne complexes needed for T-cell activation. *Science (80-.).* **249,** 30–32 (1990).

476. Paterson, L. *et al.* Controlled rotation of optically trapped microscopic particles. *Science (80-.).* **292,** 912–914 (2001).

477. Dasgupta, R., Ahlawat, S., Verma, R. S. & Gupta, P. K. Optical orientation and rotation of trapped red blood cells with Laguerre-Gaussian mode. *Opt. Express* **19,** 7680–7688 (2011).

478. Arlt, J., Garces-Chavez, V., Sibbett, W. & Dholakia, K. Optical micromanipulation using a Bessel light beam. *Opt. Commun.* **197,** 239–245 (2001).

479. Wells, A. D., Walsh, M. C., Bluestone, J. A. & Turka, L. A. Signaling through CD28 and CTLA-4 controls two distinct forms of T cell anergy. *J. Clin. Invest.* **108,** 895–903 (2001).

480. Vanasek, T. L., Khoruts, a., Zell, T. & Mueller, D. L. Antagonistic Roles for CTLA-4 and the Mammalian Target of Rapamycin in the Regulation of Clonal Anergy: Enhanced Cell Cycle Progression Promotes Recall Antigen Responsiveness. *J. Immunol.* **167,** 5636–5644 (2001).

481. Singh, R., Pervin, S., Karimi, A., Celderbaum, S. & Chaudhuri, G. Arginase Activity in Human Breast Cancer Cell Lines : N ω -Hydroxy-l-arginine Selectively Inhibits Cell Proliferation and Induces Apoptosis in MDA-MB-468 Cells. *Cancer Res.* **60,** 3305–3312 (2000).

482. Chang, C.-I., Liao, J. C. & Kuo, L. Macrophage Arginase Promotes Tumor Cell Growth and Suppresses Nitric Oxide-mediated Tumor Cytotoxicity. *Cancer Res.* **61,** 1100–1106 (2001).

483. Rodríguez, P. C. & Ochoa, A. C. Arginine regulation by myeloid derived suppressor cells and tolerance in cancer: mechanisms and therapeutic perspectives. *Immunol. Rev.* **222,** 180–191 (2008).

484. Schmielau, J. & Finn, O. J. Activated Granulocytes and Granulocyte-derived Hydrogen Peroxide Are the Underlying Mechanism of Suppression of T-Cell Function in Advanced Cancer Patients. *Cancer Res.* **61,** 4756–4760 (2001).

485. Peterman, E. J. G., Gittes, F. & Schmidt, C. F. Laser-induced heating in optical traps. *Biop* **84,** 1308–1316 (2003).

486. Simpson, N. B., McGloin, D., Dholakia, K., Allen, L. & Padgett, M. J. Optical tweezers with increased axial trapping efficiency. *J. Mod. Opt.* **45,** 1943–1949 (1998).

487. Reihani, S. N. S. & Oddershede, L. B. Optimizing immersion media refractive index improves optical trapping by compensating. *Opt. Lett.* **32,** 1998–2000 (2007).

488. Kim, H., Joo, I., Song, S. & Kim, P. Dependence of the Optical Trapping Efficiency on the Ratio of the Beam Radius-to-the Aperture Radius. *J. Korean Phys. Soc.* **43,** 348–351 (2003).

489. Mahamdeh, M., Citlali, P. C. & Schaffer, E. Under-filling trapping objectives optimizes the use of the available laser power in optical tweezers Abstract : *Opt. Express* **19,** 1260–1262 (2011).

490. Bormuth, V. *et al.* Optical trapping of coated microspheres. *Opt. Express* **16,** 13831–13844 (2008).

491. Hu, Y., Nieminen, T. a., Heckenberg, N. R. & Rubinsztein-Dunlop, H. Antireflection coating for improved optical trapping. *J. Appl. Phys.* **103,** 093119 (2008).

492. Oostrum, P. D. J. Van, Blaaderen, A. Van, Jannasch, A., Demiro, A. F. & Schaffer, E. Nanonewton optical force trap employing titania microspheres. *Nat. Photonics* **6,** 469–473 (2012).

493. Harris, J. & McConnell, G. Optical trapping and manipulation of live T cells with a low numerical aperture lens. *Opt. Express* **16,** 14036–14043 (2008).

494. Visscher, K., Brakenhoff, G. J. & Krol, J. J. Micromanipulation by " Multiple " Optical Traps Created by a Single Fast Scanning Trap Integrated With the Bilateral Confocal Scanning Laser Microscope. *Cytometry* **114,** 105–114 (1993).

495. Molloy, J. E. *et al.* Single-molecule mechanics of heavy meromyosin and Si interacting with rabbit or drosophila actins using optical tweezers. *Biophys. J.* **68,** 298–303 (1995).

496. Reicherter, M., Haist, T., Wagemann, E. U. & Tiziani, H. J. Optical particle trapping with computer-generated holograms written on a liquid-crystal display. *Opt. Lett.* **24,** 608–610 (1999).

497. Eriksson, E. *et al.* A microfluidic system in combination with optical tweezers for analyzing rapid and reversible cytological alterations in single cells upon environmental changes. *Lab Chip* **7,** 71–6 (2007).

498. Skelley, A. M., Kirak, O., Suh, H., Jaenisch, R. & Voldman, J. Microfluidic control of cell pairing and fusion. *Nat. Methods* **6,** 147–152 (2009).

499. Chen, H. D. *et al.* Application of optical tweezers in the research of molecular interaction between lymphocyte function associated antigen-1 and its monoclonal antibody. *Cell. Mol. Immunol.* **4,** 221–5 (2007).

500. Schermelleh, L., Heintzmann, R. & Leonhardt, H. A guide to super-resolution fluorescence microscopy. *J. Cell Biol.* **190,** 165–175 (2010).

501. Heller, I. *et al.* STED nanoscopy combined with optical tweezers reveals protein dynamics on densely covered DNA. *Nat. Methods* **10,** 910–916 (2013).

502. Hosseini, B. H. *et al.* Mechanical interactions between dendritic cells and T cells correlate with T cell responsiveness. *J. Immunol.* **187,** 258–265 (2011).

503. Adams, C. L., Grierson, A. M., Mowat, A. M., Harnett, M. M. & Garside, P. Differences in the Kinetics, Amplitude, and Localization of ERK Activation in Anergy and Priming Revealed at the Level of Individual Primary T Cells by Laser Scanning Cytometry. *J. Immunol.* **173,** 1579–1586 (2004).

504. Gupta, K. *et al.* Lab-on-a-chip devices as an emerging platform for stem cell biology. *Lab Chip* **10,** 2019–2031 (2010).

505. Weibel, D. B. & Whitesides, G. M. Applications of microfluidics in chemical biology. *Curr. Opin. Chem. Biol.* **10,** 2019–2031 (2006).

506. Zare, R. N. & Kim, S. Microfluidic platforms for single-cell analysis. *Annu. Rev. Biomed. Eng.* **12,** 187–201 (2010).